

DETERMINING THE LOCATIONS OF FAULTS IN DISTRIBUTION SYSTEMS

A Thesis Submitted to the College of
Graduate Studies and Research
in Partial Fulfillment of the Requirements
for the Degree of Doctor of Philosophy
in the Department of Electrical Engineering
University of Saskatchewan
Saskatoon

By
Ratan Das
Spring 1998

© Copyright Ratan Das, 1998. All Rights Reserved.



National Library
of Canada

Acquisitions and
Bibliographic Services

395 Wellington Street
Ottawa ON K1A 0N4
Canada

Bibliothèque nationale
du Canada

Acquisitions et
services bibliographiques

395, rue Wellington
Ottawa ON K1A 0N4
Canada

Your file Votre référence

Our file Notre référence

The author has granted a non-exclusive licence allowing the National Library of Canada to reproduce, loan, distribute or sell copies of this thesis in microform, paper or electronic formats.

L'auteur a accordé une licence non exclusive permettant à la Bibliothèque nationale du Canada de reproduire, prêter, distribuer ou vendre des copies de cette thèse sous la forme de microfiche/film, de reproduction sur papier ou sur format électronique.

The author retains ownership of the copyright in this thesis. Neither the thesis nor substantial extracts from it may be printed or otherwise reproduced without the author's permission.

L'auteur conserve la propriété du droit d'auteur qui protège cette thèse. Ni la thèse ni des extraits substantiels de celle-ci ne doivent être imprimés ou autrement reproduits sans son autorisation.

0-612-27401-2

Canadä

PERMISSION TO USE

The author has agreed that the Library, University of Saskatchewan, may make this thesis freely available for inspection. Moreover, the author has agreed that permission for extensive copying of this thesis for scholarly purposes may be granted by the professors who supervised the thesis work recorded herein or, in their absence, by the Head of the Department or the Dean of the College in which the thesis work was done. It is understood that due recognition will be given to the author of this thesis and to the University of Saskatchewan in any use of the material in this thesis. Copying or publication or any other use of this thesis or parts thereof for financial gain without the written approval of the author is prohibited.

Requests for permission to copy or to make any other use of the material in this thesis in whole or part should be addressed to:

Head of the Department of Electrical Engineering
University of Saskatchewan
Saskatoon SK S7N 5A9
Canada

ABSTRACT

The conventional approach for estimating the locations of transmission line shunt faults has been to measure the apparent impedance to the fault from a line terminal and to convert the reactive component of the impedance to line length. Several methods, that use the fundamental frequency voltages and currents measured at one or both line terminals, have been proposed in the past. Methods for locating faults on radial transmission lines have also been proposed. A technique for locating faults on rural distribution feeders has also been suggested. These methods do not adequately address the problems associated with the fault location on distribution systems that have single or multiphase laterals and/or tapped loads.

This thesis presents a technique that estimates the location of a shunt fault on a radial distribution system that has several single and/or multiphase laterals. Load taps and non-homogeneity of the system are taken into account. Distributed parameter models of the line and voltage dependent load models are used. The loads up to the fault are considered independently and the loads beyond the fault are consolidated to a single load at the remote end. The load constants, describing the change of load impedance with voltage, are computed from the pre-fault load voltages and currents.

The apparent location of a fault is first estimated by computing the impedance from the fundamental frequency voltage and current phasors, and converting the reactive component of the impedance to line length. The sequence voltages and currents at the nodes up to the fault are calculated. The sequence voltages at the remote end are expressed as a linear function of the distance to the fault. The sequence voltages and currents at the fault are expressed as functions of the distance to the fault as well as the impedances of loads beyond the fault. An equation for the fault impedance is then developed and its imaginary component is equated to zero. This provides a non-linear equation which is linearized and is then solved using an iterative approach. Multiple estimates may be obtained for a fault in a distribution system that has laterals. One of the estimates is identified as the most likely fault location by using information from fault indicators which are strategically placed on the laterals.

The developed technique, which can handle single-phase-to-ground, two-phase-to-ground, phase-to-phase and balanced three-phase faults was tested to evaluate its suitability. Results from computer simulations of faults on a model of a 25 kV distribution circuit of SaskPower are presented. The results indicate that the proposed technique works well for fault resistances that are of magnitudes comparable to the line impedance. It also indicates that the proposed technique is more accurate than the reactive component method.

Five thousand six hundred and sixteen cases were studied to determine the effect of the errors, in the input parameters, on the accuracy of the proposed technique. The test results indicate that the sensitivity of the proposed technique is comparable to that of the reactive component method in 80% of the cases. The proposed technique is less sensitive than the reactive component method for the remaining 20% cases.

Development of a prototype fault location system has also been presented. A modular approach was adopted in developing the system which will reduce implementation effort and time for future projects. The prototype system was tested by simulating faults on the model of the SaskPower distribution system. Ninety percent of the results reported in this thesis, show a close agreement with the results obtained from the simulations, described earlier.

ACKNOWLEDGEMENTS

The author expresses his appreciation and gratitude to Dr. M.S. Sachdev and Dr. T.S. Sidhu for their supervision of this work. Their advice and assistance in the preparation of this thesis are thankfully acknowledged.

The author also wishes to thank the advisory committee members for their suggestions and advice. Assistance provided by the computing staff of the College of Engineering and, laboratory and secretarial staff of the Department of Electrical Engineering is thankfully acknowledged. The encouragement of fellow graduate students in the Power System Research Group is appreciated.

The author acknowledges the encouragement and support provided by his spouse Nandita, and daughter Diya. Special thanks are extended to other family members for their support in making this project a reality. Financial assistance provided by the Natural Sciences and Engineering Research Council (NSERC) of Canada, through operating research grants, is thankfully acknowledged.

In the loving memory of
my mother
the source of inspiration

TABLE OF CONTENTS

	Page
PERMISSION TO USE	i
ABSTRACT	ii
ACKNOWLEDGEMENTS	iv
DEDICATION	v
TABLE OF CONTENTS	vi
LIST OF FIGURES	x
LIST OF TABLES	xv
LIST OF PRINCIPAL SYMBOLS	xx
1. INTRODUCTION	1
1.1 Fault Locating Methods	2
1.1.1 Transmission Line Fault Location Methods	2
1.1.2 Distribution Line Fault Location Methods	3
1.2 Objectives of the Thesis	4
1.3 Outline of the Thesis	5
2. DISTRIBUTION SYSTEM FAULTS	8
2.1 Introduction	8
2.2 A Typical Distribution System	8
2.2.1 Distribution system protection	10
2.3 Shunt Faults	10
2.3.1 Single-phase-to-ground faults	11
2.3.2 Two-phase-to-ground faults	11
2.3.3 Phase-to-phase faults	12
2.3.4 Balanced three-phase faults	14
2.4 Fault Resistance	16
2.4.1 Arc resistance	16
2.4.2 Ground resistance	17
2.5 Impact of Fault Resistance on Fault Location Estimates	17
2.6 Effect of Load Taps on Fault Location Estimates	21
2.7 Summary	22

3. FAULT LOCATION METHODS	23
3.1 Introduction	23
3.2 Reactive Component Method	24
3.3 Takagi Algorithm	32
3.4 Richards and Tan Algorithm	30
3.5 Srinivasan and St-Jacques Algorithm	30
3.6 Grgis Algorithm	34
3.7 Summary	37
4. DEVELOPMENT OF THE PROPOSED TECHNIQUE	38
4.1 Introduction	38
4.2 Overview of the Technique	38
4.3 Detection of Faults and Collection of Pre-fault and Fault Data	41
4.3.1 Estimating phasors	41
4.3.2 Fault detection	42
4.3.3 Collection of pre-fault and fault data	42
4.4 Estimating the Faulted Section	43
4.5 Developing an Equivalent Radial System	45
4.6 Modeling of Loads	46
4.6.1 Selecting the load model	47
4.6.2 Estimating the pre-fault loads at all nodes up to the fault	50
4.6.3 Estimating the pre-fault voltages and currents at the nodes	50
4.6.4 Estimating the load constants	53
4.7 Estimating Voltages and Currents at the Remote End and at the Fault	54
4.8 Estimating the Location of the Fault	58
4.8.1 Single-phase-to-ground faults	58
4.8.2 Two-phase-to-ground and phase-to-phase faults	61
4.8.3 Balanced three-phase faults	63
4.8.4 Generalized equation for all types of faults	64
4.9 Converting Multiple Estimates to a Single Estimate	64
4.9.1 Fault indicators	65
4.9.2 Single estimate	66
4.10 Summary	67
5. TESTING THE PROPOSED TECHNIQUE	68
5.1 Introduction	68
5.2 Distribution System Selected for the Studies	69
5.3 Studies Conducted	70
5.3.1 Single-phase-to-ground faults	70
5.3.2 Two-phase-to-ground faults	78
5.3.3 Phase-to-phase faults	85
5.3.4 Balanced three-phase faults	91
5.4 Summary	98

6. SENSITIVITY STUDIES	99
6.1 Introduction	99
6.2 Distribution System Parameters Selected for the Studies	100
6.3 Studies Conducted	100
6.3.1 Single-phase-to-ground faults	106
6.3.2 Phase-to-phase faults	114
6.4 Summary	122
7. IMPLEMENTING THE FAULT LOCATOR	123
7.1 Introduction	123
7.2 Design Requirements	123
7.3 System Overview	124
7.4 Hardware	125
7.4.1 Low pass filter boards	125
7.4.2 Data acquisition system cards	127
7.4.3 Digital signal processing card	128
7.4.4 Host personal computer	128
7.5 Software	128
7.5.1 User-Interface software	129
7.5.2 Real-time software	130
7.5.2.1 Data acquisition software	131
7.5.2.2 Application software	132
7.5.3 Off-line application software	133
7.6 Testing	134
7.6.1 Low pass filter	134
7.6.2 Real-time application software	136
7.6.3 Data acquisition software	136
7.6.4 User-Interface software	137
7.6.5 Complete fault locator	137
7.7 Summary	140
8. SUMMARY AND CONCLUSIONS	141
8.1 Summary	141
8.2 Conclusions	143
REFERENCES	145
APPENDICES	152
APPENDIX A. Representation of Various Shunt Faults	152
APPENDIX B. Least Error Squares Algorithm	161
APPENDIX C. Static Response Type Load Model	165
APPENDIX D. Voltages and Currents at the Line Terminals	167
APPENDIX E. Power Systems Simulation Software	169

APPENDIX F.	Anti-aliasing Filter	169
APPENDIX G.	Electrical Parameters of SaskPower Distribution System	173
APPENDIX H.	Additional Test Results	177
APPENDIX I.	Procedure for Estimating Fault Locations	195
APPENDIX J.	Fault Locator Hardware	197
APPENDIX K.	Testing the Real-time Application Software	202
APPENDIX L.	Real Time Playback (RTP) Simulator	205

LIST OF FIGURES

	Page
Figure 2.1. A typical distribution system.	9
Figure 2.2. Single-phase-to-ground faults experienced on three-phase lines. (a) Types of faults. (b) Sequence network diagram with faulted phase as reference.	12
Figure 2.3. Two-phase-to-ground faults. (a) Types of faults. (b) Sequence network diagram with unfaulted phase as reference.	13
Figure 2.4. Phase-to-phase faults. (a) Types of faults. (b) Sequence network diagram with unfaulted phase as reference.	14
Figure 2.5. Balanced three-phase fault. (a) Types of faults. (b) Sequence network diagram for fault with ground. (c) Sequence network diagram for fault without ground.	15
Figure 2.6. Change of the apparent impedance seen from the fault locator terminal due to the fault resistance. (a) The single line diagram of a line connected at one terminal only and disconnected from the load at the remote terminal. (b) The phasor diagram showing the line current and voltage at bus M . (c) The equivalent $R - X$ diagram.	18
Figure 2.7. Change of the apparent impedance seen from the fault locator terminal due to the fault resistance. (a) The single line diagram of a line connected to sources at both ends. (b) The phasor diagram. (c) The $R - X$ diagrams.	20
Figure 2.8. A distribution line with tapped loads, experiencing a fault.	21
Figure 3.1. (a) Single line diagram of a two machine system. (b) The system is experiencing a fault at F . (c) Equivalent circuit for calculating the pre-fault currents and their distribution. (c) Equivalent circuit for calculating the fault currents and their distribution.	25
Figure 3.2. System model used by Richards and Tan for determining fault locations using an optimization approach.	30
Figure 3.3. Faulted transmission line with load.	31

Figure 3.4.	Faulted transmission line with two load taps.	33
Figure 4.1.	The single line diagram of a distribution line experiencing a fault.	40
Figure 4.2.	Block diagram for (a) acquiring data and (b) estimating the location of the fault.	40
Figure 4.3.	Flowchart for determining the fault type and the identity of faulted phases.	43
Figure 4.4.	The single line diagram of the modified radial distribution system experiencing a fault (a) at F and (b) at F_1 .	46
Figure 4.5.	A single-phase load at node R and its sequence network representation.	48
Figure 4.6.	A phase-to-phase load at node R and its sequence network representation.	49
Figure 4.7.	A three-phase balanced load and its sequence network representation.	49
Figure 4.8.	Distribution line section between nodes M and R .	51
Figure 4.9.	The voltage and currents at node R .	52
Figure 4.10.	The pre-fault voltages and currents at nodes N and x .	53
Figure 4.11.	The voltages and currents at nodes F and N during the fault.	55
Figure 4.12.	Location of fault indicators in a typical distribution system.	55
Figure 5.1.	A single line diagram of the selected SaskPower distribution circuit.	69
Figure 5.2.	Estimation errors for the single-phase-to-ground faults when the fault resistance is 0.05 ohm.	73
Figure 5.3.	Estimation errors for the single-phase-to-ground faults when the fault resistance is 5.0 ohm.	74
Figure 5.4.	Estimation errors for the single-phase-to-ground faults when the fault resistance is 10.0 ohm.	75
Figure 5.5.	Estimation errors for the single-phase-to-ground faults when the fault resistance is 25.0 ohm.	76
Figure 5.6.	Estimation errors for the single-phase-to-ground faults when the fault resistance is 50.0 ohm.	77

Figure 5.7.	Estimation errors for the two-phase-to-ground faults when the fault resistance is 0.05 ohm.	80
Figure 5.8.	Estimation errors for the two-phase-to-ground faults when the fault resistance is 5.0 ohm.	81
Figure 5.9.	Estimation errors for the two-phase-to-ground faults when the fault resistance is 10.0 ohm.	82
Figure 5.10.	Estimation errors for the two-phase-to-ground faults when the fault resistance is 25.0 ohm.	83
Figure 5.11.	Estimation errors for the two-phase-to-ground faults when the fault resistance is 50.0 ohm.	84
Figure 5.12.	Estimation errors for the phase-to-phase faults when the fault resistance is 0.05 ohm.	86
Figure 5.13.	Estimation errors for the phase-to-phase faults when the fault resistance is 5.0 ohm.	87
Figure 5.14.	Estimation errors for the phase-to-phase faults when the fault resistance is 10.0 ohm.	88
Figure 5.15.	Estimation errors for the phase-to-phase faults when the fault resistance is 25.0 ohm.	89
Figure 5.16.	Estimation errors for the phase-to-phase faults when the fault resistance is 50.0 ohm.	90
Figure 5.17.	Estimation errors for the balanced three-phase faults when the fault resistance is 0.05 ohm.	93
Figure 5.18.	Estimation errors for the balanced three-phase faults, when the fault resistance is 5.0 ohm.	94
Figure 5.19.	Estimation errors for the balanced three-phase faults when the fault resistance is 10.0 ohm.	95
Figure 5.20.	Estimation errors for the balanced three-phase faults when the fault resistance is 25.0 ohm.	96
Figure 5.21.	Estimation errors for the balanced three-phase faults when the fault resistance is 50.0 ohm.	97
Figure 6.1.	Estimation errors for the single-phase-to-ground fault for variation in the magnitude of the estimated voltage phasor.	107

Figure 6.2.	Estimation errors for the single-phase-to-ground fault for variation in the angle of the estimated voltage phasor.	107
Figure 6.3.	Estimation errors for the single-phase-to-ground fault for variation in the magnitude of the estimated current phasor.	108
Figure 6.4.	Estimation errors for the single-phase-to-ground fault for variation in the angle of the estimated current phasor.	109
Figure 6.5.	Estimation errors for the single-phase-to-ground fault for variation in the line section lengths.	112
Figure 6.6.	Estimation errors for the single-phase-to-ground fault for variation in the line section impedances per unit length.	112
Figure 6.7.	Estimation errors for the single-phase-to-ground fault for variation in the largest connected load.	113
Figure 6.8.	Estimation errors for the single-phase-to-ground fault for variation in the equivalent load response constants.	113
Figure 6.9.	Estimation errors for the phase-to-phase fault for variation in the magnitude of the estimated voltage phasor.	115
Figure 6.10.	Estimation errors for the phase-to-phase fault for variation in the angle of the estimated voltage phasor.	115
Figure 6.11.	Estimation errors for the phase-to-phase fault for variation in the magnitude of the estimated current phasor.	116
Figure 6.12.	Estimation errors for the phase-to-phase fault for variation in the angle of the estimated current phasor.	117
Figure 6.13.	Estimation errors for the phase-to-phase fault for variation in the line section lengths.	120
Figure 6.14.	Estimation errors for the phase-to-phase fault for variation in the line section impedances per unit length.	120
Figure 6.15.	Estimation errors for the phase-to-phase fault for variation in the largest connected load.	121
Figure 6.16.	Estimation errors for the phase-to-phase fault for variation in the equivalent load response constants.	121
Figure 7.1.	Overview of the fault location system along with the testing arrangement.	125

Figure 7.2.	Hardware configuration of the fault location system for distribution network.	126
Figure 7.3.	Display of the user-interface for the fault location system.	129
Figure 7.4.	Real-time software modules.	131
Figure 7.5.	Different stages of testing in the development of the fault location system.	135
Figure 7.6.	Frequency response of the sixth order Butterworth low-pass filter.	135
Figure 7.7.	A typical fault waveform played back by the Real Time Playback Simulator.	138
Figure A.1.	Fault conditions for a phase A-to-ground fault.	153
Figure A.2.	Fault conditions for a phase B and phase C-to-ground fault.	154
Figure A.3.	Fault conditions for a phase B-to-phase C fault.	156
Figure A.4.	Fault conditions for a balanced three-phase fault, involving ground.	158
Figure A.5.	Fault conditions for a balanced three-phase fault, without ground.	160
Figure B.1.	Magnitude response of the Least Error Squares algorithm.	164
Figure D.1.	Distribution line section between nodes M and R .	167
Figure F.1.	Magnitude response of the fourth-order low-pass digital filter.	172
Figure G.1.	Single line diagram of the SaskPower 25 kV distribution system.	173
Figure J.1.	Circuit diagram of one channel of the Butterworth low-pass filter.	197
Figure J.2.	Functional block diagram of the data acquisition system.	199

LIST OF TABLES

	Page
Table 4.1. Selection of a reference phase for different types of faults.	55
Table 5.1. Multiple fault location estimates for the single-phase-to-ground fault cases between node 1 and 11 when the fault resistance is 0.05 ohm.	71
Table 5.2. Multiple fault location estimates for the single-phase-to-ground fault cases between node 12 and 21 when the fault resistance is 0.05 ohm.	72
Table 5.3. Fault location estimates for the single-phase-to-ground fault cases when the fault resistance is 0.05 ohm.	73
Table 5.4. Fault location estimates for the single-phase-to-ground fault cases when the fault resistance is 5.0 ohm.	74
Table 5.5. Fault location estimates for the single-phase-to-ground fault cases when the fault resistance is 10.0 ohm.	75
Table 5.6. Fault location estimates for the single-phase-to-ground fault cases when the fault resistance is 25.0 ohm.	76
Table 5.7. Fault location estimates for the single-phase-to-ground fault cases when the fault resistance is 50.0 ohm.	77
Table 5.8. Fault resistances selected for the two-phase-to-ground faults.	78
Table 5.9. Multiple fault location estimates for the two-phase-to-ground fault cases when the fault resistance is 0.05 ohm.	79
Table 5.10. Fault location estimates for the two-phase-to-ground fault cases when the fault resistance is 0.05 ohm.	80
Table 5.11. Fault location estimates for the two-phase-to-ground fault cases when the fault resistance is 5.0 ohm.	81
Table 5.12. Fault location estimates for the two-phase-to-ground fault cases when the fault resistance is 10.0 ohm.	82

Table 5.13.	Fault location estimates for the two-phase-to-ground fault cases when the fault resistance is 25.0 ohm.	83
Table 5.14.	Fault location estimates for the two-phase-to-ground fault cases when the fault resistance is 50.0 ohm.	84
Table 5.15.	Multiple fault location estimates for the phase-to-phase fault cases when the fault resistance is 0.05 ohm.	85
Table 5.16.	Fault location estimates for the phase-to-phase fault cases when the fault resistance is 0.05 ohm.	86
Table 5.17.	Fault location estimates for the phase-to-phase fault cases when the fault resistance is 5.0 ohm.	87
Table 5.18.	Fault location estimates for the phase-to-phase fault cases when the fault resistance is 10.0 ohm.	88
Table 5.19.	Fault location estimates for the phase-to-phase fault cases when the fault resistance is 25.0 ohm.	89
Table 5.20.	Fault location estimates for the phase-to-phase fault cases when the fault resistance is 50.0 ohm.	90
Table 5.21.	Multiple fault location estimates for the balanced three-phase fault cases when the fault resistance is 0.05 ohm.	92
Table 5.22.	Fault location estimates for the balanced three-phase fault cases when the fault resistance is 0.05 ohm.	93
Table 5.23.	Fault location estimates for the balanced three-phase fault cases when the fault resistance is 5.0 ohm.	94
Table 5.24.	Fault location estimates for the balanced three-phase fault cases when the fault resistance is 10.0 ohm.	95
Table 5.25.	Fault location estimates for the balanced three-phase fault cases when the fault resistance is 25.0 ohm.	96
Table 5.26.	Fault location estimates for the balanced three-phase fault cases when the fault resistance is 50.0 ohm.	97
Table 6.1.	Cases of estimated voltage phasor variations.	101
Table 6.2.	Cases of estimated current phasor variations.	102

Table 6.3.	Cases of estimated voltage and current phasors combined magnitude variations.	103
Table 6.4.	Cases of estimated voltage and current phasors combined magnitude and phase angle variations.	104
Table 6.5.	Cases of line and load parameters variations.	105
Table 6.6.	Estimation errors for the single-phase-to-ground fault for combined variation in magnitude and angle of the estimated voltage phasor.	108
Table 6.7.	Estimation errors for the single-phase-to-ground fault for combined variation in magnitude and angle of the estimated current phasor.	119
Table 6.8.	Estimation errors for the single-phase-to-ground fault for combined variation in magnitudes of the estimated voltage and current phasors.	110
Table 6.9.	Estimation errors for the single-phase-to-ground fault for combined variation in magnitudes and phase angles of the estimated voltage and current phasors.	111
Table 6.10.	Estimation errors for the phase-to-phase fault for combined variation in magnitude and angle of the estimated voltage phasor.	116
Table 6.11.	Estimation errors for the phase-to-phase fault for combined variation in magnitude and angle of the estimated current phasor.	117
Table 6.12.	Estimation errors for the phase-to-phase fault for combined variation in magnitudes of the estimated voltage and current phasors.	118
Table 6.13.	Estimation errors for the phase-to-phase fault for combined variation in magnitudes and phase angles of the estimated voltage and current phasors.	119
Table 7.1.	Fault location estimates obtained using non real-time and real-time testing.	139
Table B.1.	Filter coefficients for the Least Error Squares algorithm.	164
Table G.1.	Equivalent distribution system source data.	173
Table G.2.	Line data.	174
Table G.3.	Load data.	175
Table G.4.	Power factor and response constants for different types of load.	176

Table H.1.	Fault location estimates for the phase C-to-ground fault cases when the fault resistance is 0.05 ohm.	177
Table H.2.	Fault location estimates for the phase C-to-ground fault cases when the fault resistance is 5.0 ohm.	178
Table H.3.	Fault location estimates for the phase C-to-ground fault cases when the fault resistance is 10.0 ohm.	179
Table H.4.	Fault location estimates for the phase C-to-ground fault cases when the fault resistance is 25.0 ohm.	180
Table H.5.	Fault location estimates for the phase C-to-ground fault cases when the fault resistance is 50.0 ohm.	181
Table H.6.	Fault location estimates for the phase A-to-ground fault cases when the fault resistance is 0.05 ohm.	182
Table H.7.	Fault location estimates for the phase A-to-ground fault cases when the fault resistance is 5.0 ohm.	182
Table H.8.	Fault location estimates for the phase A-to-ground fault cases when the fault resistance is 10.0 ohm.	183
Table H.9.	Fault location estimates for the phase A-to-ground fault cases when the fault resistance is 25.0 ohm.	183
Table H.10.	Fault location estimates for the phase A-to-ground fault cases when the fault resistance is 50.0 ohm.	184
Table H.11.	Fault location estimates for the phase C and phase A-to-ground fault cases when the fault resistance is 0.05 ohm.	184
Table H.12.	Fault location estimates for the phase C and phase A-to-ground fault cases when the fault resistance is 5.0 ohm.	185
Table H.13.	Fault location estimates for the phase C and phase A-to-ground fault cases when the fault resistance is 10.0 ohm.	185
Table H.14.	Fault location estimates for the phase C and phase A-to-ground fault cases when the fault resistance is 25.0 ohm.	186
Table H.15.	Fault location estimates for the phase C and phase A-to-ground fault cases when the fault resistance is 50.0 ohm.	186
Table H.16.	Fault location estimates for the phase A and phase B-to-ground fault cases when the fault resistance is 0.05 ohm.	187

Table H.17.	Fault location estimates for the phase A and phase B-to-ground fault cases when the fault resistance is 5.0 ohm.	187
Table H.18.	Fault location estimates for the phase A and phase B-to-ground fault cases when the fault resistance is 10.0 ohm.	188
Table H.19.	Fault location estimates for the phase A and phase B-to-ground fault cases when the fault resistance is 25.0 ohm.	188
Table H.20.	Fault location estimates for the phase A and phase B-to-ground fault cases when the fault resistance is 50.0 ohm.	189
Table H.21.	Fault location estimates for the phase B-to-phase C fault cases when the fault resistance is 0.05 ohm.	189
Table H.22.	Fault location estimates for the phase B-to-phase C fault cases when the fault resistance is 5.0 ohm.	190
Table H.23.	Fault location estimates for the phase B-to-phase C fault cases when the fault resistance is 10.0 ohm.	190
Table H.24.	Fault location estimates for the phase B-to-phase C fault cases when the fault resistance is 25.0 ohm.	191
Table H.25.	Fault location estimates for the phase B-to-phase C fault cases when the fault resistance is 50.0 ohm.	191
Table H.26.	Fault location estimates for the phase C-to-phase A fault cases when the fault resistance is 0.05 ohm.	192
Table H.27.	Fault location estimates for the phase C-to-phase A fault cases when the fault resistance is 5.0 ohm.	192
Table H.28.	Fault location estimates for the phase C-to-phase A fault cases when the fault resistance is 10.0 ohm.	193
Table H.29.	Fault location estimates for the phase C-to-phase A fault cases when the fault resistance is 25.0 ohm.	193
Table H.30.	Fault location estimates for the phase C-to-phase A fault cases when the fault resistance is 50.0 ohm.	194
Table I.1.	Multiple fault location estimates for the single-phase-to-ground fault at node 10 when the fault resistance is 0.05 ohm.	195
Table I.2.	Fault location estimates for one apparent location.	195

LIST OF PRINCIPAL SYMBOLS

α	Phasor operator.
A, B, C, D	Line/line section constants.
A_e, B_e, C_e, D_e	Equivalent line section constants of all cascaded sections between nodes x and N .
$A_{mr}, B_{mr}, C_{mr}, D_{mr}$	Line section constants between nodes M and R .
$b_{mr}, g_{mr}, r_{mr}, x_{mr}$	Susceptance, conductance, resistance and reactance per unit length of the line section between nodes M and R , respectively.
B_{xy}, C_{xy}	Line section constants between nodes x and y .
B_n and B_r	Constants proportional to the load susceptance at nodes N and R , respectively.
d	Conductor spacing.
G_n and G_r	Constants proportional to the load conductance at node N and R , respectively.
I_f	Fault current.
I_n, I_r	Load currents at nodes N and R , respectively.
I_{f1}, I_{f2}	Fault current contribution from two terminals, respectively.
$\tilde{I}_{f1}, \tilde{I}_{f2}$	Difference between the pre-fault and fault current from two terminals, respectively.
I_{mf}	Current at bus M towards fault F .
\tilde{I}_{mf}	Difference between the pre-fault line current and the line current during the fault at bus M .

$I_{amr}, I_{bmr}, I_{cmr}$	Phasor of the phase A, phase B and phase C line currents at node M towards node R , respectively.
I_{comp}	Compensating current.
I_t and I_{tg}	Threshold currents.
I_{0mr}	Zero sequence component of the line currents at node M towards node R .
I_{0f}, I_{1f}, I_{2f}	Zero, positive and negative sequence currents flowing into the fault F , respectively.
I_{0r}, I_{1r}, I_{2r}	Zero, positive and negative sequence load currents at node R , respectively.
$I_{0xf}, I_{1xf}, I_{2xf}$	Zero, positive and negative sequence currents at node x flowing towards the fault F .
$K_a - K_w$	Complex constants/parameters.
K_{0w}, K_{1w}, K_{2w}	Zero, positive and negative sequence values of the constant K_w .
K_A, K_B, K_C, K_D	Complex parameters.
l_{mf}	Distance to the fault from bus/node M .
L_{arc}	Length of the arc in still air.
L_{mn}	Length of line/line section between buses/nodes M and N .
L_{xy}	Length of line section between nodes x and y .
n_p, n_q	Response constants for the active and reactive components of the load respectively.
P_r	Active power of the load at node R .
Q_r	Reactive power of the load at node R .
R_{arc}	Arc resistance.
R_f	Fault resistance.

s	Distance to the node F from node x , expressed as a fraction of section length between nodes x and $x + l (= y)$.
S_r	Apparent power of the load at node R .
T_{arc}	Duration of the arc.
U	Wind velocity.
V_f	Voltage at fault F .
V_m	Voltage at bus/node M .
V_m''	Difference between the pre-fault voltage and the voltage during the fault at bus M .
V_n, V_r	Voltages at nodes N and R , respectively.
V_{nom}	Nominal voltage.
V_{am}, V_{bm}, V_{cm}	Phasor of the phase A-to-ground, phase B-to-ground and phase C-to-ground voltages at node M , respectively.
V_{0f}, V_{1f}, V_{2f}	Zero, positive and negative sequence voltages with respect to ground at the fault F , respectively.
V_{0r}, V_{1r}, V_{2r}	Zero, positive and negative sequence load voltages with respect to ground at node R , respectively.
V_{0r}, V_{1r}, V_{2r}	Zero, positive and negative sequence load voltages with respect to ground at node R .
X_{m1}	Apparent reactance to the fault F from node M , for single-phase-to-ground faults.
X_{m2g}	Apparent reactance to the fault F from node M , for two-phase-to-ground faults.
X_{m3}	Positive sequence apparent reactance to the fault F from node M , for balanced three-phase faults.
X_{mr}^m	Modified reactance of section between nodes M and R .
X_{0mr}, X_{1mr}	Zero and positive sequence reactances of the section between nodes M and R , respectively.

Y_n and Y_r	Admittance of the load at nodes N and R , respectively.
Z_{app}	Computed apparent impedance.
Z_m	Impedance seen by the fault locator provided at bus M .
Z_{m1}	Apparent impedance to the fault F from node M , for single-phase-to-ground faults.
Z_{m2g}	Apparent impedance to the fault F from node M , for two-phase-to-ground faults.
Z_{m3}	Positive sequence apparent impedance to the fault F from node M , for balanced three-phase faults.
z_{mn}	Impedance per unit length of line/line section between buses/nodes M and N .
Z_{sm}, Z_{sn}	Source impedances at buses M and N , respectively.
Z_{mn}^s	Surge impedance of line/line section between buses/nodes M and N .
γ_{mn}	Propagation constant of the line/line section between buses/nodes M and N .
η	Fault current distribution factor.
θ	Argument of η .

1. INTRODUCTION

Electric power systems have grown rapidly over the past fifty years. This has resulted in a large increase of the number of lines in operation and their total length. These lines experience faults which are caused by storms, lightning, snow, freezing rain, insulation breakdown and, short circuits caused by birds and other external objects. In most cases, electrical faults manifest in mechanical damage which must be repaired before returning the line to service. The restoration can be expedited if the location of the fault is either known or can be estimated with reasonable accuracy.

Fault locators, which provide estimates for the locations of faults, are useful when overhead lines are long and patrolling is time-consuming. Also, visual inspection is difficult during adverse weather conditions. Fault locators could be relied on for obtaining the needed fault location estimates. They provide estimates for sustained as well as transient faults. Generally, transient faults cause minor damage that is not easily visible on inspection. Fault locators help identify those locations for early repairs to prevent recurrence and consequent major damages. In this manner, fault locators make a definite contribution towards increasing the availability and security of electric power systems.

The subject of fault location has been of considerable interest to electric power utility engineers and researchers for over twenty-five years. Most of the research done so far, has been aimed at finding the locations of transmission line faults. This is mainly because of the impact of transmission line faults on the power systems and the time required to physically check the lines is much larger than the faults in the subtransmission and distribution systems. Of late, the location of faults on distribution systems has started receiving some attention as utilities are operating in a deregulated environment and are competing with each other to increase the availability of power supply to the customers. Also, distribution systems are being gradually automated and microprocessor based relays [1] are being used for line protection. Therefore, development of an improved fault location technique is possible utilizing data that the relays are now able to collect.

1.1 Fault Locating Methods

Faulted lines must be repaired and returned to service in the shortest possible times to provide reliable service to the customers. Several methods of locating transmission line faults have been developed to achieve this objective. The primitive method of fault location was to visually inspect the line [2]. The procedure involved patrolling the line by foot or automobile and inspecting the line with or without the aid of binoculars.

Sectionalizing the line and energizing it in parts has been used to reduce the length of the line that must be inspected. Surge-operated targets, placed on line towers, and tracer currents have been used to further assist in locating faults. These procedures are slow, inaccurate and expensive, and are unsafe during adverse weather conditions. Other methods, proposed in the past used, include the use of annunciator ammeters, magnetic links and automatic oscillographs [2]. These methods are also not used widely because they require considerable preparatory work and skill; they are time-consuming and accuracy of the results is low. Specific methods, recently proposed for use on transmission and distribution lines, are discussed in the following sections.

1.1.1 Transmission Line Fault Location Methods

A previously proposed approach for estimating the location of transmission line faults consists of using voltages and currents measured at one or both terminals of a line. The methods can be divided into three categories. The first category is of the methods which are based on the phenomenon of traveling waves [2, 3, 4, 5]. It is well known that voltage and current traveling waves, on the inception of a fault, start and travel from the fault towards the line terminals. The methods are accurate but are complex and are difficult to apply. The accuracy of these methods depends largely on the accuracy of the estimated values of line parameters (line inductance and capacitance) and, to some degree, the network configuration as well as on the transducer accuracy and bandwidth.

The methods in the second category use the high frequency components of currents and voltages caused by the inceptions of faults and the ensuing voltage and current traveling waves between the fault and the line terminals [6]. The methods are complex and expensive because they require the use of specially tuned filters for measuring high frequency components.

The methods in the third category use the fundamental frequency voltages and currents at the terminals of a line and the parameters of the line [7, 8, 9, 10]. These methods consist of calculating line impedances as seen from the line terminals and estimating, from the calculated impedances, distances of the faults from the line terminals. The methods in this category can be further classified into two sub-categories. The first category includes the methods that use measurements from one terminal of the transmission line [7, 8, 9]. The methods in the second category use measurements taken from both terminals [10]. These methods are popular among electric power utilities because they are simple and economical compared to those based on the traveling wave and high frequency component techniques. These methods are implemented using analog as well as digital hardware including microprocessors. The emphasis, in these techniques, has been on the premise that sources of energy are connected to both terminals of the line, the line is homogeneous and not tapped.

A method that estimates fault locations on radial transmission lines has also been proposed in the past [11]. This method considers that the line is of homogeneous construction and also assumes that currents at load taps are known.

1.1.2 Distribution Line Fault Location Methods

Distribution lines are usually operated in the radial mode. Loads are usually tapped along the lines; which could be single and/or multi-phase taps. The construction of the line is usually non-homogeneous because distribution lines are extended as loads develop.

Previously proposed approaches for estimating the locations of distribution line faults consist of using voltages and currents measured at the line terminal. The methods used in this approach can be divided into two categories. The first category uses the high frequency components of currents and voltages caused by the faults which start voltage and current traveling waves between the fault and the line terminals [12]. This method is similar to that proposed for transmission lines and is complex and expensive.

The methods in the second category use the fundamental frequency voltages and currents at the terminals of a line and parameters of the line and loads [13]. This method consists of calculating the line impedance as seen from the line terminal and uses the calculated impedance to estimate the distance of the fault from the line terminals.

Reference [13] does not consider the dynamic nature of the loads and multiphase taps which are normally encountered in such cases.

Another technique, that uses the fundamental frequency components of voltages and currents measured at the line terminal, has been proposed for estimating the locations of shunt faults on radial distribution lines [14, 15]. The technique is suitable for non-homogeneous lines with or without capacitor banks and dynamic loads. However, this technique does not consider the presence of laterals in the distribution system.

Utilities estimate fault locations in distribution lines by computing the impedance seen from the line terminal from the voltages and currents available from reclosers. Portable fault locators are also used, in an off-line mode, to locate faults in distribution lines. While the former method fails to provide estimates with reasonable accuracy, the latter is cumbersome and time-consuming.

Another method, that is used to identify the faulted section, consists of using a fault indicator in each section of the line. This technique is not of much help if the section is more than a couple of miles. Most fault indicators provide indication locally which makes it difficult to use the information during inclement weather. To alleviate this problem, some manufacturers are now providing fault indicators which communicate with a remote receiver over a radio link.

1.2 Objectives of the Thesis

The work, reported in this thesis, was conducted keeping the following objectives in mind.

- To develop a technique for determining the locations of shunt faults in radial distribution systems which include several single and/or multi-phase laterals.
- To perform sensitivity studies of the developed technique.
- To design, build and test a prototype fault location system in the laboratory.

1.3 Outline of the Thesis

The thesis is organized in nine chapters and twelve appendices. The subject and organization of the thesis are described in the first chapter. Past activities in the area of fault location, and the methods presently used for locating distribution line faults are outlined.

A typical distribution system and its protection are described in Chapter 2. Different types of shunt faults experienced on distribution lines are also described. The effects of fault resistance and tapped load on the accuracy of fault location estimates are discussed. The knowledge of these effects is later used in developing a suitable technique.

The previously proposed fault location techniques are reviewed in Chapter 3. A new technique is developed in Chapter 4. This technique estimates the location of a shunt fault in a radial distribution system which may have several laterals and tapped loads. The proposed technique calculates the phasors of the fundamental frequency components of voltages and currents from measurements taken at the line terminal. This information is used along with the data on the sequence impedances of the line, the lengths of different sections, the loads and their characteristics. If necessary, it uses information from fault indicators strategically placed in the laterals. The technique is suitable for estimating the locations of single and multi-phase shunt faults either on the main feeder or on any of the laterals.

The technique was tested using the voltages and currents obtained from simulations in which faults were applied on a model of a SaskPower distribution circuit. The simulations were performed on a UNIX based SUN SPARC Workstation using the PSCAD software. The system has single and three phase laterals. Faults were applied at different locations and data on voltage and currents at the line terminal were collected. The studies were repeated using several conditions and several values of fault resistance. The reactive components of the apparent impedance were also used. The simulation studies and the test results for single-phase-to-ground, two phase-to-ground, phase-to-phase and balanced three phase faults are reported in Chapter 5.

Sensitivity studies were performed to examine the effect of errors in the input parameters on the accuracy of the proposed technique. Some of the test results are reported in Chapter 6.

The hardware and software used to build a prototype fault location system is described in Chapter 7. The modular approach, that was adopted in the development of the fault location system, is also described. The advantage of this approach is that it will be possible to use this system for implementing protection, monitoring, measurement or relay testing algorithms by modifying the appropriate software codes only. The testing procedure for the prototype system is also described in this chapter. The test results are also reported.

A brief summary of the thesis and conclusions drawn from the work reported in the thesis are outlined in Chapter 8. References are listed in Chapter 9.

This thesis also contains twelve appendices. Appendix A describes the symmetrical components representation of shunt faults discussed in chapter 2. Appendix B presents the Least Error Squares (LES) algorithm which was used for estimating phasors. Appendix C describes the static response type load models. Voltage-current relationships at the line terminals are presented in Appendix D. Appendix E presents the power system simulation software used for generating the fault data. Anti-aliasing filter used for pre-processing data obtained from simulation studies is described in Appendix F. Appendix G lists the system data used in simulating line faults. Additional test results are provided in Appendix H. An example of the fault location estimation procedure is provided in Appendix I. Appendix J describes the prototype fault location system hardware. Real-time application software testing is described in Appendix K. Appendix L describes the Real Time Playback (RTP) Simulator used for testing the implemented fault location system.

The following contributions were made by this research project.

- A technique was developed for determining the locations of shunt faults in radial distribution systems which include several laterals. The technique provides a single estimate of the fault location and is reported in Chapter 4.
- The performance of the technique was tested and is reported in Chapter 5.
- The sensitivity of the developed technique was examined and was found to be comparable to or better than the reactive component method.
- A PC based fault location system was designed, implemented and tested. The details are reported in Chapter 7.

- The modular approach was used in developing the fault location system. This general purpose system is suitable for implementing the protection, monitoring, measurement and relay testing algorithms in the laboratory.

This chapter briefly introduces the importance of fault locators. The work previously done for locating transmission and distribution system faults is also reviewed. The objectives of the research are described. The organization of the thesis is outlined and the specific contributions made by this research project are enumerated.

2. DISTRIBUTION SYSTEM FAULTS

2.1 Introduction

Methods for locating shunt faults on electric power lines have been briefly introduced in Chapter 1. The necessity for estimating locations of faults has also been discussed. As stated in Chapter 1, the objective of this project was to develop an accurate as well as practical technique for locating shunt faults on radial distribution systems that have load taps and single and/or multiphase laterals. This chapter describes a typical distribution system and reviews the shunt faults generally experienced on them. Two major components of fault resistance, arc and ground resistances, are briefly described in this chapter. The effects of fault resistance and load on the estimates of fault locations are also discussed.

2.2 A Typical Distribution System

Distribution networks of an electric power system link bulk sources of energy to customers' facilities. If an outage occurs on a distribution circuit, supply to the customers is interrupted. It is estimated that 80% of all interruptions occur due to failures in distribution systems [16].

Figure 2.1 shows a typical distribution system which includes sub-transmission circuits, substations, feeders, transformers, secondary circuits and services to customers' facilities. The sub-transmission circuits, operating at voltages ranging from 12 to 245 kV, transport energy from bulk power sources to the distribution substations. A distribution substation includes power transformers, buses, reactors, capacitors, circuit breakers, isolators and reclosers. The transformers reduce the voltages from the sub-transmission levels to lower levels for local distribution.

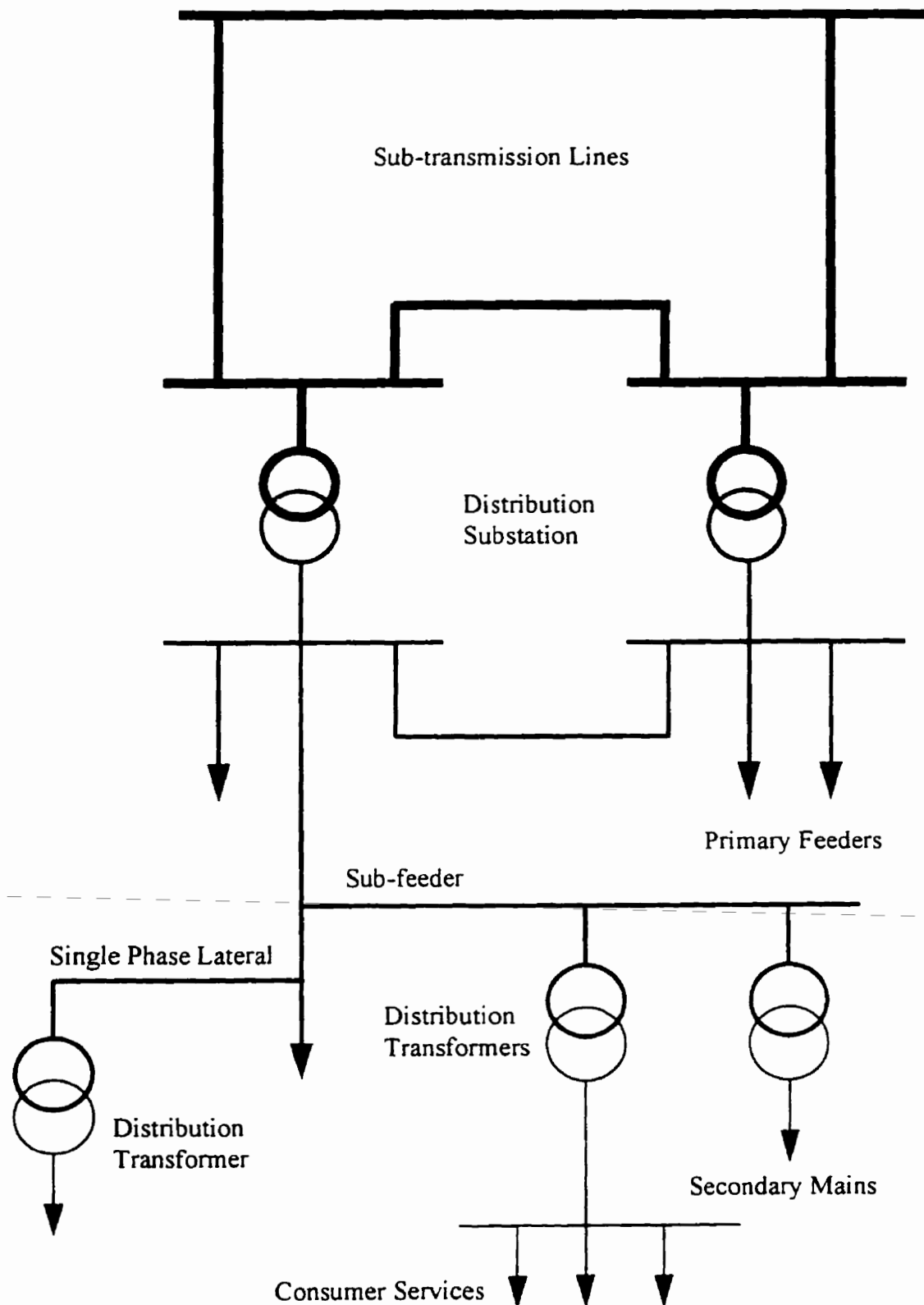


Figure 2.1. A typical distribution system.

Three-phase primary distribution feeders, which operate at voltages ranging from 4.16 to 34.5 kV, distribute energy to load centres. From these centres, the circuits branch into three-phase sub-feeders and single phase laterals. Distribution transformers of 10 to 500 kVA rating are usually installed on primary feeders and sub-feeders to reduce the distribution voltage to the utilization level. Secondary circuits facilitate distribution of energy from the distribution transformers to the customers through service drops.

2.2.1 Distribution system protection

Distribution systems generally experience shunt faults. The commonly used equipment for detecting and isolating the faulted circuits in a distribution system are [17, 18, 19]

1. Phase-overcurrent relays and
2. Ground-overcurrent relays.

Distance relays are also sometimes used in special situations, for example in feeders which have significant generation, low fault current-to-load current ratios and severe magnetizing inrush. The issues addressed, while designing the protection of a distribution system, are cold load pickup and magnetizing inrush.

Protection practices, which vary among utilities, were surveyed by the IEEE Power System Relaying Committee and are presented in a Working Group report [20]. The protection, control and operating practices of 124 distribution systems were collected and summarized in the report. A data base was established to collect information on the performance of the protection systems and to help develop a benchmark for determining future design and operational trends.

2.3 Shunt Faults

Distribution lines experience faults more often than the faults experienced by other power system facilities [21]. Most line faults are caused by insulation failure resulting in single-phase-to-ground and multi-phase short circuits. For a three-phase line, shunt faults are classified in the following four categories.

1. Single-phase-to-ground faults.
2. Two-phase-to-ground faults.
3. Phase-to-phase faults.
4. Three-phase faults.

Experience has shown that between 70 and 80 percent of all faults are single-phase-to-ground faults [22, 23, 24]. All faults, except the three-phase faults, cause power systems to operate in unbalanced modes. The use of symmetrical component theory [23, 24, 25, 26] makes it convenient to study the operation of the system during such conditions.

2.3.1 Single-phase-to-ground faults

The following three types of single-phase-to-ground faults are experienced.

1. Phase A-to-ground faults.
2. Phase B-to-ground faults.
3. Phase C-to-ground faults.

Figure 2.2 (a) depicts the electrical circuits for these faults. In this figure, R_f is the fault resistance. It can be shown that a single-phase-to-ground fault can be represented by the sequence network diagram shown in Figure 2.2 (b). The derivation of this circuit is given in Appendix A.

2.3.2 Two-phase-to-ground faults

Two-phase-to-ground faults are of the following three types.

1. Phase B and phase C-to-ground faults.
2. Phase C and phase A-to-ground faults.
3. Phase A and phase B-to-ground faults.

The single line diagram of these faults is shown in Figure 2.3 (a). When fault resistances R_{f1} and R_{f2} are equal, a two-phase-to-ground fault can be represented by the sequence network diagram shown in Figure 2.3 (b).

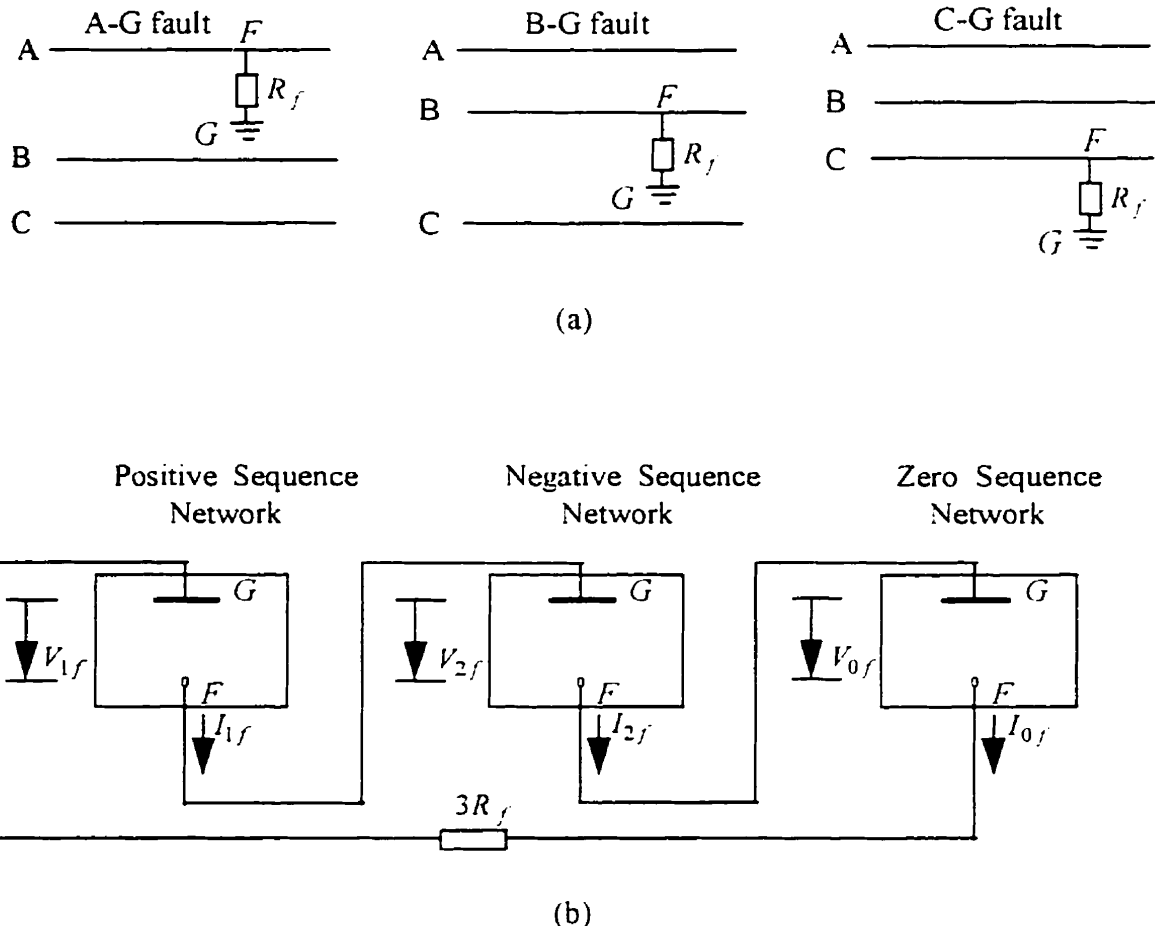


Figure 2.2. Single-phase-to-ground faults experienced on three-phase lines. (a) Types of faults. (b) Sequence network diagram with faulted phase as reference.

2.3.3 Phase-to-phase faults

The three types of phase-to-phase faults that can be experienced on lines are as follows.

1. Phase B-to-phase C faults.
2. Phase C-to-phase A faults.
3. Phase A-to-phase B faults.

These faults are shown in Figure 2.4 (a) with a fault resistance R_f . Using symmetrical component theory, a phase-to-phase fault can be represented by the sequence network diagram shown in Figure 2.4 (b).

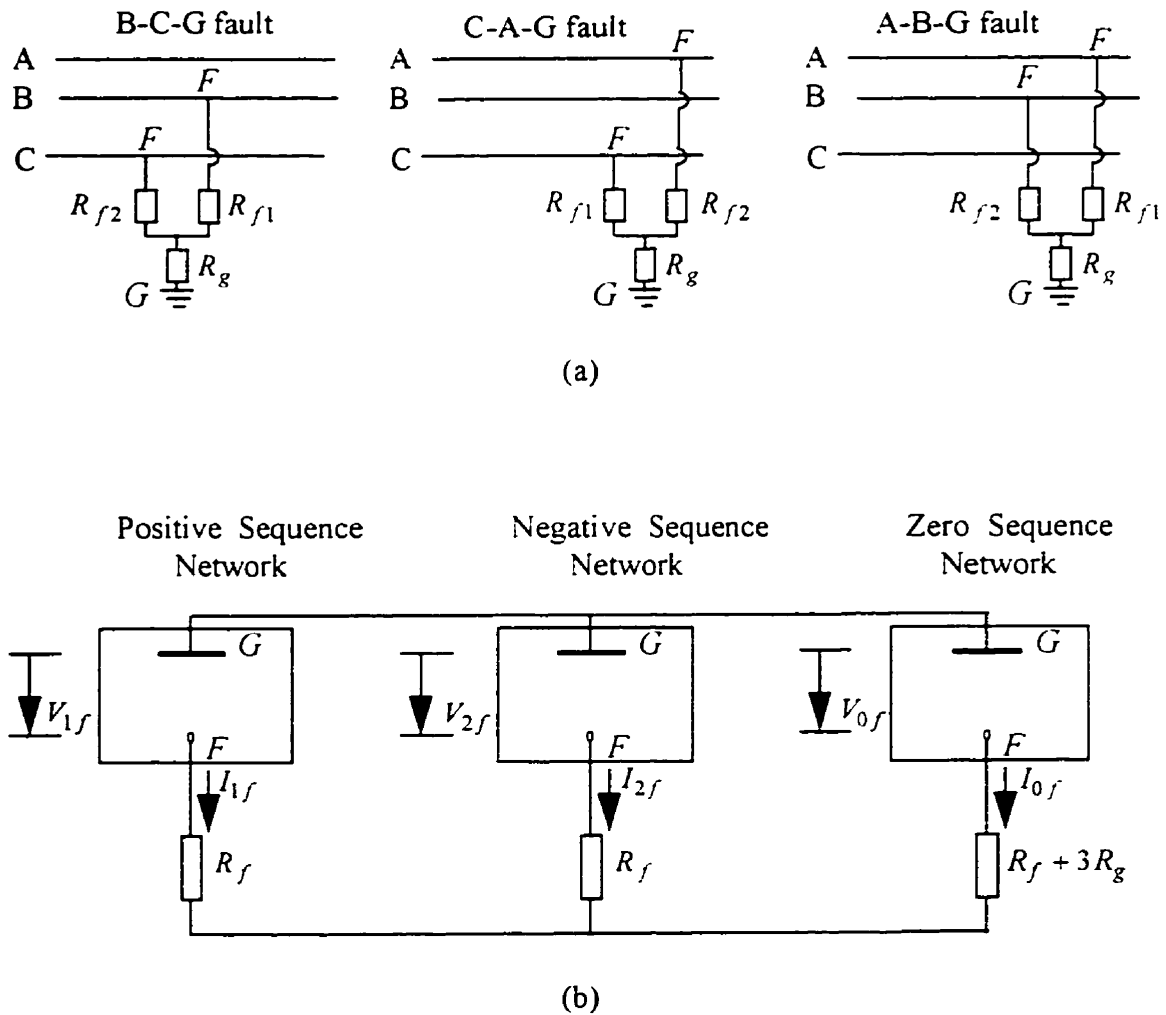


Figure 2.3. Two-phase-to-ground faults. (a) Types of faults. (b) Sequence network diagram with unfaulted phase as reference.

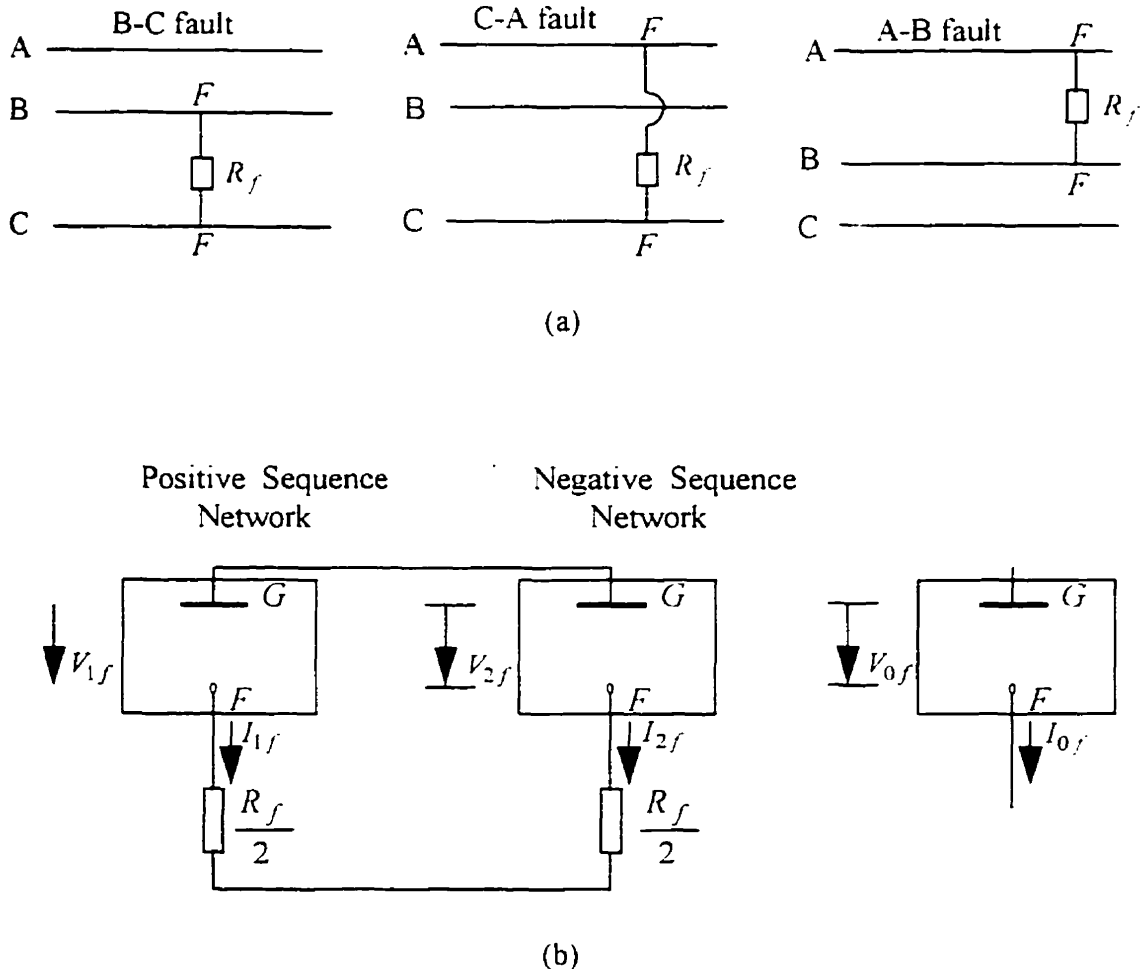


Figure 2.4. Phase-to-phase faults. (a) Types of faults. (b) Sequence network diagram with unfaulted phase as reference.

2.3.4 Balanced three-phase faults

Three-phase faults that have equal fault resistances in the three phases are called balanced three-phase faults. These faults can be further divided into two categories; those involving ground and those not involving ground as shown in Figure 2.5 (a). The ground connection is of no major significance in an otherwise balanced three phase system. A balanced three-phase fault can be represented by the sequence network diagram shown in Figure 2.5 (b) or Figure 2.5 (c) depending on the ground connection at the location of the fault.

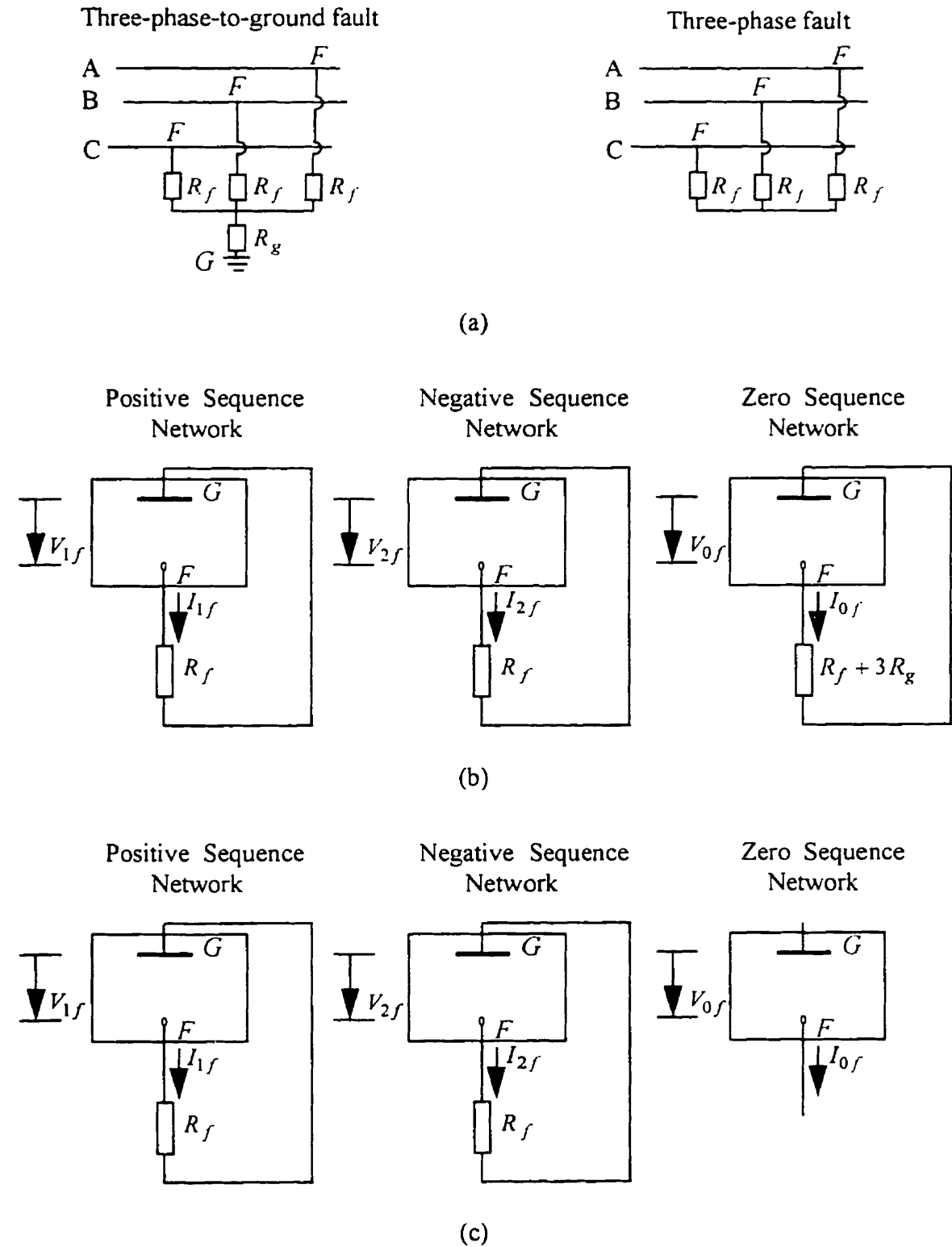


Figure 2.5. Balanced three-phase fault. (a) Types of faults. (b) Sequence network diagram for fault with ground. (c) Sequence network diagram for fault without ground.

2.4 Fault Resistance

A fault resistance consists of two major components, arc resistance and ground resistance [27, 28]. It is either constant for the duration of a fault or it varies with time due to the elongation of the arc and its ultimate extinction. In phase-to-phase faults, fault resistance is entirely due to the arc. However, for faults involving the ground, fault resistances are composed of both the arc and ground resistances. The ground resistance includes resistances of the contact between the conductor and the ground, and the resistance of the ground path for the flow of current in the ground in situations where the snapped conductor touches the ground. In situations where a broken conductor touches the tower, the ground resistance includes resistance of the contact between the conductor and the tower, and the resistance of the ground path for the flow of current in the ground and tower footings.

2.4.1 Arc resistance

Arc resistance depends on the length of the arc and the current in it as is suggested by the following equation [28].

$$R_{arc} = \frac{8750 L_{arc}}{I_f^{1.4}} \quad (2.1)$$

where: R_{arc} is the arc resistance in ohm.

L_{arc} is the length of the arc in feet in still air.

I_f is the r.m.s. fault current in amperes.

Arc length is initially equal to the spacing from the conductor to the tower, or between two conductors, but increases due to elongation of the arc caused by cross wind, convection and electromagnetic propagation. It has been suggested that arc resistance can be expressed in terms of the conductor spacing, wind velocity and time as follows [28].

$$R_{arc} = \frac{8750 (d + 3UT_{arc})}{I_f^{1.4}} \quad (2.2)$$

where: d is the conductor spacing in feet.
 U is the wind velocity in miles/hour.
 T_{arc} is the duration of arc in seconds.

This equation should be applied with care because there are limits to which an arc can stretch without either restriking or extinguishing.

2.4.2 Ground resistance

The ground resistance is the sum of the tower footing resistance at the fault location and the resistance of the current path through the ground from the fault to the source if overhead ground wires are insulated or are not used. Electric utilities measure and record data on tower footing resistances and ground resistivities. If overhead ground wires are used, the resistances of the ground path, the tower footings and ground wires form lattice networks.

The dominant resistance in the fault circuit is the resistance of the contact between the conductor and the path of the current through the ground if a conductor breaks and falls to the ground. The ground-contact resistance depends on the type of soil and moisture in it. The contact resistance also depends on the conductor voltage; it takes a finite voltage to cause the surface insulation to breakdown. Generally, the ground-contact resistances are larger than the tower footing resistances.

Fault resistances are small for inter-phase short circuits and do not exceed a few ohms. However, fault resistances are much larger for ground faults because tower footing resistances can be up to 10 ohms or even higher. Fault resistances are exceptionally large for contact with trees or for broken conductors lying on dry pavement. The fault resistance ranges from a few ohms to hundreds of ohms.

2.5 Impact of Fault Resistance on Fault Location Estimates

A single phase line that is connected to a source at one end only and supplies no load is shown in Figure 2.6 (a). The line charging current during faults is negligible and, therefore, current I_{mf} at the fault locator, is equal to the current I_f in the fault. The impedance seen from the fault locator terminal can be mathematically expressed as

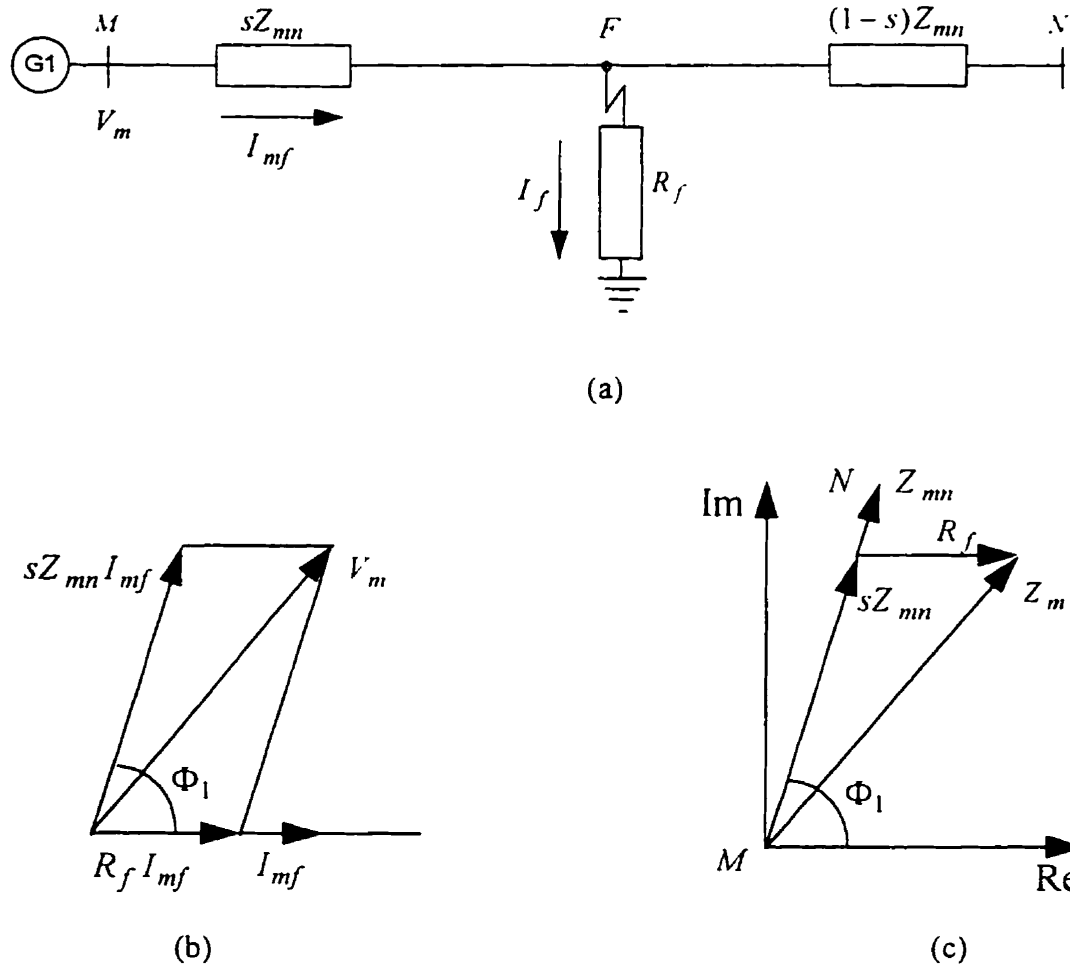


Figure 2.6. Change of the apparent impedance seen from the fault locator terminal due to the fault resistance. (a) The single line diagram of a line connected at one terminal only and disconnected from the load at the remote terminal. (b) The phasor diagram showing the line current and voltage at bus M . (c) The equivalent $R - X$ diagram.

$$Z_m = \frac{V_m}{I_{mf}} = sZ_{mn} + R_f, \quad (2.3)$$

where:
 Z_m is the impedance measured at bus M ,
 V_m is the voltage during the fault at bus M ,
 I_{mf} is the current flowing in the line at bus M and in the fault at F ,
 s is the fault distance from bus M , expressed as a fraction of the line length,
 Z_{mn} is the line impedance from bus M to N and
 R_f is the fault resistance including the resistance of the ground path.

The effect of fault resistance is shown in the phasor and $R-X$ diagrams of Figure 2.6. This figure shows that the impedance seen by the fault locator (at bus M) is greater in magnitude than the impedance of the line from bus M to fault. However, the reactive component of the apparent impedance remains equal to the reactive component of the line impedance from bus M to the fault.

It is clear from Equation 2.3 that the impedance, Z_m , is made up of the line impedance from bus M to the fault and the fault resistance. The reactive component of Z_m is independent of the fault resistance and, therefore, s can be calculated as follows.

$$s = \frac{\text{Im}(Z_m)}{\text{Im}(Z_{mn})} \quad (2.4)$$

This procedure, therefore, provides accurate estimates of fault locations if the fault current is fed from one line terminal only. In this case, the apparent fault impedance appears to be almost resistive to a fault locator that monitors the voltage and current at the source end of the line.

Now, consider the single-phase system shown in Figure 2.7 (a) which is connected to energy sources at both terminals. The impedances calculated from the fundamental frequency voltages and currents at the two line terminals can be expressed as

$$Z_m = \frac{V_m}{I_{mf}} = sZ_{mn} + R_f \left(\frac{I_f}{I_{mf}} \right) \text{ and} \quad (2.5)$$

$$Z_n = \frac{V_n}{I_{nf}} = sZ_{mn} + R_f \left(\frac{I_f}{I_{nf}} \right), \quad (2.6)$$

where: V_m and V_n are the voltages at buses M and N during the fault,
 I_{mf} and I_{nf} are the currents flowing in the line at buses M and N and,
 I_f is the fault current flowing into the fault at F .

The currents I_{mf} and I_{nf} are usually phase shifted as shown in Figure 2.9 (b). Equations 2.5 and 2.6 can be represented on the $R-X$ plane as in Figure 2.8 (c). Current in the fault resistance is phase displaced from the currents at the line terminals. Because of these phase displacements, fault location estimate obtained from the fundamental frequency voltage and current measured at the line terminal, M , is smaller

than the actual distance of the fault. The estimates obtained at bus N is larger than the actual distance of the fault.

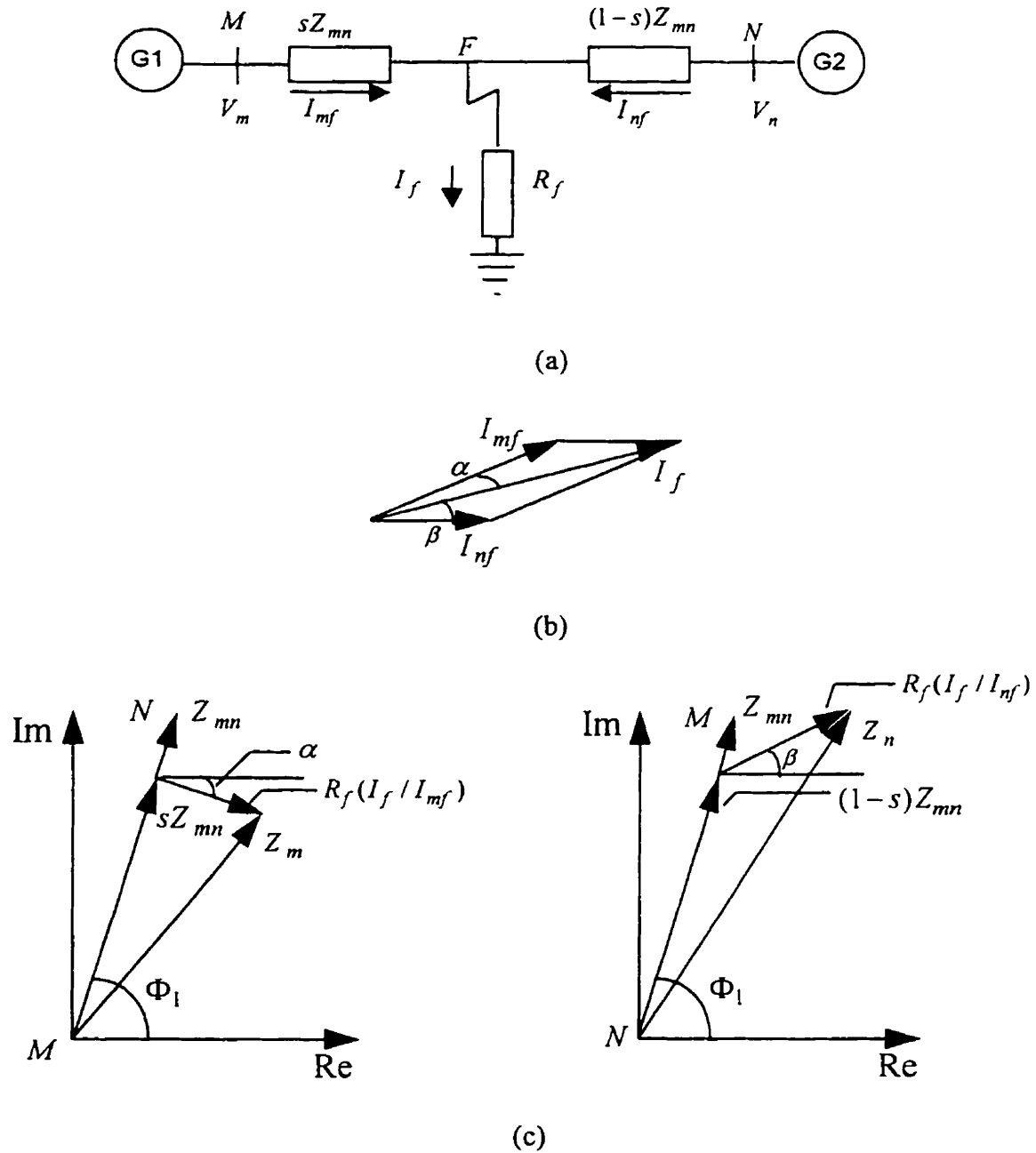


Figure 2.7. Change of the apparent impedance seen from the fault locator terminal due to the fault resistance. (a) The single line diagram of a line connected to sources at both ends. (b) The phasor diagram. (c) The $R - X$ diagrams.

Therefore, if both terminals of a line are connected to energy sources, the fault resistance appears to the fault locator as an impedance that has both resistive and reactive components. Methods that estimate fault locations from impedance measurements are, therefore, adversely affected by the fault resistance if line fault is fed from both terminals of the line. During a fault, a radial distribution line with motor loads at the end of the line is equivalent to a line connected to energy sources at both terminals. This is due to the fact that motors behave as generators for sometime after the inception of the fault [23, 24, 29]. Similarly, if there are motor load taps along a radial distribution line, it is equivalent to a line connected to multiple energy sources.

2.6 Effect of Load Taps on Fault Location Estimates

Loads in distribution lines can introduce significant errors in estimating fault locations. This, however, depends on the fault resistance and the size and characteristics of the loads. A single phase line that is connected to a source at one end, feeds two loads and is experiencing a fault, at F , is shown in Figure 2.8.

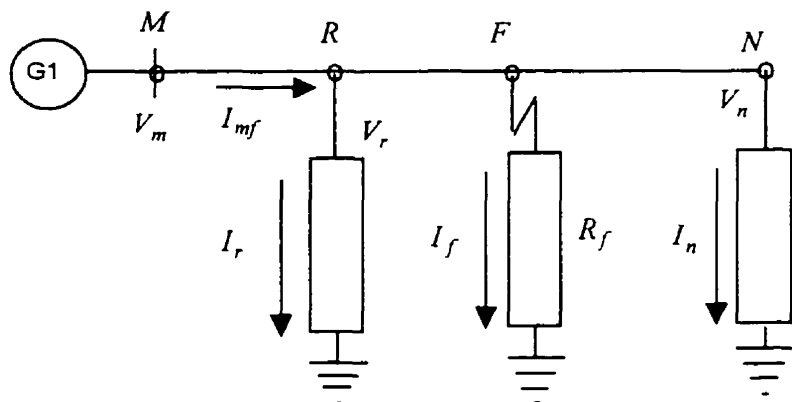


Figure 2.8. A distribution line with tapped loads, experiencing a fault.

The fault current I_f can be mathematically expressed as follows.

$$I_f = I_{mf} - I_r - I_n \quad (2.7)$$

where: I_f is the fault current flowing into the fault at F .
 I_{mf} is the line current during the fault at bus M .

I_r and I_n are the load currents during the fault at nodes R and N respectively.

Voltages, V_r and V_n , at nodes R and N respectively, largely depend on the fault resistance, line impedance and loads. The load currents, I_r and I_n , depend on the voltages, V_r and V_n , and also on the characteristics of the loads. For a large value of the fault resistance, V_r and V_n could be large making the load currents comparable to the fault current. This introduces substantial errors in measuring the fault distance if appropriate precautions are not taken.

2.7 Summary

A typical distribution system and protection has been described in this chapter. It has been shown that shunt faults, such as single-phase-to-ground, two-phase-to-ground, phase-to-phase and balanced three-phase faults, can be represented by symmetrical component network connected appropriately for each fault.

Fault resistance and its major components, arc and ground resistances, have been identified and discussed. The impact of fault resistance and load taps on the fault location estimates has been examined. It has been shown that the methods that estimate fault locations from the impedance measurements are affected by the presence of a fault resistance if the line is connected to energy sources at both terminals. The fault resistance appears to be an impedance, that has both resistive and reactive components. If there are tapped loads, the currents measured at the line terminal do not represent the currents at the fault. This usually introduces substantial errors in the estimates of the location of the fault.

3. FAULT LOCATION METHODS

3.1 Introduction

The shunt faults generally experienced on lines have been reviewed in Chapter 2. Substantial research has been done in the past to estimate the location of shunt faults on transmission lines. The methods proposed for lines fed from both terminals can be classified into two categories. The first category includes the methods that use measurement from one terminal of the transmission line. The methods in the second category use measurements taken from both terminals. Methods have also been proposed for estimating fault locations on radial transmission lines and rural distribution feeders.

Since the objective of the research conducted for this project is to estimate the locations of faults on radial distribution systems, the following methods, which are based on measurement at one terminal of the line, are reviewed in this chapter.

1. Reactive component method.
2. Takagi algorithm.
3. Richards and Tan algorithm.
4. Srinivasan and St-Jacques algorithm.
5. Grgis algorithm.

3.2 Reactive Component Method

The reactive component method [28] estimates the apparent reactance of the line from its terminal to the fault and converts the calculated reactance to distance in kilometers/miles. This basis of this method has been discussed briefly in Section 2.5.

Sant and Paithankar [8] estimated locations of transmission line faults by calculating the ratio of the reactive component of the apparent impedance to the reactance of the line. They measured the steady state fundamental frequency voltages and currents at one terminal of the line and calculated the apparent impedance from them. The authors assumed that the line is connected to a source at one terminal only and the method is, therefore, valid for those situations only.

Sant and Paithankar [30], also studied the effect of line capacitances on the fault location estimates. They assumed that the line is lossless and fault resistance is negligible. Both assumptions are not valid and, therefore, the fault location estimates obtained by using this approach are likely to have substantial errors.

3.3 Takagi Algorithm

Takagi et al. suggested an algorithm that uses the fundamental frequency voltages and currents measured at a line terminal before and during the fault [9]. This approach uses the Thevenin's equivalent of the faulted system and obtains an estimate of the distance to a fault. The Takagi algorithm is described by considering the two machine system shown in Figure 3.1 (a).

The single line diagrams of the system during and before the fault at F are shown in Figures 3.1 (b) and 3.1 (c). The Thevenin's equivalent circuit of the faulted system is shown in Figure 3.1 (d). The components of the contributed fault currents by the two systems can be calculated by using the following procedure.

1. Calculate the pre-fault currents from the system shown in Figure 3.1 (c).
2. Calculate the fault-currents and their distribution from the Thevenin's equivalent circuit shown in Figure 3.1 (d). The currents in the line at buses M and N of this circuit are \tilde{I}_{mf} and \tilde{I}_{nf} respectively.

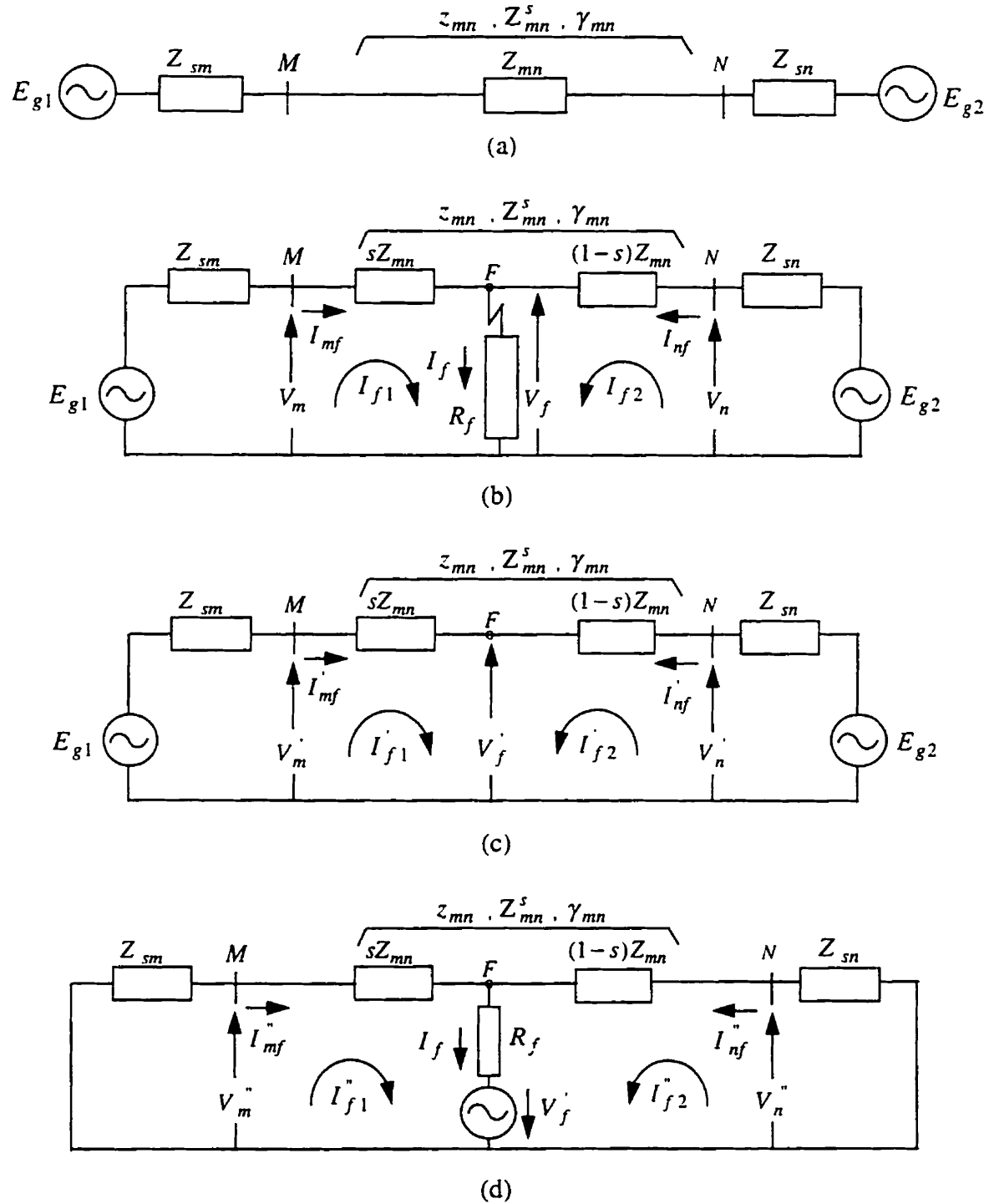


Figure 3.1. (a) Single line diagram of a two machine system. (b) The system is experiencing a fault at F . (c) Equivalent circuit for calculating the pre-fault currents and their distribution. (d) Equivalent circuit for calculating the fault currents and their distribution.

The voltage at the fault point,

$$V_f = (I_{f1} + I_{f2})R_f \quad (3.1)$$

V_f and I_{f1} expressed in terms of measurements taken at bus M are

$$V_f = V_m \cosh(\gamma_{mn} l_{mf}) - Z_{mn}^s I_{mf} \sinh(\gamma_{mn} l_{mf}) \quad (3.2)$$

$$I_{f1}'' = \frac{V_m''}{Z_{mn}^s} \sinh(\gamma_{mn} l_{mf}) - I_{mf}'' \cosh(\gamma_{mn} l_{mf}) \quad (3.3)$$

- where:
- l_{mf} is the distance from bus M to the fault,
 - V_m is the voltage at bus M during the fault,
 - I_{mf} is the fault current flowing in the line at bus M ,
 - V_f is the voltage at the fault F ,
 - I_f is the fault current,
 - I_{f1} is the fault current contribution from bus M ,
 - I_{f2} is the fault current contribution from bus N ,
 - V_m'' is the difference between the pre-fault voltage and the voltage during the fault at bus M ,
 - I_{mf}'' is the difference between the pre-fault line current and the line current during the fault at bus M ,
 - I_{f1}'' is the difference between the pre-fault and fault current contribution from bus M ,
 - I_{f2}'' is the difference between the pre-fault and fault current contribution from bus N ,
 - R_f is the fault resistance,
 - z_{mn} is the line impedance per unit length,
 - Z_{mn}^s is the line surge impedance and
 - γ_{mn} is the propagation constant per unit length of the line.

The fault current I_f is expressed as a multiple of I_{f1}'' as follows.

$$I_f = I_{f1}'' \eta \quad (3.4)$$

$$\eta = \frac{I_f}{I_{f1}''} \quad \text{and} \quad \theta = \operatorname{Arg}(\eta) \quad (3.5)$$

Equations 3.1 to 3.5 are rearranged and the following equation is obtained.

$$V_m - Z_{mn}^s I_{mf} \tanh(\gamma_{mn} l_{mf}) = \left(\frac{V_m''}{Z_{mn}^s} \tanh(\gamma_{mn} l_{mf}) - I_{mf}'' \right) \eta e^{j\theta} R_f \quad (3.6)$$

$|\eta|$ and R_f are eliminated from this equation by multiplying both sides of this equation with $\left(\frac{V_m''}{Z_{mn}^s} \tanh(\gamma_{mn} l_{mf}) - I_{mf}'' \right)^* e^{-j\theta}$ and equating their imaginary components. This provides the equation

$$\text{Im} \left(V_m - Z_{mn}^s I_{mf} \tanh(\gamma_{mn} l_{mf}) \left(\frac{V_m''}{Z_{mn}^s} \tanh(\gamma_{mn} l_{mf}) - I_{mf}'' \right)^* e^{-j\theta} \right) = 0. \quad (3.7)$$

Assuming that $\theta = 0$ and $\tanh(\gamma_{mn} l_{mf}) \equiv \gamma_{mn} l_{mf}$, $\left(\frac{V_m''}{Z_{mn}^s} \tanh(\gamma_{mn} l_{mf}) \right)^*$ can be neglected because it is small compared to $(I_{mf}'')^*$. Making these substitutions in Equation 3.7, the following equation is obtained.

$$l_{mf} = \left(\frac{\text{Im}(V_m (I_{mf}'')^*)}{\text{Im}(\gamma_{mn} Z_{mn}^s I_{mf} (I_{mf}'')^*)} \right) \quad (3.8)$$

Also, $\gamma_{mn} Z_{mn}^s = z_{mn}$ and, therefore,

$$l_{mf} = \left(\frac{\text{Im}(V_m (I_{mf}'')^*)}{\text{Im}(z_{mn} I_{mf} (I_{mf}'')^*)} \right) \quad (3.9)$$

The algorithm proposed by Takagi et al. has several weaknesses [31]. Some of these are as follows.

1. The accuracy of the algorithm depends on the value of θ used in estimating the fault location. The value of θ depends on source impedances that are not readily known because the system configuration changes from time to time. A good estimate of the system state at the time of a fault is, therefore, needed.

2. The algorithm uses differences between the pre-fault currents and the currents during the fault. The accuracy, is, therefore, affected by the fault current decrement due to changing source impedances and by the accuracy of current measuring devices.
3. The algorithm assumes that the fault locating process can be based on single phase analysis. Power systems are three-phase systems in which phases are mutually coupled. A single-phase fault changes currents in all phases and load currents in the unfaulted phases affect the current flows in the faulted phase.
4. A part of the line charging has been neglected. In long EHV lines, line charging currents can be appreciable.

However, the estimates provided by the Takagi's algorithm are substantially more accurate than the estimates provided by the reactive component method if the angle θ is small. The improvement is due to the Takagi's method taking into account the pre-fault load flows.

Schweitzer [31] suggested a method for improving the performance of the algorithm proposed by Takagi et al. The method estimates the angle θ instead of assuming it to be zero.

The angle θ is the argument of the fault current distribution factor, η . The factor, η , can be determined from the single-phase circuit, shown in Figure 3.1(d), using the following equation.

$$\eta = \frac{I_f}{I_{f1}} = 1 + \frac{\left(\frac{Z_{sm}}{Z_{mn}} + s \right)}{\left(\frac{Z_{sn}}{Z_{mn}} + (1 - s) \right)} \quad (3.10)$$

where: Z_{sm} is the source impedance at bus M .
 Z_{sn} is the source impedance at bus N .
 Z_{mn} is the total line impedance.

s is the distance to the fault, from bus M , expressed as a fraction of entire line length and is given as follows.

$$s = \frac{Z_{mn} l_{mf}}{Z_{sn}} \quad (3.11)$$

Equation 3.10 shows that θ , the argument of η , is zero if the arguments of all impedances are equal. Schweitzer [31] suggested the following two alternatives.

1. Use a constant value for the angle θ . This approach is particularly effective when phase angles of Z_{sm} and Z_{sn} are equal.
2. Use an iterative approach involving Equations 3.8 (modified by including θ), 3.10 and 3.11 to obtain a convergent solution of θ and l_{mf} .

This procedure requires that the source impedances be known; they are not always known.

Wiszniewski suggested an algorithm that uses the fundamental frequency voltages and currents measured at one terminal of a line [32]. The method is similar to the algorithm suggested by Takagi et al. [9]. Wiszniewski assumed that, for most cases, phase angle of the fault current distribution factor would be zero. He also suggested that the phase angle can either be assumed to correspond to a fault at the far end of the line or can be assigned an expected value, considering that fault can occur along the line with equal probability. The algorithm also assumes that the fault locating process can be based on a single phase analysis. This is not valid for three-phase systems that have mutual coupling between phases. Moreover, this method neglects the line charging currents. The fault location estimates obtained by this method, therefore, have substantial errors.

Erikson et al. [33] also suggested a method similar to that of Takagi et al. [9] and Wiszniewski [32]. This method also suffers from the shortcomings of the techniques of References [9] and [32] and the fault locations obtained by this method are not sufficiently accurate.

3.4 Richards and Tan Algorithm

Richards and Tan [34] considered the fault location problem as a parameter estimation of a dynamic system and compared the response of the physical system with that of a lumped parameter model. The Thevenin equivalent model used in this work includes system resistances and inductances and an unknown fault resistance as shown in Figure 3.2.

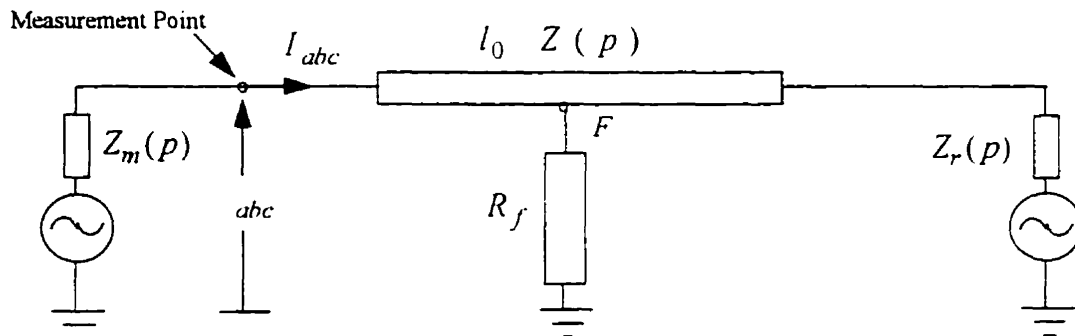


Figure 3.2. System model used by Richards and Tan for determining fault locations using an optimization approach.

The parameters of the model are varied until the observed voltages and currents match adequately with those obtained from the response of the model. An optimization technique is used to determine the fault resistance and fault location. The method needs an accurate network model including transmission lines and sources. The technique is iterative in form, is computationally expensive and can not be easily applied at every line terminal.

3.5 Srinivasan and St-Jacques Algorithm

Srinivasan and St-Jacques [11] suggested a fault location algorithm for radial transmission lines. It uses the pre-fault fundamental frequency voltages and currents and the fundamental frequency voltages and currents measured at the line terminal during the fault. Figure 3.3 shows the model of the transmission system used in their approach.

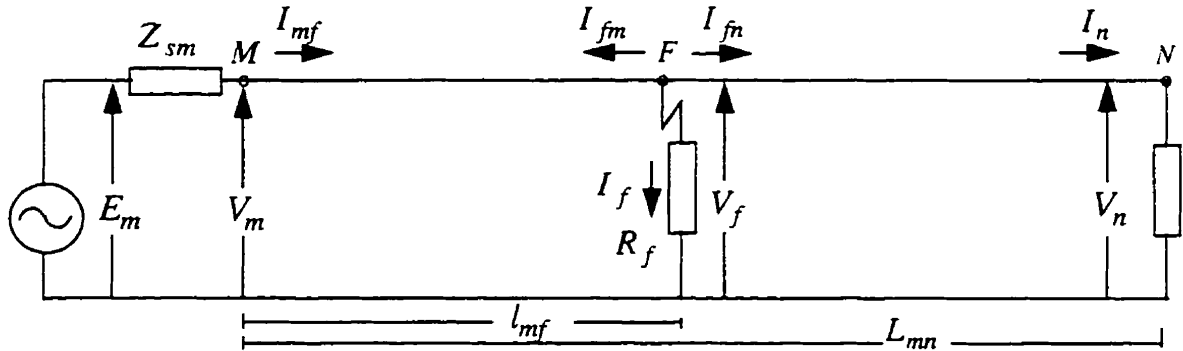


Figure 3.3. Faulted transmission line with load.

The three common types of faults are characterized by Equations 3.12, 3.14 and 3.16. The distances of the faults are estimated by equating imaginary part of the fault resistance, given by Equations 3.12, 3.14 and 3.16, to zero.

(i) Single-phase-to-ground fault

$$\left(\frac{V_{1f} + V_{2f} + V_{0f}}{I_{1f} + I_{2f} + I_{0f}} \right) = R_f \quad (3.12)$$

$$\text{Im} \left(\frac{V_{1f} + V_{2f} + V_{0f}}{I_{1f} + I_{2f} + I_{0f}} \right) = 0 \quad (3.13)$$

(ii) Phase-to-phase fault

$$\left(\frac{V_{1f} - V_{2f}}{I_{1f} - I_{2f}} \right) = R_f \quad (3.14)$$

$$\text{Im} \left(\frac{V_{1f} - V_{2f}}{I_{1f} - I_{2f}} \right) = 0 \quad (3.15)$$

(iii) Balanced three-phase fault

$$\left(\frac{V_{1f}}{I_{1f}} \right) = R_f \quad (3.16)$$

$$\text{Im}\left(\frac{V_{1f}}{I_{1f}}\right) = 0 \quad (3.17)$$

where: V_{1f} , V_{2f} and V_{0f} are the positive, negative and zero sequence voltages at the fault location.
 I_{1f} , I_{2f} and I_{0f} are the positive, negative and zero sequence fault currents.
 R_f is the fault resistance.

The authors obtained the following expressions for the sequence voltages and currents at the fault from the voltages and currents measured at terminal M (during and before fault).

$$V_f = \cosh(\gamma_{mn} l_{mf}) V_m - Z_{mn}^s \sinh(\gamma_{mn} l_{mf}) I_{mf} \quad (3.18)$$

$$\begin{bmatrix} V_n \\ I_f \end{bmatrix} = \begin{bmatrix} 1 & -Z_{mn}^s \sinh(\gamma_{mn}(L_{mn} - l_{mf})) \\ -Y_n & -\cosh(\gamma_{mn}(L_{mn} - l_{mf})) \end{bmatrix}^{-1} \begin{bmatrix} \cosh(\Gamma_{mn}) & -Z_{mn}^s \sinh(\Gamma_{mn}) \\ \sinh(\Gamma_{mn}) & -\cosh(\Gamma_{mn}) \end{bmatrix} \begin{bmatrix} V_m \\ I_{mf} \end{bmatrix} \quad (3.19)$$

where: l_{mf} is the distance from bus M to the fault, F .
 L_{mn} is the length of the line.
 V_m is the voltage at bus M .
 V_n is the voltage at node N .
 V_f is the voltage at the fault, F .
 I_{mf} is the current in the line at bus M .
 I_f is the fault current.
 R_f is the fault resistance.
 Z_{mn}^s is the surge impedance of the line.
 γ_{mn} is the propagation constant of the line.
 Y_n is the admittance of the load at node N and
 $\Gamma_{mn} = (\gamma_{mn})(L_{mn})$.

The authors used the following static response type load model.

$$Y_n = \frac{I_n}{V_n} = G_n \left| \frac{V_n}{V_{nom}} \right|^{n_p-2} + jB_n \left| \frac{V_n}{V_{nom}} \right|^{n_q-2} \quad (3.20)$$

where: V_{nom} is the nominal voltage.
 G_n and B_n are the conductance and susceptance at nominal voltage.
 n_p and n_q are the response constants for the active and reactive loads.

The load response parameters, n_p and n_q are available either from previous tests or are calculated from the load model studies conducted immediately before the inception of the fault.

For a single-phase-to-ground fault, V_f and I_f from Equations 3.18 and 3.19 are substituted in Equation 3.13 and an implicit equation in I_{mf} is obtained. Using an initial estimate for I_{mf} , this equation is solved iteratively with Equations 3.19 and 3.20 using the Newton-Raphson technique. Using a similar approach, the locations of other types of faults are determined.

The authors have mentioned that although it is possible to initially estimate the type of fault, it is equally convenient to estimate the distance, using all three possibilities and then reject the estimates that are unreasonable. The authors have also suggested an approximate closed form solution for the distance of the fault which is obtained by assuming that the transmission line is short and line charging currents can be neglected.

The authors also considered loads tapped from the line. The procedure is straightforward provided the location of the load and its model are known. The loads beyond the fault are consolidated with the load at the remote end of the line. The loads between the line terminal and the fault are handled by the following procedure. Consider a line whose single line diagram is shown in Figure 3.4.

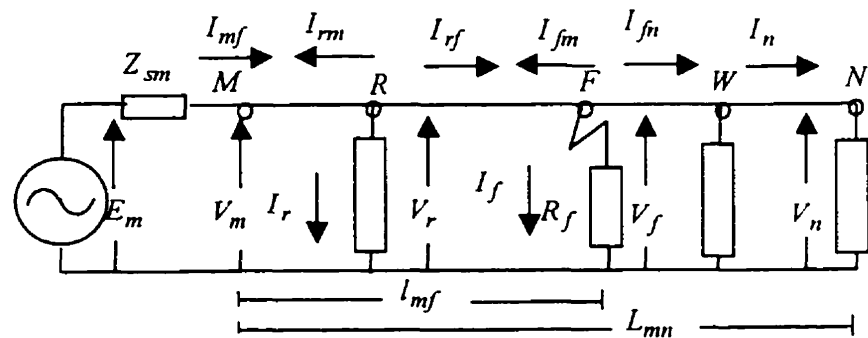


Figure 3.4. Faulted transmission line with two load taps.

Voltage and current at R can be expressed in terms of the voltage and current at M as follows.

$$\begin{bmatrix} V_r \\ I_{rm} \end{bmatrix} = \begin{bmatrix} \cosh(\gamma_{mn} l_{mr}) & -Z_{mn}^s \sinh(\gamma_{mn} l_{mr}) \\ \sinh(\gamma_{mn} l_{mr}) & Z_{mn}^s \end{bmatrix} \begin{bmatrix} V_m \\ I_{mf} \end{bmatrix} \quad (3.21)$$

$$I_{rf} = -I_{rm} - I_r \quad (3.22)$$

where: l_{mr} is the distance of the load at R from the terminal M .

The V_r and I_{rf} from Equations 3.21 and 3.22 are used in place of V_m and I_{mf} in Equations 3.18 and 3.19 respectively. Multiple load taps are treated by applying the procedure repeatedly.

The algorithm proposed by Srinivasan and St-Jacques [11] has the following weaknesses:

1. The procedure suggested for the initial estimate, considering the three types of faults, is computationally expensive.
2. The treatment of tapped loads seems to be incomplete. The suggestion of measuring currents at each intermediate tap is expensive and complex. No test results from such cases are provided.
3. The transmission line is considered to be homogeneous. This may not always be true.

However, the algorithm proposed by Srinivasan and St-Jacques [11] is an improvement over earlier methods for estimating the locations of faults on radial transmission lines.

3.6 Girgis Algorithm

Girgis et al. [13] suggested a fault location technique for rural distribution feeders. This technique estimates the fundamental frequency voltage and current phasors on the

detection of a disturbance. Changes in the magnitudes of the current phasors are used to classify the fault type and faulted phases.

The voltage and current phasors of the faulted phase are used to compute the apparent impedance. For example, when a single-phase-to-ground fault on phase A is detected, apparent impedance is calculated as follows.

$$Z_{app} = \frac{V_{select}}{I_{select}} = \frac{V_a}{I_a + I_0 \left(\frac{Z_0 - Z_1}{Z_1} \right)} \quad (3.23)$$

where: Z_{app} is the apparent impedance,
 V_a is the phasor of the Phase A-to-ground voltage,
 I_a is the phasor of the line current in phase A,
 I_0 is the phasor of the zero sequence currents and
 Z_0 and Z_1 are zero and positive sequence impedance of the line.

A compensating current fed into the fault is considered. The compensating current, I_{comp} , is considered to be proportional to the zero sequence current for single-phase-to-ground faults. The equation for apparent impedance can be expressed in terms of the distance, l , to the fault as

$$Z_{app} = l(Z_1) + \frac{(I_{comp})R_f}{I_a + kI_0} \quad (3.24)$$

where: R_f is the fault resistance,
 $I_{comp} = 3I_0$ and
 $k = \left(\frac{Z_0 - Z_1}{Z_1} \right)$.

Equation 3.24 can be expressed as

$$Z_{app} = l(R_1 + jX_1) + \frac{(I_d + jI_q)R_f}{I_{s1} + jI_{s2}} \quad (3.25)$$

where: R_1 is the positive sequence resistance of the line,
 X_1 is the positive sequence reactance of the line,

$$I_{comp} = I_d + jI_q \text{ and}$$

$$I_{select} = I_a + kI_0 = I_{s1} + jI_{s2}.$$

The value of Z_{app} is computed using Equation 3.23. Equation 3.25 can be re-written in terms of real and imaginary components, R_{app} and X_{app} , of Z_{app} as follows.

$$\begin{bmatrix} R_{app} \\ X_{app} \end{bmatrix} = \begin{bmatrix} R_1 & N \\ X_1 & M \end{bmatrix} \begin{bmatrix} I \\ R_f \end{bmatrix} \quad (3.26)$$

where: $N = \frac{(I_d I_{s1} + I_q I_{s2})}{I_{s1}^2 + I_{s2}^2}$ and $M = \frac{(-I_d I_{s2} + I_q I_{s1})}{I_{s1}^2 + I_{s2}^2}$

Eliminating the unknown R_f , the distance to the fault I , is expressed as follows.

$$I = \frac{(R_{app}M - X_{app}N)}{(R_1M - X_1N)} \quad (3.27)$$

Using a similar approach, location of other types of faults are determined.

The algorithm proposed by Girgis et al. has limitations. Some of these are:

1. The accuracy of the algorithm is affected by the dynamic nature of the loads not considered by this technique.
2. Distribution systems usually have multiphase and multiple laterals which are not considered.
3. The technique was tested for a simple system with one single-phase lateral. For a fault on the lateral, the technique provided two estimates. Reduction of multiple estimates to a single estimate has not been discussed.
4. The technique will provide inaccurate estimates for lines that have cables.

However, the algorithm proposed by Girgis et al. suggested the possibility of updating the voltage drop and current changes iteratively in each line section by using a load-flow program. Tapped loads which introduce errors in fault location estimates for a distribution system, are identified as a potential problem in this technique. This single

issue makes the fault location problem in distribution system distinctly different from that of a transmission system.

3.7 Summary

The algorithms that estimate fault locations from the fundamental frequency voltages and currents measured at one terminal of a line have been briefly described in this chapter. The problems associated with the algorithms have also been discussed. The estimates provided by the algorithms depend on factors such as source impedances, fault resistance, non-homogeneous system and tapped loads.

A distribution system is generally composed of sections which use conductors of different sizes and different configurations including sections of cables. Distribution systems also usually have several single and/or multiphase laterals. These issues and the inaccuracies introduced by tapped loads have not been adequately handled while applying these techniques to practical applications.

4. THE PROPOSED TECHNIQUE

4.1 Introduction

The fault location methods proposed in the past have been briefly reviewed in Chapter 3. They estimate the locations of faults on transmission and/or distribution lines using the fundamental frequency voltages and currents at a line terminal. None of the methods take into account the non-homogeneity of circuits encountered in a distribution system. The accuracy of these methods, if applied on a radial distribution system, will depend on the tapped loads and also on the fault resistance.

This chapter proposes a technique that estimates the location of shunt faults on radial distribution systems which usually include many laterals [35]. Like the previously proposed techniques, the method uses the fundamental frequency voltages and currents measured at the line terminal. The apparent location of a fault from the line terminal is first estimated by computing an impedance from the fundamental frequency voltage and current phasors; the reactive component of the impedance is then used to estimate the location of the fault. Intermediate load taps, laterals and non-homogeneity of the line are taken into account.

4.2 Overview of the Technique

The proposed technique is described in this chapter by considering a fault on a distribution system. The selected system consists of an equivalent source, G , the line between nodes M and N and two laterals as shown in Figure 4.1. Loads are tapped at several nodes and conductors of different types are used on this circuit.

The block diagrams shown in Figure 4.2 give an overview of the proposed technique. A detailed description of the technique is given subsequently in Sections 4.3 to 4.9. The technique consists of seven major steps:

1. Data acquisition

When a fault is detected, the fundamental frequency components of the pre-fault voltage and current phasors at node M are saved. The fundamental frequency components of voltage and current phasors at node M during the fault are estimated and the fault type is determined after a pre-set time has elapsed. These actions are taken on-line and are depicted in the Figure 4.2 (a). The pre-fault and fault data, along with line and load parameters, are used in an off-line mode to estimate the location of the fault. Necessary line and load parameters are obtained from a database.

2. Estimating the faulted section

The sequence voltages and currents at node M , before and during the fault, are calculated from the estimated phasors. A preliminary estimate of the location of the fault is made, say between nodes x and $x + l (= y)$. Line parameters, the type of fault and the phasors of the sequence voltages and currents are used to obtain this estimate. An impedance, measured at the terminal, could point to multiple locations in the system, if it has laterals. Steps 3 to 6 are applied using each of the apparent locations.

3. Modified radial system

All laterals between node M and the apparent location of the fault are ignored and the loads on a lateral are considered to be present at the node to which the lateral is connected. For example, load at nodes K and L are lumped with the load at node $x - 1$.

4. Modeling of loads

All loads up to node x are considered independently and the loads beyond the fault, node F , are assumed to be consolidated with the load at the remote node, N . Non-linear models of loads are used to take into account their dependency on voltage. The constants of load models are computed from the pre-fault load voltages and currents.

5. Estimating sequence voltages and currents at the fault and at the remote node

Using the voltage-dependent load model, determined in Step 4, sequence voltages and currents, at node x during the fault, are computed taking into account the load currents. The sequence voltages at the remote end are then calculated as a function of the distance of the fault from node x . The sequence voltages and currents at the fault node, F , are also obtained as functions of distance of the fault from node x and the impedance of the consolidated load at the remote node.

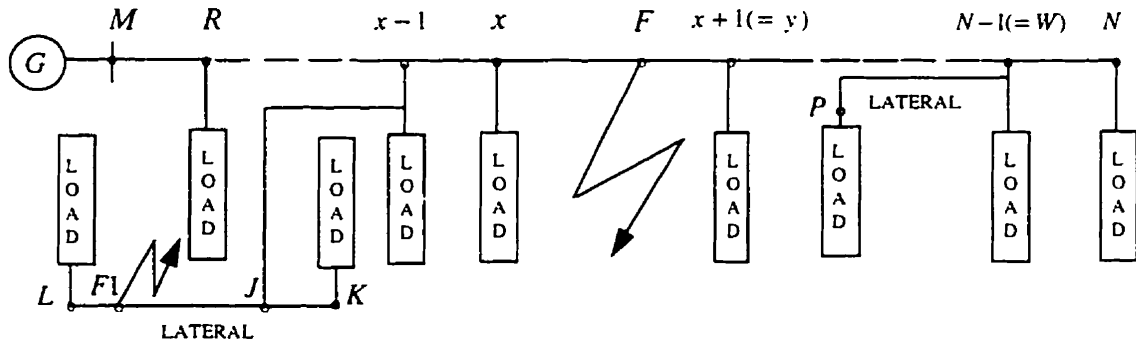


Figure 4.1. The single line diagram of a distribution system experiencing a fault.

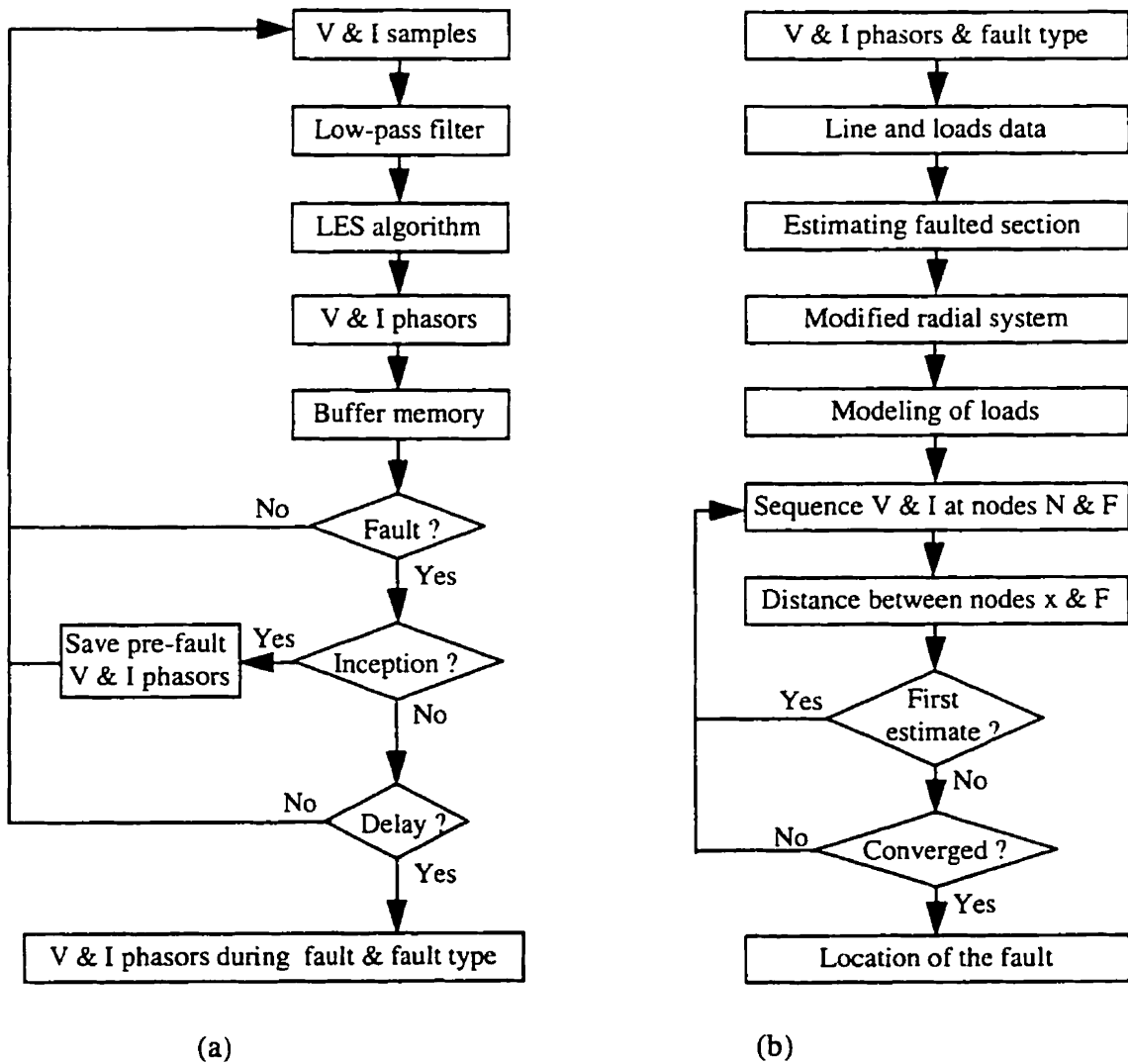


Figure 4.2. Block diagram for (a) acquiring data and (b) estimating the location of the fault.

6. Estimating the distance of fault from node x

The relationships between the sequence voltages and currents at the fault are used to estimate the distance of the fault from node x . The first estimate of the distance is obtained using the pre-fault sequence admittance of the consolidated load at node N . Subsequently, the value of the admittance is updated using the new values of the sequence voltages at node N and voltage dependent load model determined in Step 4. The procedure is repeated until a converged solution is obtained.

An attempt is made to obtain two additional estimates, for the fault location by considering that the fault is either located between the nodes $x - 1$ and x or between the nodes $x + 1$ and $x + 2$. The most plausible solution is selected and the location of the fault from the measurement node M is estimated.

7. Converting multiple estimates to a single estimate

The use steps 2 to 6 provides a single estimate if there are no laterals and multiple estimates if there are laterals. The estimates are arranged in the order of their likelihood. The technique also incorporates additional information, obtained from fault indicators strategically placed on the system, to convert multiple estimates to a single estimate.

4.3 Detection of Faults and Collection of Pre-fault and Fault Data

The first step for estimating the location of a shunt fault on a distribution line is to determine the presence of the fault and identify its type. If a fault is detected, pre-fault and fault data are collected and later used to estimate the location of the fault. This section presents a procedure for the detection of faults and collection of pre-fault and fault data.

4.3.1 Estimating phasors

The following fundamental frequency voltage and current phasors are estimated at node M in real time.

V_{am}	Phase A-to-ground voltage at node M .
V_{bm}	Phase B-to-ground voltage at node M .
V_{cm}	Phase C-to-ground voltage at node M .
I_{amr}	Phase A line current at node M towards node R .
I_{bmr}	Phase B line current at node M towards node R , and
I_{cmr}	Phase C line current at node M towards node R .

The phasors are estimated from the voltage and current samples using the Least Error Squares (LES) algorithm [36] described in Appendix B.

4.3.2 Fault detection

The line current estimates during a fault contain the load components as well as the fault components. If one or more of the line currents I_{amr} , I_{bmr} and I_{cmr} are greater than a threshold I_t , it is assumed that a fault has occurred. It is also possible to estimate the phasor of the zero sequence current from the phasors of the line currents as follows.

$$I_{0mr} = (I_{amr} + I_{bmr} + I_{cmr})/3.0 \quad (4.1)$$

where, I_{0mr} is the zero sequence component of the line currents.

The magnitude of the zero sequence current increases beyond its normal value when a ground fault is experienced. If the magnitude of the estimated zero sequence current is more than a threshold I_{tg} , it is assumed that one or two phases are short circuited to ground.

4.3.3 Collection of pre-fault and fault data

When a fault is detected, pre-fault voltage and current phasors are saved from a buffer memory. These are the phasors that were calculated one cycle before the inception of the fault. This margin is important to avoid an overlap of the pre-fault and fault data. Fault data are collected three cycles after the detection of the fault. This is done to minimize the effect of current infeed by motors. The type of fault is determined from the fault-current phasors using the logic depicted in Figure 4.3.

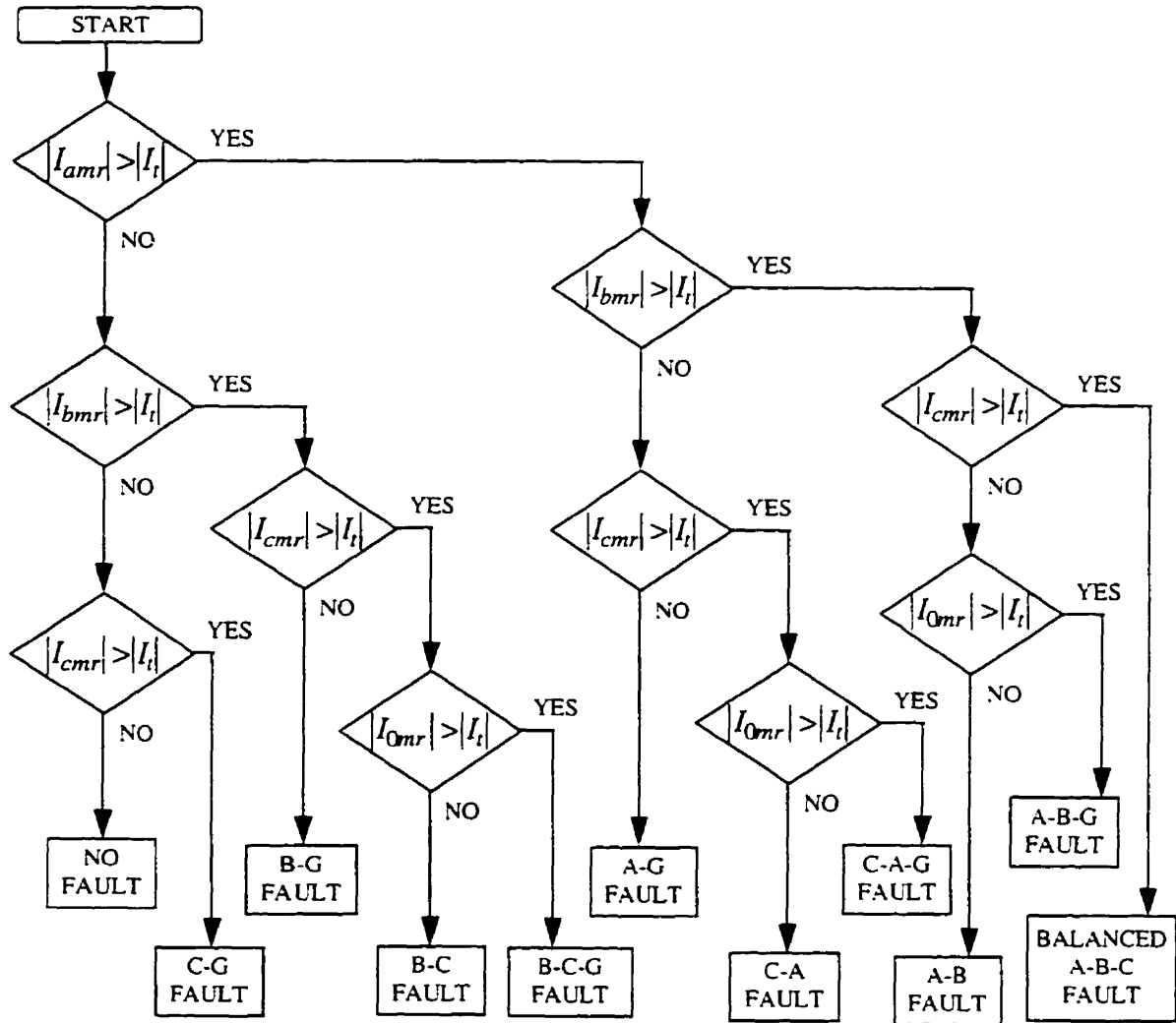


Figure 4.3. Flowchart for determining the fault type and the identity of faulted phases.

4.4 Estimating the Faulted Section

The equations needed to calculate the apparent impedance and reactance from the node M to the fault F depend on the type of the fault. Voltages and currents during a fault are used and the effects of loads and line charging are neglected. The following phasors of the sequence voltages and currents, at node M during the fault, are calculated by using Equations similar to A.4 to A.6.

V_{0m} , V_{1m} and V_{2m} Zero, positive and negative sequence voltages at node M .
 I_{0mr} , I_{1mr} and I_{2mr} Zero, positive and negative sequence currents flowing from node M to R .

(a) Single-phase-to-ground faults

For a phase A-to-ground fault,

$$Z_{m1} = \frac{V_{am}}{I_{amr}} \quad \text{and} \quad (4.2)$$

$$X_{m1} = \text{Im}(Z_{m1}) \quad (4.3)$$

where, Z_{m1} is the apparent impedance from node M to the fault.

X_{m1} is the apparent reactance from node M to the fault.

The modified reactance of the first section between node M and node R , X_{mr}^m , is computed as

$$X_{mr}^m = X_{lmr} + \frac{X_{0mr} - X_{lmr}}{3}. \quad (4.4)$$

where, X_{0mr} is the zero sequence reactance of the section between nodes M and R .

X_{lmr} is the positive sequence reactance of the section between M and R .

If the modified reactance, X_{mr}^m , is less than the apparent reactance then the fault is located beyond node R . The modified reactance of the second section is then computed using an equation similar to Equation 4.4 and added to that of the first section to obtain the total modified reactance. If this reactance is less than the apparent reactance then the fault is located beyond the first two sections. The process is continued until the total modified reactance is greater than the apparent reactance. Thus, the location of the fault, in the section between nodes x and $x+1 (= y)$, is obtained.

The apparent location for a phase B-to-ground fault and for a phase C-to-ground fault is determined in a similar manner.

(b) Two-phase-to-ground faults

For a phase B and phase C-to-ground fault,

$$Z_{m2g} = \frac{V_{bm} - V_{cm}}{I_{bmr} - I_{cnr}} \quad \text{and} \quad (4.5)$$

$$X_{m2g} = \text{Im}(Z_{m2g}) \quad (4.6)$$

where, Z_{m2g} is the apparent impedance from node M to the fault.
 X_{m2g} is the apparent reactance from node M to the fault.

If the positive sequence reactance of the first section, X_{lmr} , is less than the apparent reactance X_{m2g} , then the fault is located beyond node R . Reactance of the second section is then added to that of the first section to obtain the total reactance. If this reactance is less than the apparent reactance then the fault is located beyond the first two sections. The process is continued until the total reactance is greater than the apparent reactance. Thus, the location of the fault, in the section between nodes x and $x + 1 (= y)$, is obtained.

The apparent locations for phase C and phase A-to-ground and phase A and phase B-to-ground faults are also determined in a similar manner.

(c) Phase-to-phase faults

The apparent locations for phase-to-phase faults are also determined using the procedure used for two-phase-to-ground faults.

(d) Balanced three-phase faults

For a balanced three-phase fault,

$$Z_{m3} = \frac{V_{lm}}{I_{lmr}} \quad \text{and} \quad (4.7)$$

$$X_{m3} = \text{Im}(Z_{m3}) \quad (4.8)$$

where: Z_{m3} is the positive sequence apparent impedance from node M to the fault.
 X_{m3} is the positive sequence apparent reactance from node M to the fault.

The apparent location of the fault is determined using the procedure used for the two-phase-to-ground faults.

4.5 Developing an Equivalent Radial System

Once the location of the fault, in the section between nodes x and $x + 1 (= y)$, is established, the radial distribution system with laterals is converted to an equivalent radial system without the laterals. The load on a lateral is consolidated at its junction with the

line. The distribution system shown in Figure 4.1, for a fault at F , is modified by consolidating loads on the laterals to nodes $x - 1$ and $N - 1$ respectively. The modified system is shown in Figure 4.4 (a). If the apparent location is on a lateral, such as $F1$, the system is modified to that shown in Figure 4.4 (b). Load at node K is consolidated with the load at node J and all loads between nodes x and N are consolidated with the load at node $x - 1$. The proposed technique is described in Sections 4.6 through 4.8 considering the fault is at F .

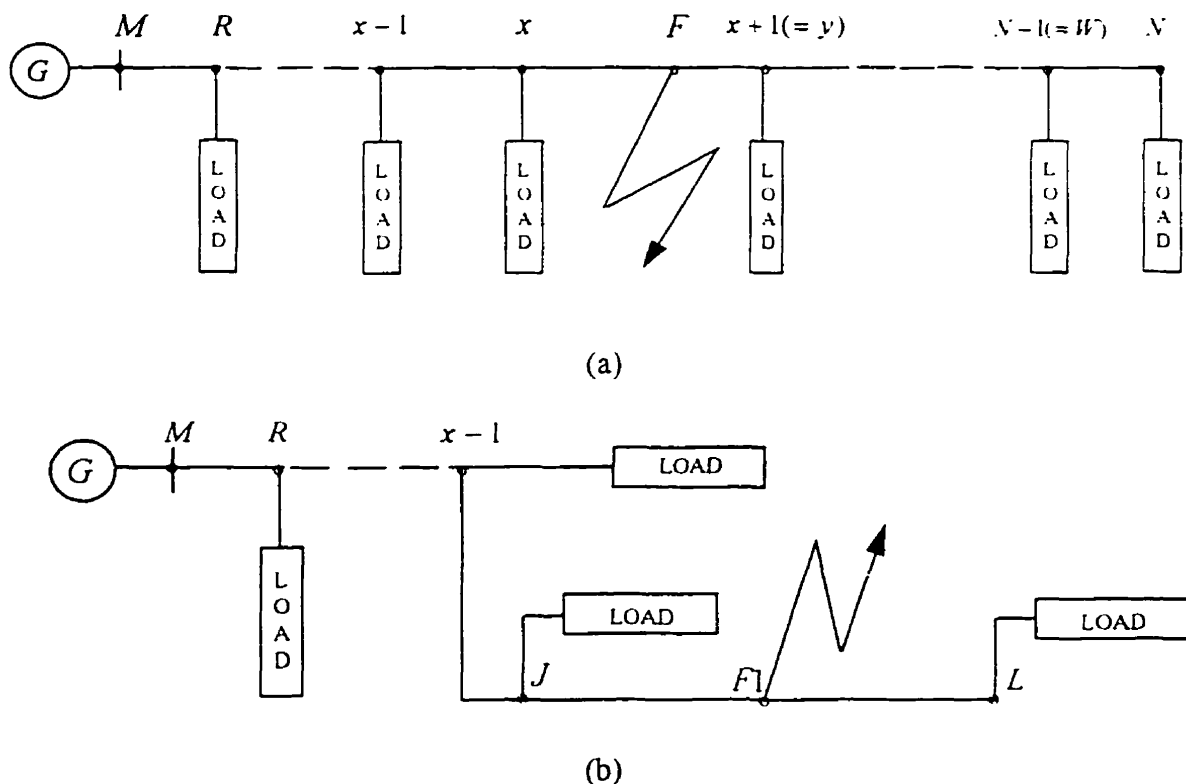


Figure 4.4. The single line diagram of the modified radial distribution system experiencing a fault at (a) at F and (b) at $F1$.

4.6 Modeling of Loads

The effects of the loads are considered by compensating for the load current. The loads at a node are assumed to depend on the voltage at the node. The constants describing the voltage-admittance relationship are estimated from the pre-fault load voltages and currents. The process consists of the following steps.

1. Selecting the load model.
2. Estimating pre-fault loads at all nodes up to x .
3. Estimating the pre-fault voltages and currents at all nodes up to x and at N .
4. Estimating the load constants.

These steps are described in Sections 4.6.1 to 4.6.4.

4.6.1 Selecting the load model

Several non-linear models have been suggested for representing loads in transmission system studies [11, 37, 38, 39, 40, 41, 42]. Similar concepts are applied in studies related to distribution systems. Static response type models were used in the work reported in this thesis for all loads up to node x and also for the consolidated load at the remote end. This model is described in Appendix C. The sequence admittances and voltages, of the consolidated load, are used in Equation C.8 to determine its load constants. However, the use of static response type models for all loads up to node x requires additional considerations depending on the load being a single-phase, phase-to-phase or three-phase type.

(a) Single-phase loads

A single-phase load is modeled as a single-phase-to-ground fault with a fault impedance equal to the load impedance. The sequence networks representation for the single-phase-to-ground faults described in Chapter 2, is used.

Figure 4.5 shows a single-phase load connected to phase A at node R , and the corresponding sequence network diagram. In this figure

V_{0r} , V_{1r} and V_{2r} are the zero, positive and negative sequence voltages at node R ,
 I_{0r} , I_{1r} and I_{2r} are the zero, positive and negative sequence load currents at
node R and
 Z_r is the load impedance.

The phase A voltage at node R , V_{ar} , in terms of the sequence voltages is given as

$$V_{ar} = V_{0r} + V_{1r} + V_{2r} \quad (4.9)$$

Load in phase B or phase C, can also be represented by similar sequence networks.

(b) Phase-to-phase loads

A phase-to-phase load is modeled as a phase-to-phase fault with the fault impedance equal to the load impedance. Figure 4.6 shows a phase-phase load connected between phases A and B at node R , and its sequence network diagrams. Development of the sequence diagram is discussed in Appendix A.

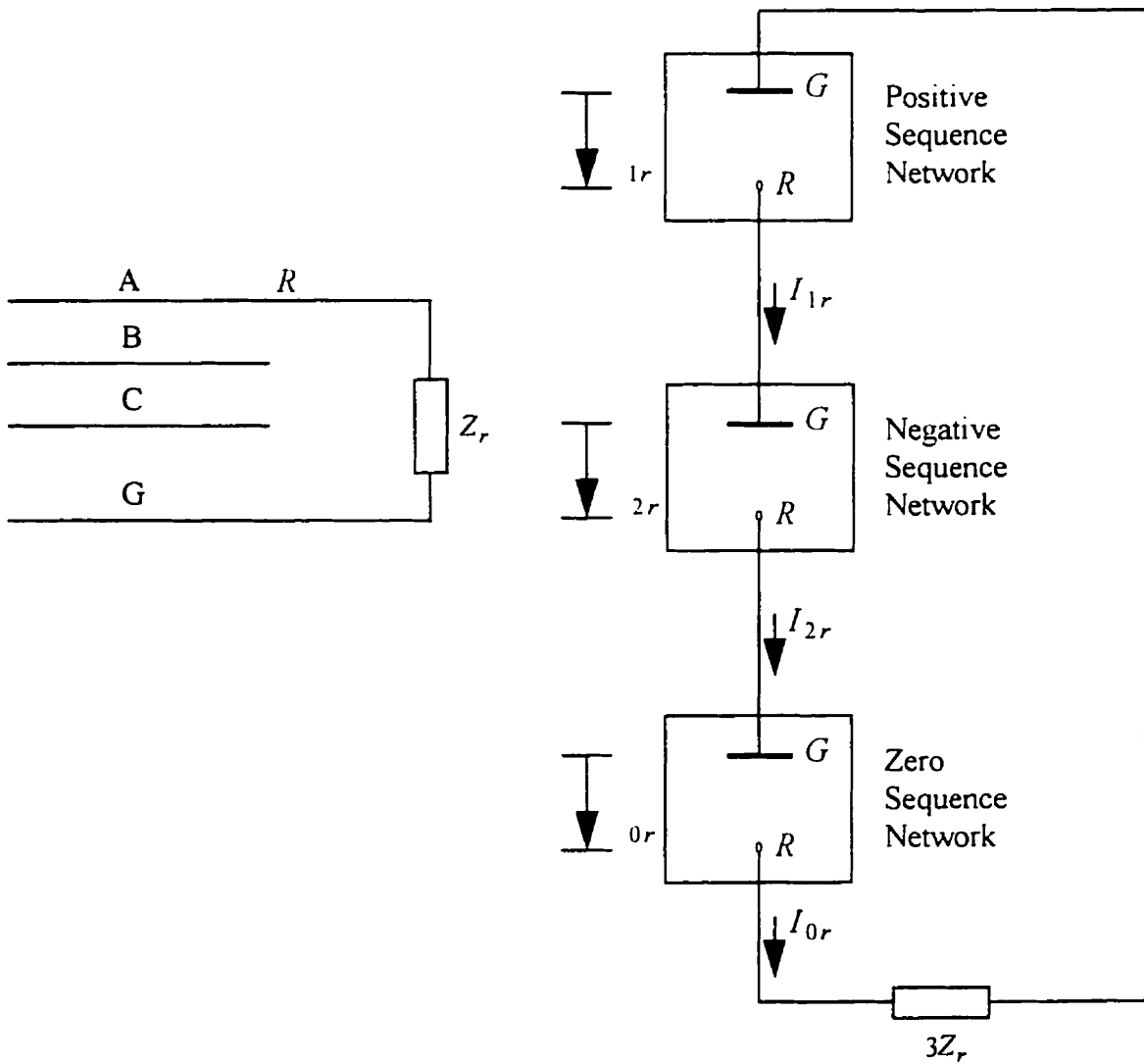


Figure 4.5. A single-phase load at node R and its sequence network representation.

(c) Three-phase loads

Three-phase loads are assumed to be balanced loads, and are modeled as balanced three-phase faults. Figure 4.7 shows a three-phase load connected between phases and

ground at node R , and its sequence network diagrams. The zero sequence network remains open circuited for a load without ground connection.

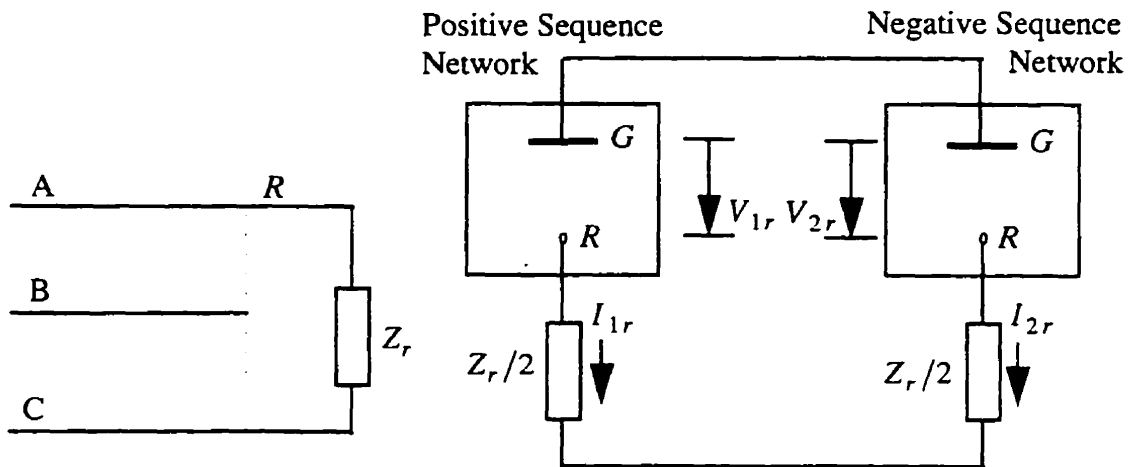


Figure 4.6. A phase-to-phase load at node R and its sequence network representation.

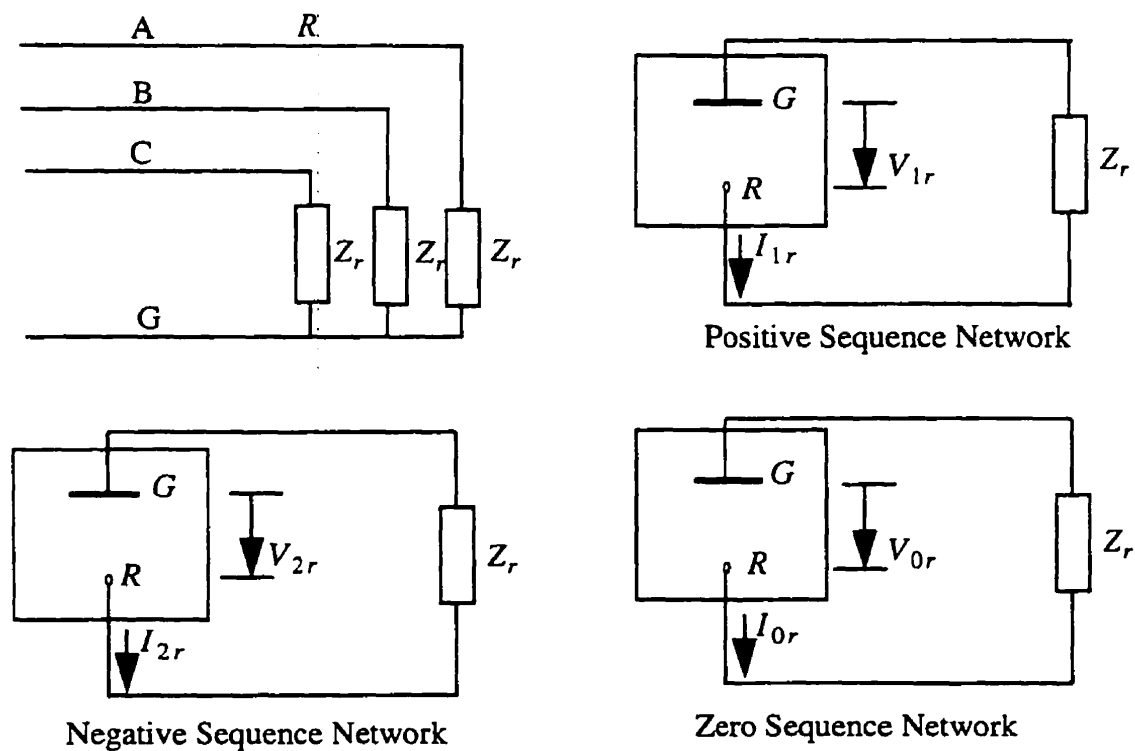


Figure 4.7. A three-phase balanced load and its sequence network representation.

4.6.2 Estimating the pre-fault loads at all nodes up to the fault

Once it is established that the fault appears to be between nodes x and $x+1$, pre-fault loads at the nodes up to node x are estimated if they are not known. These estimates are obtained by apportioning the total pre-fault load to the nodes based on the loads connected to them. For example, Load at node R is given by the equation

$$\text{Load at node } R = \frac{\text{Connected load at node } R}{\text{Total connected load}} \times \text{Total pre-fault load} . \quad (4.10)$$

The information on the connected load is taken from the load database. The total pre-fault load is calculated from the measured voltage and current phasors at node M and the reactive power used for line charging at nominal voltage.

However, if the active power, reactive power or current at a tap is either known from the SCADA system [43] or can be estimated from the metering database [44], the information is used to estimate the pre-fault apparent power at the tap. Nominal voltage and an appropriate power factor are assumed, if necessary, to compute the apparent power at a tap. The known apparent power at taps is then subtracted from the total estimated pre-fault load to obtain the remaining pre-fault load. The remaining pre-fault load is apportioned at the taps at which pre-fault loads are not known.

Load currents are zero immediately before the line is switched-into-a-fault and is energized by an auto-recloser. In those situations, total pre-fault load is assumed to determine the constants of the load model. When a line is energized by auto-reclosing, the system configuration and pre-fault loads are assumed to be the same as they were before the line was tripped. For a switching-into-a-fault, the total pre-fault load is assumed to be 60 percent of the total connected load.

4.6.3 Estimating the pre-fault voltages and currents at the nodes

The voltages and currents at the terminals of the distribution line section, shown in Figure 4.8, are described in Appendix D and are expressed as

$$\begin{bmatrix} V_r \\ I_{rm} \end{bmatrix} = \begin{bmatrix} 1 & -B_{mr} \\ C_{mr} & -1 \end{bmatrix} \begin{bmatrix} V_m \\ I_{mr} \end{bmatrix} . \quad (4.11)$$

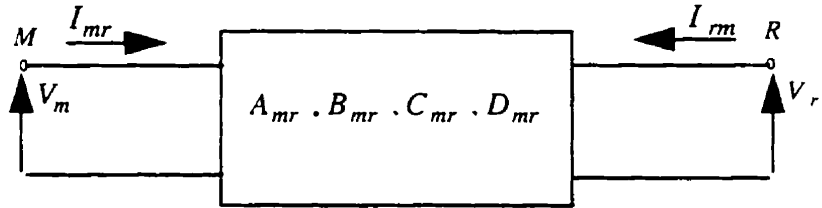


Figure 4.8. Distribution line section between nodes M and R .

The pre-fault sequence voltages and currents at node R are obtained by using this equation. The pre-fault load currents at node R are obtained by using the following procedure.

(i) Single-phase loads

The pre-fault load impedance is calculated from the apparent power drawn by the load, S_r , using

$$|Z_r| = \frac{|V_r|^2}{|S_r|}. \quad (4.12)$$

In the absence of the knowledge of the power factor of the load, a reasonable value is assumed, say between 0.8 to 0.88 (lag) for induction motor loads. The pre-fault load admittance, Y_r , and the sequence currents are then estimated using

$$Y_r = \frac{1}{Z_r} \text{ and} \quad (4.13)$$

$$I_{0r} = I_{1r} = I_{2r} = \frac{V_{0r} + V_{1r} + V_{2r}}{3Z_r}. \quad (4.14)$$

(ii) Phase-to-phase loads

The pre-fault load current, I_r , of a phase B-to-phase C load at node R is given as

$$I_r = \frac{V_{rBC}}{Z_r} \quad (4.15)$$

Pre-fault sequence currents for the load are computed from the line currents which in turn are obtained from the load current.

(ii) Three-phase loads

Three-phase loads are assumed to be balanced loads. The load admittances are computed in a similar manner to that used for single-phase loads. The pre-fault sequence currents of a three-phase load at node R are given as

$$I_{0r} = \frac{V_{0r}}{Z_r}, \quad I_{1r} = \frac{V_{1r}}{Z_r} \text{ and} \quad I_{2r} = \frac{V_{2r}}{Z_r}. \quad (4.16)$$

The current at node R , shown in Figure 4.9, is expressed by Equation 4.17.

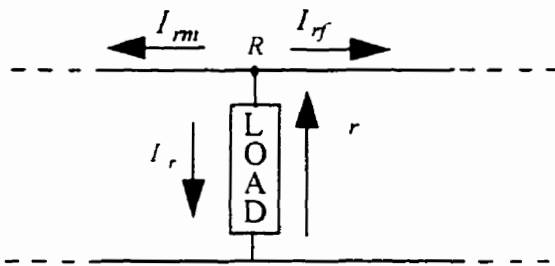


Figure 4.9. The voltage and currents at node R .

$$I_{rf} = -I_{rm} - I_r \quad (4.17)$$

where: I_{rf} is the current flowing towards the fault from node R .
 I_r is the load current at node R .

(a) Pre-fault sequence voltages and currents at all nodes up to x

The pre-fault sequence voltages and currents at node x are obtained by using equations similar to Equations 4.11 and 4.17 for each sequence component and the voltages and currents estimated for all nodes up to the node x ;

(b) Pre-fault sequence voltages and currents at the remote end

The pre-fault sequence voltages and currents at node N are estimated by assuming that all loads beyond the node x are consolidated with the load at node N as is shown in Figure 4.10.

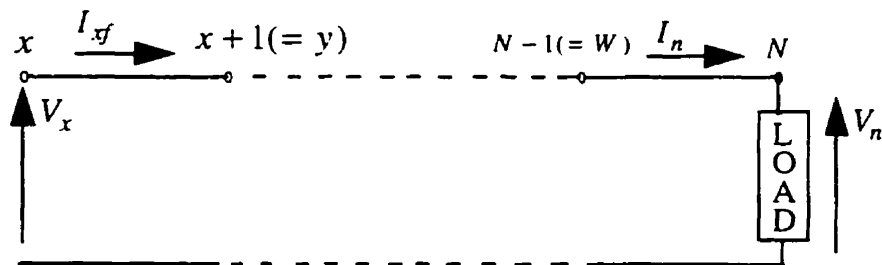


Figure 4.10. The pre-fault voltages and currents at nodes N and x .

The sequence voltages and currents at Node N are calculated using the following equation.

$$\begin{bmatrix} V_n \\ -I_n \end{bmatrix} = \begin{bmatrix} D_e & -B_e \\ C_e & -A_e \end{bmatrix} \begin{bmatrix} V_x \\ I_{xf} \end{bmatrix} \quad (4.18)$$

where: V_n and V_x are the voltages at nodes N and x .
 I_n and I_{xf} are the currents at nodes N and x .
 A_e, B_e, C_e and D_e are the constants of the cascaded sections between nodes $x + 1 (= y)$ and N .

The sequence admittances are estimated using

$$Y_n = \frac{I_n}{V_n}. \quad (4.19)$$

4.6.4 Estimating the load constants

(a) At all nodes up to x

The load constants G_r and B_r , for each single-phase load, are estimated using the pre-fault voltage, the load admittance and the appropriate values of the load response constants n_p and n_q . The values of n_p and n_q , defined in Equation C.8, are available from the load database. The load constants for each phase of a three-phase load are considered to be the same and are computed using a procedure similar to that used for single-phase loads. The load admittance, load response constants and phase-to-phase voltage are used to determine G_r and B_r of phase-to-phase loads.

(b) For the consolidated load at the remote end

The load constants proportional to the load conductances and susceptances for each sequence component are estimated using voltages and admittances obtained from Equations 4.18, 4.19 and C.8.

4.7 Estimating Voltages and Currents at the Remote End and at the Fault

This section describes the procedure for estimating the sequence currents at the fault, node F , and the sequence voltages at nodes F and N during the fault.

The sequence voltages and currents at node x must be estimated before the voltages and currents at the fault and at the remote end are estimated. The sequence voltages and currents at node R during the fault are calculated by using the measurements taken at node M and Equation 4.11. The sequence currents in the load at node R , during the fault, are obtained by using either a phase-to-ground, a phase-to-phase or a three-phase load model. The load admittances and impedances during the fault are calculated using Equations C.8 and 4.13. The currents to the next node are then calculated using Equation 4.17.

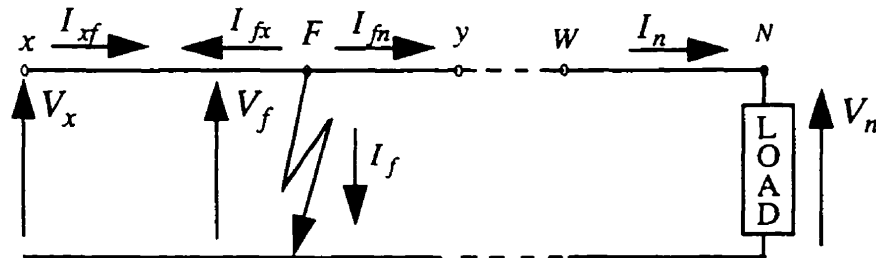
This procedure is repeated until the sequence voltages and currents at node x , during the fault, are determined.

The sequence voltages and currents at node x are estimated with phase A as reference irrespective of the type of fault. However, depending on the type of fault, these voltages and currents are converted to the sequence voltages and currents with either phase B or phase C as reference. The reference phases used for different types of faults are listed in Table 4.1.

Table 4.1. Selection of a reference phase for different types of faults.

Phase A reference	Phase B reference	Phase C reference
A-to-ground B and C-to-ground B-to-C Balanced three-phase	B-to-ground C and A-to-ground C-to-A	C-to-ground A and B-to-ground A-to-B

The sequence voltages and currents at node F , during the fault, are estimated assuming that all loads beyond the node x are consolidated with the load at node N . This is shown in Figure 4.11.

**Figure 4.11.** The voltages and currents at nodes F and N during the fault.

The voltages and currents at node F can be expressed as a function of voltages and currents at node x as follows.

$$\begin{bmatrix} V_f \\ I_{fx} \end{bmatrix} = \begin{bmatrix} 1 & -sB_{xy} \\ sC_{xy} & -1 \end{bmatrix} \begin{bmatrix} V_x \\ I_{xf} \end{bmatrix} \quad (4.20)$$

where: s is the distance to the node F from node x , expressed as a fraction of section length between nodes x and $x+1 (= y)$, and is given as

$$l_{xf} = sL_{xy} \quad (4.21)$$

B_{xy} and C_{xy} are the constants of section between the nodes x and $x+1 (= y)$.

The sequence voltages and currents at nodes N and F , during the fault, are given as

$$\begin{bmatrix} V_n \\ -I_n \end{bmatrix} = \begin{bmatrix} D_e & -B_e \\ C_e & -A_e \end{bmatrix} \begin{bmatrix} 1 & -(1-s)B_{xy} \\ -(1-s)C_{xy} & 1 \end{bmatrix} \begin{bmatrix} V_f \\ I_{fn} \end{bmatrix}. \quad (4.22)$$

Rearranging the equation provides

$$\begin{bmatrix} V_n \\ -I_n \end{bmatrix} = \begin{bmatrix} K_a + sK_b & K_c + sK_d \\ K_e + sK_f & K_g + sK_h \end{bmatrix} \begin{bmatrix} V_f \\ I_{fn} \end{bmatrix}, \quad (4.23)$$

where: K 's are complex constants, and are given as

$$\begin{aligned} K_a &= D_e + B_e C_{xy}, \\ K_b &= -B_e C_{xy}, \\ K_c &= -B_e - D_e B_{xy}, \\ K_d &= D_e B_{xy}, \\ K_e &= C_e + A_e C_{xy}, \\ K_f &= -A_e C_{xy}, \\ K_g &= -A_e - C_e B_{xy} \text{ and} \\ K_h &= C_e B_{xy}. \end{aligned} \quad (4.24)$$

The current at node F , I_{fn} shown in Figure 4.9, is given as

$$I_{fn} = -I_{fx} - I_f. \quad (4.25)$$

Substituting I_{fn} from this equation into Equation 4.23 provides

$$\begin{bmatrix} V_n \\ -I_n \end{bmatrix} = \begin{bmatrix} K_a + sK_b & K_c + sK_d \\ K_e + sK_f & K_g + sK_h \end{bmatrix} \begin{bmatrix} V_f \\ -I_{fx} \end{bmatrix} + \begin{bmatrix} K_a + sK_b & K_c + sK_d \\ K_e + sK_f & K_g + sK_h \end{bmatrix} \begin{bmatrix} 0 \\ -I_f \end{bmatrix}. \quad (4.26)$$

Substituting V_f and I_{fx} from Equation 4.20 in this equation and rearranging the resulting equation provides

$$\begin{bmatrix} V_n \\ -I_n \end{bmatrix} = \begin{bmatrix} K_a + sK_b & K_c + sK_d \\ K_e + sK_f & K_g + sK_h \end{bmatrix} \begin{bmatrix} 1 & -sB_{xy} \\ -sC_{xy} & 1 \end{bmatrix} \begin{bmatrix} V_x \\ I_{xf} \end{bmatrix} - I_f \begin{bmatrix} K_c + sK_d \\ K_g + sK_h \end{bmatrix}. \quad (4.27)$$

Substituting I_n from Equation 4.19 and rearranging , Equation 4.27 can be restated as

$$\begin{bmatrix} V_n \\ -V_n Y_n \end{bmatrix} + I_f \begin{bmatrix} K_c + sK_d \\ K_g + sK_h \end{bmatrix} = \begin{bmatrix} K_a + sK_b & K_c + sK_d \\ K_e + sK_f & K_g + sK_h \end{bmatrix} \begin{bmatrix} 1 & -sB_{xy} \\ -sC_{xy} & 1 \end{bmatrix} \begin{bmatrix} V_x \\ I_{xf} \end{bmatrix}. \quad (4.28)$$

Rearranging Equation 4.28 and neglecting the terms of second and higher order, the following equation is obtained.

$$\begin{bmatrix} 1 & K_c + sK_d \\ -Y_n & K_g + sK_h \end{bmatrix} \begin{bmatrix} V_n \\ I_f \end{bmatrix} = \begin{bmatrix} K_a + sK_i & K_c + sK_j \\ K_e + sK_k & K_g + sK_l \end{bmatrix} \begin{bmatrix} V_x \\ I_{xf} \end{bmatrix} \quad (4.29)$$

where: K 's are complex constants, and are given as

$$\begin{aligned} K_i &= K_b - K_c C_{xy}, \\ K_j &= K_d - K_a B_{xy}, \\ K_k &= K_f - K_g C_{xy} \text{ and} \\ K_l &= K_h - K_e B_{xy}. \end{aligned} \quad (4.30)$$

Rearranging this equation provides

$$\begin{bmatrix} V_n \\ I_f \end{bmatrix} = \frac{\begin{bmatrix} K_g + sK_h & -K_c - sK_d \\ Y_n & 1 \end{bmatrix} \begin{bmatrix} K_a + sK_i & K_c + sK_j \\ K_e + sK_k & K_g + sK_l \end{bmatrix}}{K_g + sK_h + Y_n(K_c + sK_d)} \begin{bmatrix} V_x \\ I_{xf} \end{bmatrix}. \quad (4.31)$$

Neglecting the second and higher order terms, Equation 4.31 becomes

$$\begin{bmatrix} V_n \\ I_f \end{bmatrix} = \frac{1}{K_v + sK_w} \begin{bmatrix} K_m + sK_n & sK_p \\ K_q + sK_r & K_v + sK_u \end{bmatrix} \begin{bmatrix} V_x \\ I_{xf} \end{bmatrix} \quad (4.32)$$

where: K 's are complex parameters, and are given as

$$\begin{aligned} K_m &= K_g K_a - K_c K_e, \\ K_n &= K_h K_a + K_g K_i - K_d K_e - K_c K_k, \\ K_p &= K_h K_c + K_g K_j - K_d K_g - K_c K_l, \\ K_q &= Y_n K_a + K_e, \\ K_r &= Y_n K_i + K_k, \\ K_u &= Y_n K_j + K_l, \\ K_v &= Y_n K_c + K_g \text{ and} \\ K_w &= Y_n K_d + K_h. \end{aligned} \quad (4.33)$$

The parameters K_m to K_w , calculated using Equation 4.33, are used to compute the voltages at node N and the fault currents at node F . The sequence voltages and currents at node F and the sequence voltages at node N are obtained by using Equations 4.20 and 4.32 as follows.

$$\begin{aligned} V_{0f} &= V_{0x} - sB_{0xy}I_{0xf}, \\ V_{1f} &= V_{1x} - sB_{1xy}I_{1xf}, \\ V_{2f} &= V_{2x} - sB_{2xy}I_{2xf}, \\ I_{0f} &= \frac{1}{K_{0v} + sK_{0w}} \{(K_{0q} + sK_{0r})V_{0x} + (K_{0v} + sK_{0u})I_{0xf}\}, \\ I_{1f} &= \frac{1}{K_{1v} + sK_{1w}} \{(K_{1q} + sK_{1r})V_{1x} + (K_{1v} + sK_{1u})I_{1xf}\} \text{ and} \\ I_{2f} &= \frac{1}{K_{2v} + sK_{2w}} \{(K_{2q} + sK_{2r})V_{2x} + (K_{2v} + sK_{2u})I_{2xf}\}. \end{aligned} \quad (4.34)$$

$$\begin{aligned} V_{0n} &= \frac{1}{K_{0v} + sK_{0w}} \{(K_{0m} + sK_{0n})V_{0x} + sK_{0p}I_{0xf}\}, \\ V_{1n} &= \frac{1}{K_{1v} + sK_{1w}} \{(K_{1m} + sK_{1n})V_{1x} + sK_{1p}I_{1xf}\} \text{ and} \\ V_{2n} &= \frac{1}{K_{2v} + sK_{2w}} \{(K_{2m} + sK_{2n})V_{2x} + sK_{2p}I_{2xf}\}. \end{aligned} \quad (4.35)$$

4.8 Estimating the Location of the Fault

This section describes the procedure used for estimating s , the distance from node x to the fault F , as a fraction of the length of the line from node x to node $x+1 (=y)$. The voltage-current relationships at the fault, described in Chapter 2, and the resistive nature of the fault impedance are used to estimate s .

4.8.1 Single-phase-to-ground faults

The voltage of the faulted phase, V_f , for a single-phase-to-ground fault at F is given by the following equation.

$$V_f = I_f R_f \quad (4.36)$$

where: I_f is the fault current and
 R_f is the fault resistance.

Expressing the phase voltage and fault current in terms of the sequence components and rearranging provides

$$\frac{V_{0f} + V_{1f} + V_{2f}}{I_{0f} + I_{1f} + I_{2f}} = R_f. \quad (4.37)$$

Equating the imaginary components of both sides of this equation provides

$$\text{Im} \left(\frac{V_{0f} + V_{1f} + V_{2f}}{I_{0f} + I_{1f} + I_{2f}} \right) = 0 \quad (4.38)$$

Substituting the sequence voltages and currents from Equation 4.34, the following equation is obtained.

$$\text{Im} \left\{ \frac{(V_{0x} + V_{1x} + V_{2x}) - s(B_{0xy}I_{0xf} + B_{1xy}I_{1xf} + B_{2xy}I_{2xf})}{\frac{1}{K_{0v} + sK_{0w}} \{(K_{0q} + sK_{0r})V_{0x} + (K_{0v} + sK_{0u})I_{0xf}\} + \frac{1}{K_{1v} + sK_{1w}} \{(K_{1q} + sK_{1r})V_{1x} + (K_{1v} + sK_{1u})I_{1xf}\} + \frac{1}{K_{2v} + sK_{2w}} \{(K_{2q} + sK_{2r})V_{2x} + (K_{2v} + sK_{2u})I_{2xf}\}} \right\} = 0 \quad (4.39)$$

The following equation is obtained by rationalizing this equation.

$$\text{Im} \left\{ \frac{\{(V_{0x} + V_{1x} + V_{2x}) - s(B_{0xy}I_{0xf} + B_{1xy}I_{1xf} + B_{2xy}I_{2xf})\} \{(K_{0v} + sK_{0w})(K_{1v} + sK_{1w})(K_{2v} + sK_{2w})\}}{(K_{1v} + sK_{1w})(K_{2v} + sK_{2w})\{(K_{0q} + sK_{0r})V_{0x} + (K_{0v} + sK_{0u})I_{0xf}\} + (K_{2v} + sK_{2w})(K_{0v} + sK_{0w})\{(K_{1q} + sK_{1r})V_{1x} + (K_{1v} + sK_{1u})I_{1xf}\} + (K_{0v} + sK_{0w})(K_{1v} + sK_{1w})\{(K_{2q} + sK_{2r})V_{2x} + (K_{2v} + sK_{2u})I_{2xf}\}} \right\} = 0 \quad (4.40)$$

Neglecting the second and higher order terms, the following equation is obtained

$$\text{Im}\left(\frac{K_A + sK_B}{K_C + sK_D}\right) = 0 \quad (4.41)$$

where: K_A to K_D are complex parameters and are given as

$$\begin{aligned} K_A &= (V_{0x} + V_{1x} + V_{2x})(K_{0v}K_{1v}K_{2v}), \\ K_B &= [(V_{0x} + V_{1x} + V_{2x})\{K_{1v}(K_{2v}K_{0w} + K_{2w}K_{0v}) + (K_{1w}K_{0v}K_{2v})\}] - \\ &\quad [(B_{0xy}I_{0xf} + B_{1xy}I_{1xf} + B_{2xy}I_{2xf})(K_{0v}K_{1v}K_{2v})], \\ K_C &= \{(K_{1v}K_{2v})(K_{0q}V_{0x} + K_{0v}I_{0xf})\} + \\ &\quad \{(K_{2v}K_{0v})(K_{1q}V_{1x} + K_{1v}I_{1xf})\} + \\ &\quad \{(K_{0v}K_{1v})(K_{2q}V_{2x} + K_{2v}I_{2xf})\} \text{ and} \\ K_D &= \{(K_{1v}K_{2v})(K_{0r}V_{0x} + K_{0u}I_{0xf}) + (K_{1v}K_{2w} + K_{1w}K_{2v})(K_{0q}V_{0x} + K_{0v}I_{0xf})\} + \\ &\quad \{(K_{2v}K_{0v})(K_{1r}V_{1x} + K_{1u}I_{1xf}) + (K_{2v}K_{0w} + K_{2w}K_{0v})(K_{1q}V_{1x} + K_{1v}I_{1xf})\} + \\ &\quad \{(K_{0v}K_{1v})(K_{2r}V_{2x} + K_{2u}I_{2xf}) + (K_{0v}K_{1w} + K_{0w}K_{1v})(K_{2q}V_{2x} + K_{2v}I_{2xf})\}. \end{aligned} \quad (4.42)$$

The complex parameters K_A to K_D are expressed in terms of their real and imaginary components as follows.

$$K_A = K_{AR} + jK_{AI}, \quad K_B = K_{BR} + jK_{BI}, \quad K_C = K_{CR} + jK_{CI}, \quad K_D = K_{DR} + jK_{DI} \quad (4.43)$$

Making these substitutions in Equation 4.41 and rationalizing the resulting equation provides

$$\text{Im}\left(\frac{\{(K_{AR} + sK_{BR}) + j(K_{AI} + sK_{BI})\}\{(K_{CR} + sK_{DR}) - j(K_{CI} + sK_{DI})\}}{\{(K_{CR} + sK_{DR}) + j(K_{CI} + sK_{DI})\}\{(K_{CR} + sK_{DR}) - j(K_{CI} + sK_{DI})\}}\right) = 0 \quad (4.44)$$

Equation 4.44 is restated as

$$(K_{AI} + sK_{BI})(K_{CR} + sK_{DR}) - (K_{AR} + sK_{BR})(K_{CI} + sK_{DI}) = 0. \quad (4.45)$$

Neglecting second and higher order terms and rearranging provides

$$s = \frac{K_{AR}K_{CI} - K_{AI}K_{CR}}{(K_{CR}K_{BI} - K_{CI}K_{BR}) + (K_{DR}K_{AI} - K_{DI}K_{AR})} \quad (4.46)$$

The value of s is calculated using the following iterative procedure.

1. The parameters K_m , K_n and K_p are computed using Equation 4.33.
2. The parameters K_q to K_w , defined in Equation 4.33, are computed using the pre-fault admittance of the consolidated load at node N .
3. The parameters K_A , K_B , K_C and K_D , defined in Equation 4.42, are computed using the values of K_q , K_r , K_u , K_v and K_w , computed in Step 2.
4. The value of s is calculated from Equation 4.46 by using the parameters K_A , K_B , K_C and K_D computed in Step 3.
5. The voltages at the node N are computed using Equation 4.35, the parameters computed in Steps 1 and 2 and the value of s computed in Step 4.
6. The new voltages at the node N and Equation C.8 are used to obtain the updated sequence admittances of the consolidated load.
7. The parameters K_q , K_r , K_u , K_v and K_w are updated using the new values of the admittance of the consolidated load at the node N , computed in Step 6.
8. The parameters K_A , K_B , K_C and K_D are updated by using the values of K_q , K_r , K_u , K_v and K_w , computed in Step 7.
9. The value of s is obtained using Equation 4.46 and the updated values of the parameters K_A , K_B , K_C and K_D computed in Step 8.
10. The convergence of the value of s is checked. The voltages at node N are updated using the parameters computed in Steps 1 and 7 and the value of s computed in Step 9, if the solution is not converged. The procedure is repeated, starting with Step 6, until a converged solution is obtained.

4.8.2 Two-phase-to-ground and phase-to-phase faults

The fault resistance R_f , when a two-phase-to-ground fault is experienced, can be expressed as

$$\left(\frac{V_{1f} - V_{2f}}{I_{1f} - I_{2f}} \right) = R_f. \quad (4.47)$$

One half of the fault resistance, when a phase-to-phase fault is experienced, can be expressed as

$$\left(\frac{V_{1f} - V_{2f}}{I_{1f} - I_{2f}} \right) = \frac{R_f}{2}. \quad (4.48)$$

Since R_f is resistive, Equations 4.47 and 4.48 provides

$$\text{Im} \left(\frac{V_{1f} - V_{2f}}{I_{1f} - I_{2f}} \right) = 0. \quad (4.49)$$

Substituting the sequence voltages and currents from Equation 4.34, the following equation is obtained.

$$\text{Im} \left(\frac{\{(V_{1x} - V_{2x}) - s(B_{1xy}I_{1xf} - B_{2xy}I_{2xf})\}\{(K_{1v} + sK_{1w})(K_{2v} + sK_{2w})\}}{(K_{2v} + sK_{2w})\{(K_{1q} + sK_{1r})V_{1x} + (K_{1v} + sK_{1u})I_{1xf}\} - (K_{1v} + sK_{1w})\{(K_{2q} + sK_{2r})V_{2x} + (K_{2v} + sK_{2u})I_{2xf}\}} \right) = 0 \quad (4.50)$$

Neglecting the second and higher order terms, the following equation is obtained

$$\text{Im} \left(\frac{K_{A2} + sK_{B2}}{K_{C2} + sK_{D2}} \right) = 0 \quad (4.51)$$

where: K_{A2} to K_{D2} are complex parameters and are given as

$$\begin{aligned} K_{A2} &= (V_{1x} - V_{2x})(K_{1v}K_{2v}), \\ K_{B2} &= (V_{1x} - V_{2x})(K_{1v}K_{2w} + K_{1w}K_{2v}) - (B_{1xy}I_{1xf} - B_{2xy}I_{2xf})(K_{1v}K_{2v}), \\ K_{C2} &= K_{2v}(K_{1q}V_{1x} + K_{1v}I_{1xf}) - K_{1v}(K_{2q}V_{2x} + K_{2v}I_{2xf}) \text{ and} \\ K_{D2} &= \{K_{2v}(K_{1r}V_{1x} + K_{1u}I_{1xf}) + K_{2w}(K_{1q}V_{1x} + K_{1v}I_{1xf})\} - \\ &\quad \{K_{1v}(K_{2r}V_{2x} + K_{2u}I_{2xf}) + K_{1w}(K_{2q}V_{2x} + K_{2v}I_{2xf})\}. \end{aligned} \quad (4.52)$$

Following the procedure used for the single-phase-to-ground faults, the distance s is calculated using an iterative approach.

4.8.3 Balanced three-phase faults

The fault resistance R_f , when a balanced three-phase fault is experienced, can be expressed as

$$\frac{V_{1f}}{I_{1f}} = R_f \quad (4.53)$$

Since R_f is resistive,

$$\operatorname{Im}\left(\frac{V_{1f}}{I_{1f}}\right) = 0. \quad (4.54)$$

Substituting the sequence voltages and currents from Equation 4.34, the following equation is obtained.

$$\operatorname{Im}\left(\frac{(V_{1x} - sB_{1xy}I_{1xf})(K_{1v} + sK_{1w})}{(K_{1q} + sK_{1r})V_{1x} + (K_{1v} + sK_{1u})I_{1xf}}\right) = 0 \quad (4.55)$$

Neglecting the second and higher order terms, the following equation is obtained

$$\operatorname{Im}\left(\frac{K_{A3} + sK_{B3}}{K_{C3} + sK_{D3}}\right) = 0 \quad (4.56)$$

where: K_{A3} - K_{D3} are complex parameters and are given as

$$\begin{aligned} K_{A3} &= V_{1x}K_{1v}, \\ K_{B3} &= V_{1x}K_{1w} - B_{1xy}I_{1xf}K_{1v}, \\ K_{C3} &= K_{1q}V_{1x} + K_{1v}I_{1xf} \text{ and} \\ K_{D3} &= K_{1r}V_{1x} + K_{1u}I_{1xf}. \end{aligned} \quad (4.57)$$

Following the procedure used for the single-phase-to-ground faults, the distance s is calculated using an iterative approach.

4.8.4 Generalized equation for all types of faults

One of the equations from 4.41, 4.51 and 4.56 is to be solved, depending on the type of the fault, to obtain the value of s . All these equations are similar except that the values of the parameters K_A, K_B, K_C and K_D are different. Parameters of Equation 4.51 for two-phase-to-ground faults and phase-to-phase faults, defined in Equation 4.52, are obtained from parameters for single-phase-to-ground faults, defined in Equation 4.42, by substituting

$$\begin{aligned} V_{2x} &= -V_{2x}, & I_{2xf} &= -I_{2xf}, & V_{0x} &= I_{0xf} = 0, \\ K_{0v} &= 1 \quad \text{and} & K_{0w} &= 0. \end{aligned} \quad (4.58)$$

Two-phase-to-ground faults and phase-to-phase faults are, therefore, special cases of single phase-to-ground faults for finding s . The equations used for single-phase-to-ground faults are used in these cases, by selecting appropriate values.

Also, the parameters of Equation 4.56 for balanced three-phase faults, defined in Equation 4.57, are obtained from parameters for two-phase-to-ground faults and phase-to-phase faults defined in Equation 4.52, by substituting

$$V_{2x} = I_{2xf} = 0, \quad K_{2v} = 1 \quad \text{and} \quad K_{2w} = 0. \quad (4.59)$$

A balanced three-phase fault is, therefore, a special case of a two-phase-to-ground fault or phase-to-phase fault, as far as the determination of s is concerned. The equations used for single-phase-to-ground faults are, therefore, used in this case, by setting appropriate values of parameters.

The Equation 4.41, derived for single-phase-to-ground faults, is suitable for all types of faults and is a general equation for finding s . The parameters of this equation, defined in equation 4.42, are modified depending on the type of the fault.

4.9 Converting Multiple Estimates to a Single Estimate

The fault location technique could provide multiple estimates if the distribution system has laterals. The number of estimates, for a fault, depends on the system

configuration and the location of the fault. It is, therefore, necessary to convert the multiple estimates to a single estimate.

Software-based fault indicators are developed for this purpose. They detect downstream faults irrespective of their location. These indicators are located at the beginning of each tap and are shown for a typical distribution system in Figure 4.12. Information from the fault indicators is combined with multiple estimates, obtained by using methodologies described above, to arrive at a single estimate for the location of a fault.

4.9.1 Fault indicators

Several Faulted Circuit Indicators (FCI) have been suggested in the past [45, 46] for use in distribution systems. Fault indicators are designed to sense a current level which is either a preset magnitude or a change in current level. They indicate the occurrence of a fault downstream of their locations. Different methods, including flashing LED, strobe, mechanical flag, acoustic pulse, radio frequency signal or SCADA contact signal, are used for indication.

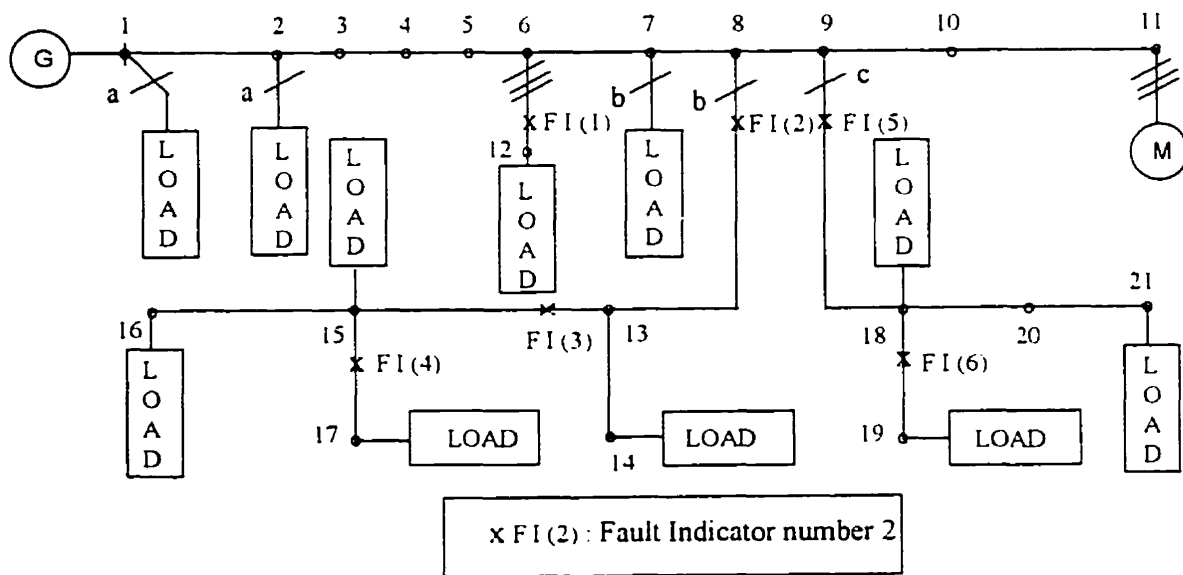


Figure 4.12. Location of fault indicators in a typical distribution system.

Earlier generations of fault indicators were primarily based on preset current levels. They require coordination for their settings and their operation is delayed to avoid misoperation on inrush currents. Of late, two techniques of implementing fault indicators have been introduced [45, 46]. These techniques do not require coordination of the settings. One method is based on load leveling and the other is based on an adaptive trip setting.

In this project, software-based fault indicators were developed to take advantage of load leveling and adaptive trip features. Each developed fault indicator has two modules: one based on load leveling and the other based on an adaptive trip setting. The fault indicator operates if either of the modules detects the presence of a fault. The load-leveling module is an overcurrent relay. Its trip level is adjusted based on the load current and is set twice the load current. The current level has to be stable for 10 seconds for implementing a change in the setting. If the current drops below a preset minimum value, the setting is not reduced further. This module will not operate if the current during a fault is close to or less than load current.

The adaptive trip setting module is based on the rate of rise of the current followed by a decrease in current. The decrease of current is detected when the current becomes less than a set value but is more than zero. This feature is provided to avoid the effect of induced currents from adjacent phases.

4.9.2 Single estimate

The methodology used to convert multiple estimates to a single estimate by combining the information from fault indicators is straightforward and is described by using the system shown in Figure 4.12. This distribution system has six fault indicators placed at the beginning of each tap. Information from these indicators and multiple estimates are used by the proposed technique.

For example, for a fault between nodes 13 and 14, the proposed technique may initially estimate four possible locations: first between nodes 9 and 10, second between nodes 13 and 14, third between nodes 15 and 16 and, fourth between nodes 15 and 17. In case only the FI (2), placed at the beginning of the lateral from node 8, detects a fault, it can be concluded that the estimate which indicates the fault to be between nodes 13 and

14 must be selected. However, for a fault between nodes 15 and 17, Fault Indicators 2, 3 and 4 would operate.

Different fault indicators will operate depending on the location of the fault. This information can be effectively combined with the multiple estimates to arrive at a single estimate.

4.10 Summary

A new technique for estimating the locations of shunt faults on a radial distribution system including laterals, has been presented in this chapter. Load currents at different taps are estimated. All loads beyond the fault are assumed to be consolidated at the end of the line. Static response type load models have been used. Non-homogeneity of the line is taken into account. The apparent location of a fault from the line terminal is first estimated by computing impedance from the fundamental frequency voltage and current phasors, and then converting the reactive component of the impedance to line length. The estimate of the fault location is an iterative process based on the apparent location of the fault, voltage-current relationship at the fault, and the resistive nature of the fault impedance. It is shown that multiple estimates obtained from the technique can be reduced to a single estimate by using information from fault indicators strategically placed in the system.

The proposed technique, however, has one apparent drawback. The estimation procedure is not valid if the fault resistance is zero. But, it is practically impossible to have a fault with exactly zero resistance.

5. TESTING THE PROPOSED TECHNIQUE

5.1 Introduction

A digital technique for estimating locations of shunt faults on radial distribution system, with laterals, has been presented in the previous chapter. The technique was tested extensively to evaluate its suitability. Data for the tests were generated by simulations performed using the PSCAD/EMTDC [47].

Several programs were developed for testing the proposed technique. A program, the acquisition module, was developed for estimating the fundamental frequency voltages and currents at the line terminal and for detecting the type of fault. This program processes the raw data using an anti-aliasing filter. The program then estimates the fundamental frequency components of voltages and currents using a least error squares algorithm.

Another program, the evaluation module, was developed for estimating the fault locations from the system data and the information provided by the acquisition module. A fault indicator module indicates the location of downstream faults and helps in selecting a location if there are multiple estimates.

Simulations were performed on a UNIX-based SUN SPARC workstation and the programs were tested using three different FORTRAN compilers available at the University of Saskatchewan. All platforms take only a few seconds to execute the evaluation module which is intended to be executed in an off-line mode.

Several fault locations and fault resistance values were used in the tests. The results obtained by the proposed technique were also compared with the distance of the fault and the values obtained by using the reactive component method. The results are presented in this chapter. Some details of tests conducted to evaluate the proposed technique are also provided. The simulation software and the anti-aliasing filter are briefly described in Appendices E and F respectively.

5.2 Distribution System Selected for the Studies

The SaskPower distribution circuit, shown in Figure 5.1, was selected for the studies reported in this chapter. The line between nodes 1 and 11 is 37 km long and consists of sections of different lengths which are made of different types of conductors. Single or three phase loads are tapped at all nodes except for nodes 3, 4, 5, 10 and 20. Nodes 3, 4 and 5 divide the 16 km section of the line from node 2 to node 6 in four sections. Node 20 divides the section from node 18 to node 21 in two sections. Node 10 is the junction of two sections made of different types of conductors. An equivalent source, G , is connected to node 1. Six fault indicators are placed in the section between nodes:

6 & 12, 8 & 13, 13 & 15, 15 & 17, 9 & 18 and 18 & 19.

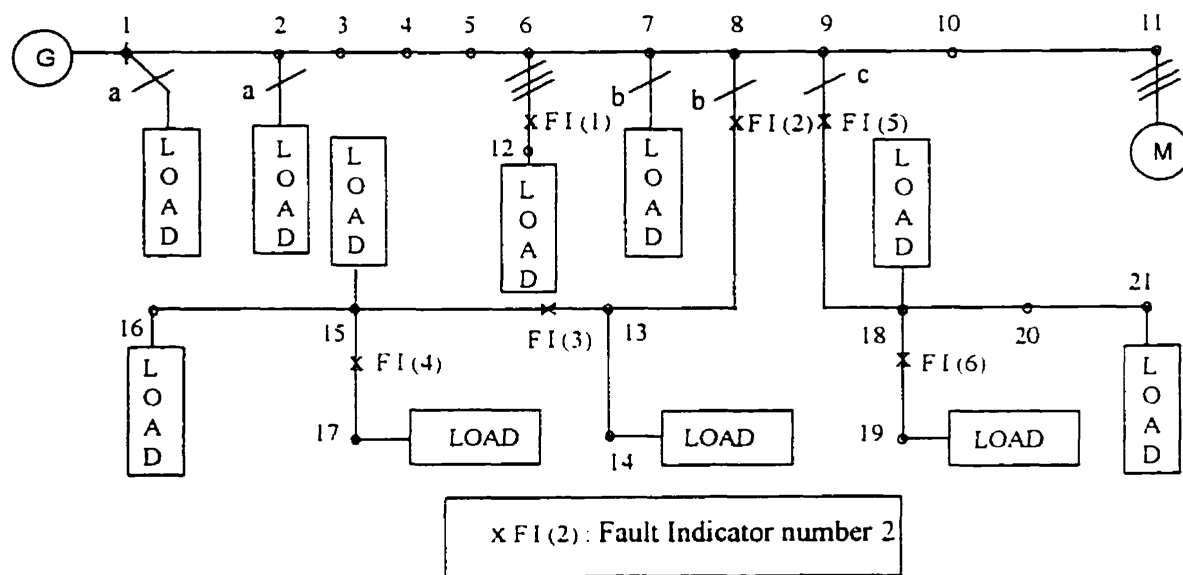


Figure 5.1. A single line diagram of the selected SaskPower distribution circuit.

All line sections were modeled by equivalent pi networks and all loads were modeled as voltage dependent loads. The load response constants of the equivalent load at the remote end of the modified radial system, for different types of faults at various locations, were chosen after considering the types of loads. The parameters of the equivalent source, the distribution line and the loads are given in Appendix G.

It was assumed that the pre-fault and fault data collected by the acquisition module will be transmitted to the evaluation module over a suitable communication system when this technique is implemented on a distribution system. For the studies reported in this chapter, the data were stored in a file.

5.3 Studies Conducted

Single-phase-to-ground, two-phase-to-ground, phase-to-phase and balanced three-phase faults were simulated at all nodes of the distribution circuit shown in Figure 5.1. Different fault resistance values were used in these simulations. The procedure described in Chapter 4 was used for estimating the locations of faults. Results for phase B-to-ground (phase C-to-ground in case of C-phase laterals), phase B and phase C-to-ground and phase A-to-phase B are reported in this chapter. Additional results are given in Appendix H.

5.3.1 Single-phase-to-ground faults

The proposed technique was tested for estimating the location of single-phase-to-ground faults. A fault resistance of 0.05 ohm was used in these cases. Multiple estimates obtained for faults at different locations are listed in Tables 5.1 and 5.2. The distance of the simulated fault locations and the fault locations estimated from the reactive components of the apparent impedance are also listed. All distances recorded in the table are from node 1. A sample fault location estimation procedure is described in detail in Appendix I.

Using additional information, described in Chapter 4, single estimate for a location of fault is obtained and are listed in Table 5.3. Estimation errors, expressed as percentage of the line length, were calculated and are shown in Figures 5.2. The results indicate that the distances of the faults, estimated by the proposed technique are substantially more accurate than the distances estimated by the reactive components of the apparent impedances.

These studies were repeated using fault resistances of 5.0, 10.0, 25.0 and 50.0 ohms. The estimated fault locations are listed in Tables 5.4 to 5.7. The distance of the simulated fault locations and the fault locations estimated from the reactive components

of the apparent impedances are also listed in the tables. All distances shown in the tables are from node 1. Estimation errors, expressed as percentages of the line length, were calculated and are shown in Figures 5.3 to 5.6.

Table 5.1. Multiple fault location estimates for the single-phase-to-ground fault cases between node 1 and 11 when the fault resistance is 0.05 ohm.

Fault Node Number	Distance of the Fault (km)	Fault Location Estimate by using the			
		Reactive Component Method		Proposed Technique	
		Fault between Nodes	Distance (km)	Fault between Nodes	Distance (km)
1	0.000	1 & 2	0.000	1 & 2	0.000
2	2.414	2 & 3	2.421	1 & 2	2.410
3	6.437	3 & 4	6.444	2 & 3	6.430
4	10.461	3 & 4	10.445	3 & 4	10.451
5	14.484	4 & 5	14.423	4 & 5	14.474
6	18.507	5 & 6	18.017	5 & 6	18.501
		5 & 6	18.017	5 & 6	18.505
7	22.530	6 & 7	21.871	6 & 7	22.525
		6 & 12	21.871	12 & xx	23.588
8	27.680	7 & 8	26.721	7 & 8	27.675
		7 & 8	26.721	7 & 8	27.676
9	30.094	8 & 9	28.965	8 & 9	30.090
		8 & 13	29.016	13 & 14	30.137
		8 & 13	29.016	13 & 14	30.138
10	34.600	9 & 10	32.936	9 & 10	34.566
		14 & xx	33.142	14 & xx	34.954
		15 & 16	33.142	15 & 16	34.419
		15 & 17	33.142	15 & 17	34.418
11	37.014	10 & 11	35.131	10 & 11	37.006
		14 & xx	35.409	14 & xx	36.636
		16 & xx	35.409	16 & xx	36.819
		17 & xx	35.409	17 & xx	36.795

Note: xx indicate that fault is identified beyond the last node of the line.

Table 5.2. Multiple fault location estimates for the single-phase-to-ground fault cases between node 12 and 21 when the fault resistance is 0.05 ohm.

Fault Node Number	Distance of the Fault (km)	Fault Location Estimate by using the			
		Reactive Component Method		Proposed Technique	
		Fault between Nodes	Distance (km)	Fault between Nodes	Distance (km)
12	20.921	6 & 12	20.258	6 & 12	20.835
		6 & 7	20.258	6 & 7	20.892
13	30.094	8 & 13	28.775	8 & 13	30.048
		8 & 9	28.733	8 & 9	29.990
14	32.508	13 & 14	31.210	14 & xx	32.759
		13 & 15	31.210	13 & 15	32.468
		9 & 10	31.077	9 & 10	32.282
15	32.508	13 & 15	31.223	13 & 15	32.482
		13 & 14	31.223	13 & 14	32.777
		9 & 10	31.089	9 & 10	32.297
16	34.922	15 & 16	33.832	16 & xx	35.243
		15 & 17	33.832	17 & xx	35.225
		9 & 10	33.601	9 & 10	34.453
17	34.922	15 & 17	33.833	17 & xx	35.232
		15 & 16	33.833	16 & xx	35.251
		9 & 10	33.601	9 & 10	34.458
18	32.508	9 & 18	30.942	9 & 18	32.471
		9 & 10	30.910	9 & 10	32.421
19	34.922	18 & 19	33.013	19 & xx	35.133
		18 & 20	33.013	19 & 20	35.087
		9 & 10	32.903	10 & 11	34.603
20	35.727	18 & 20	33.806	18 & 20	35.614
		18 & 19	33.806	18 & 19	36.176
		9 & 10	33.666	10 & 11	35.363
21	38.946	20 & 21	37.513	21 & xx	39.519
		10 & 11	37.299	11 & xx	38.303

Note: **xx** indicate that fault is identified beyond the last node of the line.

Table 5.3. Fault location estimates for the single-phase-to-ground fault cases when the fault resistance is 0.05 ohm.

Fault Node Number	Distance of the Fault (km)	Distance Estimated by using the	
		Reactive Component Method (km)	Proposed Technique (km)
1	0.000	0.000	0.000
2	2.414	2.421	2.410
3	6.437	6.444	6.430
4	10.461	10.445	10.451
5	14.484	14.423	14.474
6	18.507	18.017	18.501
7	22.530	21.871	22.525
8	27.680	26.721	27.675
9	30.094	28.965	30.090
10	34.600	32.936	34.566
11	37.014	35.131	37.006
12	20.921	20.258	20.835
13	30.094	28.775	30.048
14	32.508	31.210	32.759
15	32.508	31.223	32.482
16	34.922	33.832	35.243
17	34.922	33.833	35.232
18	32.508	30.942	32.471
19	34.922	33.013	35.133
20	35.727	33.806	35.614
21	38.946	37.513	39.519

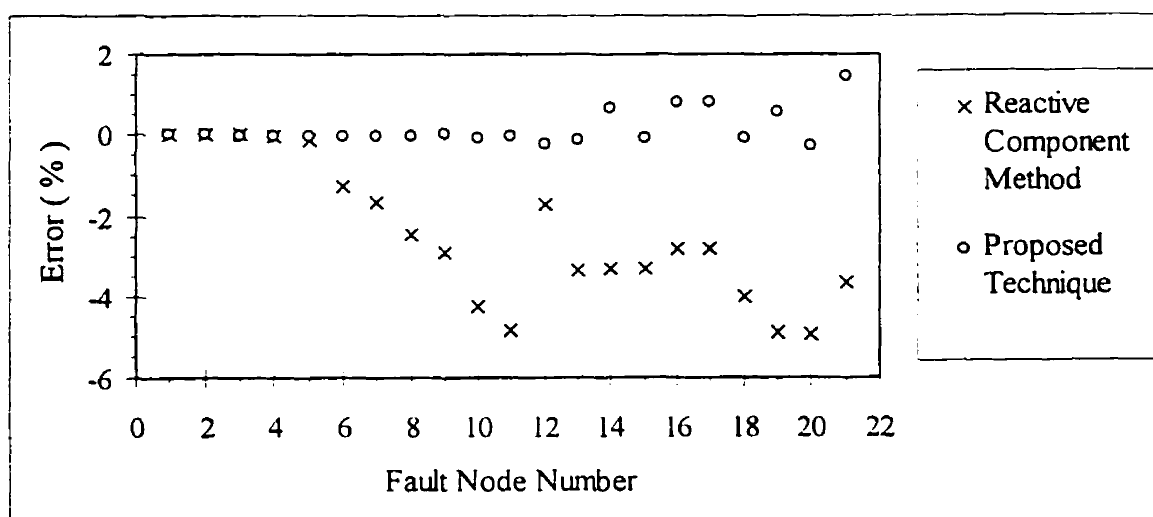


Figure 5.2. Estimation errors for the single-phase-to-ground faults when the fault resistance is 0.05 ohm.

Table 5.4. Fault location estimates for the single-phase-to-ground fault cases when the fault resistance is 5.0 ohm.

Fault Node Number	Distance of the Fault (km)	Distance Estimated by using the	
		Reactive Component Method (km)	Proposed Technique (km)
1	0.000	-0.040	0.026
2	2.414	2.330	2.434
3	6.437	6.274	6.447
4	10.461	10.207	10.462
5	14.484	14.129	14.477
6	18.507	17.659	18.539
7	22.530	21.471	22.562
8	27.680	26.298	27.704
9	30.094	28.541	30.135
10	34.600	32.588	34.611
11	37.014	35.421	37.047
12	20.921	19.875	21.091
13	30.094	28.801	30.022
14	32.508	31.340	32.753
15	32.508	31.348	32.459
16	34.922	34.058	35.275
17	34.922	34.060	35.254
18	32.508	30.869	32.440
19	34.922	33.120	35.145
20	35.727	34.011	35.612
21	38.946	37.856	39.587

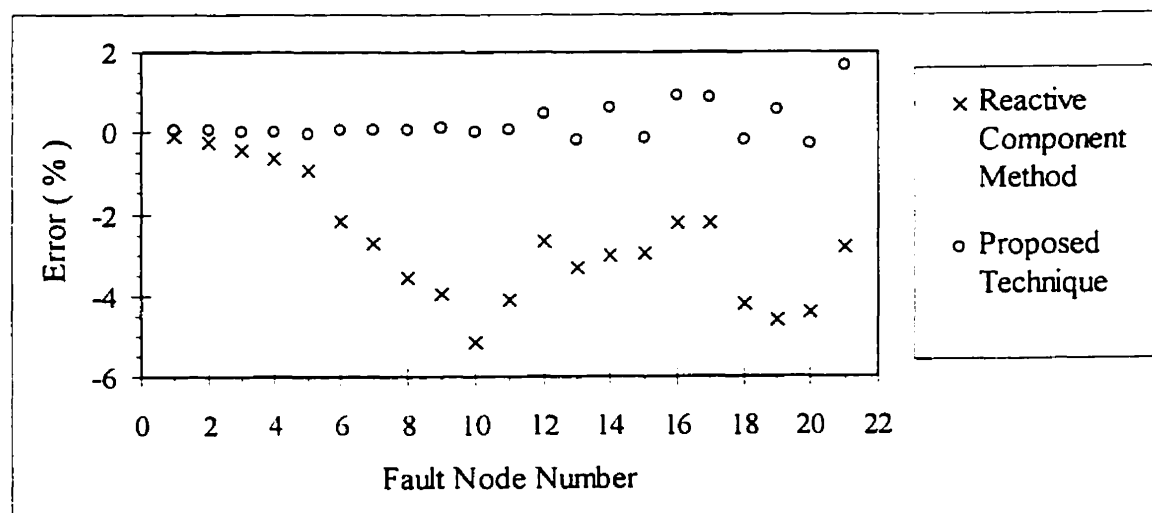


Figure 5.3. Estimation errors for the single-phase-to-ground faults when the fault resistance is 5.0 ohm.

Table 5.5. Fault location estimates for the single-phase-to-ground fault cases when the fault resistance is 10.0 ohm.

Fault Node Number	Distance of the Fault (km)	Distance Estimated by using the	
		Reactive Component Method (km)	Proposed Technique (km)
1	0.000	-0.013	0.023
2	2.414	2.310	2.423
3	6.437	6.183	6.425
4	10.461	10.055	10.431
5	14.484	13.706	14.445
6	18.507	17.493	18.534
7	22.530	21.260	22.563
8	27.680	26.096	27.730
9	30.094	28.311	30.148
10	34.600	33.088	34.630
11	37.014	35.285	37.074
12	20.921	19.679	21.291
13	30.094	28.882	29.991
14	32.508	31.477	32.758
15	32.508	31.502	32.430
16	34.922	34.359	35.266
17	34.922	34.362	35.246
18	32.508	30.864	32.403
19	34.922	33.259	35.125
20	35.727	34.163	35.526
21	38.946	38.303	39.684

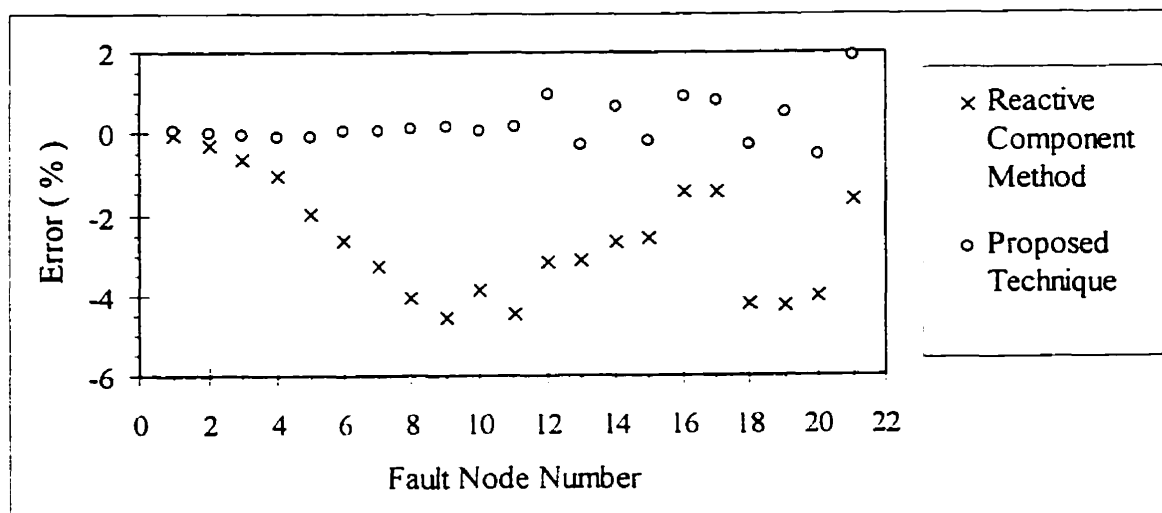


Figure 5.4. Estimation errors for the single-phase-to-ground faults when the fault resistance is 10 ohm.

Table 5.6. Fault location estimates for the single-phase-to-ground fault cases when the fault resistance is 25.0 ohm.

Fault Node Number	Distance of the Fault (km)	Distance Estimated by using the	
		Reactive Component Method (km)	Proposed Technique (km)
1	0.000	0.395	0.000
2	2.414	2.688	2.417
3	6.437	6.495	6.543
4	10.461	10.263	10.471
5	14.484	14.002	14.426
6	18.507	17.712	18.381
7	22.530	21.906	22.479
8	27.680	26.708	27.707
9	30.094	28.919	30.075
10	34.600	33.144	34.622
11	37.014	35.289	37.074
12	20.921	19.998	21.602
13	30.094	29.341	30.155
14	32.508	32.207	32.665
15	32.508	32.252	32.653
16	34.922	35.460	35.311
17	34.922	35.462	35.290
18	32.508	31.152	32.584
19	34.922	34.047	35.178
20	35.727	35.148	35.391
21	38.946	39.661	39.778

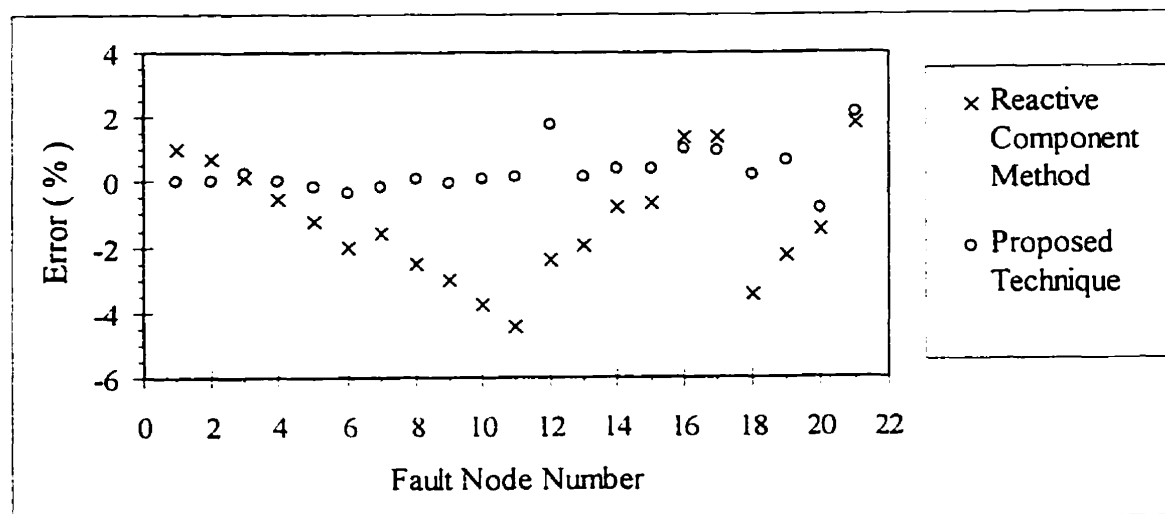


Figure 5.5. Estimation errors for the single-phase-to-ground faults when the fault resistance is 25.0 ohm.

Table 5.7. Fault location estimates for the single-phase-to-ground fault cases when the fault resistance is 50.0 ohm.

Fault Node Number	Distance of the Fault (km)	Distance Estimated by using the	
		Reactive Component Method (km)	Proposed Technique (km)
1	0.000	2.113	0.000
2	2.414	4.359	2.215
3	6.437	8.099	6.218
4	10.461	11.825	10.012
5	14.484	15.553	13.850
6	18.507	19.271	17.722
7	22.530	22.943	22.205
8	27.680	27.580	27.277
9	30.094	29.688	29.794
10	34.600	33.559	34.385
11	37.014	35.622	36.878
12	20.921	21.357	20.963
13	30.094	30.746	29.816
14	32.508	34.180	32.383
15	32.508	34.253	32.341
16	34.922	37.969	35.229
17	34.922	37.979	35.175
18	32.508	32.605	33.030
19	34.922	36.137	34.977
20	35.727	37.331	35.957
21	38.946	42.289	39.785

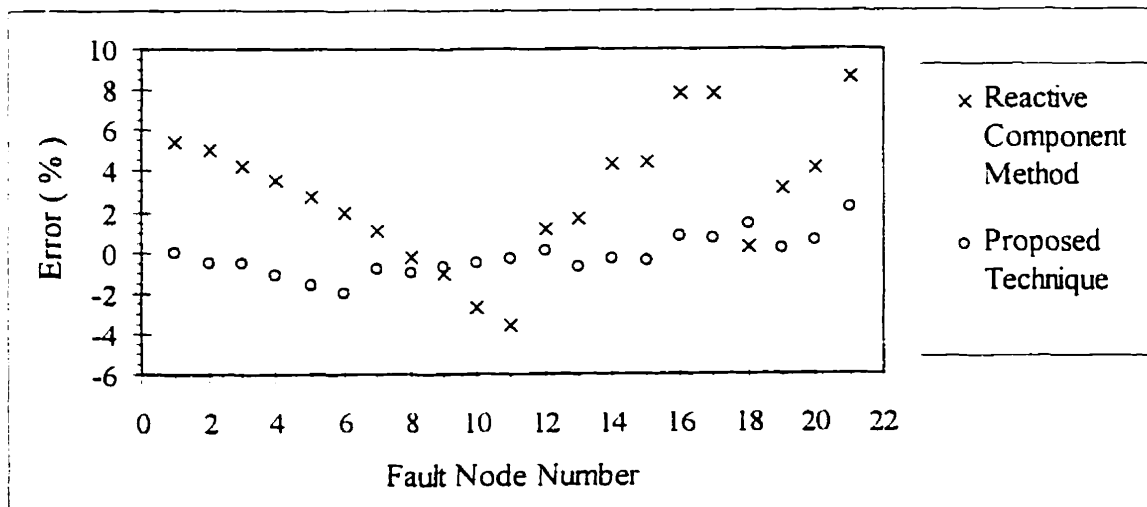


Figure 5.6. Estimation errors for the single-phase-to-ground faults when the fault resistance is 50.0 ohm.

An examination of Figures 5.2 to 5.6 reveals that the distances of the faults estimated by the proposed technique are substantially more accurate than the distances estimated by the reactive components of the apparent impedances. The results also show that the estimates of fault locations provided by the proposed technique are within 1.0% of line length for fault resistances up to 10.0 ohms except for the faults at node 21. For all other cases, it is less than 2.2% of the line length. The reason for the increase in errors with increased fault resistance is due to the fact that the effect of loads is not totally compensated by the proposed technique. With an increase in fault resistance, the fault current reduces, and the load currents increase and, consequently, the errors increase.

5.3.2 Two-phase-to-ground faults

The proposed technique was also tested for estimating locations of two-phase-to-ground faults. Fault resistances used in these studies are listed in Table 5.8. Multiple estimates obtained for faults at different locations for 0.05 ohm fault resistance are listed in Table 5.9. The simulated fault locations and the fault locations estimated from the reactive components of the apparent impedance are also listed in the table. Using the additional information, a single estimate for a location of fault is obtained and are listed in Table 5.10. The fault locations estimated by the proposed technique for other fault resistance situations are listed in Tables 5.11 to 5.14. Estimation errors, expressed as a percentage of the line length, were calculated and are shown in Figures 5.7 to 5.11.

Table 5.8. Fault resistances selected for the two-phase-to-ground faults.

R_f^* (ohm)	R_g^* (ohm)
0.05	0.0
5.0	0.0
10.0	0.0
25.0	0.0
50.0	0.0

* Refer to Figure 2.3 (b), for definition of R_f and R_g .

Table 5.9. Multiple fault location estimates for the two-phase-to-ground fault cases when the fault resistance is 0.05 ohm.

Fault Node Number	Distance of the Fault (km)	Fault Location Estimate by using the			
		Reactive Component Method		Proposed Technique	
		Fault between Nodes	Distance (km)	Fault between Nodes	Distance (km)
1	0.000	1 & 2	0.176	1 & 2	0.000
2	2.414	2 & 3	2.420	1 & 2	2.411
3	6.437	2 & 3	6.405	2 & 3	6.432
4	10.461	3 & 4	10.381	3 & 4	10.456
5	14.484	4 & 5	14.351	4 & 5	14.479
6	18.507	5 & 6	18.319	5 & 6	18.504
7	22.530	6 & 7	22.288	5 & 6	22.529
		12 & xx	22.288	12 & xx	22.765
8	27.680	7 & 8	27.246	8 & 9	27.688
9	30.094	8 & 9	29.629	9 & 10	30.096
10	34.600	9 & 10	34.082	10 & 11	34.560
11	37.014	10 & 11	36.432	10 & 11	37.004
12	20.921	6 & 12	20.663	6 & 12	20.866
		6 & 7	20.663	6 & 7	20.895

Note: **xx** indicate that fault is identified beyond the last node of the line.

An examination of the results shows that the distances of the faults estimated by the proposed technique are substantially more accurate than those estimated by the reactive components of apparent impedances. The results also show that the estimates of fault locations provided by the proposed technique are within 0.9% of the line length except that the estimate is within 1.9% of the line length for the fault at node 12.

Table 5.10. Fault location estimates for the two-phase-to-ground fault cases when the fault resistance is 0.05 ohm.

Fault Node Number	Distance of the Fault (km)	Distance Estimated by using the	
		Reactive Component Method (km)	Proposed Technique (km)
1	0.000	0.176	0.000
2	2.414	2.420	2.411
3	6.437	6.405	6.432
4	10.461	10.381	10.456
5	14.484	14.351	14.479
6	18.507	18.319	18.504
7	22.530	22.288	22.529
8	27.680	27.246	27.688
9	30.094	29.629	30.096
10	34.600	34.082	34.560
11	37.014	36.432	37.004
12	20.921	20.663	20.866

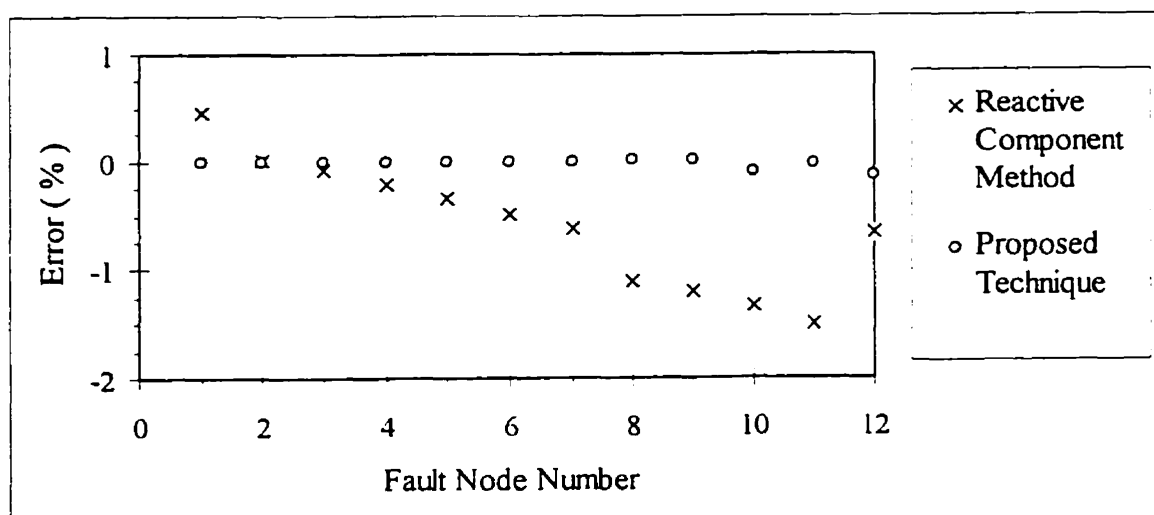


Figure 5.7. Estimation errors for the two-phase-to-ground faults when the fault resistance is 0.05 ohm.

Table 5.11. Fault location estimates for the two-phase-to-ground fault cases when the fault resistance is 5.0 ohm.

Fault Node Number	Distance of the Fault (km)	Distance Estimated by using the	
		Reactive Component Method (km)	Proposed Technique (km)
1	0.000	0.322	0.000
2	2.414	2.266	2.397
3	6.437	6.209	6.464
4	10.461	10.153	10.504
5	14.484	14.098	14.539
6	18.507	18.046	18.552
7	22.530	21.753	22.580
8	27.680	27.023	27.806
9	30.094	29.393	30.230
10	34.600	33.809	34.801
11	37.014	36.120	37.190
12	20.921	20.340	21.267

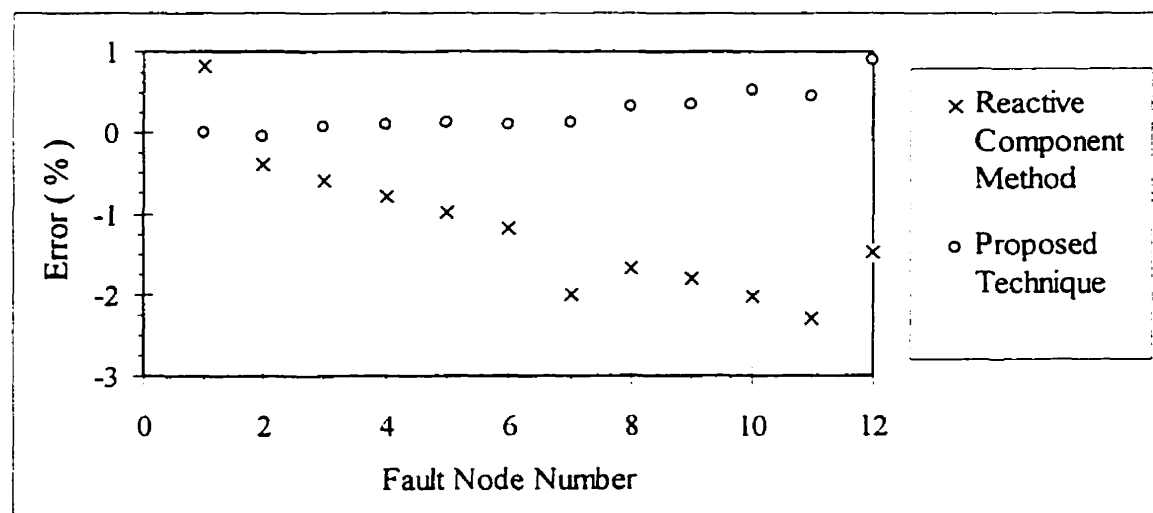


Figure 5.8. Estimation errors for the two-phase-to-ground faults when the fault resistance is 5.0 ohm.

Table 5.12. Fault location estimates for the two-phase-to-ground fault cases when the fault resistance is 10.0 ohm.

Fault Node Number	Distance of the Fault (km)	Distance Estimated by using the	
		Reactive Component Method (km)	Proposed Technique (km)
1	0.000	-0.108	0.000
2	2.414	2.261	2.309
3	6.437	6.211	6.431
4	10.461	10.158	10.490
5	14.484	14.102	14.537
6	18.507	18.023	18.568
7	22.530	21.952	22.632
8	27.680	27.019	27.856
9	30.094	29.379	30.285
10	34.600	33.797	34.926
11	37.014	36.094	37.335
12	20.921	20.371	21.515

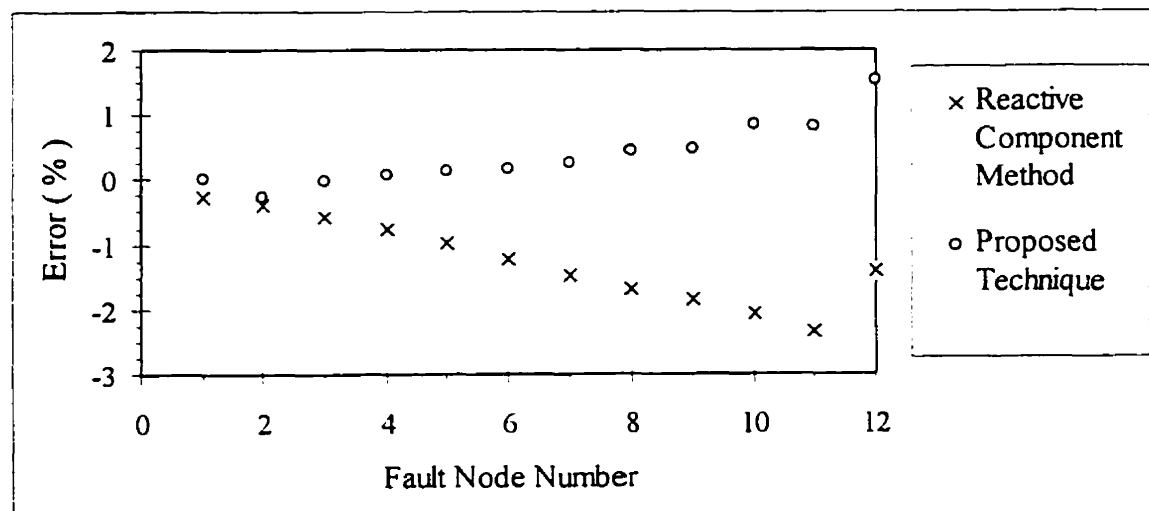


Figure 5.9. Estimation errors for the two-phase-to-ground faults when the fault resistance is 10.0 ohm.

Table 5.13. Fault location estimates for the two-phase-to-ground fault cases when the fault resistance is 25.0 ohm.

Fault Node Number	Distance of the Fault (km)	Distance Estimated by using the	
		Reactive Component Method (km)	Proposed Technique (km)
1	0.000	0.483	0.000
2	2.414	2.896	2.171
3	6.437	6.828	6.462
4	10.461	10.780	10.444
5	14.484	14.725	14.489
6	18.507	18.665	18.465
7	22.530	22.332	22.629
8	27.680	27.260	27.768
9	30.094	29.544	30.132
10	34.600	33.675	34.911
11	37.014	35.901	37.348
12	20.921	20.872	21.649

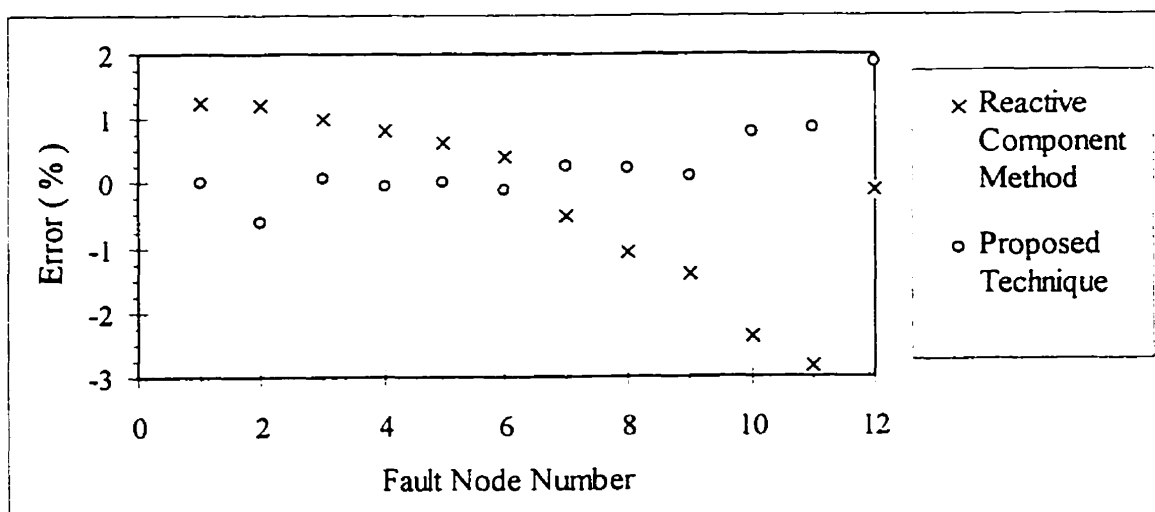


Figure 5.10. Estimation errors for the two-phase-to-ground faults when the fault resistance is 25.0 ohm.

Table 5.14. Fault location estimates for the two-phase-to-ground fault cases when the fault resistance is 50.0 ohm.

Fault Node Number	Distance of the Fault (km)	Distance Estimated by using the	
		Reactive Component Method (km)	Proposed Technique (km)
1	0.000	3.474	0.000
2	2.414	5.763	2.364
3	6.437	9.571	6.519
4	10.461	13.352	10.506
5	14.484	17.147	14.502
6	18.507	20.935	18.594
7	22.530	24.552	22.601
8	27.680	29.241	27.625
9	30.094	31.400	30.002
10	34.600	35.382	34.479
11	37.014	37.538	37.007
12	20.921	23.173	20.647

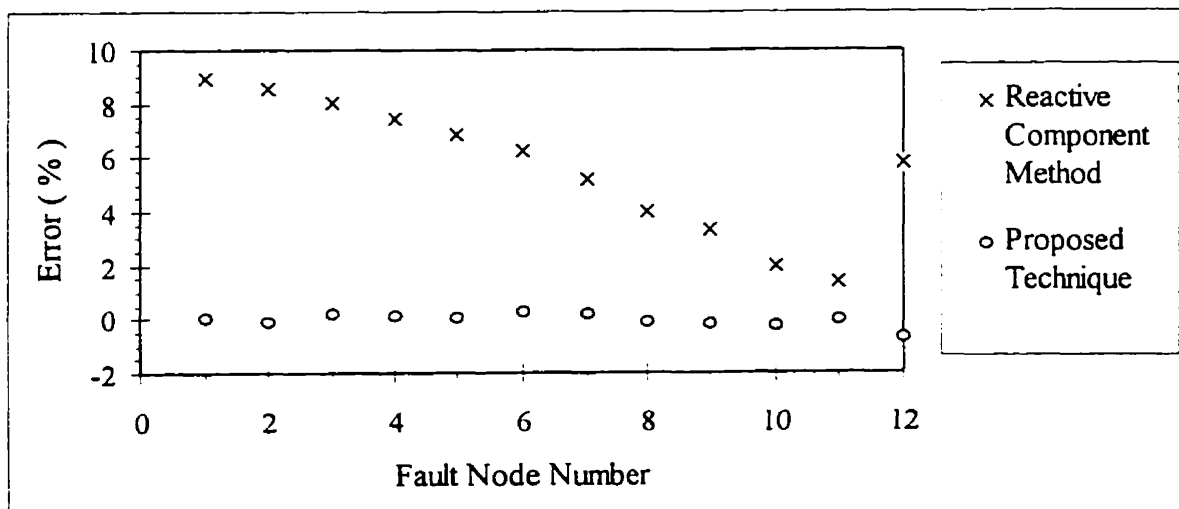


Figure 5.11. Estimation errors for the two-phase-to-ground faults when the fault resistance is 50.0 ohm.

5.3.3 Phase-to-phase faults

The proposed technique was also tested for estimating locations of phase-to-phase faults. Fault resistance values of 0.05, 5.0, 10.0, 25.0 and 50.0 ohms were used in these cases also. Multiple estimates obtained for faults at different locations for 0.05 ohm fault resistance are listed in Table 5.15. Using additional information, single estimates for each fault location are obtained. Those estimates are listed in Table 5.16. The fault locations estimated by the proposed technique for other fault resistance situations are listed in Tables 5.17 to 5.20. The estimation errors, expressed as a percentage of the line length, were calculated and are shown in Figures 5.12 to 5.16.

Table 5.15. Multiple fault location estimates for the phase-to-phase fault cases when the fault resistance is 0.05 ohm.

Fault Node Number	Distance of the Fault (km)	Fault Location Estimate by using the			
		Reactive Component Method		Proposed Technique	
		Fault between Nodes	Distance (km)	Fault between Nodes	Distance (km)
1	0.000	1 & 2	-0.001	1 & 2	0.000
2	2.414	2 & 3	2.417	1 & 2	2.408
3	6.437	2 & 3	6.438	2 & 3	6.436
4	10.461	3 & 4	10.443	3 & 4	10.457
5	14.484	4 & 5	14.433	4 & 5	14.483
6	18.507	5 & 6	17.999	5 & 6	18.508
7	22.530	6 & 7	21.868	6 & 7	22.517
		12 & xx	21.868	12 & xx	22.606
8	27.680	7 & 8	26.780	8 & 9	27.677
9	30.094	8 & 9	29.066	9 & 10	30.113
10	34.600	9 & 10	33.327	10 & 11	34.598
11	37.014	10 & 11	35.577	10 & 11	37.032
12	20.921	6 & 12	20.280	6 & 12	20.879
		6 & 7	20.280	6 & 7	20.894

Note: xx indicate that fault is identified beyond the last node of the line.

Table 5.16. Fault location estimates for the phase-to-phase fault cases when the fault resistance is 0.05 ohm.

Fault Node Number	Distance of the Fault (km)	Distance Estimated by using the	
		Reactive Component Method (km)	Proposed Technique (km)
1	0.000	-0.001	0.000
2	2.414	2.417	2.408
3	6.437	6.438	6.436
4	10.461	10.443	10.457
5	14.484	14.433	14.483
6	18.507	17.999	18.508
7	22.530	21.868	22.517
8	27.680	26.780	27.677
9	30.094	29.066	30.113
10	34.600	33.327	34.598
11	37.014	35.577	37.032
12	20.921	20.280	20.879

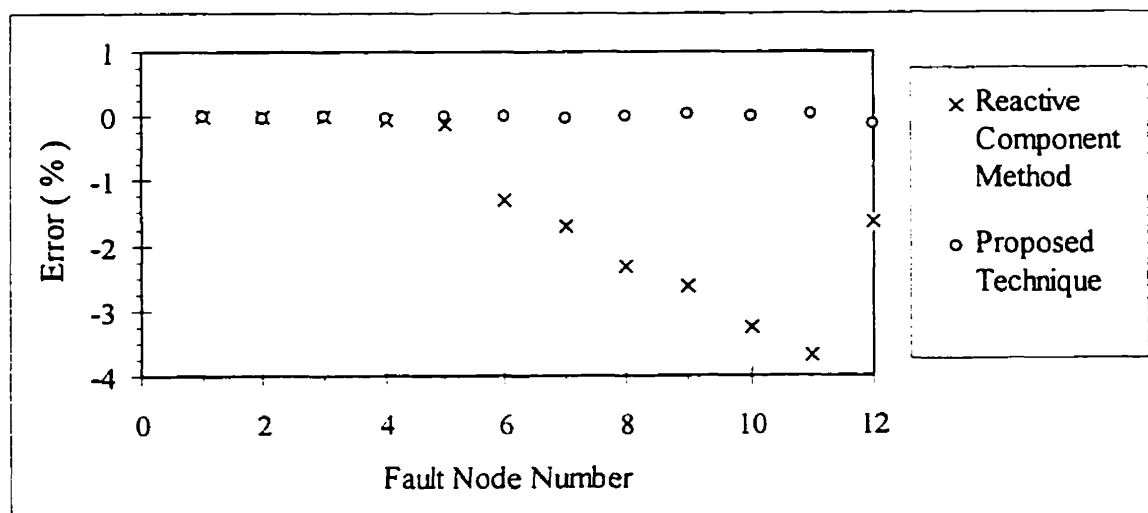


Figure 5.12. Estimation errors for the phase-to-phase faults when the fault resistance is 0.05 ohm.

Table 5.17. Fault location estimates for the phase-to-phase fault cases when the fault resistance is 5.0 ohm.

Fault Node Number	Distance of the Fault (km)	Distance Estimated by using the	
		Reactive Component Method (km)	Proposed Technique (km)
1	0.000	-0.084	0.028
2	2.414	2.308	2.434
3	6.437	6.278	6.449
4	10.461	10.233	10.465
5	14.484	14.176	14.482
6	18.507	17.695	18.533
7	22.530	21.534	22.576
8	27.680	26.431	27.829
9	30.094	28.705	30.127
10	34.600	32.940	34.610
11	37.014	35.122	37.055
12	20.921	19.979	21.218

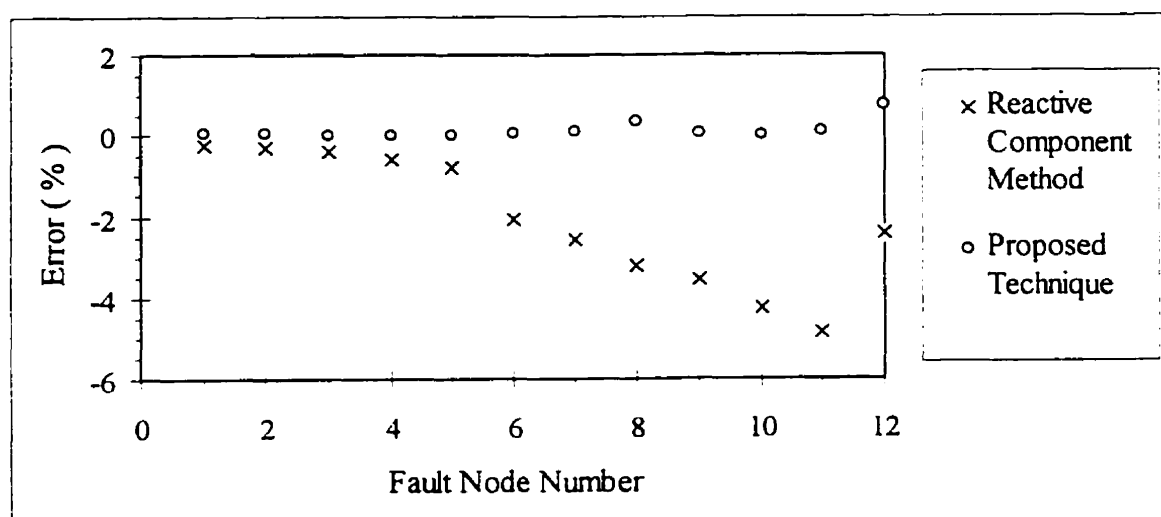


Figure 5.13. Estimation errors for the phase-to-phase faults when the fault resistance is 5.0 ohm.

Table 5.18. Fault location estimates for the phase-to-phase fault cases when the fault resistance is 10.0 ohm.

Fault Node Number	Distance of the Fault (km)	Distance Estimated by using the	
		Reactive Component Method (km)	Proposed Technique (km)
1	0.000	-0.115	0.047
2	2.414	2.244	2.448
3	6.437	6.162	6.456
4	10.461	10.070	10.465
5	14.484	13.676	14.487
6	18.507	17.493	18.547
7	22.530	21.302	22.609
8	27.680	26.187	27.965
9	30.094	28.447	30.132
10	34.600	32.717	34.682
11	37.014	34.908	37.088
12	20.921	19.775	21.537

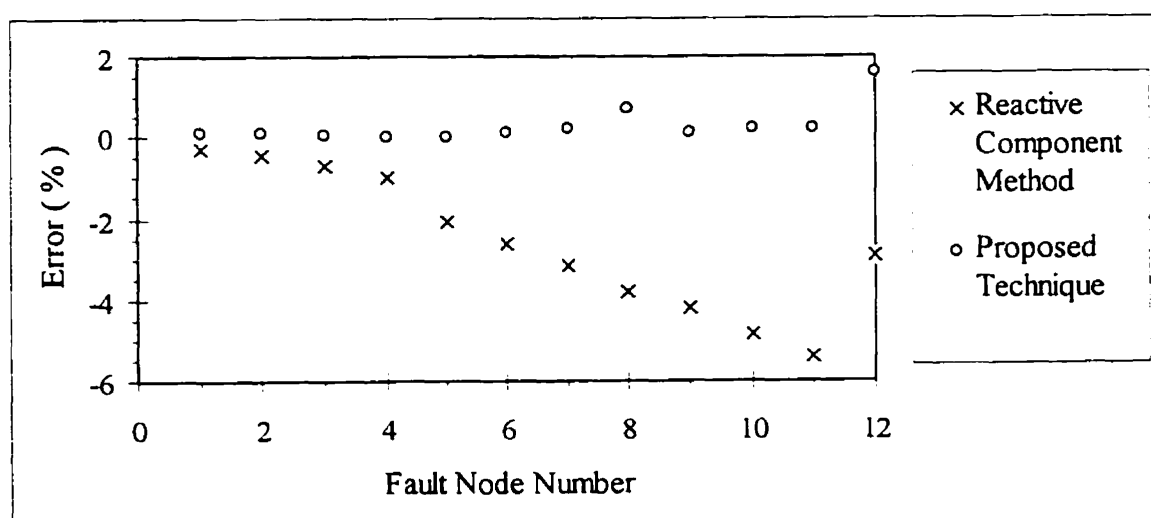


Figure 5.14. Estimation errors for the phase-to-phase faults when the fault resistance is 10.0 ohm.

Table 5.19. Fault location estimates for the phase-to-phase fault cases when the fault resistance is 25.0 ohm.

Fault Node Number	Distance of the Fault (km)	Distance Estimated by using the	
		Reactive Component Method (km)	Proposed Technique (km)
1	0.000	-0.037	0.000
2	2.414	2.258	2.377
3	6.437	6.077	6.361
4	10.461	9.806	10.368
5	14.484	13.586	14.363
6	18.507	17.358	18.366
7	22.530	21.109	22.546
8	27.680	26.136	28.386
9	30.094	28.375	30.129
10	34.600	33.369	34.740
11	37.014	35.606	37.153
12	20.921	19.633	20.676

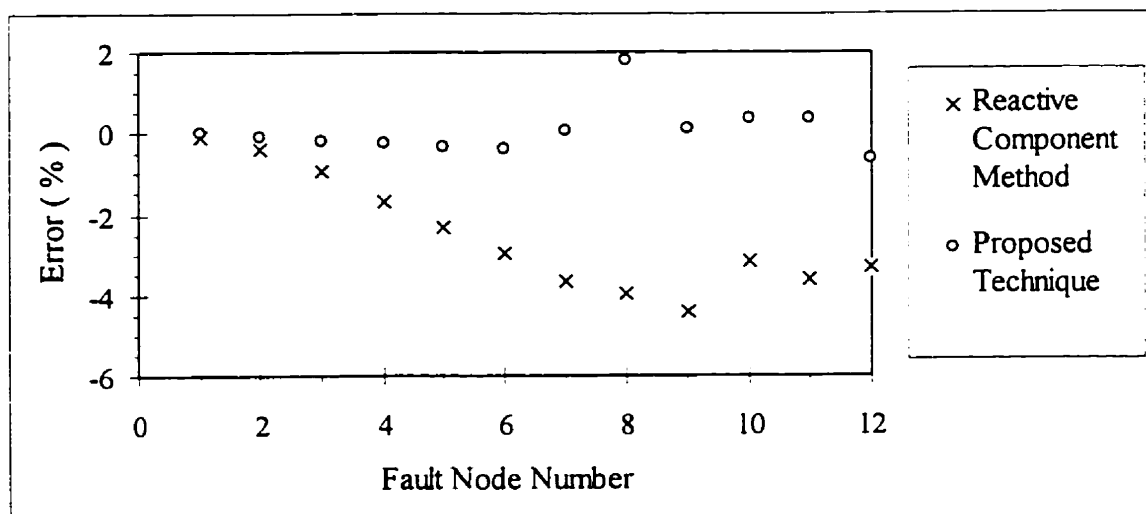


Figure 5.15. Estimation errors for the phase-to-phase faults when the fault resistance is 25.0 ohm.

Table 5.20. Fault location estimates for the phase-to-phase fault cases when the fault resistance is 50.0 ohm.

Fault Node Number	Distance of the Fault (km)	Distance Estimated by using the	
		Reactive Component Method (km)	Proposed Technique (km)
1	0.000	0.527	0.000
2	2.414	2.818	2.139
3	6.437	6.604	6.019
4	10.461	10.365	9.925
5	14.484	14.290	13.875
6	18.507	18.384	17.818
7	22.530	22.224	22.084
8	27.680	27.095	28.175
9	30.094	29.359	29.652
10	34.600	33.634	34.402
11	37.014	35.877	36.881
12	20.921	20.687	19.906

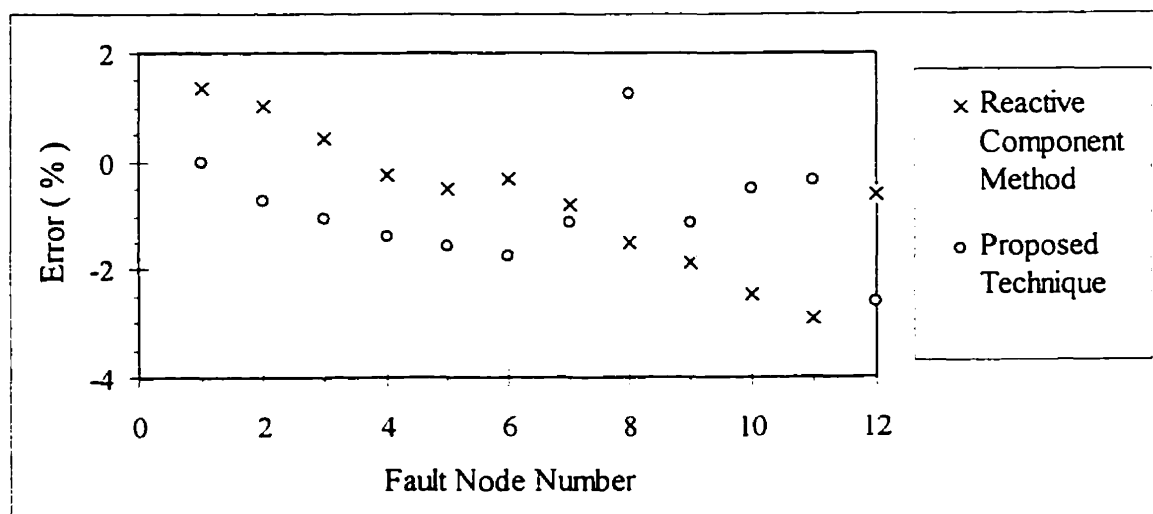


Figure 5.16. Estimation errors for the phase-to-phase faults when the fault resistance is 50.0 ohm.

An examination of the results shows that the distances of the faults estimated by the proposed technique are substantially more accurate than those estimated by the reactive components of apparent impedances. The results also show that the estimates of fault locations provided by the proposed technique are within 0.8% of the line length up to 25.0 ohm fault resistance except that the estimate is within 1.6% of the line length for the fault at node 12. For a 50.0 ohm fault resistance, the estimation errors are less than 2.7% of the line length.

5.3.4 Balanced three-phase faults

The proposed technique was tested for estimating locations of balanced three-phase faults. Fault resistance values used are the same as listed in Table 5.8. Fault resistance values of 0.05, 5.0, 10.0, 25.0 and 50.0 ohms were used in these cases also. Multiple estimates obtained for faults at different locations for 0.05 ohm fault resistance are listed in Table 5.21. Using additional information, single estimates for each fault location are obtained. Those estimates are listed in Table 5.22. The fault locations estimated by the proposed technique for other fault resistance situations are listed in Tables 5.23 to 5.26. The estimation errors, expressed as a percentage of the line length, were calculated and are shown in Figures 5.17 to 5.21.

An examination of the results shows that the distances of the faults estimated by the proposed technique are substantially more accurate than those estimated by the reactive components of apparent impedances. The results also show that the estimates of fault locations provided by the proposed technique are within 1.25% of the line length.

Table 5.21. Multiple fault location estimates for the balanced three-phase fault cases when the fault resistance is 0.05 ohm.

Fault Node Number	Distance of the Fault (km)	Fault Location Estimate by using the			
		Reactive Component Method		Proposed Technique	
		Fault between Nodes	Distance (km)	Fault between Nodes	Distance (km)
1	0.000	1 & 2	0.024	1 & 2	0.000
2	2.414	2 & 3	2.465	1 & 2	2.305
3	6.437	3 & 4	6.557	2 & 3	6.193
4	10.461	4 & 5	10.671	3 & 4	10.205
5	14.484	5 & 6	14.800	4 & 5	14.217
6	18.507	6 & 7	18.940	5 & 6	18.368
7	22.530	7 & 8	23.064	6 & 7	22.395
		12 & xx	23.087	12 & xx	22.765
8	27.680	8 & 9	27.790	8 & 9	27.457
9	30.094	9 & 10	30.211	9 & 10	30.014
10	34.600	10 & 11	34.726	10 & 11	34.422
11	37.014	10 & 11	37.137	10 & 11	36.900
12	20.921	6 & 12	21.372	6 & 12	20.982
		6 & 7	21.372	6 & 7	20.732

Note: **xx** indicate that fault is identified beyond the last node of the line.

Table 5.22. Fault location estimates for the balanced three-phase fault cases when the fault resistance is 0.05 ohm.

Fault Node Number	Distance of the Fault (km)	Distance Estimated by using the	
		Reactive Component Method (km)	Proposed Technique (km)
1	0.000	0.024	0.000
2	2.414	2.465	2.305
3	6.437	6.557	6.193
4	10.461	10.671	10.205
5	14.484	14.800	14.217
6	18.507	18.940	18.368
7	22.530	23.064	22.395
8	27.680	27.790	27.457
9	30.094	30.211	30.014
10	34.600	34.726	34.422
11	37.014	37.137	36.900
12	20.921	21.372	20.982

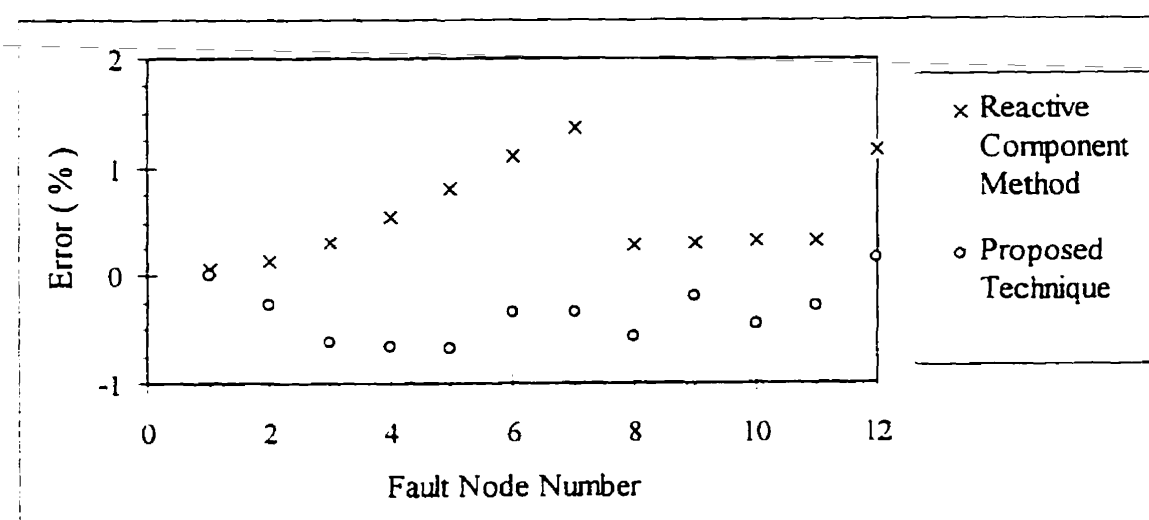


Figure 5.17. Estimation errors for the balanced three-phase faults when the fault resistance is 0.05 ohm.

Table 5.23. Fault location estimates for the balanced three-phase fault cases when the fault resistance is 5.0 ohm.

Fault Node Number	Distance of the Fault (km)	Distance Estimated by using the	
		Reactive Component Method (km)	Proposed Technique (km)
1	0.000	-0.118	0.000
2	2.414	2.343	2.273
3	6.437	6.453	6.253
4	10.461	10.570	10.257
5	14.484	14.690	14.264
6	18.507	18.813	18.273
7	22.530	22.283	22.290
8	27.680	27.393	27.371
9	30.094	29.778	29.877
10	34.600	34.210	34.325
11	37.014	36.571	36.797
12	20.921	21.257	20.885

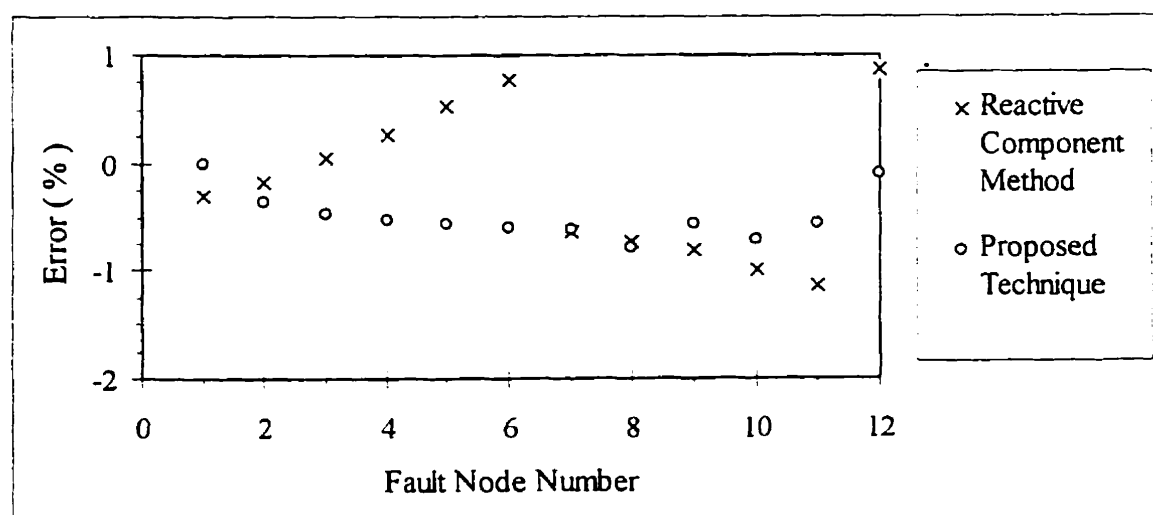


Figure 5.18. Estimation errors for the balanced three-phase faults when the fault resistance is 5.0 ohm.

Table 5.24. Fault location estimates for the balanced three-phase fault cases when the fault resistance is 10.0 ohm.

Fault Node Number	Distance of the Fault (km)	Distance Estimated by using the	
		Reactive Component Method (km)	Proposed Technique (km)
1	0.000	-0.131	0.000
2	2.414	2.338	2.246
3	6.437	6.453	6.220
4	10.461	10.565	10.210
5	14.484	14.677	14.201
6	18.507	18.149	18.202
7	22.530	22.109	22.204
8	27.680	27.161	27.296
9	30.094	29.511	29.760
10	34.600	33.882	34.220
11	37.014	35.580	36.668
12	20.921	20.516	20.768

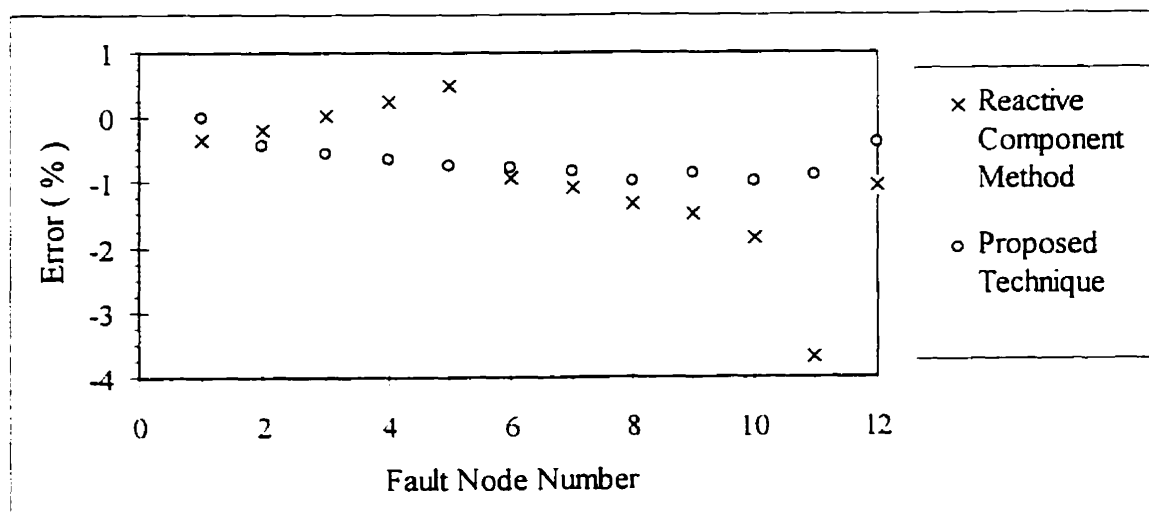


Figure 5.19. Estimation errors for the balanced three-phase faults when the fault resistance is 10.0 ohm.

Table 5.25. Fault location estimates for the balanced three-phase fault cases when the fault resistance is 25.0 ohm.

Fault Node Number	Distance of the Fault (km)	Distance Estimated by using the	
		Reactive Component Method (km)	Proposed Technique (km)
1	0.000	0.479	0.000
2	2.414	2.914	2.275
3	6.437	6.707	6.289
4	10.461	10.600	10.291
5	14.484	14.494	14.283
6	18.507	18.381	18.274
7	22.530	22.241	22.262
8	27.680	26.736	27.384
9	30.094	28.976	29.824
10	34.600	33.124	34.275
11	37.014	35.398	36.719
12	20.921	20.698	20.634

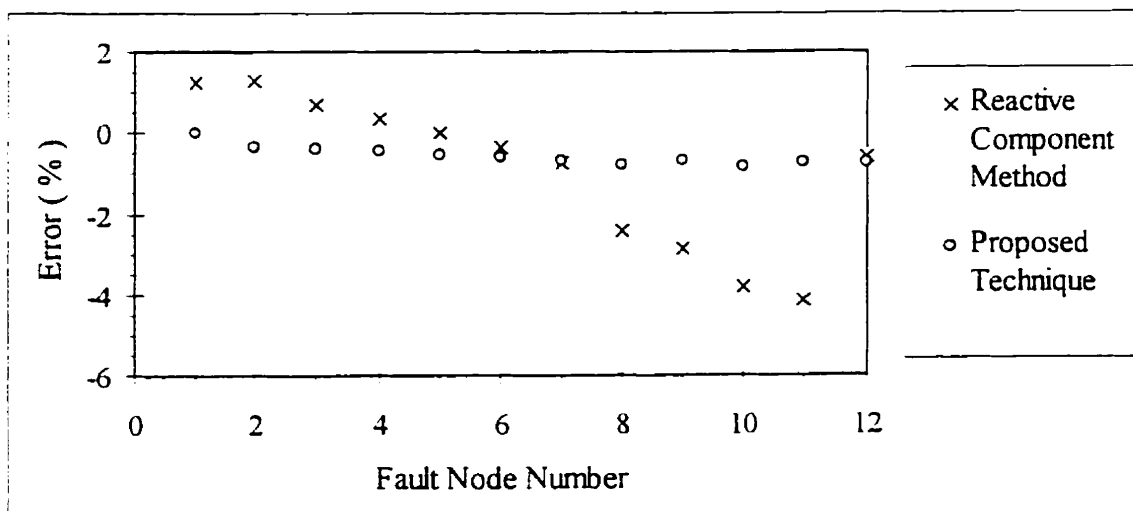


Figure 5.20. Estimation errors for the balanced three-phase faults when the fault resistance is 25.0 ohm.

Table 5.26. Fault location estimates for the balanced three-phase fault cases when the fault resistance is 50.0 ohm.

Fault Node Number	Distance of the Fault (km)	Distance Estimated by using the	
		Reactive Component Method (km)	Proposed Technique (km)
1	0.000	3.349	0.000
2	2.414	5.622	2.273
3	6.437	9.366	6.393
4	10.461	13.103	10.514
5	14.484	16.851	14.607
6	18.507	20.577	18.684
7	22.530	24.206	22.790
8	27.680	28.850	28.067
9	30.094	30.969	30.521
10	34.600	34.920	35.080
11	37.014	37.056	37.489
12	20.921	22.764	20.721

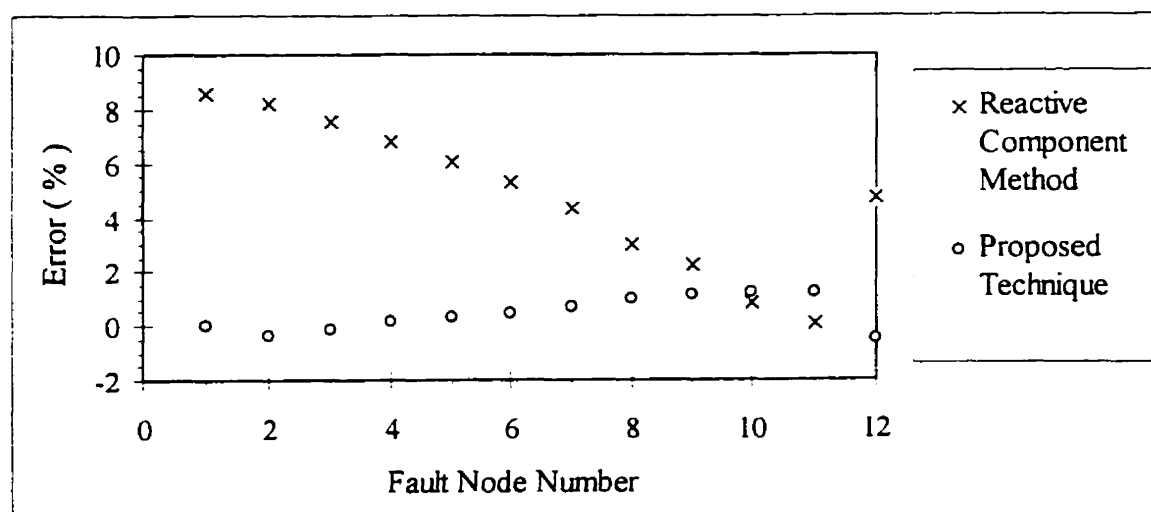


Figure 5.21. Estimation errors for the balanced three-phase when the fault resistance is 50.0 ohm.

5.4 Summary

The technique for estimating locations of shunt faults on a radial distribution circuit which has tapped loads and laterals, has been tested using simulated fault data. Test results for single-phase-to-ground, two-phase-to-ground, phase-to-phase and balanced three-phase faults have been presented. Fault resistances ranging from 0.05 to 50 ohms were used in these studies. The studies show that the locations of faults estimated by the proposed technique are more accurate than the estimates provided by the reactive components of the apparent impedances. The studies also demonstrate that the accuracy of results provided by the proposed technique is good even if the fault resistances are comparable to the line impedances.

6. SENSITIVITY STUDIES

6.1 Introduction

A technique for estimating location of shunt faults on radial distribution circuits, which include tapped loads and laterals, has been presented in Chapter 4. The technique was tested to evaluate its suitability and test results have been presented Chapter 5. Test results revealed that the locations of faults estimated by the proposed technique are more accurate than the estimates provided by the reactive components of the apparent impedances.

The accuracy of the fault location estimates depends on the accuracy of the input parameters. The accuracy of the voltage and current phasors depends on the quality of transducers that sample voltages and currents. Line parameters depend on different factors including the resistivity of the soil and ambient temperature. Accuracy of the load estimates depends on the estimated pre-fault voltage and current phasors. It also depends on the technique used to estimate the loads at the taps.

Sensitivity studies were performed to determine the effect of the errors in the input parameters on the accuracy of the proposed technique. Several fault locations and fault resistance values were used. The distribution system used in Chapter 5 was also used for the studies reported in this chapter. The results obtained by the proposed technique were also compared with the simulated location of faults and the estimates provided by the reactive component method. Some of the results are presented in this chapter.

6.2 Distribution System Parameters Selected for the Studies

The model of the SaskPower distribution circuit, shown in Figure 5.1, was used for the sensitivity studies reported in this chapter. Input parameters identified for the studies are the estimates of the voltage and current phasors, the line length, the line impedance per unit length, the largest load and load response constants of the equivalent load.

All errors in the input data were introduced during the off-line process of estimating the location of the fault by varying the estimated voltage and/or current phasors or by varying the load and line parameters. The ranges of errors in voltage and current phasors were selected considering the IEC standards for voltage and current transformers [52, 53]. Errors in voltage phasor magnitudes were varied from -5% to +5% while errors for current phasors magnitude were varied from -3% to +3%. The angles of the voltage and current phasors were varied from -1° to $+1^\circ$. The cases of voltage and current phasor errors considered in the studies are listed in Tables 6.1 to 6.4.

Errors in the length and impedance per unit length were varied from -3% and +3%. The impact of load errors was studied by varying the largest load from -20% to +20% of the value used in Chapter 5. The equivalent load response constants were varied from -10% to +10%. The cases of varying the line and load parameters are listed in Table 6.5. A total of 104 cases were identified for the sensitivity studies for each location and for each type of fault. These are reported in the following sections.

6.3 Studies Conducted

Single-phase-to-ground and phase-to-phase faults were identified as possible candidates for sensitivity studies. All faults start as single-phase-to-ground or phase-to-phase faults and sometimes extend to two-phase-to-ground or three-phase faults. It was, therefore, decided to perform sensitivity studies for single-phase-to-ground and phase-to-phase fault situations only. Faults were applied at all nodes (node 1 to node 21). Different fault resistance values were used. The procedure described in Chapter 4 was used for estimating the locations of faults. Some of the results for phase B-to-ground and phase B-to-phase C faults are reported in the following sections.

Table 6.1. Cases of estimated voltage phasor variations.

Case Number	Voltage	
	Magnitude (%)	Phase Angle (Degree)
1	+5.0	0.0
2	+3.0	0.0
3	+1.0	0.0
4	-1.0	0.0
5	-3.0	0.0
6	-5.0	0.0
7	0.0	+1.0
8	0.0	+0.5
9	0.0	-0.5
10	0.0	-1.0
11	+1.0	-0.25
12	+1.0	+0.25
13	-1.0	-0.25
14	-1.0	+0.25
15	+3.0	-0.5
16	+3.0	+0.5
17	-3.0	-0.5
18	-3.0	+0.5
19	+5.0	-1.0
20	+5.0	+1.0
21	-5.0	-1.0
22	-5.0	+1.0

Table 6.2. Cases of estimated current phasor variations.

Case Number	Current	
	Magnitude (%)	Phase Angle (Degree)
23	+3.0	0.0
24	+1.0	0.0
25	-1.0	0.0
26	-3.0	0.0
27	0.0	+1.0
28	0.0	+0.5
29	0.0	-0.5
30	0.0	-1.0
31	+1.0	-0.5
32	+1.0	+0.5
33	-1.0	-0.5
34	-1.0	+0.5
35	+3.0	-1.0
36	+3.0	+1.0
37	-3.0	-1.0
38	-3.0	+1.0

Table 6.3. Cases of estimated voltage and current phasors combined magnitude variations.

Case Number	Voltage Magnitude (%)	Current Magnitude (%)
39	+5.0	+3.0
40	+5.0	+1.0
41	+5.0	-1.0
42	+5.0	-3.0
43	+3.0	+3.0
44	+3.0	+1.0
45	+3.0	-1.0
46	+3.0	-3.0
47	+1.0	+3.0
48	+1.0	+1.0
49	+1.0	-1.0
50	+1.0	-3.0
51	-1.0	+3.0
52	-1.0	+1.0
53	-1.0	-1.0
54	-1.0	-3.0
55	-3.0	+3.0
56	-3.0	+1.0
57	-3.0	-1.0
58	-3.0	-3.0
59	-5.0	+3.0
60	-5.0	+1.0
61	-5.0	-1.0
62	-5.0	-3.0

Table 6.4. Cases of estimated voltage and current phasors combined magnitude and phase angle variations.

Case Number	Voltage		Current	
	Magnitude (%)	Phase Angle (Degree)	Magnitude (%)	Phase Angle (Degree)
63	+5.0	+1.0	+3.0	+1.0
64	+5.0	+1.0	+1.0	+0.5
65	+5.0	+1.0	-1.0	-0.5
66	+5.0	+1.0	-3.0	-1.0
67	+3.0	+0.5	+3.0	+1.0
68	+3.0	+0.5	+1.0	+0.5
69	+3.0	+0.5	-1.0	-0.5
70	+3.0	+0.5	-3.0	-1.0
71	+1.0	+0.25	+3.0	+1.0
72	+1.0	+0.25	+1.0	+0.5
73	+1.0	+0.25	-1.0	-0.5
74	+1.0	+0.25	-3.0	-1.0
75	-1.0	+0.25	+3.0	+1.0
76	-1.0	-0.25	+1.0	+0.5
77	-1.0	-0.25	-1.0	-0.5
78	-1.0	-0.25	-3.0	-1.0
79	-3.0	-0.5	+3.0	+1.0
80	-3.0	-0.5	+1.0	+0.5
81	-3.0	-0.5	-1.0	-0.5
82	-3.0	-0.5	-3.0	-1.0
83	-5.0	-1.0	+3.0	+1.0
84	-5.0	-1.0	+1.0	+0.5
85	-5.0	-1.0	-1.0	-0.5
86	-5.0	-1.0	-3.0	-1.0

Table 6.5. Cases of line and load parameters variations.

Case Number	Line and Load Parameter Variations			
	Line Section Length (%)	Line Section Impedance per km (%)	Largest Load (%)	Equivalent Load Response Constant (%)
87	+3.0	0.0	0.0	0.0
88	+1.0	0.0	0.0	0.0
89	-1.0	0.0	0.0	0.0
90	-3.0	0.0	0.0	0.0
91	0.0	+3.0	0.0	0.0
92	0.0	+1.0	0.0	0.0
93	0.0	-1.0	0.0	0.0
94	0.0	-3.0	0.0	0.0
95	0.0	0.0	+20.0	0.0
96	0.0	0.0	+10.0	0.0
97	0.0	0.0	+5.0	0.0
98	0.0	0.0	-5.0	0.0
99	0.0	0.0	-10.0	0.0
100	0.0	0.0	-20.0	0.0
101	0.0	0.0	0.0	+10.0
102	0.0	0.0	0.0	+5.0
103	0.0	0.0	0.0	-5.0
104	0.0	0.0	0.0	-10.0

6.3.1 Single-phase-to-ground faults

Sensitivity of the proposed technique was tested for estimating the locations of single-phase-to-ground faults. Fault resistance values of 10.0 ohms and 15.0 ohms were used in these cases, considering 10.0 ohms for tower footing resistance and 5.0 ohms for arc resistance. The results for faults at node 7, when the fault resistance is 15.0 ohms are shown. The results for other cases are similar.

The location of the fault was calculated for different errors in the magnitude of the voltage phasors of the faulted phase. Estimation errors, expressed as percentage of the line length, are shown in Figure 6.1. Figure 6.2 shows the estimation errors when the estimate of the phase angle of the phasor is in error. Table 6.6 shows the error in the location estimates due to errors in the magnitudes and angles of the voltage phasor of the faulted phase. This results show that the errors change linearly with the change of phasor magnitude error when the reactive component method is used. These variations are non-linear for the proposed technique. This is due to the non-linear effect of loads. Results also indicate that the proposed technique is less sensitive than reactive component method.

Estimation errors in the location of the fault were also calculated for errors in the magnitudes and phase angles of the current phasor of the faulted phase. These results are shown in Figure 6.3, Figure 6.4 and Table 6.7. These figures and table show that the sensitivity of the proposed technique and the reactive component method are similar.

Tables 6.8 and 6.9 show the estimation errors when the magnitudes and angles of the voltage and current phasors are simultaneously in error. These tables show that the sensitivity of the proposed technique is similar to that of the reactive component method.

Estimation errors in the location of the fault were also calculated for errors in the line and load parameters. The results, shown in Figures 6.5 to 6.8, lead to the conclusion that the sensitivity of the proposed technique is similar to that of the reactive component method. Load parameter variations do not affect the reactive component method while it affects the proposed technique marginally.

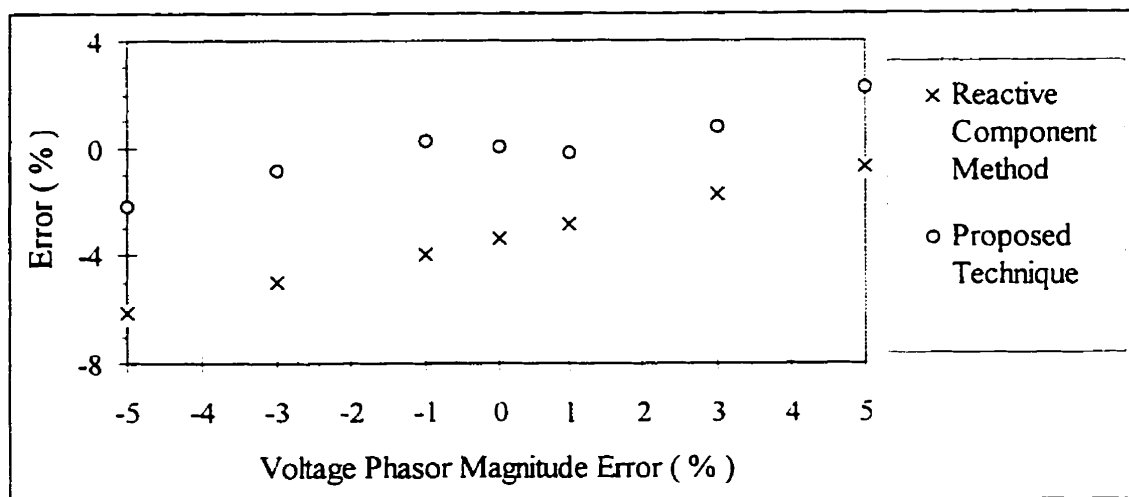


Figure 6.1. Estimation errors for the single-phase-to-ground fault for variation in the magnitude of the estimated voltage phasor.

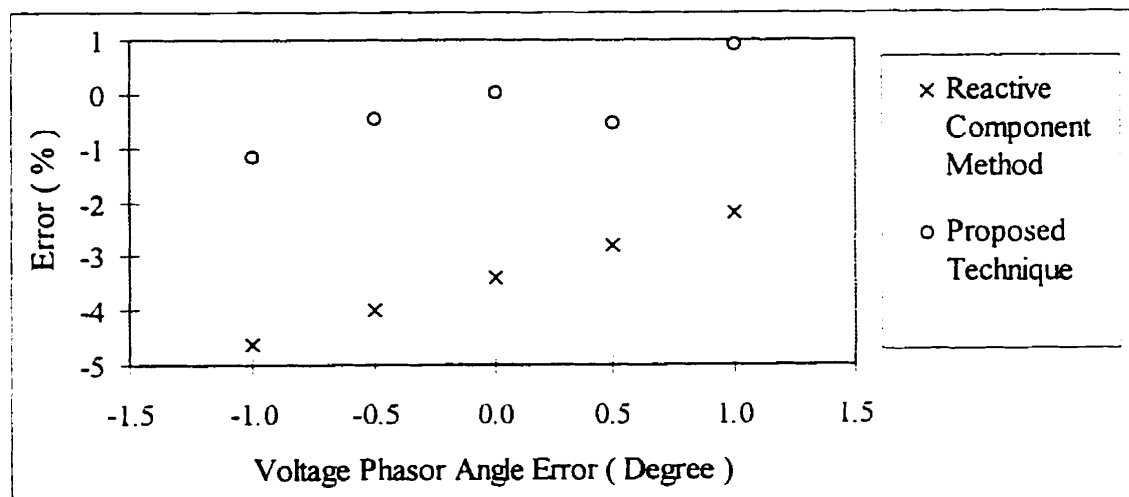


Figure 6.2. Estimation errors for the single-phase-to-ground fault for variation in the angle of the estimated voltage phasor.

Table 6.6. Estimation errors for the single-phase-to-ground fault for combined variation in magnitude and angle of the estimated voltage phasor.

Voltage Phasor		Error in Estimated Fault Location by using the	
Magnitude Error (%)	Phase Angle Error (Degree)	Reactive Component Method (%)	Proposed Technique (%)
-5.0	-1.00	-7.27	-3.38
-5.0	1.00	-4.99	-1.09
-3.0	-0.50	-5.62	-1.51
-3.0	0.50	-4.45	-0.27
-1.0	-0.25	-4.24	0.07
-1.0	0.25	-3.65	0.74
0.0	0.00	-3.40	0.02
1.0	-0.25	-3.16	-0.46
1.0	0.25	-2.55	0.06
3.0	-0.50	-2.39	-0.03
3.0	0.50	-1.15	1.87
5.0	-1.00	-1.95	1.00
5.0	1.00	0.56	3.77

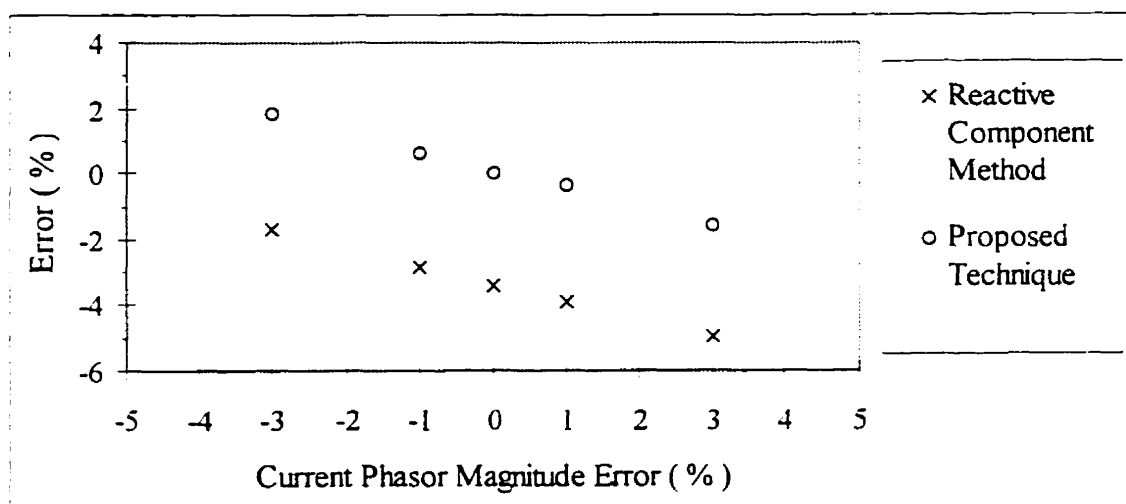


Figure 6.3. Estimation errors for the single-phase-to-ground fault for variation in the magnitude of the estimated current phasor.

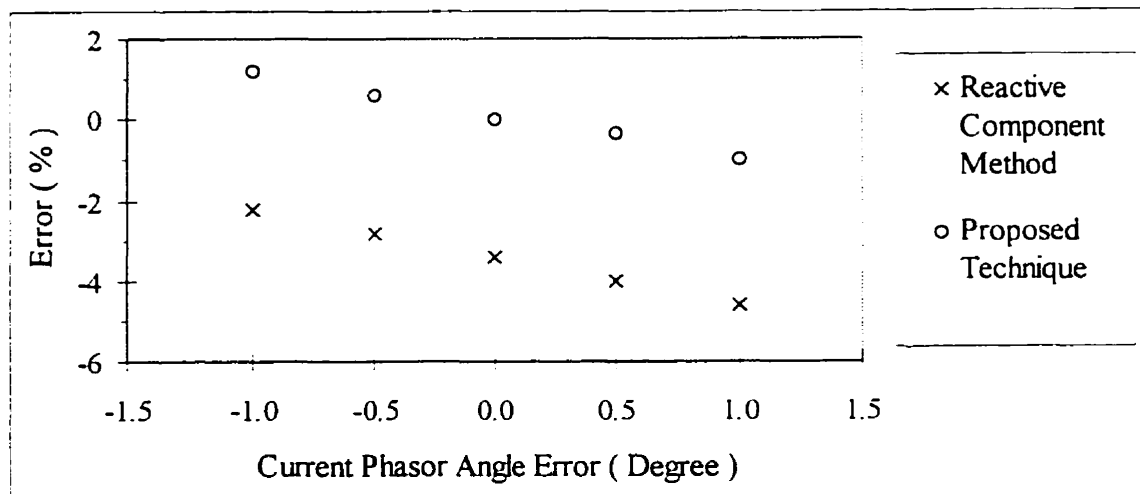


Figure 6.4. Estimation errors for the single-phase-to-ground fault for variation in the angle of the estimated current phasor.

Table 6.7. Estimation errors for the single-phase-to-ground fault for combined variation in magnitude and angle of the estimated current phasor.

Current Phasor		Error in Estimated Fault Location by using the	
Magnitude Error (%)	Phase Angle Error (Degree)	Reactive Component Method (%)	Proposed Technique (%)
-3.0	-1.00	-0.49	3.08
-3.0	1.00	-2.96	0.66
-1.0	-0.50	-2.25	1.22
-1.0	0.50	-3.46	0.03
0.0	0.00	-3.40	0.02
1.0	-0.50	-3.35	0.00
1.0	0.50	-4.54	-0.96
3.0	-1.00	-3.83	-0.35
3.0	1.00	-6.16	-2.78

Table 6.8. Estimation errors for the single-phase-to-ground fault for combined variation in magnitudes of the estimated voltage and current phasors.

Magnitude Error		Error in Estimated Fault Location by using the	
Voltage Phasor (%)	Current Phasor (%)	Reactive Component Method (%)	Proposed Technique (%)
-5.0	-3.0	-4.52	-0.50
-5.0	-1.0	-5.60	-1.63
-5.0	1.0	-6.63	-2.72
-5.0	3.0	-7.63	-3.78
-3.0	-3.0	-3.40	0.53
-3.0	-1.0	-4.50	-0.27
-3.0	1.0	-5.56	-1.41
-3.0	3.0	-6.57	-2.51
-1.0	-3.0	-2.28	2.20
-1.0	-1.0	-3.40	0.89
-1.0	1.0	-4.48	0.01
-1.0	3.0	-5.52	-1.21
0.0	0.0	-3.40	0.02
1.0	-3.0	-1.16	1.38
1.0	-1.0	-2.30	0.22
1.0	1.0	-3.40	-0.81
1.0	3.0	-4.46	-2.02
3.0	-3.0	-0.03	3.02
3.0	-1.0	-1.20	1.52
3.0	1.0	-2.32	-0.28
3.0	3.0	-3.40	-1.95
5.0	-3.0	1.06	4.35
5.0	-1.0	-0.10	2.97
5.0	1.0	-1.25	1.62
5.0	3.0	-2.34	0.03

Table 6.9. Estimation errors for the single-phase-to-ground fault for combined variation in magnitudes and phase angles of the estimated voltage and current phasors.

Voltage Phasor		Current Phasor		Error in Estimated Fault Location by using the	
Magnitude Error (%)	Phase Angle Error (Degree)	Magnitude Error (%)	Phase Angle Error (Degree)	Reactive Component Method (%)	Proposed Technique (%)
-5.0	-1.00	-3.0	-1.00	-4.52	-0.62
-5.0	-1.00	-1.0	-0.50	-6.18	-2.30
-5.0	-1.00	1.0	0.50	-8.35	-4.44
-5.0	-1.00	3.0	1.00	-9.88	-6.02
-3.0	-0.50	-3.0	-1.00	-2.80	0.98
-3.0	-0.50	-1.0	-0.50	-4.50	-0.40
-3.0	-0.50	1.0	0.50	-6.72	-2.60
-3.0	-0.50	3.0	1.00	-8.29	-4.23
-1.0	-0.25	-3.0	-1.00	-1.36	2.72
-1.0	-0.25	-1.0	-0.50	-3.10	0.89
-1.0	-0.25	1.0	0.50	-5.37	-1.11
-1.0	-0.25	3.0	1.00	-6.97	-2.87
0.0	0.00	0.0	0.0	-3.40	0.02
1.0	0.25	-3.0	-1.00	0.39	3.60
1.0	0.25	-1.0	-0.50	-1.39	1.42
1.0	0.25	1.0	0.50	-3.70	-1.15
1.0	0.25	3.0	1.00	-5.35	-3.11
3.0	0.50	-3.0	-1.00	1.82	5.46
3.0	0.50	-1.0	-0.50	0.04	3.33
3.0	0.50	1.0	0.50	-2.32	-0.08
3.0	0.50	3.0	1.00	-4.00	-2.71
5.0	1.00	-3.0	-1.00	3.57	7.11
5.0	1.00	-1.0	-0.50	1.75	5.10
5.0	1.00	1.0	0.50	-0.62	2.44
5.0	1.00	3.0	1.00	-2.34	0.21

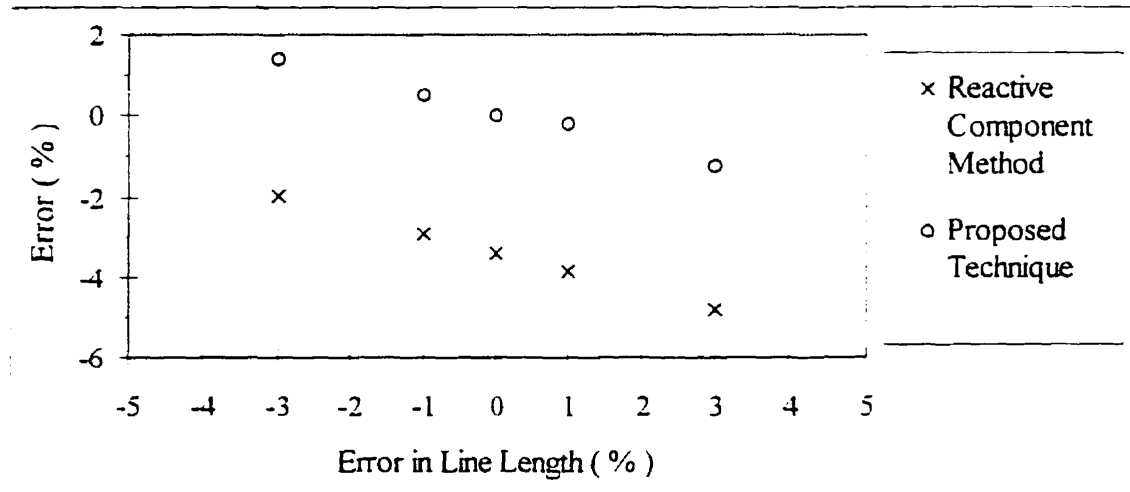


Figure 6.5. Estimation errors for the single-phase-to-ground fault for variation in the line section lengths.

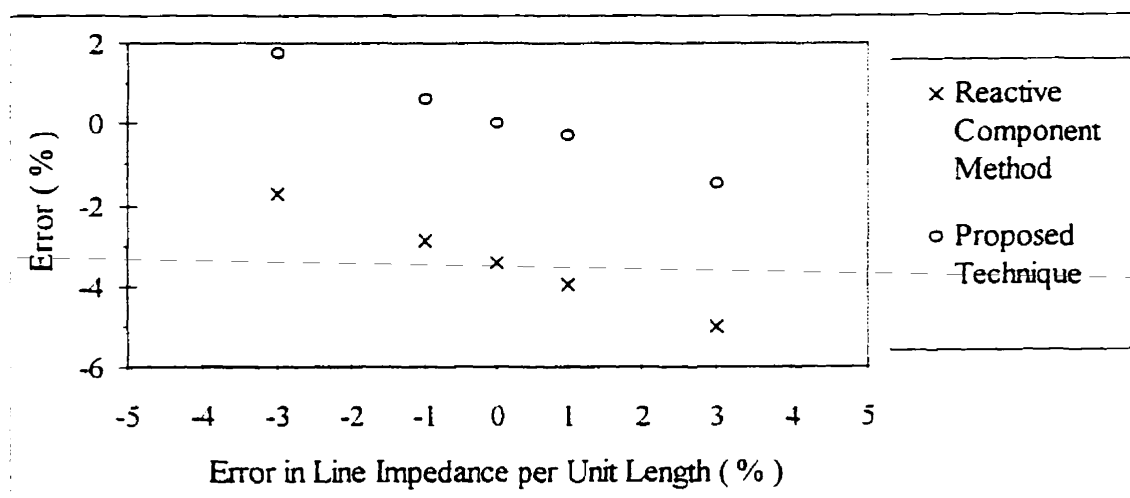


Figure 6.6. Estimation errors for the single-phase-to-ground fault for variation in the line section impedances per unit length.

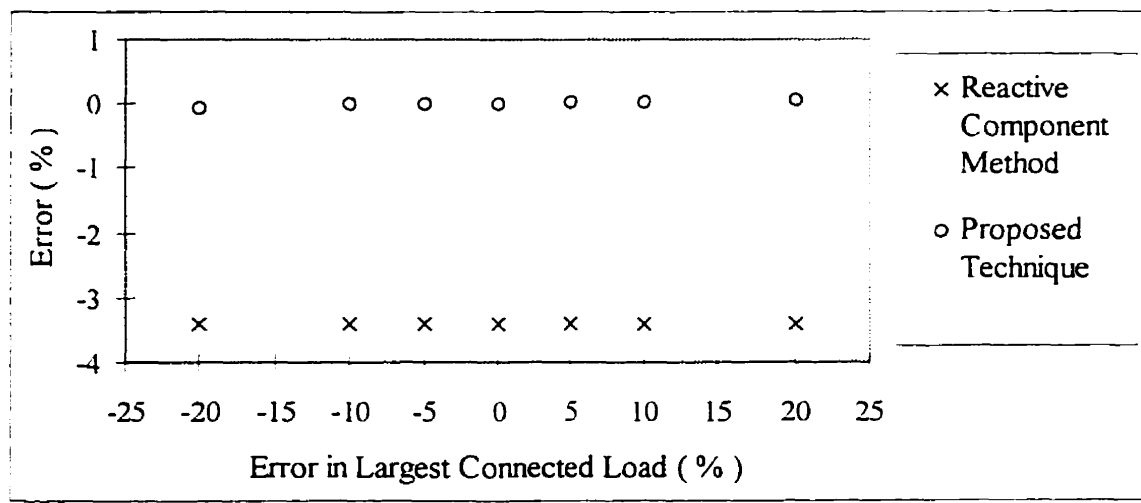


Figure 6.7. Estimation errors for the single-phase-to-ground fault for variation in the largest connected load.

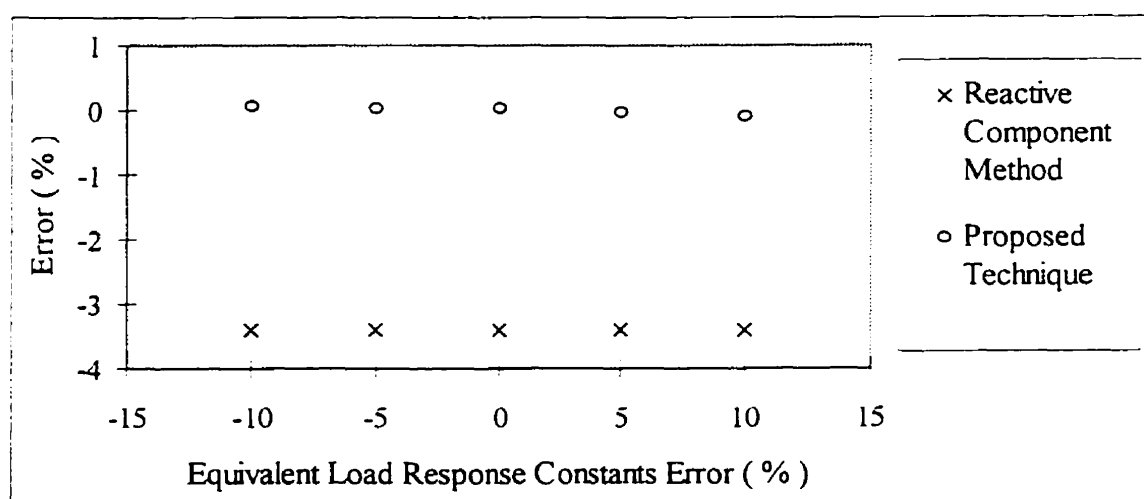


Figure 6.8. Estimation errors for the single-phase-to-ground fault for variation in the equivalent load response constants.

6.3.2 Phase-to-phase faults

Sensitivity of the proposed technique was also tested for estimating the location of phase-to-phase faults. A fault resistance of 5.0 ohms was used in these cases because this is a typical value of an arc resistance. Results for faults at node 7 are presented in this section. The results for faults at other locations are similar.

The location of the fault was calculated for errors in the magnitude of the voltage phasor of one of the faulted phases. Errors in the estimates provided by the proposed technique and those provided by the reactive component method are shown in Figure 6.9. Figure 6.10 shows the errors in the location estimated due to the errors in the angle of the voltage phasor of the faulted phase. Table 6.10 shows the errors when the magnitude and angle of the voltage phasor of one of the faulted phase are in error. The results show that the error varies linearly with the change of phasor magnitude error when the reactive component method is used. The changes in these errors are non-linear when the proposed technique is used. The results also show that the proposed technique is as sensitive as the reactive component method.

Estimation errors in the location of the fault were also calculated for errors in the magnitudes and phase angles of the current phasor of one of the faulted phases. These results are shown in Figure 6.11, Figure 6.12 and Table 6.11. These figures and table show that the sensitivity of the proposed technique and the reactive component method are similar.

Tables 6.12 and 6.13 show the estimation errors when the magnitudes and angles of voltage and current phasors are simultaneously in error. These tables show that the sensitivity of the proposed technique is similar to that of the reactive component method.

Estimation errors in the location of the fault were also calculated for errors in the line and load parameters. The results, shown in Figures 6.13 to 6.16, indicate that the sensitivity of the proposed technique is similar to that of the reactive component method. Load parameter variations do not affect the reactive component method while it affects the proposed technique marginally.

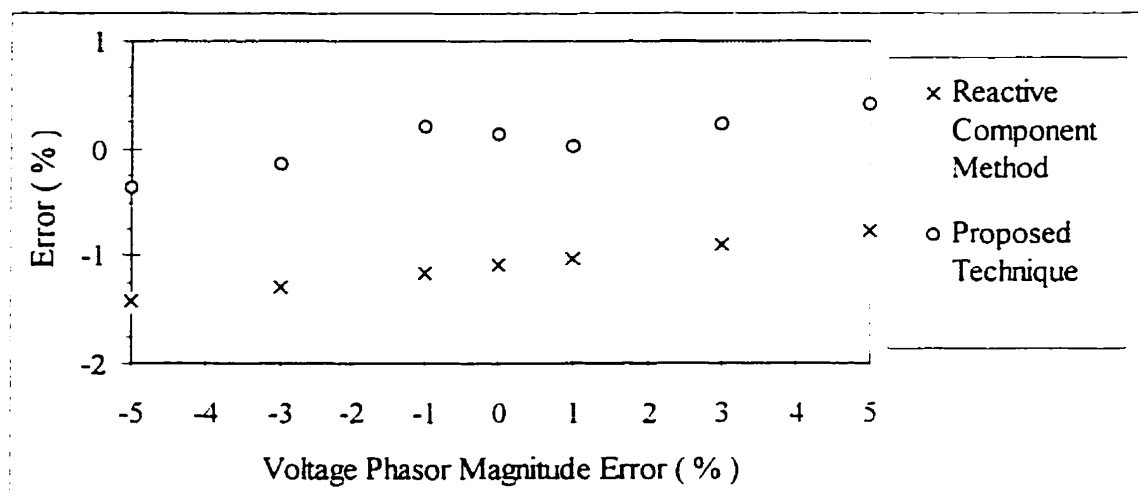


Figure 6.9. Estimation errors for the phase-to-phase fault for variation in the magnitude of the estimated voltage phasor.

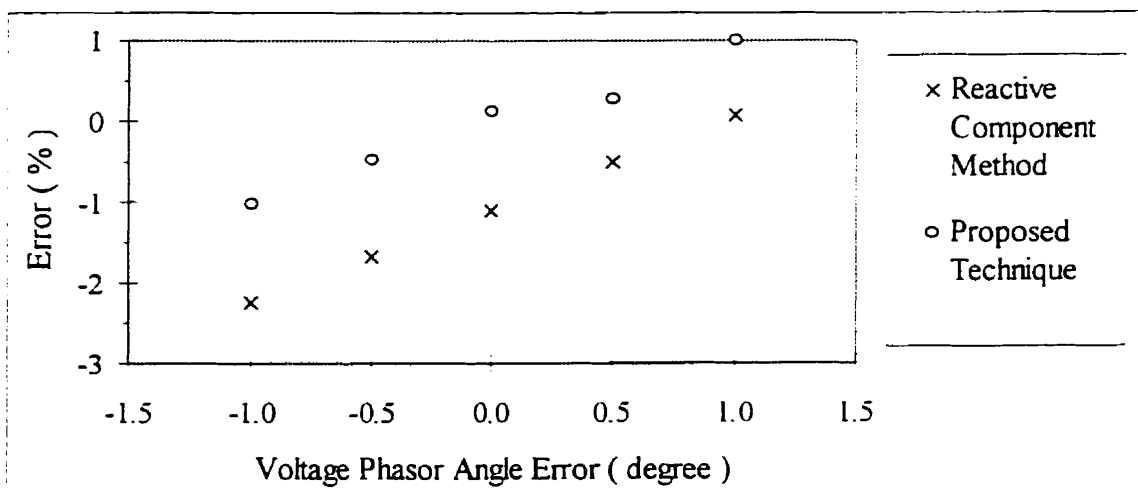


Figure 6.10. Estimation errors for the phase-to-phase fault for variation in the angle of the estimated voltage phasor.

Table 6.10. Estimation errors for the phase-to-phase fault for combined variation in magnitude and angle of the estimated voltage phasor.

Voltage Phasor		Error in Estimated Fault Location by using the	
Magnitude Error (%)	Phase Angle Error (Degree)	Reactive Component Method (%)	Proposed Technique (%)
-5.0	-1.00	-2.53	-1.42
-5.0	1.00	-0.31	0.74
-3.0	-0.50	-1.85	-0.67
-3.0	0.50	-0.72	0.45
-1.0	-0.25	-1.45	-0.14
-1.0	0.25	-0.87	0.53
0.0	0.00	-1.09	0.14
1.0	-0.25	-1.32	-0.25
1.0	0.25	-0.73	0.31
3.0	-0.50	-1.50	-0.42
3.0	0.50	-0.30	0.79
5.0	-1.00	-1.99	-0.84
5.0	1.00	0.44	1.56

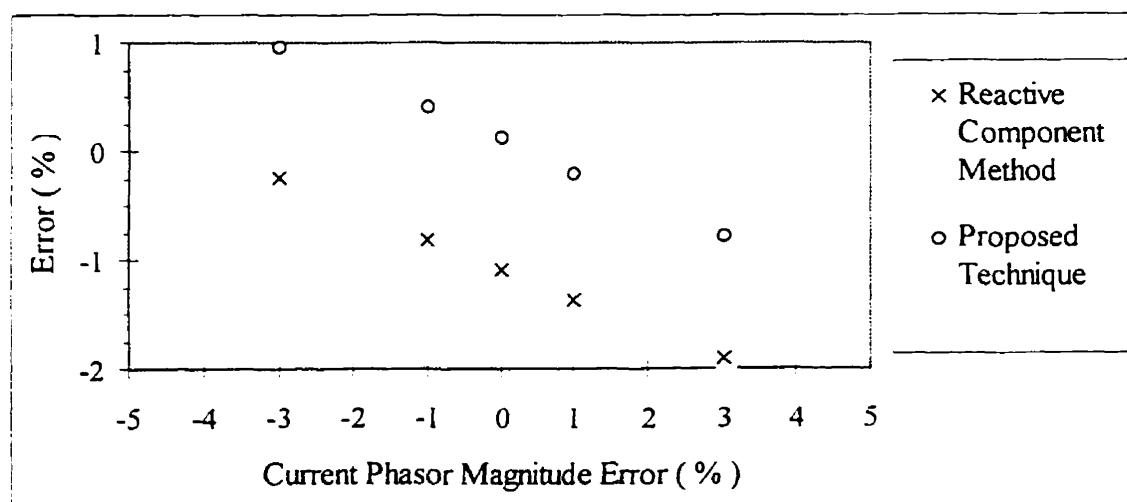


Figure 6.11. Estimation errors for the phase-to-phase fault for variation in the magnitude of the estimated current phasor.

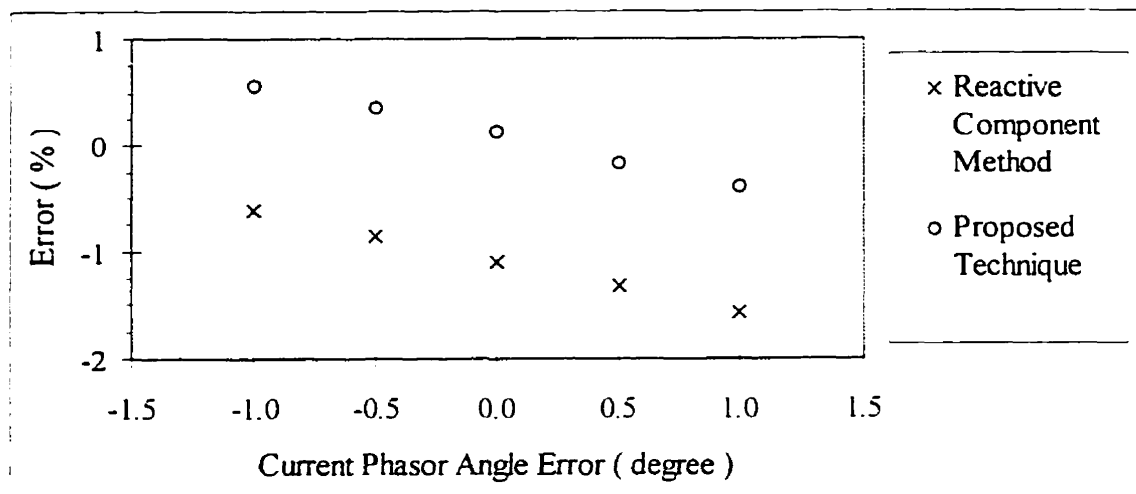


Figure 6.12. Estimation errors for the phase-to-phase fault for variation in the angle of the estimated current phasor.

Table 6.11. Estimation errors for the phase-to-phase fault for combined variation in magnitude and angle of the estimated current phasor.

Current Phasor		Error in Estimated Fault Location by using the	
Magnitude Error (%)	Phase Angle Error (Degree)	Reactive Component Method (%)	Proposed Technique (%)
-3.0	-1.00	0.23	1.41
-3.0	1.00	-0.73	0.53
-1.0	-0.50	-0.57	0.63
-1.0	0.50	-1.06	0.19
0.0	0.00	-1.09	0.14
1.0	-0.50	-1.12	0.08
1.0	0.50	-1.61	-0.44
3.0	-1.00	-1.43	-0.32
3.0	1.00	-2.39	-1.22

Table 6.12. Estimation errors for the phase-to-phase fault for combined variation in magnitudes of the estimated voltage and current phasors.

Magnitude Error		Error in Estimated Fault Location by using the	
Voltage Phasor (%)	Current Phasor (%)	Reactive Component Method (%)	Proposed Technique (%)
-5.0	-3.0	-0.58	0.52
-5.0	-1.0	-1.14	-0.10
-5.0	1.0	-1.69	-0.63
-5.0	3.0	-2.23	-1.16
-3.0	-3.0	-0.44	0.75
-3.0	-1.0	-1.01	0.21
-3.0	1.0	-1.56	-0.40
-3.0	3.0	-2.10	-0.93
-1.0	-3.0	-0.31	1.08
-1.0	-1.0	-0.88	0.51
-1.0	1.0	-1.43	-0.11
-1.0	3.0	-1.97	-0.67
0.0	0.0	-1.09	0.14
1.0	-3.0	-0.18	0.93
1.0	-1.0	-0.75	0.37
1.0	1.0	-1.30	-0.31
1.0	3.0	-1.85	-0.88
3.0	-3.0	-0.05	1.08
3.0	-1.0	-0.62	0.52
3.0	1.0	-1.17	-0.16
3.0	3.0	-1.72	-0.72
5.0	-3.0	0.08	1.26
5.0	-1.0	-0.49	0.70
5.0	1.0	-1.04	0.15
5.0	3.0	-1.59	-0.53

Table 6.13. Estimation errors for the phase-to-phase fault for combined variation in magnitudes and phase angles of the estimated voltage and current phasors.

Voltage Phasor		Current Phasor		Error in Estimated Fault Location by using the	
Magnitude Error (%)	Phase Angle Error (Degree)	Magnitude Error (%)	Phase Angle Error (Degree)	Reactive Component Method (%)	Proposed Technique (%)
-5.0	-1.00	-3.0	-1.00	-1.25	-0.21
-5.0	-1.00	-1.0	-0.50	-2.03	-0.95
-5.0	-1.00	1.0	0.50	-3.02	-1.89
-5.0	-1.00	3.0	1.00	-3.78	-2.62
-3.0	-0.50	-3.0	-1.00	-0.55	0.62
-3.0	-0.50	-1.0	-0.50	-1.35	-0.19
-3.0	-0.50	1.0	0.50	-2.36	-1.14
-3.0	-0.50	3.0	1.00	-3.13	-1.88
-1.0	-0.25	-3.0	-1.00	-0.13	1.17
-1.0	-0.25	-1.0	-0.50	-0.93	0.40
-1.0	-0.25	1.0	0.50	-1.96	-0.64
-1.0	-0.25	3.0	1.00	-2.74	-1.41
0.0	0.00	0.0	0.00	-1.09	0.14
1.0	0.25	-3.0	-1.00	0.58	1.63
1.0	0.25	-1.0	-0.50	-0.21	0.83
1.0	0.25	1.0	0.50	-1.25	-0.34
1.0	0.25	3.0	1.00	-2.04	-1.16
3.0	0.50	-3.0	-1.00	1.02	2.11
3.0	0.50	-1.0	-0.50	0.23	1.31
3.0	0.50	1.0	0.50	-0.82	0.26
3.0	0.50	3.0	1.00	-1.63	-0.68
5.0	1.00	-3.0	-1.00	1.76	2.90
5.0	1.00	-1.0	-0.50	0.96	2.08
5.0	1.00	1.0	0.50	-0.08	1.04
5.0	1.00	3.0	1.00	-0.89	0.24

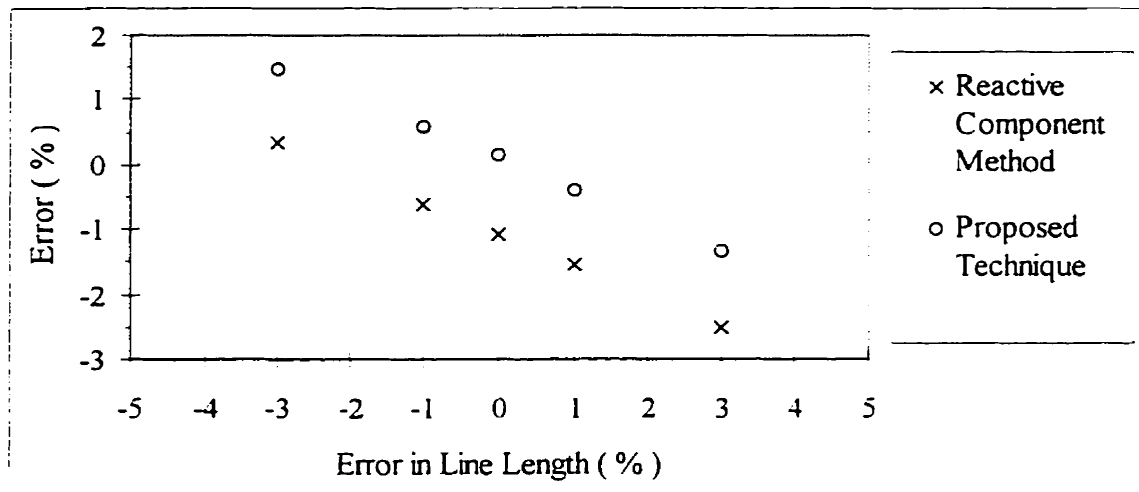


Figure 6.13. Estimation errors for the phase-to-phase fault for variation in the line section lengths.

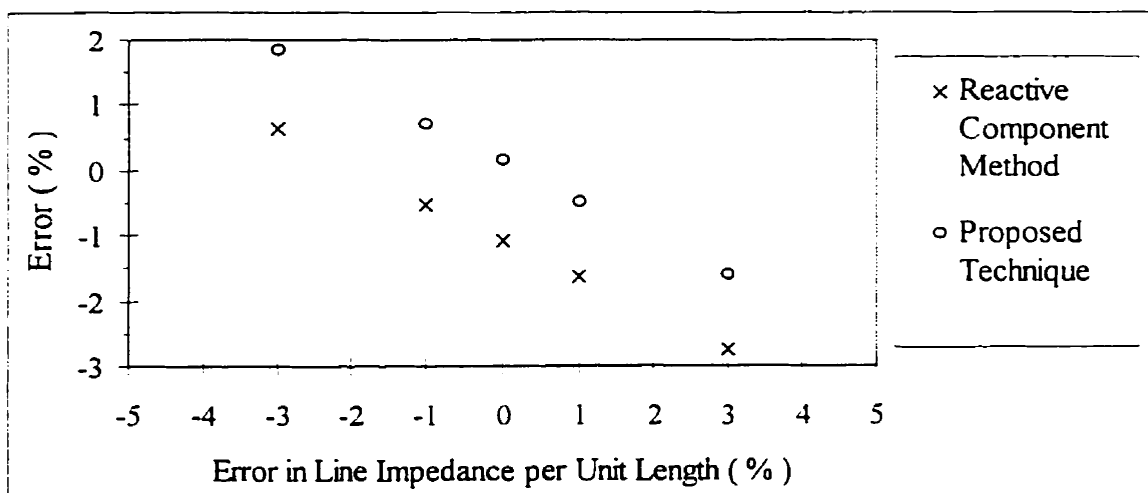


Figure 6.14. Estimation errors for the phase-to-phase fault for variation in the line section impedances per unit length.

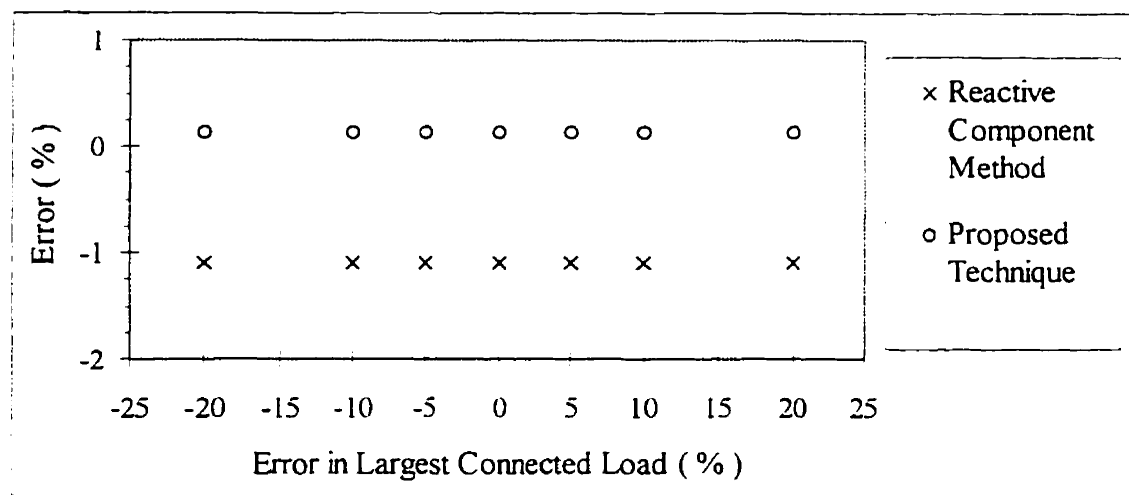


Figure 6.15. Estimation errors for the phase-to-phase fault for variation in the largest connected load.

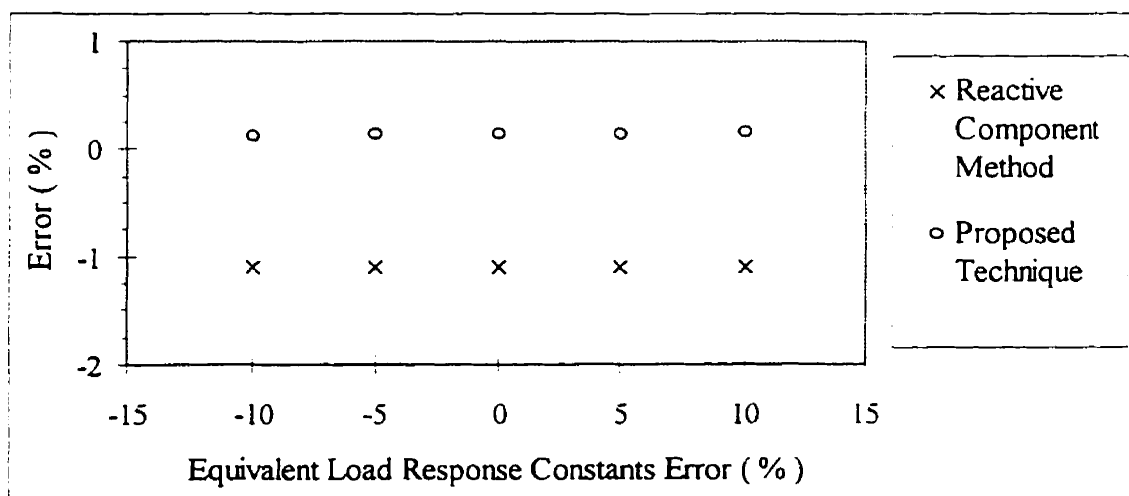


Figure 6.16. Estimation errors for the phase-to-phase fault for variation in the equivalent load response constants.

6.4 Summary

Sensitivity studies of the proposed technique for estimating locations of shunt faults on a radial distribution circuit which includes tapped loads and laterals was performed using simulated fault data. A total of 5,616 cases were studied, out of which 104 cases are reported in this chapter. Additional sensitivity studies are included in an internal report of the Department of Electrical Engineering [54]. Samples of test results for single-phase-to-ground and phase-to-phase faults have been presented. Fault resistance of 5.0 ohms was used for phase-to-phase faults and fault resistances of 10.0 and 15.0 ohms were used for single-phase-to-ground faults.

The studies presented in this chapter show that the proposed technique is less sensitive to voltage phasors errors compared to the reactive component method. Both methods have comparable sensitivity to errors in the current phasors, line section length and line impedances per unit length. The errors in the load parameters do not affect the reactive component method while its effect on the proposed technique is marginal.

7. IMPLEMENTING THE FAULT LOCATOR

7.1 Introduction

A digital technique for estimating the locations of shunt faults on radial distribution circuits, that have tapped loads and laterals, has been presented in Chapter 4. The technique was tested in an off-line mode to evaluate its suitability. Sensitivity of the proposed technique was also studied. Samples of test results have been presented in Chapters 5 and 6. The results show that the proposed technique is suitable for estimating the locations of shunt faults on radial distribution circuits.

The prototype of a fault locator was developed and the proposed technique was implemented on it. The fault locator and sample test results from its use are presented in this chapter.

The design requirements of the prototype system are first identified. The system hardware and software are then described. The procedure for testing the fault locator, by using a playback simulator, is then reported.

7.2 Design Requirements

Six design requirements for the prototype fault locator were identified. They are as follows.

1. The hardware should be suitable for implementing the proposed technique for locating faults in radial distribution systems.
2. The system should make use of the hardware available in the laboratory [55, 56] as far as possible.

3. The hardware should be suitable for future implementations of relaying, monitoring, measurement or relay testing algorithm.
4. The user interface should be suitable for developing and testing protective devices in the future.
5. It should be possible to use the data files from simulations and records obtained from distribution systems to test the fault locator using a real-time playback simulator.
6. The hardware and software should be modular to make it convenient to develop, test and maintain them. Modular approach will help to meet the requirements mentioned under serial number 4.

7.3 System Overview

The fault locator was developed keeping in mind the requirements outlined in the previous section. The equipment needed for testing the fault locator are shown in Figure 7.1. Power Systems Analysis Laboratory at the University of Saskatchewan has sixteen personal computers and three workstations; the workstations and three personal computers are connected to the computer system of the university via an Ethernet link.

One of the three personal computers is equipped with hardware and software suitable for use as a Real Time Playback Simulator. This personal computer (PC) was used for testing the fault location system. Another PC, which is equipped with a Digital Signal Processing (DSP) board and a Data Acquisition System (DAS) board, was used to implement the fault locator. Faults were simulated, in the selected distribution circuit, on one of the SUN SPARC workstations. Data files produced by the simulations were used to test the fault locator.

Low-pass filters were designed and built. They were used as anti-aliasing filters and were placed between the playback PC and the PC used as a fault locator. Output signals from the low-pass filter boards are connected to the termination interface board by using coaxial cables. The interface board is connected to the Data Acquisition System Boards. The status monitoring signals are brought out to the termination interface board by means of a ribbon cable.

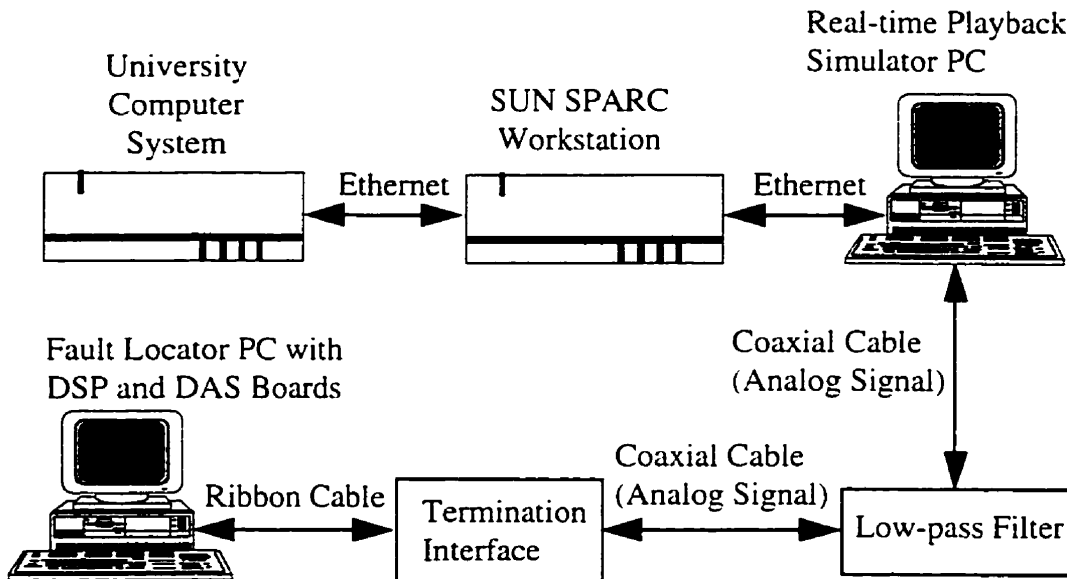


Figure 7.1. Overview of the fault location system along with the testing arrangement.

7.4 Hardware

The hardware of the fault location system was selected keeping in mind the requirements outlined in Section 7.2. Figure 7.2 shows the organization of the hardware. It has four major components: low-pass filter boards, data acquisition system (DAS) cards, a digital signal processing (DSP) card and a host personal computer. This section briefly describes the features of low-pass filter boards and other system hardware components which are available from commercial products.

7.4.1 Low-pass filter boards

The low-pass filter is required to band-limit the analog voltage and current signals to the data acquisition system and prevent aliasing in samples of voltage and current signals. Design requirements mentioned in Section 7.2 was followed while designing the low-pass filter. Cut-off frequency of the low-pass filter depends on the frequency at which voltage and current signals are subsequently sampled by the data acquisition system. It was decided to design two filter boards each capable of handling four signal channels.

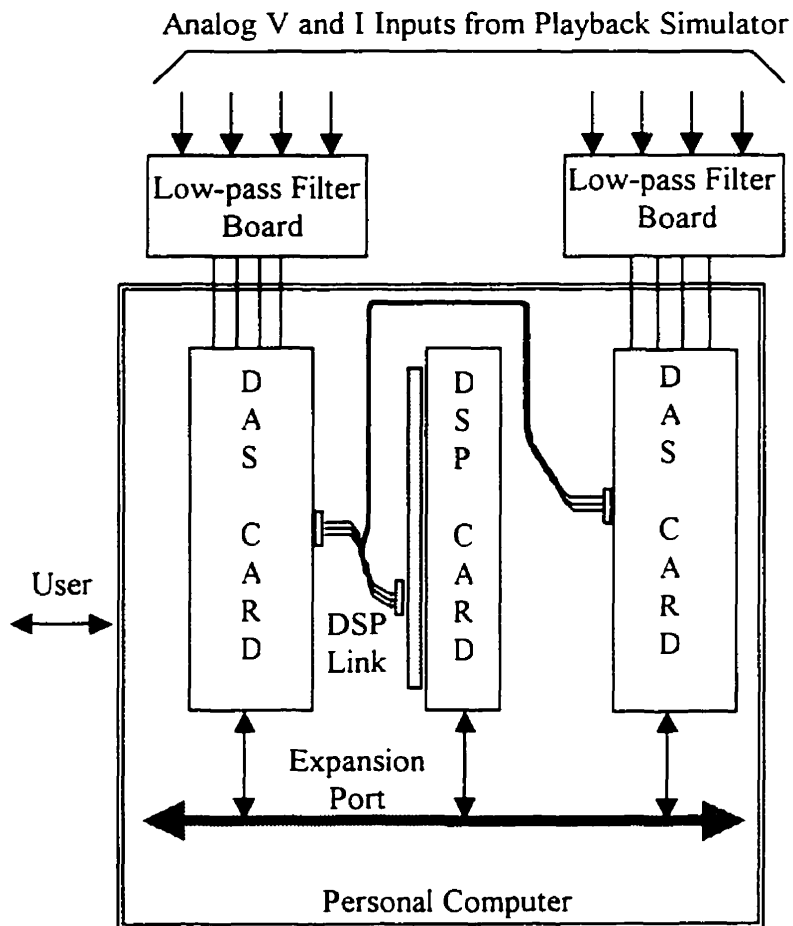


Figure 7.2. Hardware configuration of the fault location system for distribution network.

In order to use the same hardware for future requirements of different cut-off frequencies, it was decided to use switched capacitor filters [57]. Switched capacitor filters overcome some of the problems inherent in the standard active filters, while providing some new capabilities. Switched capacitor filters need no external resistors or capacitors and their cut-off frequencies are set to a typical accuracy of $\pm 0.3\%$ by an external clock frequency. This allows consistent, repeatable filter design whose cut-off frequencies are variable over a wide range by simply changing the clock frequency.

Ideally, the low-pass filter should have an abrupt transition from pass band to stop band which is known as brick-wall characteristics [58]. Another, requirement is that the ripple in pass band should be as small as possible.

The characteristics of the Butterworth low-pass filter matches closely with the requirement of the anti-aliasing filter and it was decided to use the Butterworth characteristics. It has nearly flat passband, roll-off is smooth and monotonic, with a roll-off rate is 20 db/decade or 6 db/octave for every pole. It was decided to have an attenuation of 80 db or more per decade. Any Butterworth filter of order 4 or above would provide the desired attenuation.

National Semiconductor Corporation's MF6CN-100 [57], a 6th order Butterworth low-pass filter, was selected for designing the low pass filter as it is readily available in the electrical engineering laboratory at the University of Saskatchewan. It is widely used in other equipment at the department with a satisfactory performance record. Use in other equipment at the department will enable easy availability of spares while having reduced inventory. Further details of the low pass filter are given in Appendix J.

7.4.2 Data acquisition system cards

The 4 Channel Analog Interface Card [60] from Spectrum Signal Processing was used as a data acquisition system card. Two such cards were used to collect data from eight channels. Each card supports four analog input channels and two analog output channels. A reloadable up-counter provides a hardware generated programmable sample rate clock. The A/D and D/A sections can also be triggered by means of external input signals or by software. Analog signal and digital control and status connections were made via a 25 way 'D' type connector. The card occupied a short PC slot and powered from the bus. All control and data signals were transferred via 50-way DSPLINK2 connector from the Digital Signal Processor card. Further details of data acquisition system cards are given in Appendix J.

7.4.3 Digital signal processing card

The PC/C31 card [61, 62], based around the TMS320C31 Digital Signal Processor from Texas Instruments [63], was used as a Digital Signal Processor Card. The TMS320C31 is a low cost variant of the Texas Instruments' 32 bit floating-point TMS320C30 DSP and is code compatible with it. C31 has a core architecture optimized for real-time operations integrated with a 32 bit timer, a DMA controller and a serial port. It has 32 bit data bus and 24 bit address bus. PC/C31 is a full height, two-thirds length PC AT card and occupies one 16 bit PC slot and draws power from the PC bus.

7.4.4 Host personal computer

The PC/C31 DSP card and DAS cards were placed into the expansion ports of an IBM compatible personal computer based on Intel Corporation's 486 processor, running at 66 MHz. The host PC controls the operation of the DSP card and provides access to the software development system of the DSP. It also provides the graphical user interface with the fault location system which is necessary to coordinate the operation of various hardware and software modules to achieve the objective.

The host PC is also equipped with 800 MB Hard Drive, 8 MB RAM and 1.44 MB Floppy Drive. The operating system of the host PC is Microsoft Windows for Workgroups Version 3.11. The PC is connected to the University computer system via Ethernet link.

Host PC also runs the DOS executable file which estimates the location of fault from the real-time data obtained from the DSP and data from files stored in the PC.

7.5 Software

The software for the fault location system was also developed keeping in mind the requirements outlined in Section 7.2 and using a modular approach. Software developed for this project can be classified in three categories, each serving a specific purpose. User-interface software loads the program in the DSP's memory and executes it. Real-time software acquires real-time voltage and current samples, estimates phasors, detects

faults and saves the required data. Once the fault data is saved, user-interface software transfers the data to the PC and coordinates the execution of the off-line software to estimate the location of the fault. The following sections describe the software.

7.5.1 User-interface software

The user-interface software provides a graphical interface with the fault locator and coordinates the operation of other modules. This software was written in Microsoft VISUAL BASICTM [64] where the development system is also installed in the fault locator PC. PC/C31 Intelligent Interface Library Windows support software [65] was used while developing the user-interface. The display of the developed user-interface is shown in Figure 7.3.

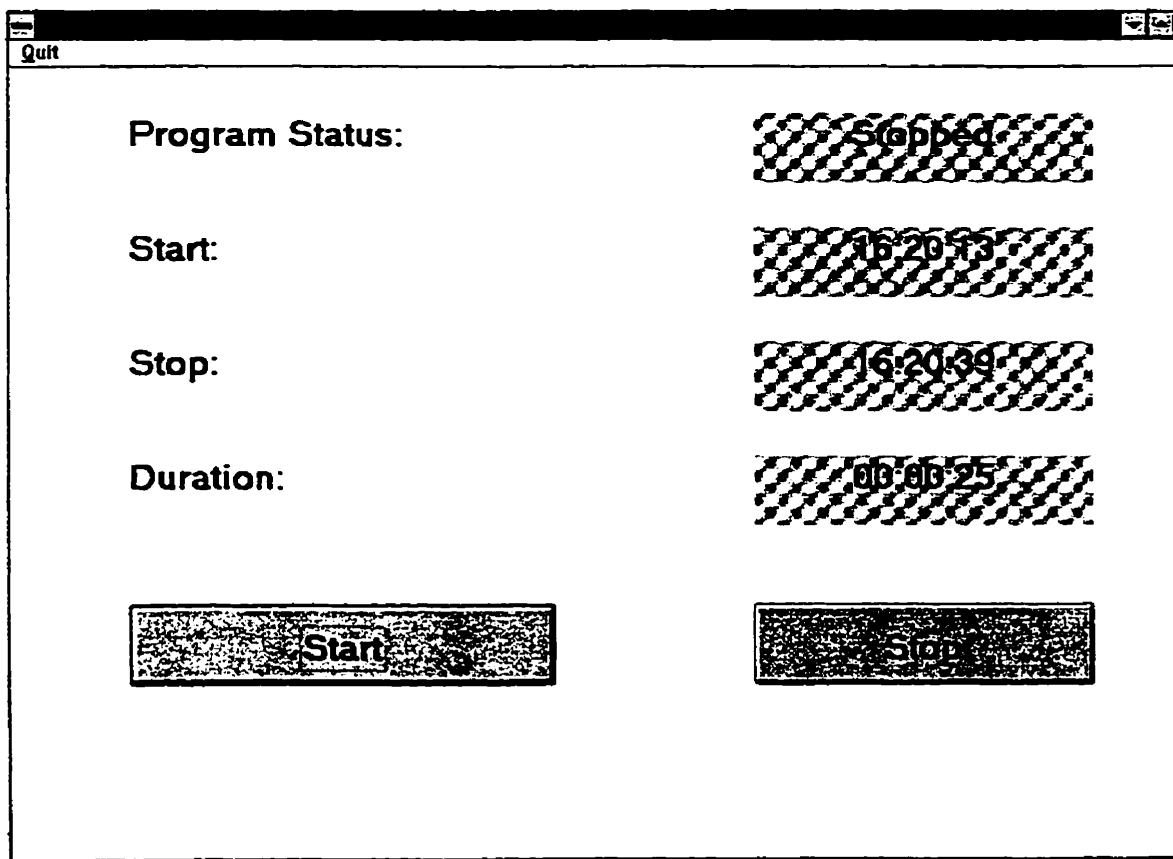


Figure 7.3. Display of the user-interface for the fault location system.

Once the user-interface is opened by clicking on its icon in the program manager of the WINDOWS™ operating system, the software resets the DSP, releases it from the reset and enables the DPRAM. Then the executable real-time codes available in the host PC is loaded into the DSP's memory. If there is a problem with any of the processes, an alarm is displayed in the program in the program status window.

Once the 'Start' button in the user-interface window is clicked, the software runs the DSP code from the prespecified memory location. While the real-time software runs, 'processing' is displayed in the program status window. Each time the real-time software is compiled to generate an executable file, its map file has to be checked for determining the starting location of the program and the user-interface software has to be modified accordingly.

While the DSP runs the real-time software, user-interface software waits for a signal from the DSP that appropriate data has been written in the DPRAM. On receiving the signal, user-interface software reads the data from the pre-defined locations, writes them in an output file and signals back to the DSP that DPRAM is free for further writing.

User-interface software runs the executable file of the off-line software in DOS shell. The off-line software uses the data file generated by the user-interface software along with other data file to estimate the location of the fault. The location of the fault is written in DOS mode in the monitor screen and in an output file. Once a confirmation is received from the user, the off-line program stops and the user interface program resets the DSP. User-interface software then estimates the duration of the run and displays it in a specified window. The program then stops and this status is displayed on the screen. The program can be stopped at any time by clicking on the 'Stop' button in the user-interface window.

7.5.2 Real-time software

Real-time software, written in ANSI C, runs on the DSP. ANSI C source program is converted to the source code of the DSP. The conversion process involves compiling, assembling and linking the source files to create an executable object file [66, 67]. Modular structure of the real-time software makes it easy to adapt the software for other projects.

The real-time software consists of two components: data acquisition software and application software. Application software consists of three software modules: phasor estimation, overcurrent relaying and data management and are shown in Figure 7.4. All software modules are executed sequentially. Data acquisition software controls the operation of the data acquisition system when it acquires voltage and current samples. The signals are taken at a specified rate and are stored in specified memory locations. The signals are subsequently processed by the application software modules before the next set of samples are acquired by the data acquisition system. The modules of the real-time software are briefly described in the following sections.

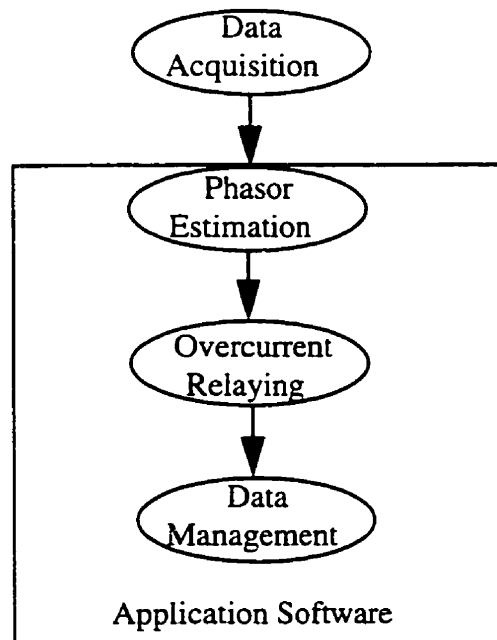


Figure 7.4. Real-time software modules.

7.5.2.1 Data acquisition software

The data acquisition software consist of two routines, a main routine and an interrupt service routine. The main routine initializes the system and controls the sampling rate using a sample-rate timer which is on one of the DAS card. The output of the timer, which is available at PIN 13, is connected to the 'Trigger In' (PIN 23) of the

second card. This ensures that the eight channels, four per card, are sampled synchronously.

The main routine loads the timer with the appropriate hexadecimal number which is stored in a specified DSP memory location. This number corresponds to the selected sampling rate, which was 720 Hz for this project. The main routine enables the interrupts after loading the timer. The timer generates an interrupt after its timeout and reloads itself from an on-board counter. The interrupt also enables the execution of the interrupt service routine described hereafter.

The execution of the interrupt service routine is described by using the block diagram of the data acquisition system shown in Figure I.2. The timeout signal triggers the sample/hold devices which sample the signals and put them into the hold mode. The Analog-to-digital converter (ADC) starts converting after a pre-set delay of 1 μ s. This delay is incorporated to allow to settle input signals. Typical conversion time for each channel is 3 μ s. ADC signals the end-of-conversion by making the EOC bit high which is read by the DSP through the status register. The DSP then reads the data from the ADC, stores the information in a specified location and initiates the conversion of the next channel by writing the channel number in the control register. The process is repeated until the data from all the channels are acquired and quantized.

The 12 bit data read from all channels are converted into 32 bit data after the conversion of all the channels. The data are then converted to appropriate primary signals by using the information on the resolution of the ADC and the ratio of the transducer used in the channel. Before the interrupt is again generated by the timer, application software modules are executed within the Interrupt Service Routine. Once all the software modules are executed, the program control goes to the main routine. It waits for another interrupt which initiates the processes of acquiring the next set of samples and their processing.

7.5.2.2 Application software

Real-time application software consists of the three modules shown in Figure 7.4. Phasor-estimation software module estimates the phasors of voltage and current signals from the samples acquired by the data acquisition software using LES algorithm described in Appendix B. It also estimates the r.m.s values and phase angles of the

phasor. This module uses a circular buffer memory to store the quantized values of signals in each channel. The circular buffer memory facilitates easy manipulation of data required for phasor computation.

The overcurrent relaying software module detects the presence of fault using the overcurrent algorithm described in Section 4.3.2. For the purpose of detecting ground faults, it estimates the zero-sequence component of the currents at the line terminal from the estimated phasors of the line currents. This software module sets two flags which indicate the presence and type of fault.

The data management software module stores the estimated information on the phasors in a one-cycle circular buffer memory. If a fault is detected then it retrieves the pre-fault phasors of voltages and currents from the buffer and writes them in the appropriate DPRAM locations along with information concerning the type of fault. This module collects the information of phasors of voltages and currents during the fault and the type of faults after a 3 cycle time delay. This module also detects the auto-reclosing condition.

Once all the information for a fault is written in the DPRAM, the data management software module signals the user-interface software to read data from the DPRAM, otherwise, it returns the control of the program to the main routine.

7.5.3 Off-line application software

The off-line application software is essentially the same as that used for testing the proposed technique, using non real-time data. The software has been tailored to work in coordination with the user-interface software which obtains information from the real-time software and writes it to a output file.

The off-line application software has two components: one implements the fault indicator and provides this information to the second component. This component uses the information to estimate the location of the fault from the data collected in real-time, and the line and load parameters stored in the host PC. Off-line application software is written in FORTRAN using the Microsoft FORTRAN Professional Development System [68].

The fault indicator component of the off-line application software implements the load balancing and adaptive trip feature described in Section 4.9. This component has a modular structure and consists of 18 modules. These modules implement different features, such as, low pass filtering, phasor estimation, load balancing and adaptive trip algorithm. This component of the software also provides an output on the monitor screen and writes data in an output file.

The other component of the off-line application software integrates the information generated by the fault indicator module with the information generated by the real-time software, line and load database, and estimates the location of the fault. This component also has a modular structure and consists of 81 modules that implement the proposed technique described in Chapter 4. Errors in the estimated voltage and current phasors, and line and load parameters, described in Chapter 6, are compensated, if they are known, without recompiling the software.

The modular structure of the off-line application software facilitated the development of this component in Microsoft FORTRAN version 5.1 that is based on DOS. The executable file is limited to 318 kBytes. This is achieved by using some of the advanced features of FORTRAN 90 that the compiler provides.

7.6 Testing

The proposed fault location system was implemented and tested in the laboratory. Testing of the hardware and software components of the system was done during the various stages of the development, shown in Figure 7.5.

7.6.1 Low pass filter

Low-pass filters were implemented in a circuit board with ICs and discrete components. Cut-off frequency of 240 Hz was selected the low-pass filters. The selected cut-off frequency is less than the Nyquist frequency of 360 Hz and the sampling frequency was 720 Hz. The filter was tested using a spectrum analyzer. The frequency response of one of the filter built is shown in Figure 7.6. The response indicates that the performance of the filter, is close to the expected response.

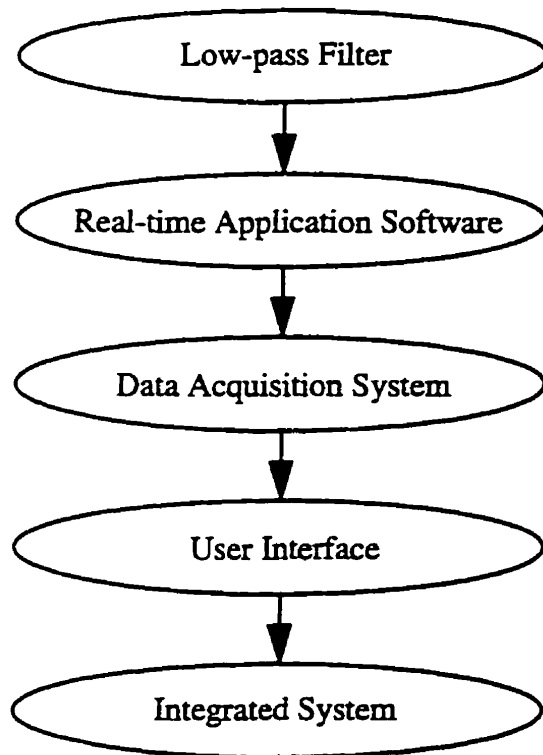


Figure 7.5. Different stages of testing in the development of the fault location system.

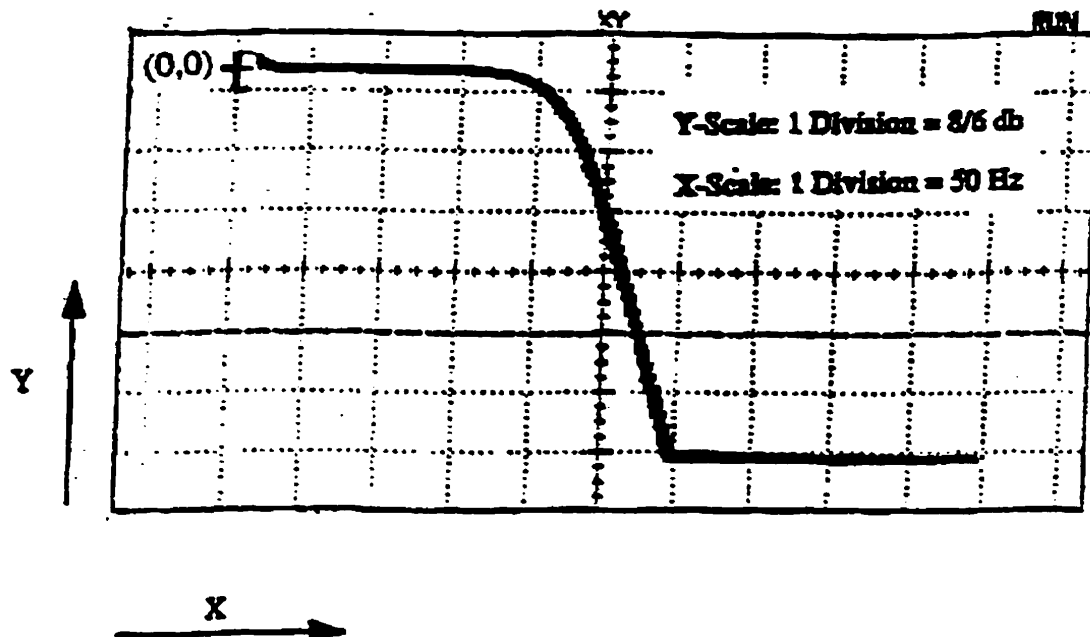


Figure 7.6. Frequency response of the sixth order Butterworth low-pass filter.

7.6.2 Real-time application software

The real-time application software was tested by including a datafile, containing simulated fault information, in the software. This datafile was used earlier for off-line testing of the proposed technique. The testing of the real-time application software was done on another PC equipped with a TMS320C30 Evaluation Module (EVM) [69]. The debugging of the program was done by using the TMS320C30 C Source Debugger [70]. Appendix K gives an overview of the testing system used and the procedures followed.

This testing of the real-time application software is required to confirm that the software can be executed within the inter-sampling time. Benchmarking of the real time application software indicates that it can be executed within 0.2 millisecond for each pass of the program. This is much less than the available inter-sampling time of 1.38 millisecond for 720 Hz sampling frequency. Even if the software overhead for data acquisition system is added, it is expected to be much less than the inter-sampling time. Results from these tests are also similar to that of non real-time tests except that all phasors are shifted by an equal amount of angle. Real-time software correctly detects all types of faults and the testing was done for one of the location of the fault.

7.6.3 Data acquisition software

The data acquisition software was tested by applying a sinusoidal test waveform from the FDF Dynamic Frequency Source of the Doble Engineering Company. The level of the signal was first checked with an oscilloscope to ensure that it is less than ± 2.0 Volt so that data acquisition card is not stressed. Initial testing of the data acquisition software is done by using the MPC View C source debugger [71] available from Spectrum Signal Processing, manufacturer of DSP and DAS Cards.

MPC view is a Windows based user-interface and allows different functions like load, display and execution of DSP code. It also allows data management facility and all data in the DSP including memory and registers can be viewed in a desired format: floating-point, hexadecimal or decimal. MPC view can also be interfaced with an Intelligent Interface Library (IIL).

Testing of the data acquisition system revealed that the on-board low-pass filters in the two DAS cards have significantly different group delays that resulted in a phase-shift

between the signals acquired by the two boards. The amount of phase-shift was determined and software compensation was provided to eliminate the undesired phase-shift between signals acquired by the two boards.

7.6.4 User-interface software

User-interface software was added at this stage and the data acquisition system was tested by applying a FDF Dynamic Frequency Source of the Doble Engineering Company. Real-time application software was then integrated with the data acquisition software and the user-interface software. The integrated real-time system, without the off-line application software, was then tested by playing back simulated fault waveforms in the Real Time Playback (RTP) simulator [72], the RTP simulator is described in Appendix L.

The estimated phasors from the real-time system were found to match closely with that obtained from non real-time studies. The off-line application software was then integrated with the user-interface software to have the complete fault location system.

7.6.5 Complete fault locator

The complete fault locator was tested by playing back the simulated fault data in RTP. The test set-up is shown in Figure 7.1. Simulations were carried out in a SUN Sparc workstation on the model of a SaskPower system, described in Section 5.2, and the datafile for playback was generated. This datafile was then played back using the RTP simulator.

A fault waveform, for a B-phase-to-ground fault in the test system, played back by the RTP unit is shown in Figure 7.7. Phase voltage in volts, line current in amperes and time in milliseconds is shown in the diagram.

Simulations were done for all types of faults: single-phase-to-ground (L-G), two-phase-to-ground (L-L-G), phase-to-phase (L-L) and balanced three-phase (L-L-L-G). Several fault locations were used in the simulations. Each simulation generates two sets of data file: one was used for non real-time testing as described in Chapter 5 and the other was used for playback in the RTP. Results obtained from non real-time testing

were compared with that obtained using the real-time playback unit. Results are also compared for both the reactive component method and the proposed technique and are shown in Table 7.1.

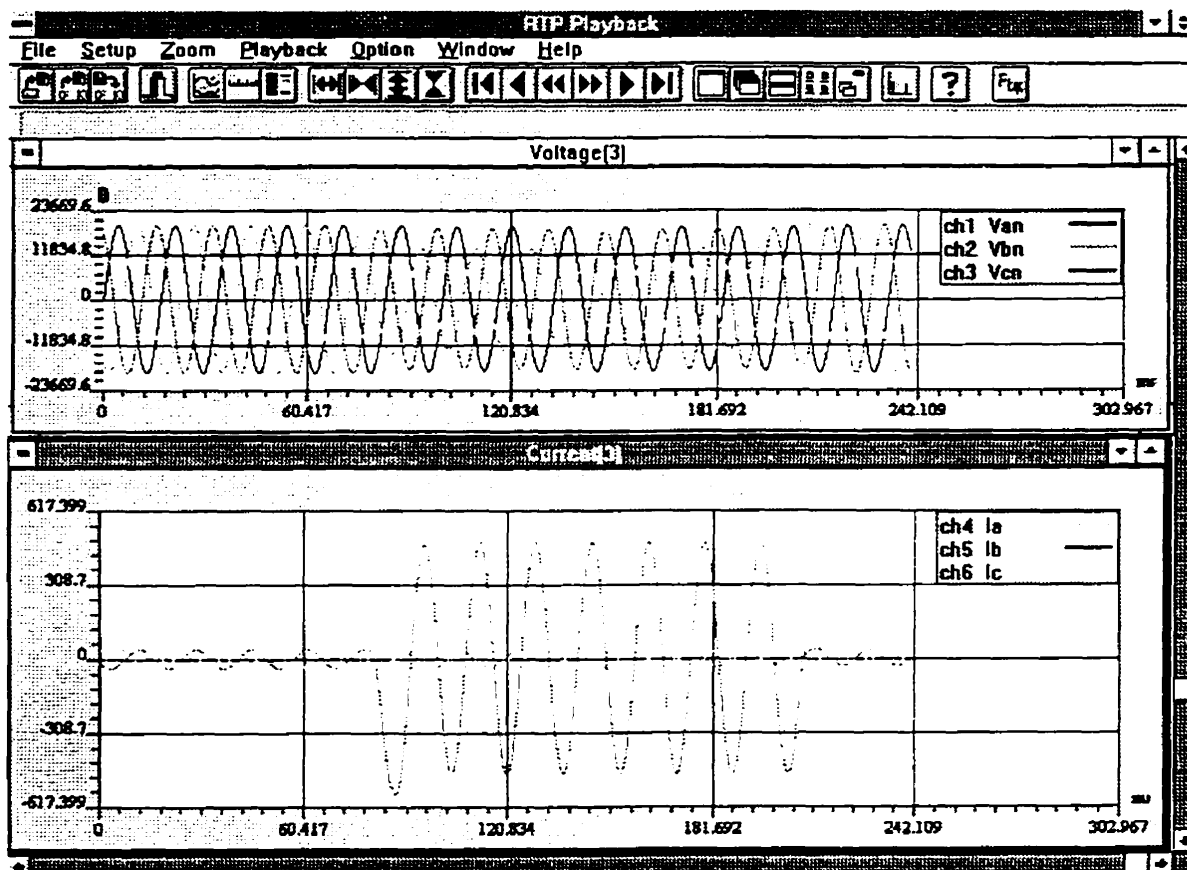


Figure 7.7. A typical fault waveform played back by the Real Time Playback Simulator.

Results indicate that the location of faults obtained using the implemented fault locator are close to that obtained in non real-time testing using the proposed technique. The same is generally true for the reactive component method except for two fault situations out of twenty-four cases of faults simulated.

Table 7.1. Fault location estimates obtained using non real-time and real-time testing.

Type of fault	Fault Node Number	Distance of the Fault (km)	Distance of the Fault Estimated using			
			Reactive Component Method		Proposed Technique	
			Non real-time (km)	Playback (km)	Non real-time (km)	Playback (km)
L-G	2	2.414	2.278	2.227	2.409	2.347
	7	22.530	21.078	21.411	22.546	22.574
	8	27.680	25.845	26.344	27.698	28.257
	10	34.600	33.109	33.315	34.744	34.789
	12	20.921	19.505	19.767	21.112	20.834
	13	30.094	28.924	29.264	30.052	30.138
	16	34.922	34.460	34.733	35.087	35.549
	18	32.508	31.118	28.584	32.359	32.284
	19	34.922	33.506	30.639	35.006	35.448
L-L-G	2	2.414	2.261	1.943	2.309	2.312
	7	22.530	21.952	20.920	22.632	22.162
	8	27.680	27.019	25.839	27.856	27.407
	10	34.600	33.797	32.306	34.926	34.434
	12	20.921	20.371	19.024	21.515	21.091
L-L	2	2.414	2.244	2.194	2.448	2.492
	7	22.530	21.302	21.818	22.609	22.605
	8	27.680	26.187	26.794	27.965	27.961
	10	34.600	32.717	33.377	34.682	34.903
	12	20.921	19.775	20.234	21.537	20.871
L-L-L-G	2	2.414	2.338	4.315	2.246	2.322
	7	22.530	22.109	21.730	22.204	22.695
	8	27.680	27.161	27.381	27.296	27.671
	10	34.600	33.882	34.276	34.220	33.285
	12	20.921	20.516	20.960	20.768	21.260

7.7 Summary

The technique for estimating locations of shunt faults on a radial distribution system which has tapped loads and many laterals, has been implemented using laboratory facilities. Commercially available hardware components were used as far as possible.. Low-pass filter design and building is described. The testing of hardware and software components in different stages of development is described in this chapter.

The prototype fault locator was tested by playing back simulated data in a Real Time Playback simulator. Performance of the implemented fault location system is encouraging and the estimates of the fault location provided by it matches closely with the non real-time test results which are reported in Chapter 5.

8. SUMMARY AND CONCLUSIONS

8.1 Summary

A good estimate of the location of a fault substantially reduces the time required to restore the faulted line to service. The time taken to locate a fault could be substantially longer than the time needed to repair if a proper fault locating device is not used. The objective of the research, outlined in this thesis, was to develop a technique that would estimate the locations of shunt faults on radial distribution systems with laterals. Work in this area already reported in the literature has been briefly reviewed in Chapter 1.

A typical distribution system and the protection provided on it are described in Chapter 2. Shunt faults experienced on electric lines have been reviewed in that chapter. The nature of fault resistance has been described and the effect of fault resistance on fault location estimates has been discussed. The impact of tapped loads on fault location estimates has also been discussed.

A review of the previously published literature revealed that several methods use the fundamental frequency voltages and currents at one of the line terminals. Also, previously published work reported algorithms for estimating the location of faults on radial transmission lines with tapped loads. These methods have been briefly reviewed in Chapter 3. It has been shown that they are not suitable for use on radial distribution systems which include several single and multiphase laterals and has dynamic load taps along the line.

A new technique that estimates the location of a shunt fault on a radial distribution system, which includes several laterals, has been proposed in Chapter 4. The possible location of a fault from the line terminal is first estimated by computing the apparent impedance from the fundamental frequency voltage and current phasors and converting the reactive component of the impedance to line length. The distribution system, with laterals, is then modified to a form without laterals.

Static response type load models are used. Single-phase, phase-to-phase and three-phase loads are modeled using the symmetrical components approach. Load currents at the taps, during the fault, are estimated from the pre-fault voltages and currents, and calculated fault voltages and currents. Voltages and currents at the fault are calculated using telegraphic equations as functions of distance of the fault location from the source-side node and the admittances of the loads beyond the fault. The loads beyond the fault are assumed to be consolidated at the end of the line. The distance of the fault from the nearest node, close to the measurement terminal, is solved iteratively by linearizing a higher order equation that is obtained by using the appropriate voltage-current relationship at the fault. The technique is suitable for considering single-phase-to-ground, two-phase-to-ground, phase-to-phase and balanced three-phase faults.

The proposed technique was tested using data obtained from simulation studies on a model of a 25 kV distribution circuit of SaskPower. The system was simulated on a SUN SPARC workstation using the PSCAD, a simulation software. Faults were applied at different locations of the system model. The data, obtained from the simulations, were then used to estimate the locations of faults. The studies were repeated using several values of fault resistances. Fault locations were also estimated by using the reactive components of the apparent impedances. Test results for single phase-to-ground, two-phase-to-ground, phase-to-phase and three phase faults are reported in Chapter 5. A study of the results indicates that the proposed technique is more accurate than the traditional reactive component method. It also demonstrates that the proposed technique is quite accurate even if the fault resistance is numerically comparable to the line impedance.

The effect of errors in the input parameters on the accuracy of the proposed technique was analyzed by performing sensitivity studies. Some test results from these studies are reported in Chapter 6. The studies indicate that the proposed technique is less sensitive to the errors in estimated voltage phasors than the reactive component method. However, the sensitivity of both methods is comparable for errors in the estimated current phasors, line section lengths and line impedances per unit length. Errors in the load parameters affect the accuracy of the proposed technique slightly whereas it does not affect the reactive component method.

The proposed technique was implemented on a prototype fault location system that was designed and built in the laboratory using commercially available hardware as far as possible. Chapter 7 describes the hardware and the software designed for the fault location system. The modular approach used in developing the hardware and software provided a DSP based system that can be used to implement protection, monitoring or relay testing algorithms by modifying a few software modules. The prototype fault location system was tested by playing back the fault data via a Real Time Playback (RTP) Simulator. Test results are also reported in Chapter 7; are encouraging because they match closely with the results obtained from the non real-time tests.

8.2 Conclusions

The research work presented in this thesis indicates that the proposed technique is simple and accurate. The technique provides a single estimate for the location of the fault even if a distribution circuit has many laterals. The results obtained from simulation studies indicate that the proposed technique has acceptable accuracy even when the magnitude of the fault resistance is comparable to the line impedance.

The real time component of the proposed technique can be implemented in a digital relay used for protecting the line. The off-line component can be implemented as a fault analysis package on a personal computer. This facility can be located in the substation for analyzing all faults on lines emanating from the substation. Alternately, the facility can be located in a Control Center and can be used for analyzing faults in all the distribution circuits of a utility.

Another alternative is to implement the off-line component in the relay if the relay is equipped with a microcomputer other than the one used for real-time data collection and analysis. This approach was successfully implemented in the fault location system using a personal computer with DSP and data acquisition cards.

REFERENCES

1. Sachdev, M.S., (Coordinator), IEEE Tutorial Course Text, *Advancements in Microprocessor Based Protection and Communication*, IEEE Operations Center, Publication No. 97TP120-0, 1997, pp. 1-127.
2. Stringfield, T.W., Marihart, D.J. and Stevens, R.F., "Fault Location Methods for Overhead Lines", *Transactions of the AIEE, Part III - Power Apparatus and Systems*, Vol. 76, August 1957, pp. 518-530.
3. Desikachar, K.V. and Singh, L.P., "Digital Travelling-Wave Protection of Transmission Lines", *Electric Power Systems Research*, Vol. 7, No. 1, January 1984, pp. 19-28.
4. Ibe, A.O. and Cory, B.J., "A Travelling Wave-Based Fault Locator for Two- and Three-Terminal Networks", *IEEE Transactions on Power Systems*, Vol. PWRD-1, No. 2, April 1986, pp. 283- 288.
5. Ranjbar, A.M., Shirani, A.R. and Fathi, A.F., "A New Approach for Fault Location Problem on Power Lines", *IEEE Transactions on Power Delivery*, Vol. 7, No. 1, January 1992, pp. 146-151.
6. Johns, A.T. and Agarwal, P., " A New Approach to Power Line Protection Based upon the Detection of Fault Induced High Frequency Signals", *IEE Proceedings*, Vol. 137, Pt. C, No. 4, July 1990, pp. 307-313.
7. Carr, J. and Jackson, R.V., "Frequency Domain Analysis Applied to Digital Transmission Line Protection by Digital Computer", *IEEE Transactions on Power Apparatus and Systems*, Vol. PAS-95, No. 4, July/August 1975, pp. 1157-1166.
8. Sant, M.T. and Paithankar, Y.G., "Online Digital Fault Locator for Overhead Transmission Line" , *IEE Proceedings*, Vol. 126, No. 11, November 1979, pp. 1181-1185.

9. Takagi, T., Yamakoshi, Y., Yamaura, M., Kondow, R. and Matsushima, T., "Development of a New Type Fault locator Using the One-terminal Voltage and Current Data", *IEEE Transactions on Power Apparatus and Systems*, Vol. PAS-101, No 8, August 1982, pp. 2892-2898.
10. Sachdev, M.S., and Agarwal, R., "A Technique for Estimating Transmission Line Fault Locations from Digital Impedance Relay Measurements", *IEEE Transactions on Power Delivery*, Vol. 3, No. 1, January 1988, pp. 121-129.
11. Srinivasan, K. and St-Jacques, A., "A New Fault Location Algorithm for Radial Transmission Line with Loads", *IEEE Transactions on Power Delivery*, Vol. 4, No. 3, July 1989, pp. 1676-1682.
12. Johns, A.T., Lai, L.L., El-Hami, M. and Daruvala, D.J., "New Approach to Directional Fault Location for Overhead Power Distribution Feeders", *IEE Proceedings*, Vol. 138, Pt. C, No. 4, July 1991, pp. 351-357.
13. Girgis, Adly A., Fallon, Christopher M. and Lubkeman, David L., "A Fault Location Technique for Rural Distribution Feeders", *IEEE Transactions on Industry Applications*, Vol. 29, No. 6, November/December 1993, pp. 1170-1175.
14. Das, Ratan, "Estimating Locations of Shunt Faults on Distribution Lines", *M.Sc. Thesis, College of Graduate Studies and Research, University of Saskatchewan, Saskatchewan*, 1995.
15. Das, Ratan, Sachdev M.S. and Sidhu T.S., "A Technique for Estimating Locations of Shunt Faults on Distribution Lines", *Conference Proceedings of the IEEE WESCANEX*, May 15-16, 1995, Vol. 1, pp. 6-11.
16. Canadian Electricity Association, "1996 Annual Service Continuity Report on Distribution System Performance in Canadian Electrical Utilities", May 1997.
17. Mason, C. Russell, *The Art and Science of Protective Relaying*, John Wiley & Sons, Inc., 1956.
18. GEC Measurements, *Protective Relays Application Guide*, Stafford, England, 1987.
19. Horowitz, S.H. and Phadke, A.G., *Protective System Relaying*, Research Studies Press Ltd., Taunton, England, 1992.

20. IEEE Power System Relaying Committee of the IEEE Power Engineering Society, "Distribution Line Protection Practices: Industry Survey Analysis", *IEEE Transactions on Power Apparatus and Systems*, Vol. PAS-102, No. 10, October 1983, pp. 3279-3285.
21. Westinghouse Electric Corporation, *Electric Utility Engineering Reference Book: distribution systems*, Vol. 3, Pittsburgh, Pennsylvania, USA, 1965.
22. Westinghouse Electric Corporation, *Electrical Transmission and Distribution Reference Book*, Pittsburgh, Pennsylvania, USA, 1964.
23. Stevenson Jr., William D., *Elements of Power Systems Analysis*, McGraw-Hill Book Company, Inc., 1975.
24. Anderson, Paul M., *Analysis of Faulted Power Systems*, IEEE Press, 1995.
25. Wagner, C.F. and Evans, R.D., *Symmetrical Components*, McGraw-Hill Book Company, Inc., 1933.
26. Elmore, Walter A., (Editor), ABB Power T&D Company Inc., *Protective Relaying Theory and Applications*, Marcel Dekker Inc., 1994.
27. Gilkeson, C.L., Jeanne, P.A. and Vaage, E.F., "Power System Faults to Ground, Part II", *Transactions of the AIEE*, Vol. 56, No. 4, April 1937, pp. 428-433 and 474.
28. Warrington, A.R. Van C., *Protective Relays, Their Theory and Practice*, Vol. I, Chapman and Hall Ltd. London, 1968.
29. Clarke, Edith, *Circuit Analysis of A-C Power Systems*, Vol. II, John Wiley & Sons, Inc., 1950.
30. Sant, M. T. and Paithankar, Y. G., "Fault Locator for Long EHV Transmission lines", *Electric Power Systems Research*, Vol. 6, No. 4, December 1983, pp. 305-310.
31. Schweitzer III, Edmund O., "Evaluation and Development of Transmission Line Fault-Locating Techniques which uses Sinusoidal Steady-State Information" , *presented at the Ninth Annual Protective Relay Conference*, Spokane, Washington, October ,1982.

32. Wiszniewski, A., "Accurate Fault Impedance Locating Algorithm", *IEE Proceedings*, Vol. 130, Pt. C, No. 6, November 1983, pp. 311-314.
33. Eriksson, L., Saha, M.M. and Rockefeller, G.D., "An Accurate Fault Locator with Compensation for Apparent Reactance in the Fault Resistance Resulting from Remote-End Infeed", *IEEE Transactions on Power Apparatus and Systems*, Vol. PAS-104, No. 2, February 1985, pp. 424-436.
34. Richards, Gill G. and Tan, Owen T., "An Accurate Fault Location Estimator for Transmission lines", *IEEE Transactions on Power Apparatus and Systems*, Vol. PAS-101, No. 4 , April 1982, pp. 945-950.
35. Sachdev, M.S., Das, R. and Sidhu, T.S., "Determining Location of Faults in Distribution Systems", *Proceedings of the IEE International Conference on Developments in Power System Protection*, Nottingham, UK, March 25-27, 1997.
36. Sachdev, M.S. and Baribeau, M.A., "A New Algorithm for Digital Impedance Relays", *IEEE Transactions on Power Apparatus and Systems*, Vol. PAS-98, No. 6, November/December 1979, pp. 2232-2240.
37. IEEE Power System Engineering Committee, "System Load Dynamics-Simulation Effects and Determination of Load Constants", *IEEE Transactions on Power Apparatus and Systems*, Vol. PAS-92, March 1973, pp. 600-609.
38. Concordia, C., "Representation of Loads", *IEEE PES Winter Power Meeting*, New York, 1975, Monograph 75 - CH 0970-4-PWR, pp. 41-45.
39. Shackshaft , G., Symons, O.C. and Hadwick, J.G., "General-Purpose Model of Power-System Loads", *IEE Proceedings*, Vol. 124, No. 8, August 1977, pp. 715-723.
40. Shackshaft , G., and Ashmole, P.H., "The Influence of Load Characteristics on Power System Performance - A C.E.G.B. Viewpoint", *CIGRE 1978 Session*, Paper 31-02, August 30 - September 7, Paris, France.
41. Srinivasan, K., Nguyen, C.T., Robichaud, Y, St. Jacques, A. and Rogers, G. J., "Load Response Coefficients Monitoring System: Theory and Field Experience", *IEEE transactions on Power Apparatus and Systems*, Vol. PAS-100, No. 8, August 1981, pp. 3818-3827.
42. El-Hawary, M.E., "Incorporation of Load Modeling in Load Flow Studies", *Transactions of the Engineering and Operating Division, Canadian Electrical Association*, Vol. 22, part 4, 1983, Paper No. 83-SP-160, pp. 1-14.

43. IEEE Task Group on Long Range Distribution System Design of the Working Group on Distribution System Design, of the Distribution Subcommittee, of the Transmission and Distribution Subcommittee, "The Distribution System of the Year 2000", *IEEE Transactions on Power Apparatus and Systems*, Vol. PAS-101, No. 8, August 1982, pp. 2485-2490.
44. Baran, Mesut E., Zhu, Jinxiang and Kelly, Arthur W., "Meter Placement for Real-Time Monitoring of Distribution Feeders", *IEEE Transactions on Power Systems*, Vol. 11, No. 1, February 1996, pp. 332-337.
45. Klusmeyer, Terry R., "Elimination of Faulted Circuit Indicator Coordination Concerns", *IEEE/PES Transmission and Distribution Conference*, September 15 - 20, 1996, Los Angeles, California.
46. Van Le, A., "Overhead & Underground SCADA: Radio Faulted Circuit Indicators and Applications", *IEEE/PES Transmission and Distribution Conference*, September 15 - 20, 1996, Los Angeles, California.
47. Manitoba HVDC Research Center, *PSCAD/EMTDC Manuals*, Winnipeg, 1994.
48. Swift, G.W., "The Spectra of Fault-Induced Transients", *IEEE Transactions on Power Apparatus and Systems*, Vol. PAS-98, No. 3, May/June 1979, pp. 940-947.
49. IEEE Power System Relaying Committee, "Fault Induced Wave Distortion of Interest to Relay Engineers", *IEEE Transactions on Power Apparatus and Systems*, Vol. PAS-104, December 1985, pp. 3574-3584.
50. Oppenheim, Alan V. and Schafer, Ronald W., *Digital Signal Processing*, Prentice-Hall, Inc., Englewood Cliffs, New Jersey, 1975.
51. Rabiner, Lawrence R. and Gold, Bernard, *Theory and Application of Digital Signal Processing*, Prentice-Hall, Inc., Englewood Cliffs, New Jersey, 1975.
52. International Electrotechnical Commission, *IEC 60186 Amd.2 Ed. 2.0: Voltage transformers*, Geneva, Switzerland, Sept. 1995.
53. International Electrotechnical Commission, *IEC 60044-1: Instrument transformers - Part 1: Current transformers*, Geneva, Switzerland, Dec. 1996.

54. Das, R., "Sensitivity Studies of the Fault Location Technique for a Radial Distribution System with Laterals", *Report of the Department of Electrical Engineering, University of Saskatchewan*, Saskatchewan, 1997.
55. Sachdev, M.S. and Sidhu, T.S., "A Laboratory for Research and Teaching of Microprocessor-Based Power System", *IEEE Transactions on Power Systems*, Vol. 11, No. 2, May 1996, pp. 599-606.
56. Sidhu, T.S., Sachdev, M.S. and Das, R., "Modern Relays: Research and Teaching Using PCs", *IEEE Computer Application in Power*, Vol. 10, No. 2, April 1997, pp. 50-55.
57. National Semiconductor Corporation, *Linear Databook 2*, 1987.
58. Valkenburg, M.E. Van, *Analog Filter Design*, CBS College Publishing, New York, 1982.
59. Texas Instruments Inc., *Linear Circuits, Operational Amplifiers, Databook*, Volume 1, 1992.
60. Spectrum Signal Processing Inc., *4 Channel Analog I/O Board User's Manual: Version 2.1*, 1988.
61. Spectrum Signal Processing Inc., *PC/C31 Real Time Application Board Technical Reference Manual: Version 1.06*, 1995.
62. Spectrum Signal Processing Inc., *PC/C31 Board User Guide: Version 1.04*, 1995.
63. Texas Instruments Inc., *TMS320C3x User's Guide: Revision F*, 1992.
64. Microsoft Corporation , *Microsoft Visual Basic Programming System for Windows, Programmer's Guide and Language Reference: Version 3.0*, 1993.
65. Spectrum Signal Processing Inc., *PC/C31 Intelligent Interface Library Windows Support Software User Manual: Version 1.01*, 1995.
66. Texas Instruments Inc., *TMS320 Floating-Point DSP Optimizing C Compiler, Microprocessor Development systems, User's Guide: Revision A*, 1991.
67. Texas Instruments Inc., *TMS320 Floating-Point DSP Assembly Language Tools, Microprocessor Development systems, User's Guide: Revision A*, 1991.

68. Microsoft Corporation , *Microsoft FORTRAN Development System Version 5.1: Environment and Tools, and Reference*, 1993.
69. Texas Instruments Inc., *Digital Signal Processing Applications with the TMS320C30 Evaluation Module, Selected Application Notes, Microprocessor Development systems: Revision A*, 1991.
70. Texas Instruments Inc., *TMS320C3x C Source Debugger User's Guide, Microprocessor Development systems: Revision F*, 1991.
71. Spectrum Signal Processing Inc., *MPC View for PC C31, User Manual: Version 1.01*, 1995.
72. Manitoba HVDC Research Center, *Real Time Playback (RTP) and PSCAD/EMTDC Recorder Component User's Guide*, Winnipeg, 1997.

APPENDICES

Appendix A. Representation of Various Shunt Faults

Using symmetrical component theory [22, 23, 24, 25, 26], three phase unbalanced voltages or currents can be represented by three sets of voltages and currents, in which two sets are balanced while the third set has co-phasor quantities. Thus, a set of unbalanced currents, I_{af} , I_{bf} and I_{cf} , can be represented as

$$I_{af} = (I_{0f} + I_{1f} + I_{2f}) \quad (\text{A.1})$$

$$I_{bf} = (I_{0f} + a^2 I_{1f} + aI_{2f}) \quad (\text{A.2})$$

$$I_{cf} = (I_{0f} + aI_{1f} + a^2 I_{2f}) \quad (\text{A.3})$$

where: I_{0f} , I_{1f} and I_{2f} are the zero, positive and negative sequence currents with phase A as reference.

$a = 1\angle 120^\circ$ is the phasor operator.

The relationship between the sequence quantities and line currents can be alternatively expressed by Equations A.4 to A.6.

$$I_{0f} = \frac{1}{3}(I_{af} + I_{bf} + I_{cf}) \quad (\text{A.4})$$

$$I_{1f} = \frac{1}{3}(I_{af} + aI_{bf} + a^2 I_{cf}) \quad (\text{A.5})$$

$$I_{2f} = \frac{1}{3}(I_{af} + a^2 I_{bf} + aI_{cf}) \quad (\text{A.6})$$

A.1 Single-phase-to-ground faults

Consider a phase A-to-ground fault through a fault resistance R_f as in Figure A.1.

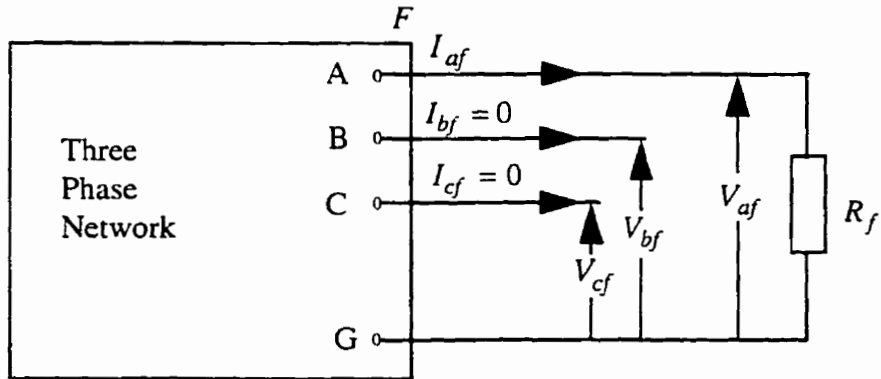


Figure A.1. Fault conditions for a phase A-to-ground fault.

The operating parameters at the fault, F , can be expressed by the following equations.

$$I_{bf} = I_{cf} = 0 \quad (\text{A.7})$$

$$V_{af} = I_{af} R_f \quad (\text{A.8})$$

where: I_{af} , I_{bf} and I_{cf} are the phase A, B and C currents flowing into the fault.
 V_{af} is the phase A voltage at the fault.

Using the symmetrical components and phase A as reference; the zero, positive and negative sequence components of the fault currents can be obtained as shown in Equations A.4 to A.6.

Substituting values of I_{bf} and I_{cf} from Equation A.7 in the Equations A.4 to A.6 provides

$$I_{0f} = I_{1f} = I_{2f} = \frac{1}{3}(I_{af}) \quad (\text{A.9})$$

Expressing V_{af} as a sum of its symmetrical components and substituting I_{af} with $3I_{0f}$, the following equation is obtained.

$$V_{0f} + V_{1f} + V_{2f} = I_{0f}(3R_f) \quad (\text{A.10})$$

where: V_{0f} , V_{1f} and V_{2f} are the zero, positive and negative sequence fault voltages of phase A at F .

Equations A.9 and A.10 lead to the conclusion that the sequence networks circuit, shown in Figure 2.2 (b), can be used to represent a phase A to ground fault.

Phase B-to-ground and phase C-to-ground faults can be represented by similar circuits if phase B and phase C are used as the reference phases for defining symmetrical components.

A.2 Two-phase-to-ground faults

Consider a phase B and phase C-to-ground fault through fault resistances R_f and R_g as shown in Figure A.2.

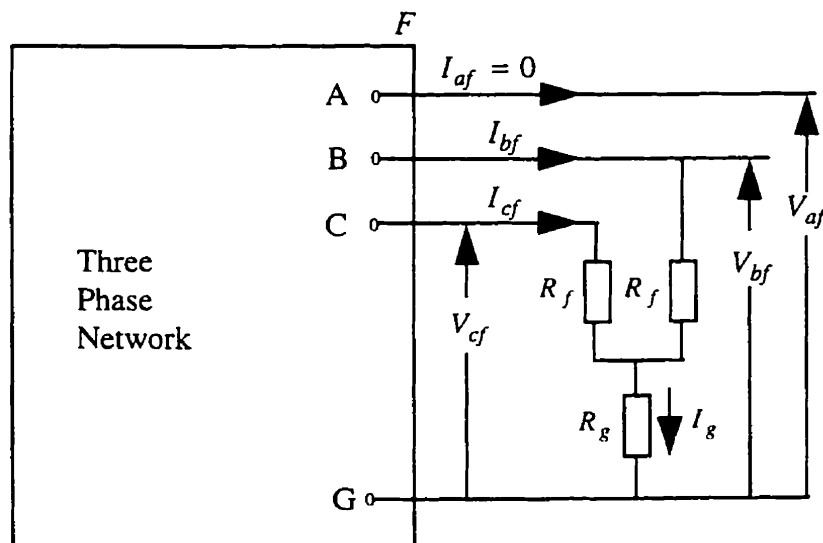


Figure A.2. Fault conditions for a phase B and phase C-to-ground fault.

The operating parameters at the fault, F , can be expressed by the following equations.

$$I_{af} = 0 \quad \text{and} \quad I_{bf} + I_{cf} = I_g \quad (\text{A.11})$$

$$V_{bf} = I_{bf} R_f + I_g R_g \quad (\text{A.12})$$

$$V_{cf} = I_{cf} R_f + I_g R_g \quad (\text{A.13})$$

where: V_{bf} and V_{cf} are phase B and phase C fault voltages at F .

Subtracting Equation A.13 from Equation A.12 and adding Equations A.12 and A.13, the following equations are obtained.

$$V_{bf} - V_{cf} = (I_{bf} - I_{cf}) R_f \quad (\text{A.14})$$

$$V_{bf} + V_{cf} = (I_{bf} + I_{cf}) R_f + 2I_g R_g \quad (\text{A.15})$$

Using the symmetrical components with phase A as reference and expressing currents with their symmetrical components, Equations A.1 to A.3 are obtained. Similar equations can be obtained for voltages and are shown as follows:

$$V_{af} = (V_{0f} + V_{1f} + V_{2f}) \quad (\text{A.16})$$

$$V_{bf} = (V_{0f} + a^2 V_{1f} + a V_{2f}) \quad (\text{A.17})$$

$$V_{cf} = (V_{0f} + a V_{1f} + a^2 V_{2f}) \quad (\text{A.18})$$

Substituting I_{af} from Equation A.1 in A.11, the following equation is obtained.

$$(I_{0f} + I_{1f} + I_{2f}) = 0 \quad (\text{A.19})$$

Substituting, V_{bf} , V_{cf} , I_{bf} and I_{cf} from Equations A.17, A.18, A.2 and A.3 in Equations A.14 and A.15 respectively, and rearranging, the following equations are obtained.

$$(V_{1f} - I_{1f} R_f) = (V_{2f} - I_{2f} R_f) \quad (\text{A.20})$$

$$[2V_{0f} + (a^2 + a)(V_{1f} + V_{2f})] = [2I_{0f} + (a^2 + a)(I_{1f} + I_{2f})](R_f + 2R_g) \quad (\text{A.21})$$

Substituting, $a^2 + a = -1$ and $(V_{2f} - I_{2f} R_f)$ from Equation A.20 in Equation A.21 and rearranging, the following equation is obtained.

$$[V_{0f} - I_{0f}(R_f + 2R_g)] = (V_{1f} - I_{1f} R_f) - (I_{1f} + I_{2f}) R_g \quad (\text{A.22})$$

Substituting, $I_{1f} + I_{2f} = -I_{0f}$ from Equation A.19, in Equation A.22 and rearranging, the following equation is obtained.

$$[V_{0f} - I_{0f}(R_f + 3R_g)] = (V_{1f} - I_{1f}R_f) \quad (\text{A.23})$$

From Equations A.20 and A.23, it is clear that:

$$(V_{1f} - I_{1f}R_f) = (V_{2f} - I_{2f}R_f) = [V_{0f} - I_{0f}(R_f + 3R_g)] \quad (\text{A.24})$$

Equations A.19 and A.24, lead to the conclusion that the sequence networks circuit, shown in Figure 2.3 (b), can be used to represent a phase B and phase C-to-ground fault.

Phase C and phase A-to-ground, and phase A and phase B-to-ground faults can be represented by similar circuits if phase B and phase C are used as the reference phases for defining the symmetrical components.

A.3 Phase-to-phase faults

Consider a phase B-to-phase C fault through a fault resistance R_f as shown in Figure A.3.

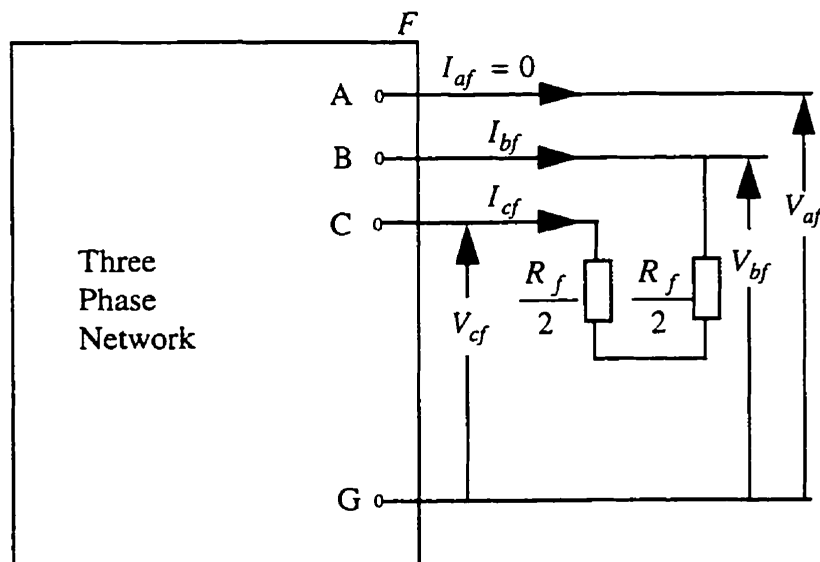


Figure A.3. Fault conditions for a phase B-to-phase C fault.

The operating parameters at the fault, F , can be expressed by the following equations.

$$I_{af} = 0 \quad \text{and} \quad I_{bf} + I_{cf} = 0 \quad (\text{A.25})$$

$$V_{bf} - I_{bf} \left(\frac{R_f}{2} \right) = V_{cf} - I_{cf} \left(\frac{R_f}{2} \right) \quad (\text{A.26})$$

Using symmetrical components with phase A as reference and Equation A.25, the zero, positive and negative sequence components of the fault current can be obtained as follows.

$$I_{0f} = \frac{1}{3}(I_{af} + I_{bf} + I_{cf}) = 0 \quad (\text{A.27})$$

$$I_{1f} = \frac{1}{3}(a - a^2)(I_{bf}) \quad (\text{A.28})$$

$$I_{2f} = -\frac{1}{3}(a - a^2)(I_{bf}) \quad (\text{A.29})$$

Equations A.27 to A.29, provide:

$$I_{0f} = 0 \quad \text{and} \quad I_{1f} = -I_{2f} \quad (\text{A.30})$$

Expressing V_{bf} , V_{cf} , I_{bf} and I_{cf} in their symmetrical components and substituting V_{bf} , V_{cf} , I_{bf} and I_{cf} from Equations A.17, A.18, A.2 and A.3 in Equation A.26 and rearranging, the following equation is obtained.

$$\left[V_{1f} - I_{1f} \left(\frac{R_f}{2} \right) \right] = \left[V_{2f} - I_{2f} \left(\frac{R_f}{2} \right) \right] \quad (\text{A.31})$$

Equations A.30 and A.31, lead to the conclusion that the sequence networks circuit, shown in Figure 2.4 (b), can be used to represent a phase B-to-phase C fault.

Phase C-to-phase A and phase A-to-phase B faults can be represented by similar circuits if phase B and phase C are used as the reference phases for defining the symmetrical components.

A.4 Balanced three-phase faults

Consider a balanced three-phase fault, involving ground, through fault resistances R_f and R_g as shown in Figure A.4.

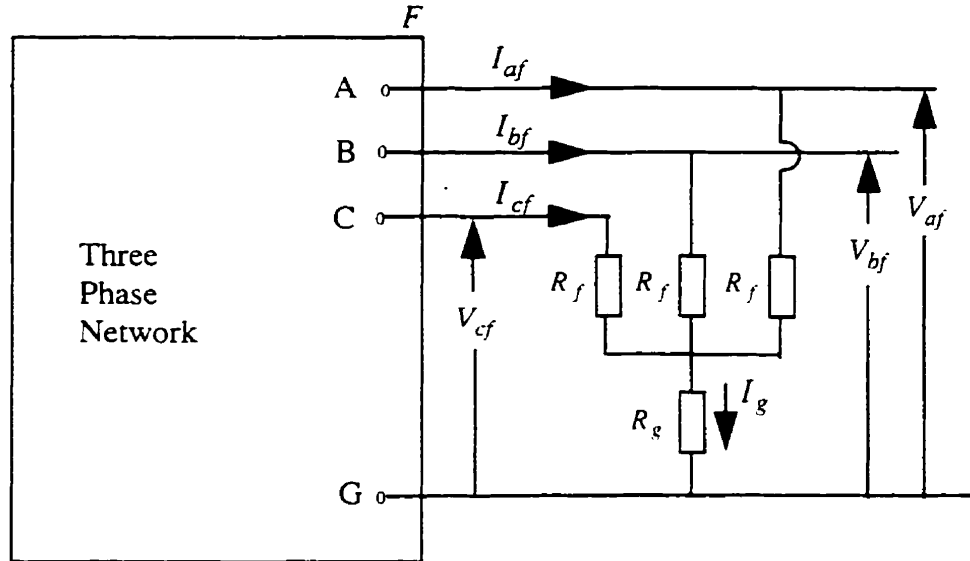


Figure A.4. Fault conditions for a balanced three-phase fault, involving ground.

The operating parameters at the fault, F , can be expressed by the following equations.

$$I_{af} + I_{bf} + I_{cf} = I_g \quad (\text{A.32})$$

$$V_{af} = I_{af}R_f + I_gR_g \quad (\text{A.33})$$

$$V_{bf} = I_{bf}R_f + I_gR_g \quad (\text{A.34})$$

$$V_{cf} = I_{cf}R_f + I_gR_g \quad (\text{A.35})$$

Subtracting Equation A.35 from Equation A.34 and adding Equations A.34 and A.35, the following equations are obtained.

$$V_{bf} - V_{cf} = (I_{bf} - I_{cf})R_f \quad (\text{A.36})$$

$$V_{bf} + V_{cf} = (I_{bf} + I_{cf})R_f + 2I_gR_g \quad (\text{A.37})$$

Using symmetrical component theory with phase A as reference and expressing voltages and currents with their symmetrical components, Equations A.16 to A.18 and A.1 to A.3 are obtained.

Substituting, V_{bf} , V_{cf} , I_{bf} and I_{cf} from Equations A.17, A.18, A.2 and A.3 in Equations A.36 and A.37, and rearranging, following equations are obtained.

$$(V_{1f} - I_{1f} R_f) = (V_{2f} - I_{2f} R_f) \quad (\text{A.38})$$

$$[V_{0f} - I_{0f}(R_f + 3R_g)] = (V_{1f} - I_{1f} R_f) \quad (\text{A.39})$$

Adding Equations A.33, A.34 and A.35, the following equation is obtained.

$$V_{af} + V_{bf} + V_{cf} = (I_{af} + I_{bf} + I_{cf})R_f + 3I_g R_g \quad (\text{A.40})$$

Substituting I_g from Equation A.32, in A.40, the following equation is obtained.

$$V_{af} + V_{bf} + V_{cf} = (I_{af} + I_{bf} + I_{cf})(R_f + 3R_g) \quad (\text{A.41})$$

Substituting, V_{af} , V_{bf} , V_{cf} , I_{af} , I_{bf} and I_{cf} from Equations A.16 to A.18 and A.1 to A.3 in Equation A.41, and rearranging, the following equation is obtained.

$$[V_{0f} - I_{0f}(R_f + 3R_g)] = 0 \quad (\text{A.42})$$

Equations A.38, A.39 and A.42 provide:

$$(V_{1f} - I_{1f} R_f) = (V_{2f} - I_{2f} R_f) = [V_{0f} - I_{0f}(R_f + 3R_g)] = 0 \quad (\text{A.43})$$

Equation A.43, leads to the conclusion that the sequence networks circuit, shown in Figure 2.5 (b), can be used to represent a balanced three-phase fault, involving ground, through fault resistances R_f and R_g as shown in Figure 2.5 (a).

Consider a balanced three-phase fault, without ground, through fault resistance R_f as shown in Figure A.5. Proceeding in a similar way, the fault condition can be represented by Figure 2.5 (c) which is similar to Figure 2.5 (b) except that the zero sequence network is open-circuited.

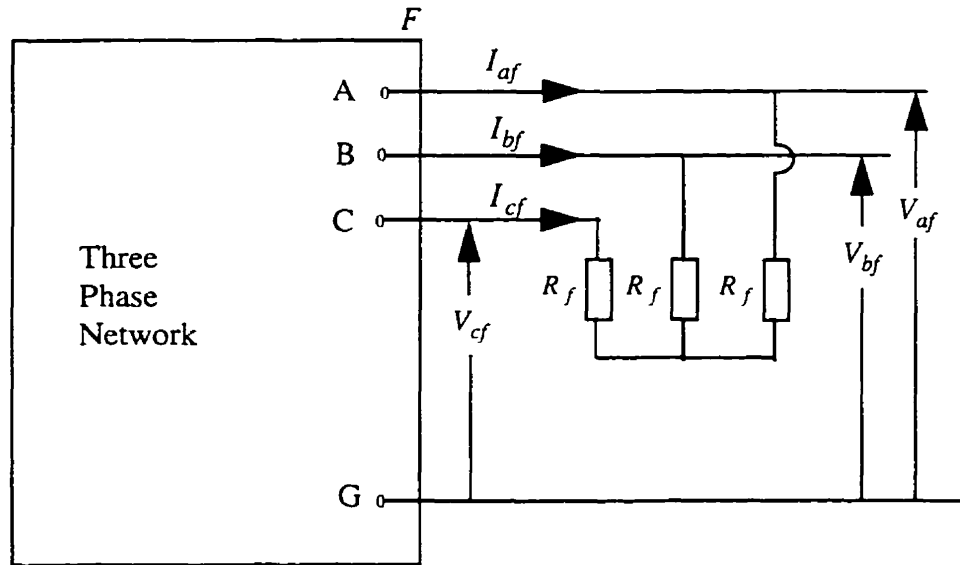


Figure A.5. Fault conditions for a balanced three-phase fault, without ground.

There is no connection to ground at the fault, therefore, the resistance R_g approaches an infinite value. This can alternatively be stated by the following equation which represents the fault conditions at fault point F .

$$I_{af} + I_{bf} + I_{cf} = 0 \quad (\text{A.44})$$

Substituting, I_{af} , I_{bf} and I_{cf} from Equations A.1 to A.3 in Equation A.44, and rearranging, following equation is obtained.

$$I_{0f} = 0 \quad (\text{A.45})$$

Positive and negative sequence networks are same as that of balanced three-phase fault involving ground.

Appendix B. Least Error Squares Algorithm

Least Error Squares (LES) algorithm [36] is used to estimate the phasors of the fundamental and harmonic frequency components of voltages and currents. It is based on minimizing the mean-square error between the actual and assumed waveforms. The voltage and/or current waveform is modeled as a combination of the fundamental frequency component, an exponentially decaying dc component and harmonics of specified orders.

$$x(t) = X_0 e^{-t/\tau} + \sum_{n=1}^N X_n \sin(n\omega_0 t + \theta_n) \quad (\text{B.1})$$

- where:
- $x(t)$ is the instantaneous value of the signal at time t .
 - τ is the time constant of the decaying dc component.
 - N is the highest order of the harmonic component present in the signal.
 - ω_0 is the fundamental frequency of the system.
 - X_0 is the magnitude of the dc offset at $t = 0$.
 - X_n is the peak value of the n^{th} harmonic component.
 - θ_n is the phase angle of the n^{th} harmonic component.

Expressing the decaying dc component by the Taylor series expansion and retaining the first two terms, the following equation is obtained.

$$x(t) = X_0 - \left(\frac{X_0}{\tau} \right) t + \sum_{n=1}^N X_n \sin(n\omega_0 t + \theta_n) \quad (\text{B.2})$$

For further discussion on this subject, assume that each input is composed of an exponentially decaying dc component, the fundamental frequency component and components of the second, third, fourth and fifth harmonics. For $t = t_1$, Equation B.2 can, therefore, expressed as

$$\begin{aligned} x(t_1) = X_0 - \left(\frac{X_0}{\tau} \right) t_1 &+ X_1 \sin(\omega_0 t_1 + \theta_1) + X_2 \sin(2\omega_0 t_1 + \theta_2) \\ &+ X_3 \sin(3\omega_0 t_1 + \theta_3) + X_4 \sin(4\omega_0 t_1 + \theta_4) \\ &+ X_5 \sin(5\omega_0 t_1 + \theta_5) \end{aligned} \quad (\text{B.3})$$

Using trigonometric identities, Equation B.3 can be rewritten as

$$\begin{aligned}
x(t_1) = X_0 - \left(\frac{X_0}{\tau} \right) t_1 + & (X_1 \cos \theta_1) \sin \omega_0 t_1 + (X_1 \sin \theta_1) \cos \omega_0 t_1 \\
& + (X_2 \cos \theta_2) \sin 2\omega_0 t_1 + (X_2 \sin \theta_2) \cos 2\omega_0 t_1 \\
& + (X_3 \cos \theta_3) \sin 3\omega_0 t_1 + (X_3 \sin \theta_3) \cos 3\omega_0 t_1 . \quad (\text{B.4}) \\
& + (X_4 \cos \theta_4) \sin 4\omega_0 t_1 + (X_4 \sin \theta_4) \cos 4\omega_0 t_1 \\
& + (X_5 \cos \theta_5) \sin 5\omega_0 t_1 + (X_5 \sin \theta_5) \cos 5\omega_0 t_1
\end{aligned}$$

This equation can be expressed as

$$\begin{aligned}
x(t_1) = & a_{11}x_1 + a_{12}x_2 + a_{13}x_3 + a_{14}x_4 + a_{15}x_5 + a_{16}x_6 + a_{17}x_7 \\
& + a_{18}x_8 + a_{19}x_9 + a_{110}x_{10} + a_{111}x_{11} + a_{112}x_{12} \quad (\text{B.5})
\end{aligned}$$

where: $x_1 = X_0$, $x_2 = -X_0 / \tau$, $x_3 = X_1 \cos \theta_1$, $x_4 = X_1 \sin \theta_1$,
 $x_5 = X_2 \cos \theta_2$, $x_6 = X_2 \sin \theta_2$, $x_7 = X_3 \cos \theta_3$, $x_8 = X_3 \sin \theta_3$,
 $x_9 = X_4 \cos \theta_4$, $x_{10} = X_4 \sin \theta_4$, $x_{11} = X_5 \cos \theta_5$, $x_{12} = X_5 \sin \theta_5$,
 $a_{11} = 1$, $a_{12} = t_1$, $a_{13} = \sin(\omega_0 t_1)$, $a_{14} = \cos(\omega_0 t_1)$,
 $a_{15} = \sin(2\omega_0 t_1)$, $a_{16} = \cos(2\omega_0 t_1)$, $a_{17} = \sin(3\omega_0 t_1)$, $a_{18} = \cos(3\omega_0 t_1)$,
 $a_{19} = \sin(4\omega_0 t_1)$, $a_{110} = \cos(4\omega_0 t_1)$, $a_{111} = \sin(5\omega_0 t_1)$, $a_{112} = \cos(5\omega_0 t_1)$.

The signal is sampled at intervals of Δt seconds and Equation B.5, can be rewritten as follows by substituting $t_1 = m\Delta t$.

$$\begin{aligned}
x(m\Delta t) = & a_{m1}x_1 + a_{m2}x_2 + a_{m3}x_3 + a_{m4}x_4 + a_{m5}x_5 + a_{m6}x_6 + a_{m7}x_7 \\
& + a_{m8}x_8 + a_{m9}x_9 + a_{m10}x_{10} + a_{m11}x_{11} + a_{m12}x_{12} + a_{m13}x_{13} \quad (\text{B.6})
\end{aligned}$$

where: $\Delta t = \frac{1}{f_s}$, (B.7)

f_s is the sampling frequency.

m is the sample number.

The a -coefficients are now redefined as follows:

$a_{m1} = 1$, $a_{m2} = m\Delta t$, $a_{m3} = \sin(\omega_0 m\Delta t)$, $a_{m4} = \cos(\omega_0 m\Delta t)$, $a_{m5} = \sin(2\omega_0 m\Delta t)$,
 $a_{m6} = \cos(2\omega_0 m\Delta t)$, $a_{m7} = \sin(3\omega_0 m\Delta t)$, $a_{m8} = \cos(3\omega_0 m\Delta t)$,
 $a_{m9} = \sin(4\omega_0 m\Delta t)$, $a_{m10} = \cos(4\omega_0 m\Delta t)$, $a_{m11} = \sin(5\omega_0 m\Delta t)$, $a_{m12} = \cos(5\omega_0 m\Delta t)$.

Thirteen equations, similar to B.6, can be formed using thirteen consecutive samples. These can be written as

$$\begin{matrix} [A] & [X] & = & [x] \\ 13 \times 12 & 12 \times 1 & & 13 \times 1 \end{matrix} \quad (\text{B.8})$$

The least error squares estimate of $[X]$ is given by the following equation.

$$[X] = \left[[A^T][A] \right]^{-1} [A^T] [x] = [A]^+ [x] \quad (\text{B.9})$$

where: $[A]^+$ is the left pseudo-inverse of $[A]$.

The elements of the 3rd and 4th rows of $[A]^+$, are the coefficients of the filter for estimating the real and imaginary components of the fundamental frequency phasor of the signal. These coefficients can be calculated in the off-line mode.

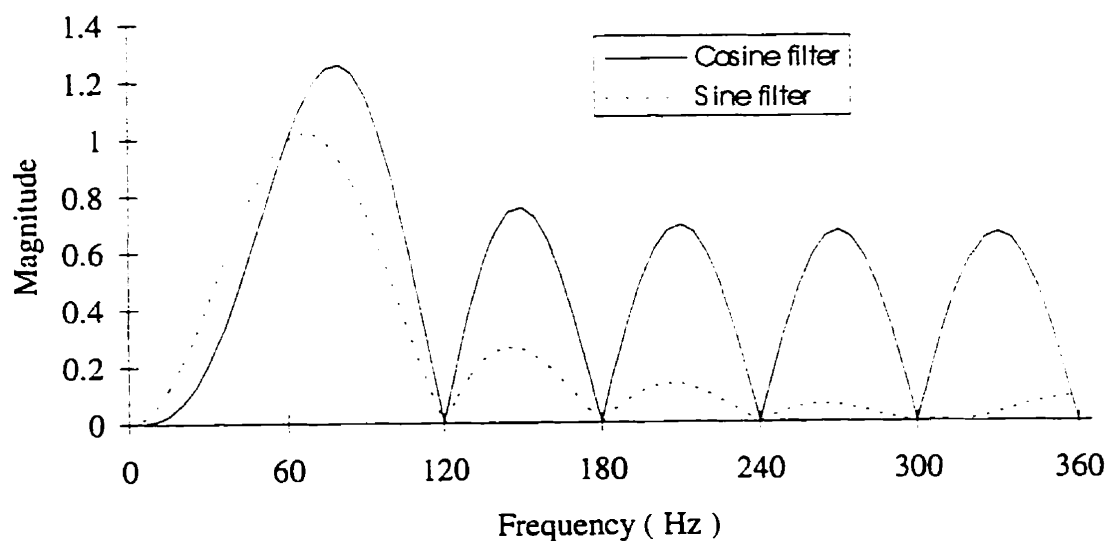
For the work reported in this thesis, sampling frequency of 720 Hz was used. The time coinciding with the seventh sample was considered to be zero. The filter coefficients, for estimating the real and imaginary components of the fundamental frequency phasor of the signal, are given in Table B.1. The real and imaginary components of the fundamental frequency phasor are calculated by multiplying the coefficients with the samples. The transfer function of the cosine and sine filters in the z -plane is given by

$$\begin{aligned} H(z) = & C(1)z^{-6} + C(2)z^{-5} + C(3)z^{-4} + C(4)z^{-3} + C(5)z^{-2} + C(6)z^{-1} + C(7) \\ & + C(8)z^1 + C(9)z^2 + C(10)z^3 + C(11)z^4 + C(12)z^5 + C(13)z^6 \end{aligned} \quad (\text{B.10})$$

The magnitude response of the LES algorithm obtained by using the numerical values of the filter coefficients and substituting z with $e^{j\omega\Delta t}$ in Equation B.10 and evaluating the resulting equation. The responses are shown in Figure B.1.

Table B.1. Filter coefficients for the Least Error Squares algorithm.

Coefficient Number	Cosine Filter (Real)	Sine Filter (Imaginary)
$C(1)$	0.31100423	-0.08695652
$C(2)$	-0.08333333	-0.13709119
$C(3)$	-0.14433757	-0.09057971
$C(4)$	-0.16666667	0.00724638
$C(5)$	-0.14433757	0.07608695
$C(6)$	-0.08333333	0.15158394
$C(7)$	0.00000000	0.15942029
$C(8)$	0.08333333	0.15158394
$C(9)$	0.14433757	0.07608695
$C(10)$	0.16666667	0.00724638
$C(11)$	0.14433757	-0.09057971
$C(12)$	0.08333333	-0.13709119
$C(13)$	-0.31100423	-0.08695652

**Figure B.1.** Magnitude response of the Least Error Squares algorithm.

Appendix C. Static Response Type Load Model

Static response type models [11] have been found to explain satisfactorily the behavior of large composite loads at most points. These can be mathematically expressed as

$$\frac{\partial P_r}{P_r} = n_p \frac{\partial |V_r|}{|V_r|} \text{ and} \quad (\text{C.1})$$

$$\frac{\partial Q_r}{Q_r} = n_q \frac{\partial |V_r|}{|V_r|}, \quad (\text{C.2})$$

where: P_r is the active power of the load at node R .
 Q_r is the reactive power of the load at node R .
 V_r is the voltage at the node R .
 n_p and n_q are the response constants for the active and reactive components of the load respectively.

The relationship between the complex power and voltage can be expressed as follows.

$$P_r + j Q_r = K_p |V_r|^{n_p} + j K_q |V_r|^{n_q} \quad (\text{C.3})$$

$$P_r + j Q_r = V_r I_r^* = |V_r| \angle \theta_v I_r^* \quad (\text{C.4})$$

where: K_p and K_q are real constants.

Equating Equations C.3 and C.4, the following equation is obtained.

$$|V_r| \angle \theta_v I_r^* = K_p |V_r|^{n_p} + j K_q |V_r|^{n_q} \quad (\text{C.5})$$

Rearranging Equation C.5, the following equation is obtained.

$$I_r^* = \left(K_p |V_r|^{n_p - 2} + j K_q |V_r|^{n_q - 2} \right) V_r^* \quad (\text{C.6})$$

Conjugating both side of Equation C.6 and rearranging, the following equation is obtained.

$$\frac{I_r}{V_r} = \left(K_p |V_r|^{n_p - 2} - j K_q |V_r|^{n_q - 2} \right) \quad (\text{C.7})$$

Equation C.7 can be restated as Equation C.8.

$$Y_r = \left(G_r |V_r|^{n_p - 2} + jB_r |V_r|^{n_q - 2} \right) \quad (\text{C.8})$$

where: Y_r is the load admittance.

G_r is the constant proportional to load conductance.

B_r is the constant proportional to load susceptance.

If Y_r is measured at a specified voltage (e.g. pre-fault voltage), and n_p and n_q are known, the values of G_r and B_r can be determined. The values of G_r and B_r can then be used to determine Y_r at any other voltage.

The values of n_p and n_q for three types of loads are as follows.

$n_p = n_q = 0$ for constant power load.

$n_p = n_q = 1$ for constant current load.

$n_p = n_q = 2$ for constant impedance load.

Different methods for obtaining a practical value of n_p and n_q for a particular type of load have been suggested [37, 39, 40, 41]. In the absence of detailed data, the values of n_p and n_q can be assumed.

Appendix D. Voltages and Currents at the Line Terminals

The voltages and currents at the terminals of the distribution line section, shown in Figure D.1, are related by the following equation [23].

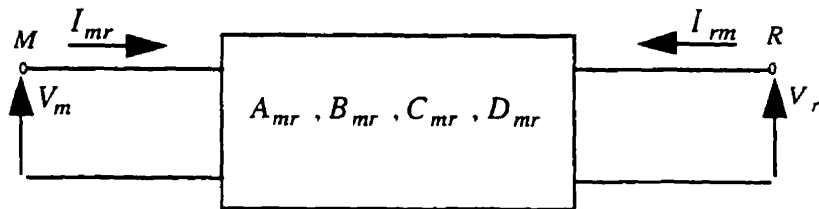


Figure D.1. Distribution line section between nodes M and R .

$$\begin{bmatrix} V_r \\ I_{rm} \end{bmatrix} = \begin{bmatrix} D_{mr} & -B_{mr} \\ C_{mr} & -A_{mr} \end{bmatrix} \begin{bmatrix} V_m \\ I_{mr} \end{bmatrix} \quad (\text{D.1})$$

- where: V_m and V_r are voltages at nodes M and R respectively.
 I_{mr} and I_{rm} are currents entering into the section from nodes M and R .
 A_{mr}, B_{mr}, C_{mr} and D_{mr} are the distribution section constants.

The constants A_{mr}, B_{mr}, C_{mr} and D_{mr} are given as

$$\begin{aligned} A_{mr} &= \cosh(\gamma_{mr} L_{mr}), \\ B_{mr} &= Z_{mr}^s \sinh(\gamma_{mr} L_{mr}), \\ C_{mr} &= \frac{\sinh(\gamma_{mr} L_{mr})}{Z_{mr}^s} \quad \text{and} \\ D_{mr} &= \cosh(\gamma_{mr} L_{mr}); \end{aligned} \quad (\text{D.2})$$

- where: γ_{mr} is the propagation constant per unit length,
 L_{mr} is the length of the section and
 Z_{mr}^s is the surge impedance of the section.

The propagation constant and surge impedance for the section are obtained from the following equations.

$$\gamma_{mr} = \sqrt{(r_{mr} + jx_{mr})(g_{mr} + jb_{mr})} \quad (\text{D.3})$$

$$Z_{mr}^s = \sqrt{\frac{r_{mr} + jx_{mr}}{g_{mr} + jb_{mr}}} \quad (\text{D.4})$$

- where:
- r_{mr} is the section resistance per unit length.
 - x_{mr} is the section reactance per unit length.
 - g_{mr} is the section conductance per unit length.
 - b_{mr} is the section susceptance per unit length.

As the length of sections in a distribution line are short; the A, B, C and D constants of each section can be approximated as

$$\begin{aligned} A &= 1, \\ B &= Z^s \gamma L, \\ C &= \frac{\gamma L}{Z^s} \text{ and} \\ D &= 1. \end{aligned} \quad (\text{D.5})$$

Substituting A and D , Equation D.1 is restated by the following equation.

$$\begin{bmatrix} V_r \\ I_{mr} \end{bmatrix} = \begin{bmatrix} 1 & -B_{mr} \\ C_{mr} & -1 \end{bmatrix} \begin{bmatrix} V_m \\ I_{mr} \end{bmatrix} \quad (\text{D.6})$$

Appendix E. Power Systems Simulation Software

This appendix gives a brief description of the power systems simulation software, PSCAD/EMTDC [47], which was used for generating fault data for a SaskPower distribution system. EMTDC and PSCAD are a group of related software packages which provide the user with a flexible power systems electromagnetic transients simulation tool. EMTDC is the software which actually performs the electromagnetic transients analysis on the user defined power system. The various software modules which comprise PSCAD are the graphical user interface to EMTDC. PSCAD, enables the user to select preprogrammed models of power system components to graphically build the power system networks. The built-in library of PSCAD, has models of voltage and current sources, machines, lines, transformers, switches and measuring instruments among many other power system apparatus models.

Compilation of the PSCAD network generates FORTRAN source code. The source code is then compiled using EMTDC which generates executable code that runs in the UNIX environment of the SUN SPARC workstation. Fault data generated by EMTDC was stored in a file. This data file was used for testing the proposed technique.

Appendix F. Anti-aliasing Filter

The voltages and currents during a fault consist of decaying dc, fundamental frequency (60 Hz) and high frequency components [48, 49]. The high frequency components, whose frequencies depend on the distance to the fault, are due to traveling wave phenomenon. Additionally, harmonics of the 60 Hz components are produced because of non-linearities in the power system.

The Least Error Squares (LES) algorithm was used to estimate the fundamental frequency components of the voltage and current signals from the samples obtained from the simulation of faults. Depending on the rate at which the voltages and currents are sampled, some of the high frequency components can appear to be components of power frequency [50]. The sampling frequency for the LES algorithm was selected as 720 Hz.

An anti-aliasing digital filter was designed to pre-process the voltage and current samples obtained from simulation studies before presenting to the LES algorithm. The principle of anti-aliasing dictates that the cut-off frequency of the designed low-pass filter should be less than one-half of the sampling frequency of the LES algorithm. A fourth-order low-pass digital filter with a cut-off frequency of 240 Hz was selected.

A fourth order analog filter is obtained by cascading four first order filters to have better roll-off characteristic. The transfer function of such a filter is given as

$$H(s) = \left[\frac{k}{s+k} \right]^4. \quad (\text{F.1})$$

where: k is a constant and

s is the Laplace operator.

In order to obtain the frequency response of the filter, the Laplace operator s , is replaced by $j\Omega$ and the following equation is obtained.

$$H(j\Omega) = \left[\frac{k}{j\Omega + k} \right]^4 \quad (\text{F.2})$$

The amplitude response of this analog filter should be -3dB at the cut-off frequency, Ω_c . This requirement dictates that the following equation must be satisfied.

$$\left| \frac{k}{j\Omega_c + k} \right|^4 = \frac{1}{\sqrt{2}} \quad (\text{F.3})$$

The solution of the Equation F.3, provide the following relation between k and Ω_c .

$$k = 2.2989592\Omega_c \quad (\text{F.4})$$

Digital implementation of the analog filter was performed using the bilinear transformation [51]. In this transformation, there is a conformal mapping from the s -plane to the z -plane and is given as follows.

$$s \rightarrow \frac{2}{\Delta T} \left(\frac{1 - z^{-1}}{1 + z^{-1}} \right) \quad (\text{F.5})$$

$$\Delta T = \frac{1}{F_s} \quad (\text{F.6})$$

where: ΔT is the sampling interval.
 F_s is the sampling frequency, 28800 Hz in this case.

Due to the warping effect, the cut-off frequency of the digital filter is some what different than that of its corresponding analog filter. The cut-off frequency of the analog filter for a selected digital filter cut-off frequency is given by the following equation.

$$\Omega_c = \frac{2}{\Delta T} \tan\left(\frac{\omega_c \Delta T}{2}\right) \quad (\text{F.7})$$

where: ω_c is the cut-off frequency of the digital filter, 240 Hz in this case.

Substituting values of ΔT and ω_c in Equation F.7, the cut-off frequency of the analog filter, Ω_c is obtained as 1508.3091 radians/second. Substituting value of Ω_c in Equation F.4, the value of k is obtained as 3467.5411. The transfer function for the fourth-order analog filter that has a cut-off frequency of 1508.3091 radians/second can, therefore, be expressed by the following equation.

$$H(s) = \left[\frac{3467.5411}{s + 3467.5411} \right]^4 \quad (\text{F.8})$$

Transfer function for the digital low-pass filter is obtained by substituting s in Equation F.8, from Equation F.5 and is given by the following equation.

$$H(z) = \left[\frac{1 + z^{-1}}{17.611195 - 15.611195z^{-1}} \right]^4 \quad (\text{F.9})$$

Equation F.9 is restated by the following equation.

$$H(z) = 1.0395484 \times 10^{-5} \left[\frac{1 + z^{-1}}{1 - 0.88643587z^{-1}} \right]^4 \quad (\text{F.10})$$

Rearranging Equation F.10, the transfer function of the designed low-pass digital filter is obtained as follows.

$$H(z) = \frac{1.0395484 \times 10^{-5} (1 + 4z^{-1} + 6z^{-2} + 4z^{-3} + z^{-4})}{(1 - 3.5457435z^{-1} + 4.7146113z^{-2} - 2.7861337z^{-3} + 0.61743222z^{-4})} \quad (\text{F.11})$$

Since, $H(z) = \frac{Y(z)}{X(z)}$, Equation F.11 is restated as follows.

$$\frac{Y(z)}{X(z)} = \frac{1.0395484 \times 10^{-5} (1 + 4z^{-1} + 6z^{-2} + 4z^{-3} + z^{-4})}{(1 - 3.5457435z^{-1} + 4.7146113z^{-2} - 2.7861337z^{-3} + 0.61743222z^{-4})} \quad (\text{F.12})$$

Rearranging Equation F.12, the following equation is obtained.

$$\begin{aligned} Y(z)(1 - 3.5457435z^{-1} + 4.7146113z^{-2} - 2.7861337z^{-3} + 0.61743222z^{-4}) \\ = 1.0395484 \times 10^{-5} (1 + 4z^{-1} + 6z^{-2} + 4z^{-3} + z^{-4}) X(z) \end{aligned} \quad (\text{F.13})$$

Equation F.13 is restated in terms of a sequence of n samples as follows.

$$\begin{aligned} y(n) &= 1.0395484 \times 10^{-5} (x(n) + 4x(n-1) + 6x(n-2) + 4x(n-3) + x(n-4)) \\ &\quad + 3.5457435y(n-1) - 4.7146113y(n-2) + 2.7861337y(n-3) \\ &\quad - 0.61743222y(n-4) \end{aligned} \quad (\text{F.14})$$

Equation F.14 was used to implement the digital low-pass filter.

By substituting $z = e^{j\omega\Delta T}$ into Equation F.11, the magnitude response of this filter is obtained and is shown in Figure F.1.

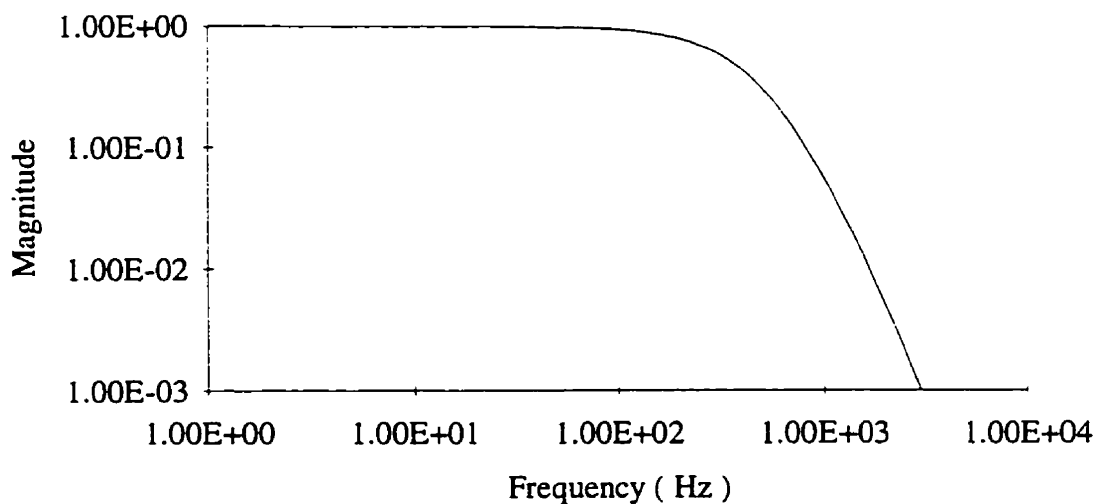


Figure F.1. Magnitude response of the fourth-order low-pass digital filter.

Appendix G. Electrical Parameters of SaskPower Distribution System

The model of the SaskPower distribution system selected for testing the proposed technique in Chapter 5, is again shown in Figure G.1.

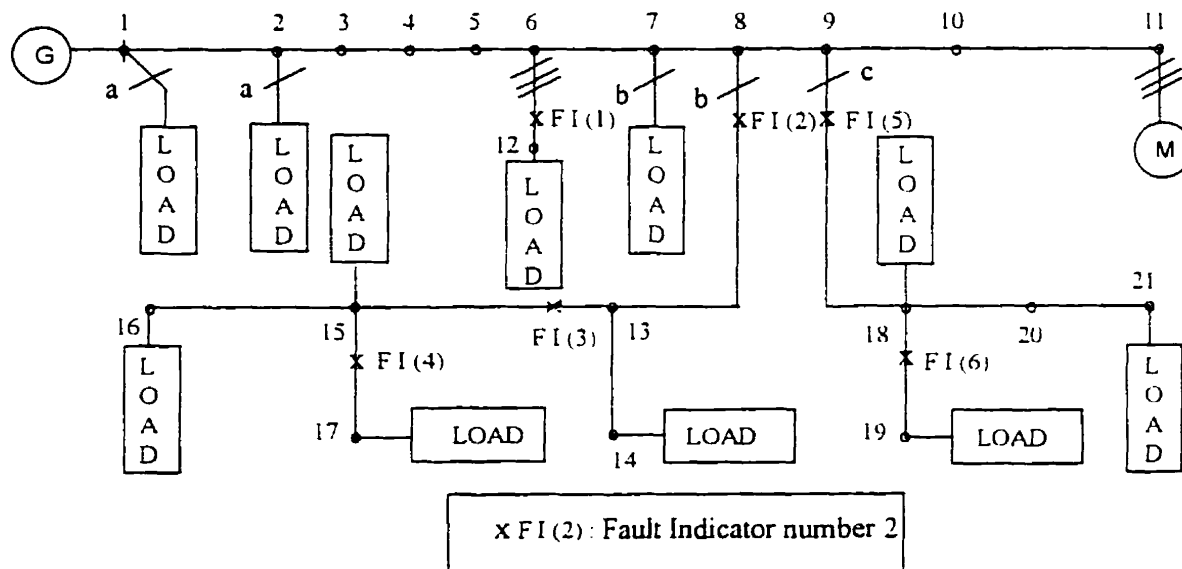


Figure G.1. Single line diagram of SaskPower 25 kV distribution system.

The electrical parameters of the system are given in Tables G.1, G.2 and G3.

Table G.1. Equivalent distribution system source data.

Base Voltage (kV)	Base Capacity (MVA)	Positive and Negative Sequence Impedance (p.u.)	Zero Sequence Impedance (p.u.)
25	00	$0.68283 + j2.98139$	$0.09496 + j1.39289$

Table G.2. Line data.

Section Between Nodes	Length of Section (km)	Series Impedance (Ohms / km)		Shunt Admittance (Mhos / km)	
		Positive & Negative Sequence	Zero Sequence	Positive & Negative Sequence	Zero Sequence
1 & 2	2.414	0.3480 + j0.5166	0.5254 + j1.704	j3.74 E-06	j2.49 E-06
2 & 6	16.092	0.3480 + j0.5166	0.5254 + j1.704	j3.74 E-06	j2.49 E-06
6 & 7	4.023	0.3480 + j0.5166	0.5254 + j1.704	j3.74 E-06	j2.49 E-06
7 & 8	5.150	0.5519 + j0.5390	0.7290 + j1.727	j3.59 E-06	j2.39 E-06
8 & 9	2.414	0.5519 + j0.5390	0.7290 + j1.727	j3.59 E-06	j2.39 E-06
9 & 10	4.506	0.5519 + j0.5390	0.7290 + j1.727	j3.59 E-06	j2.39 E-06
10 & 11	2.414	0.3480 + j0.5166	0.5254 + j1.704	j3.74 E-06	j2.49 E-06
11 & 12	2.414	0.3480 + j0.5166	0.5254 + j1.704	j3.74 E-06	j2.49 E-06
8 & 13	2.414	7.3977 + j0.8998	7.3977 + j0.8998	j2.51 E-06	j2.51 E-06
13 & 14	2.414	7.3977 + j0.8998	7.3977 + j0.8998	j2.51 E-06	j2.51 E-06
13 & 15	2.414	7.3977 + j0.8998	7.3977 + j0.8998	j2.51 E-06	j2.51 E-06
15 & 16	2.414	7.3977 + j0.8998	7.3977 + j0.8998	j2.51 E-06	j2.51 E-06
15 & 17	2.414	7.3977 + j0.8998	7.3977 + j0.8998	j2.51 E-06	j2.51 E-06
9 & 18	2.414	7.3977 + j0.8998	7.3977 + j0.8998	j2.51 E-06	j2.51 E-06
18 & 19	2.414	7.3977 + j0.8998	7.3977 + j0.8998	j2.51 E-06	j2.51 E-06
18 & 20	3.219	7.3977 + j0.8998	7.3977 + j0.8998	j2.51 E-06	j2.51 E-06
20 & 21	3.219	7.3977 + j0.8998	7.3977 + j0.8998	j2.51 E-06	j2.51 E-06

Table G.3. Load data.

Node Number	Phase	Connected Size (kVA)	Composition (%)		
			Heating	Lighting	Motor
1	A	15.0	99.8	0.1	0.1
2	A	15.0	99.8	0.1	0.1
7	B	15.0	99.8	0.1	0.1
11	A, B & C	1000.0	0.1	0.1	99.8
12	A, B & C	67.5	99.8	0.1	0.1
14	B	15.0	99.8	0.1	0.1
15	B	15.0	99.8	0.1	0.1
16	B	7.5	99.8	0.1	0.1
17	B	15.0	99.8	0.1	0.1
18	C	25.0	99.8	0.1	0.1
19	C	15.0	99.8	0.1	0.1
21	C	15.0	99.8	0.1	0.1

Load at a node is generally a mixture of heating, lighting and motor loads. Approximate composition of load is expected to be known for a particular node. Due to limitations in power systems simulation software, load at all nodes except at node number 11 was simulated as constant impedance load having a power factor 0.8 lag. Load at node number 11 was simulated with an available model of 500 h.p., 4.6 kV induction motor. The motor was connected to the 25 kV system through a 1000 kVA transformer having negligible loss.

The power factor and response constants of heating, lighting and motor loads are given in Table G.4.

Table G.4. Power factor and response constants for different types of load.

Type of Load	Power Factor	Response constant	
		Active	Reactive
Heating	1.0	2.0	2.0
Lighting	0.85 lag	1.4	1.4
Motor	0.8 lag	1.4	1.5 / 4.0*

* For balanced three-phase fault.

Response constant of equivalent active load, assumed consolidated with the load at the remote node, depends on the location of the fault. It was selected between 1.3 to 2.0. The same for reactive load was chosen between 1.5 to 2.0 for all types of fault except for balanced three-phase fault. For balanced three-phase fault, response constant of reactive load was chosen as 4.0.

Appendix H. Additional Test Results

Test results for phase C-to-ground, phase A-to-ground, phase C and phase A-to-ground, phase A and phase B-to-ground, phase B-to-phase C and, phase C-to-phase A faults are given in the Tables H.1 to H.30.

Table H.1. Fault location estimates for the phase C-to-ground fault cases when the fault resistance is 0.05 ohm.

Fault Node Number	Distance of the Fault (km)	Distance Estimated by using the	
		Reactive Component Method (km)	Proposed Technique (km)
1	0.000	0.395	0.000
2	2.414	2.840	2.417
3	6.437	6.459	6.444
4	10.461	10.479	10.470
5	14.484	14.494	14.497
6	18.507	18.497	18.526
7	22.530	22.457	22.542
8	27.680	27.340	27.693
9	30.094	29.692	30.108
10	34.600	33.872	34.568
11	37.014	36.169	37.006
12	20.921	20.809	20.856
18	32.508	30.942	32.471
19	34.922	33.013	35.133
20	35.727	33.806	35.614
21	38.946	37.513	39.519

Table H.2. Fault location estimates for the phase C-to-ground fault cases when the fault resistance is 5.0 ohm.

Fault Node Number	Distance of the Fault (km)	Distance Estimated by using the	
		Reactive Component Method (km)	Proposed Technique (km)
1	0.000	0.515	0.024
2	2.414	2.428	2.434
3	6.437	6.504	6.448
4	10.461	10.559	10.463
5	14.484	14.595	14.480
6	18.507	17.659	18.539
7	22.530	22.136	22.569
8	27.680	27.125	27.727
9	30.094	29.452	30.134
10	34.600	33.527	34.608
11	37.014	35.789	37.046
12	20.921	20.517	21.102
18	32.508	30.869	32.440
19	34.922	33.120	35.145
20	35.727	34.011	35.612
21	38.946	37.856	39.587

Table H.3. Fault location estimates for the phase C-to-ground fault cases when the fault resistance is 10.0 ohm.

Fault Node Number	Distance of the Fault (km)	Distance Estimated by using the	
		Reactive Component Method (km)	Proposed Technique (km)
1	0.000	0.685	0.020
2	2.414	2.501	2.424
3	6.437	6.652	6.426
4	10.461	10.753	10.431
5	14.484	14.616	14.443
6	18.507	18.107	18.541
7	22.530	21.995	22.569
8	27.680	26.939	27.730
9	30.094	29.010	30.155
10	34.600	33.240	34.623
11	37.014	35.479	37.065
12	20.921	20.379	21.308
18	32.508	30.864	32.403
19	34.922	33.259	35.125
20	35.727	34.163	35.526
21	38.946	38.303	39.684

Table H.4. Fault location estimates for the phase C-to-ground fault cases when the fault resistance is 25.0 ohm.

Fault Node Number	Distance of the Fault (km)	Distance Estimated by using the	
		Reactive Component Method (km)	Proposed Technique (km)
1	0.000	0.355	0.000
2	2.414	2.931	2.406
3	6.437	6.635	6.526
4	10.461	10.401	10.470
5	14.484	14.233	14.422
6	18.507	18.051	18.393
7	22.530	21.840	22.570
8	27.680	26.495	27.675
9	30.094	28.727	30.090
10	34.600	32.819	34.577
11	37.014	34.969	37.022
12	20.921	20.257	21.637
18	32.508	31.152	32.584
19	34.922	34.047	35.178
20	35.727	35.148	35.391
21	38.946	39.661	39.778

Table H.5. Fault location estimates for the phase C-to-ground fault cases when the fault resistance is 50.0 ohm.

Fault Node Number	Distance of the Fault (km)	Distance Estimated by using the	
		Reactive Component Method (km)	Proposed Technique (km)
1	0.000	2.084	0.000
2	2.414	4.320	2.169
3	6.437	8.037	6.156
4	10.461	11.734	9.947
5	14.484	15.414	13.776
6	18.507	19.073	17.679
7	22.530	22.681	22.151
8	27.680	27.271	27.208
9	30.094	29.416	29.749
10	34.600	33.297	34.289
11	37.014	35.385	36.804
12	20.921	21.159	21.060
18	32.508	32.605	33.030
19	34.922	36.137	34.977
20	35.727	37.331	35.957
21	38.946	42.289	39.785

Table H.6. Fault location estimates for the phase A-to-ground fault cases when the fault resistance is 0.05 ohm.

Fault Node Number	Distance of the Fault (km)	Distance Estimated by using the	
		Reactive Component Method (km)	Proposed Technique (km)
1	0.000	-0.001	0.000
2	2.414	2.417	2.411
3	6.437	6.428	6.432
4	10.461	10.411	10.456
5	14.484	14.367	14.485
6	18.507	18.288	18.510
7	22.530	21.802	22.547
8	27.680	26.599	27.700
9	30.094	28.816	30.114
10	34.600	32.981	34.605
11	37.014	34.991	37.046
12	20.921	20.206	20.850

Table H.7. Fault location estimates for the phase A-to-ground fault cases when the fault resistance is 5.0 ohm.

Fault Node Number	Distance of the Fault (km)	Distance Estimated by using the	
		Reactive Component Method (km)	Proposed Technique (km)
1	0.000	-0.043	0.027
2	2.414	2.325	2.435
3	6.437	6.258	6.450
4	10.461	10.171	10.472
5	14.484	14.063	14.485
6	18.507	17.605	18.557
7	22.530	21.383	22.585
8	27.680	26.158	27.734
9	30.094	28.377	30.166
10	34.600	32.435	34.700
11	37.014	34.595	37.094
12	20.921	19.819	21.109

Table H.8. Fault location estimates for the phase A-to-ground fault cases when the fault resistance is 10.0 ohm.

Fault Node Number	Distance of the Fault (km)	Distance Estimated by using the	
		Reactive Component Method (km)	Proposed Technique (km)
1	0.000	-0.017	0.025
2	2.414	2.304	2.427
3	6.437	6.163	6.431
4	10.461	10.013	10.443
5	14.484	13.846	14.458
6	18.507	17.412	18.557
7	22.530	21.146	22.582
8	27.680	25.899	27.761
9	30.094	28.091	30.183
10	34.600	32.224	34.721
11	37.014	34.361	37.108
12	20.921	19.605	21.316

Table H.9. Fault location estimates for the phase A-to-ground fault cases when the fault resistance is 25.0 ohm.

Fault Node Number	Distance of the Fault (km)	Distance Estimated by using the	
		Reactive Component Method (km)	Proposed Technique (km)
1	0.000	0.403	0.000
2	2.414	2.680	2.428
3	6.437	6.432	6.549
4	10.461	10.157	10.485
5	14.484	13.875	14.459
6	18.507	17.538	18.428
7	22.530	21.167	22.502
8	27.680	26.196	27.714
9	30.094	28.571	30.160
10	34.600	32.666	34.740
11	37.014	34.963	37.148
12	20.921	19.675	21.639

Table H.10. Fault location estimates for the phase A-to-ground fault cases when the fault resistance is 50.0 ohm.

Fault Node Number	Distance of the Fault (km)	Distance Estimated by using the	
		Reactive Component Method (km)	Proposed Technique (km)
1	0.000	2.178	0.000
2	2.414	4.406	2.250
3	6.437	8.089	6.250
4	10.461	11.747	10.058
5	14.484	15.396	13.901
6	18.507	19.024	17.794
7	22.530	22.607	22.307
8	27.680	27.132	27.405
9	30.094	29.243	29.897
10	34.600	33.180	34.570
11	37.014	35.286	37.017
12	20.921	21.115	21.150

Table H.11. Fault location estimates for the phase C and phase A-to-ground fault cases when the fault resistance is 0.05 ohm.

Fault Node Number	Distance of the Fault (km)	Distance Estimated by using the	
		Reactive Component Method (km)	Proposed Technique (km)
1	0.000	1.329	0.000
2	2.414	2.510	2.416
3	6.437	6.668	6.442
4	10.461	10.411	10.456
5	14.484	15.139	14.491
6	18.507	19.428	18.516
7	22.530	23.297	22.536
8	27.680	27.558	27.685
9	30.094	29.935	30.100
10	34.600	34.357	34.572
11	37.014	36.726	37.011
12	20.921	21.618	20.872

Table H.12. Fault location estimates for the phase C and phase A-to-ground fault cases when the fault resistance is 5.0 ohm.

Fault Node Number	Distance of the Fault (km)	Distance Estimated by using the	
		Reactive Component Method (km)	Proposed Technique (km)
1	0.000	1.431	0.000
2	2.414	2.470	2.394
3	6.437	6.762	6.461
4	10.461	11.078	10.502
5	14.484	15.409	14.535
6	18.507	19.081	18.557
7	22.530	22.030	22.601
8	27.680	27.052	27.817
9	30.094	29.397	30.238
10	34.600	33.748	34.809
11	37.014	36.055	37.200
12	20.921	20.439	21.256

Table H.13. Fault location estimates for the phase C and phase A-to-ground fault cases when the fault resistance is 10.0 ohm.

Fault Node Number	Distance of the Fault (km)	Distance Estimated by using the	
		Reactive Component Method (km)	Proposed Technique (km)
1	0.000	-0.125	0.000
2	2.414	2.508	2.308
3	6.437	6.892	6.434
4	10.461	11.273	10.493
5	14.484	14.827	14.539
6	18.507	18.254	18.554
7	22.530	21.754	22.631
8	27.680	26.732	27.887
9	30.094	29.042	30.290
10	34.600	33.332	34.907
11	37.014	35.587	37.313
12	20.921	20.190	21.495

Table H.14. Fault location estimates for the phase C and phase A-to-ground fault cases when the fault resistance is 25.0 ohm.

Fault Node Number	Distance of the Fault (km)	Distance Estimated by using the	
		Reactive Component Method (km)	Proposed Technique (km)
1	0.000	0.529	0.000
2	2.414	3.136	2.186
3	6.437	6.718	6.440
4	10.461	10.571	10.484
5	14.484	14.303	14.558
6	18.507	18.116	18.508
7	22.530	21.906	22.673
8	27.680	26.710	27.920
9	30.094	28.944	30.142
10	34.600	33.157	34.968
11	37.014	35.326	37.383
12	20.921	20.412	21.685

Table H.15. Fault location estimates for the phase C and phase A-to-ground fault cases when the fault resistance is 50.0 ohm.

Fault Node Number	Distance of the Fault (km)	Distance Estimated by using the	
		Reactive Component Method (km)	Proposed Technique (km)
1	0.000	3.605	0.035
2	2.414	5.898	2.645
3	6.437	9.632	6.855
4	10.461	13.352	10.834
5	14.484	17.071	14.802
6	18.507	20.862	18.724
7	22.530	24.445	23.044
8	27.680	29.047	28.414
9	30.094	31.197	29.708
10	34.600	35.169	34.736
11	37.014	37.492	37.271
12	20.921	23.068	20.719

Table H.16. Fault location estimates for the phase A and phase B-to-ground fault cases when the fault resistance is 0.05 ohm.

Fault Node Number	Distance of the Fault (km)	Distance Estimated by using the	
		Reactive Component Method (km)	Proposed Technique (km)
1	0.000	0.002	0.000
2	2.414	2.464	2.411
3	6.437	6.598	6.432
4	10.461	10.750	10.455
5	14.484	14.912	14.483
6	18.507	18.411	18.503
7	22.530	22.376	22.529
8	27.680	27.375	27.690
9	30.094	29.708	30.111
10	34.600	34.039	34.567
11	37.014	35.565	37.020
12	20.921	20.743	20.854

Table H.17. Fault location estimates for the phase A and phase B-to-ground fault cases when the fault resistance is 5.0 ohm.

Fault Node Number	Distance of the Fault (km)	Distance Estimated by using the	
		Reactive Component Method (km)	Proposed Technique (km)
1	0.000	-0.139	0.000
2	2.414	2.329	2.383
3	6.437	6.436	6.448
4	10.461	10.535	10.488
5	14.484	14.628	14.520
6	18.507	17.868	18.545
7	22.530	21.753	22.580
8	27.680	26.677	27.795
9	30.094	28.966	30.226
10	34.600	32.658	34.804
11	37.014	34.839	37.198
12	20.921	20.183	21.252

Table H.18. Fault location estimates for the phase A and phase B-to-ground fault cases when the fault resistance is 10.0 ohm.

Fault Node Number	Distance of the Fault (km)	Distance Estimated by using the	
		Reactive Component Method (km)	Proposed Technique (km)
1	0.000	-0.133	0.000
2	2.414	2.290	2.280
3	6.437	6.324	6.461
4	10.461	10.354	10.464
5	14.484	13.735	14.524
6	18.507	17.574	18.534
7	22.530	21.396	22.606
8	27.680	26.269	27.874
9	30.094	28.506	30.288
10	34.600	32.341	34.937
11	37.014	34.485	37.340
12	20.921	19.864	21.518

Table H.19. Fault location estimates for the phase A and phase B-to-ground fault cases when the fault resistance is 25.0 ohm.

Fault Node Number	Distance of the Fault (km)	Distance Estimated by using the	
		Reactive Component Method (km)	Proposed Technique (km)
1	0.000	0.523	0.000
2	2.414	2.821	2.033
3	6.437	6.516	6.311
4	10.461	10.268	10.365
5	14.484	14.026	14.397
6	18.507	17.769	18.432
7	22.530	21.562	22.498
8	27.680	26.885	27.948
9	30.094	29.116	30.254
10	34.600	33.262	35.062
11	37.014	35.686	37.530
12	20.921	20.010	21.721

Table H.20. Fault location estimates for the phase A and phase B-to-ground fault cases when the fault resistance is 50.0 ohm.

Fault Node Number	Distance of the Fault (km)	Distance Estimated by using the	
		Reactive Component Method (km)	Proposed Technique (km)
1	0.000	3.290	0.000
2	2.414	5.577	1.808
3	6.437	9.351	6.135
4	10.461	13.107	10.129
5	14.484	16.889	14.124
6	18.507	20.653	18.108
7	22.530	24.298	22.000
8	27.680	28.985	28.149
9	30.094	31.127	29.812
10	34.600	35.058	34.743
11	37.014	37.225	37.234
12	20.921	22.882	20.656

Table H.21. Fault location estimates for the phase B-to-phase C fault cases when the fault resistance is 0.05 ohm.

Fault Node Number	Distance of the Fault (km)	Distance Estimated by using the	
		Reactive Component Method (km)	Proposed Technique (km)
1	0.000	0.022	0.000
2	2.414	2.422	2.410
3	6.437	6.407	6.439
4	10.461	10.383	10.461
5	14.484	14.353	14.485
6	18.507	18.322	18.504
7	22.530	22.291	22.518
8	27.680	27.252	27.671
9	30.094	29.632	30.104
10	34.600	34.081	34.581
11	37.014	36.429	37.019
12	20.921	20.668	20.889

Table H.22. Fault location estimates for the phase B-to-phase C fault cases when the fault resistance is 5.0 ohm.

Fault Node Number	Distance of the Fault (km)	Distance Estimated by using the	
		Reactive Component Method (km)	Proposed Technique (km)
1	0.000	-0.047	0.039
2	2.414	2.329	2.449
3	6.437	6.286	6.465
4	10.461	10.241	10.483
5	14.484	14.195	14.501
6	18.507	18.150	18.544
7	22.530	22.105	22.583
8	27.680	27.105	27.833
9	30.094	29.480	30.129
10	34.600	33.915	34.617
11	37.014	36.246	37.052
12	20.921	20.505	21.233

Table H.23. Fault location estimates for the phase B-to-phase C fault cases when the fault resistance is 10.0 ohm.

Fault Node Number	Distance of the Fault (km)	Distance Estimated by using the	
		Reactive Component Method (km)	Proposed Technique (km)
1	0.000	-0.079	0.062
2	2.414	2.285	2.470
3	6.437	6.228	6.480
4	10.461	10.172	10.492
5	14.484	14.118	14.505
6	18.507	18.064	18.565
7	22.530	22.007	22.619
8	27.680	27.038	27.965
9	30.094	29.408	30.144
10	34.600	33.824	34.674
11	37.014	36.244	37.092
12	20.921	20.421	21.554

Table H.24. Fault location estimates for the phase B-to-phase C fault cases when the fault resistance is 25.0 ohm.

Fault Node Number	Distance of the Fault (km)	Distance Estimated by using the	
		Reactive Component Method (km)	Proposed Technique (km)
1	0.000	-0.029	0.028
2	2.414	2.349	2.419
3	6.437	6.309	6.412
4	10.461	10.266	10.398
5	14.484	14.214	14.386
6	18.507	18.138	18.470
7	22.530	22.068	22.637
8	27.680	27.124	28.280
9	30.094	29.516	30.117
10	34.600	33.854	34.681
11	37.014	36.150	37.098
12	20.921	20.501	20.716

Table H.25. Fault location estimates for the phase B-to-phase C fault cases when the fault resistance is 50.0 ohm.

Fault Node Number	Distance of the Fault (km)	Distance Estimated by using the	
		Reactive Component Method (km)	Proposed Technique (km)
1	0.000	0.544	0.000
2	2.414	2.969	2.230
3	6.437	6.983	6.154
4	10.461	10.870	10.094
5	14.484	14.745	14.031
6	18.507	18.598	17.977
7	22.530	22.480	22.238
8	27.680	27.357	28.067
9	30.094	29.628	29.696
10	34.600	33.832	34.244
11	37.014	36.067	36.701
12	20.921	20.913	20.066

Table H.26. Fault location estimates for the phase C-to-phase A fault cases when the fault resistance is 0.05 ohm.

Fault Node Number	Distance of the Fault (km)	Distance Estimated by using the	
		Reactive Component Method (km)	Proposed Technique (km)
1	0.000	0.049	0.000
2	2.414	2.511	2.417
3	6.437	6.514	6.435
4	10.461	10.465	10.462
5	14.484	14.479	14.486
6	18.507	18.488	18.506
7	22.530	22.490	22.525
8	27.680	27.574	27.669
9	30.094	29.947	30.103
10	34.600	34.361	34.588
11	37.014	36.725	37.019
12	20.921	20.853	20.894

Table H.27. Fault location estimates for the phase C-to-phase A fault cases when the fault resistance is 5.0 ohm.

Fault Node Number	Distance of the Fault (km)	Distance Estimated by using the	
		Reactive Component Method (km)	Proposed Technique (km)
1	0.000	-0.025	0.038
2	2.414	2.409	2.449
3	6.437	6.441	6.468
4	10.461	10.319	10.489
5	14.484	14.306	14.509
6	18.507	18.285	18.552
7	22.530	22.260	22.593
8	27.680	27.313	27.839
9	30.094	29.671	30.135
10	34.600	34.047	34.623
11	37.014	36.376	37.057
12	20.921	20.648	21.228

Table H.28. Fault location estimates for the phase C-to-phase A fault cases when the fault resistance is 10.0 ohm.

Fault Node Number	Distance of the Fault (km)	Distance Estimated by using the	
		Reactive Component Method (km)	Proposed Technique (km)
1	0.000	-0.109	0.059
2	2.414	2.328	2.470
3	6.437	6.381	6.484
4	10.461	10.210	10.503
5	14.484	14.168	14.517
6	18.507	18.122	18.579
7	22.530	22.070	22.640
8	27.680	27.098	27.993
9	30.094	29.439	30.143
10	34.600	33.781	34.676
11	37.014	36.087	37.072
12	20.921	20.478	21.553

Table H.29. Fault location estimates for the phase C-to-phase A fault cases when the fault resistance is 25.0 ohm.

Fault Node Number	Distance of the Fault (km)	Distance Estimated by using the	
		Reactive Component Method (km)	Proposed Technique (km)
1	0.000	-0.025	0.030
2	2.414	2.361	2.433
3	6.437	6.216	6.432
4	10.461	10.111	10.435
5	14.484	14.003	14.424
6	18.507	17.902	18.484
7	22.530	21.784	22.663
8	27.680	26.730	28.333
9	30.094	29.030	30.040
10	34.600	33.164	34.580
11	37.014	35.382	37.020
12	20.921	20.240	20.739

Table H.30. Fault location estimates for the phase C-to-phase A fault cases when the fault resistance is 50.0 ohm.

Fault Node Number	Distance of the Fault (km)	Distance Estimated by using the	
		Reactive Component Method (km)	Proposed Technique (km)
1	0.000	0.621	0.000
2	2.414	2.934	2.293
3	6.437	6.777	6.267
4	10.461	10.612	10.171
5	14.484	14.440	14.095
6	18.507	18.258	18.023
7	22.530	22.055	22.400
8	27.680	26.929	28.272
9	30.094	29.167	29.670
10	34.600	33.327	34.204
11	37.014	35.519	36.658
12	20.921	20.551	20.130

Appendix I. Procedure for Estimating Fault Locations

The procedure for estimating the location of a fault is described in this Appendix by considering that a single-phase-to-ground fault has occurred at Node 10 and the fault resistance is 0.05 ohms. The procedure described in the thesis provided four locations where the fault could be; these locations are listed in Table 5.1. Part of this table is reproduced here for ready reference.

Table I.1. Multiple fault location estimates for the single-phase-to-ground fault at node 10 when the fault resistance is 0.05 ohm.

Fault Node Number	Distance of the Fault (km)	Fault Location Estimate by using the			
		Reactive Component Method		Proposed Technique	
		Fault between Nodes	Distance (km)	Fault between Nodes	Distance (km)
10	34.600	9 & 10	32.936	9 & 10	34.566
		14 & xx	33.142	14 & xx	34.954
		15 & 16	33.142	15 & 16	34.419
		15 & 17	33.142	15 & 17	34.418

Note: **xx** indicate that fault is identified beyond the last node of the line.

For each apparent location, say for the location between Nodes 9 and 10, two additional locations, one between nodes 8 and 9 and the other between Nodes 10 and 11 were considered. The values of s calculated for these locations were:

Table I.2. Fault location estimates for one apparent location.

Apparent Locations Between Nodes	The Estimate of s
9 and 10	0.9926
8 and 9	2.42
10 and 11	None*

* None signifies that the convergence is not obtained.

The location corresponding to the estimate of s that is between 0 and 1 is the most likely location of the fault. It was, therefore, concluded that the fault is between Nodes 9 and 10. The estimated distance from Node 1 to the fault worked out to 34.566 km.

Using a similar approach, the estimates of s were obtained for the remaining three apparent locations listed in Table I.1. Four possible locations for a fault at Node 10 were identified in this manner. These estimates were converted to a single estimate using the information obtained from the fault indicators.

Appendix J. Fault Locator Hardware

The hardware of the fault locator has four major components: low-pass filter boards, data acquisition system (DAS) cards, a digital signal processing (DSP) card and a host personal computer. This section describes the features of low-pass filter boards and other system hardware components that are available from commercial products.

J.1 Low-pass Filter Boards

The low-pass filter is required to band-limit the analog voltage and current signals to the data acquisition system and prevent aliasing in samples of voltage and current signals. The circuit diagram of one channel of the low-pass filter is shown in Figure J.1.

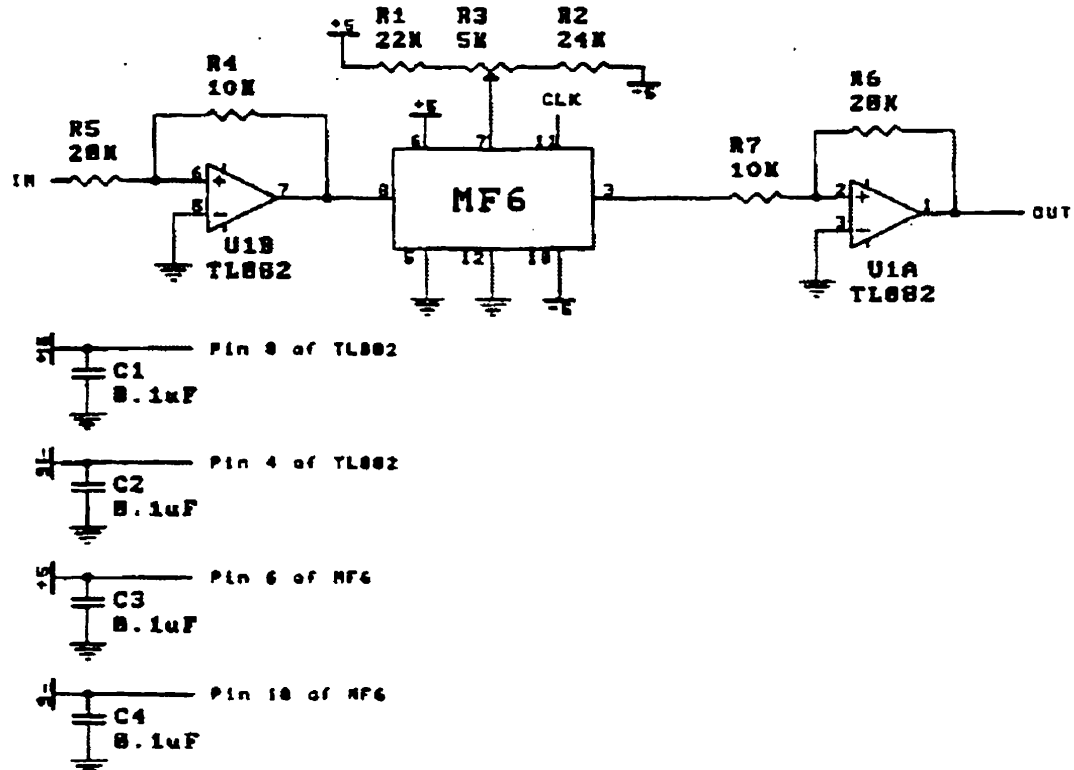


Figure J.1. Circuit diagram of one channel of the Butterworth low-pass filter.

MF6CN-100 is a low cost, easy to use 6th order low-pass filter with 14-pin DIP packaging. The ratio of clock frequency to cut-off frequency is internally set to 100:1. The maximum clock frequency is 1 MHz, giving the MF6CN-100 a maximum cut-off frequency of 10 kHz. A TTL logic compatible clock signal is provided to MF6CN-100 from a signal generator for tighter cut-off frequency control. The Pin 7 of MF6CN-100 is provided to adjust the filter's offset voltage and off-set adjustment arrangement is shown in Figure J.1. The output voltage swing of the filter is +3.5 V to -3.8 V.

Two operational amplifiers available from a TL082 chip [59] are provided at the input and output of the filter for the purpose of buffering the signals. As an additional feature, gain of the operational amplifier at the input of the filter is set to 0.5 while the operational amplifier at the output of the filter has a gain of 2.0. This feature extends the range of signals that can be filtered to $\pm 5.0\text{V}$ from $\pm 2.5\text{V}$.

The filters on both boards are powered from a commercially available $\pm 15\text{V}$ power supply. Additional power supply of $\pm 5\text{V}$ required for MF6CN-100 is derived in each board by using two voltage regulators, IC type 7805 for +5V and 7905 for -5V.

J.2 Data Acquisition System Cards

Figure J.2 shows the functional block diagram of the data acquisition of input channels [60]. These blocks are: Analog Signal Conditioning, Quad Sample/Hold, Analog-to-Digital conversion (ADC), the sample rate timer and the Control and Status Registers with the associated interrupt control.

Analog signal conditioning block consists of a unity gain low offset operational amplifier that buffers the input signal from the low-pass filter. A ± 2.5 Volt analog input signal range provides full scale operation of the ADC and it is necessary to limit the input signals below ± 3.0 Volt to prevent damage to the quad sample/hold chip. The signal conditioning block also has programmable 3rd order Butterworth low-pass analog filters to suppress unwanted high frequencies. They are only suitable as anti-aliasing filters if the sampling frequency is very much higher than the maximum input frequency component. As in the present project, the sampling frequency is not very much higher than the input frequency component, an external low-pass filter is used as an anti-aliasing filter and the low pass filters are described in the previous section.

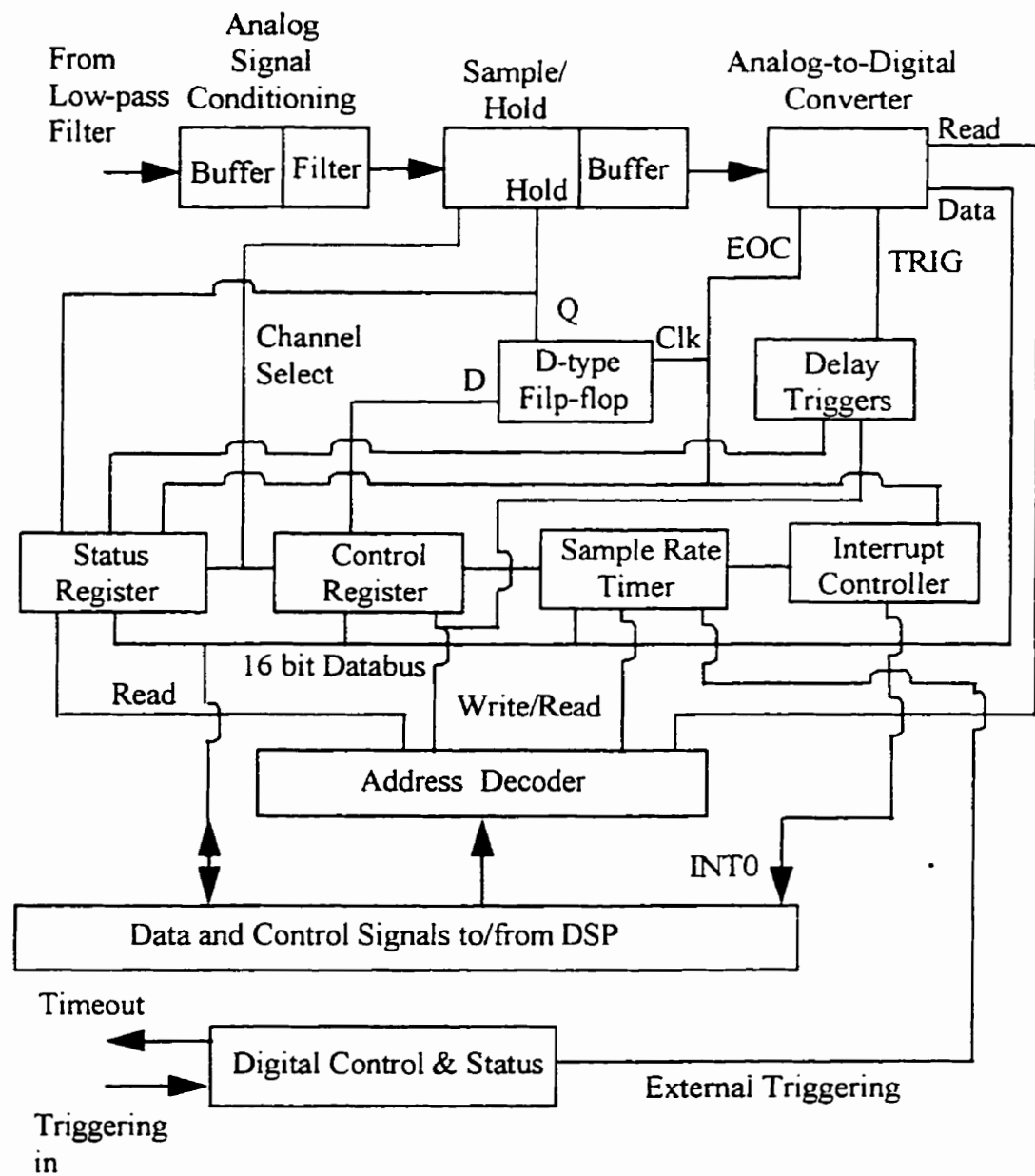


Figure J.2. Functional block diagram of the data acquisition system.

The outputs from the four filters in analog signal conditioning block are fed into a quad sample/hold chip. This device also performs multiplexing the signals to a single analog channel. Channel selection is performed by the control register. Output from the multiplexer is shifted in dc level and becomes the input to a single analog-to-digital converter (ADC).

The sample/hold chip also features on-chip digital intelligence and measurement circuitry capable of calibrating all four input channels. The effect of calibration is an automatic nulling of dc offsets in sample/hold and multiplexer components. For each channel, the device internally deselects the input signal and switches a known reference voltage to the input of the track-and-hold-amplifier. In the calibration mode, it uses an internal microcontroller and special nulling circuitry to reduce all errors at the output to less than ± 700 microvolt.

The conversion of a channel, presented to the ADC by the sample/hold as selected by the control register, is initiated by the trigger signal to the ADC. ADC signals the end-of-conversion by setting the EOC bit high which is read by the DSP through the status register. Once the EOC is high, DSP reads the data from the ADC and resets the EOC and initiate next conversion.

The sample rate timer is a 16-bit up counter running with an 8 MHz. The counter has a programmable input register from which the counter is loaded every time the maximum count value FFFF (hexadecimal) is reached.

Control and Status Registers are mapped into the lower 8 bits of the 16 bit word. The least significant 2 bits of the Control Register determine the channel to be converted. Other bits control the timeout interrupts (bit 2), operation of the timer (bit 4), initiation of S/H calibration cycle (bit 5), HOLD flip-flop (bit 6), end-of-conversion (bit 7) and an output flag for controlling the external circuitry (bit 3). Bits within the Status Register reflect the current operational state of the board and provide pollable flags indicating end-of-conversion and timeout events.

One DSP card can support four numbers of 4 Channel I/O cards. Each card is mapped to a specific base address in the DSP. Links (LK1) are provided on each DAS card to select the base address from four possible locations. Base address for the DAS cards was selected by providing links in position c and d respectively.

J.3 Digital Signal Processing Card

The PC/C31 card [61, 62] is a real-time applications platform from Spectrum Signal Processing Inc. PC/C31 card available at the University of Saskatchewan is equipped with a 33.3 MHz C31 processor which gives a performance of 16.7 Million Instructions Per Second (MIPS). A peak floating-point performance of 33.3 Million Floating-point Operations Per Second (MFLOPS) can be obtained from the processor.

PC/C31 card has one 32k x 32 bank of fast (zero wait state) SRAM, 2k x 32 Dual-port RAM (DPRAM) which is shared with the PC, and 32k x 8 EPROM (two wait states) which is used to boot up the TMS320C31 DSP. DPRAM on the card provides 2k x 32 on the DSP side and 8k x 8 (4k x 16) on the PC side.

The PC/C31 card is suitable for PC AT and compatibles as it uses the 16 bit interfaces. It is not necessary to write code to access the PC interface directly as the interface library, provided with PC/C31 development support package, allows easy access to card features.

Communication between the PC and the Card takes place over two autonomous interfaces. A memory-mapped interface, consist of DPRAM, allows fast information exchange between the PC and DSP without disrupting the process of either device. Simultaneous accesses are allowed unless the same address is being written to from both sides. In this case, user transparent arbitration is implemented to allow one side to gain control. I/O Mapped Interface provides access to various card facilities, such as resets and interrupts, through software programmable control registers.

The PC/C31 card is equipped with Loughborough Sound Images (LSI) Ltd.' DSPLINK2 digital system expansion interface. It consists of a 32 bit memory-mapped (256 locations) high speed, bi-directional bus that allows input/output directly to/from the DSP, without using the I/O bus on the PC. DSPLINK2 interface is used to communicate with data acquisition system cards described in the previous section.

There are four maskable interrupt lines (/INT0, 1, 2, 3) to the TMS320C31 DSP driven by DSPLINK2, PC and other optional peripheral devices. DSPLINK2 has one maskable interrupt /INT0 which is routed to the TMS320C31 processor via the processor's /INT2 line. The DSP can interrupt the PC on one of the six maskable interrupt request lines (/IRQ3, 4, 5, 6, 7 and 9).

Appendix K. Testing the Real-time Application Software

This section gives a brief overview of the TMS320C30-based system that was used for testing the real-time application software. An IBM-compatible PC was used as the host machine in the system. The TMS320C30 Evaluation Module (EVM) is a development tool from Texas Instruments and was used for executing and debugging applications program using the TMS320C30 C source debugger. Floating-point DSP applications can be evaluated and developed using the module. Each EVM includes a PC bus compatible card and software package.

K.1 Hardware

The hardware components of the EVM card include:

- TMS320C30, a 33-MFLOPS, 32-bit floating-point DSP,
- 16K-word zero-wait-state SRAM, allowing on-board coding of the algorithms,
- Port for host-PC communications and
- Multiprocessor serial port providing connections to multiple EVMs.

Loading of the code is done through the emulation port. A shared bi-directional 16-bit register is used for communication between the host and TMS320C30 after the code has been loaded since there is no direct host access into the TMS320C30 memory. The TMS320C30 has direct interface to SRAM which supports zero wait-state memory accesses on primary bus.

K.2. Software

The system has software tools to develop, debug, benchmark and run real-time algorithms. These include the TMS320C3x assembler/linker, C source debugger and an optimizing ANSI C compiler, a program loader and example applications software.

The EVM provides a window-based mouse-driven user-interface that enables downloading, execution and debugging of assembly code or C code.

K.3. Testing Procedure

Testing of the real-time application software was performed using code generation and execution steps. The ANSI C program written for the real-time application software was converted to the DSP code, which is executed after loading into the DSP.

The TMS320 floating-point C compiler consists of three different programs: the parser, the optimizer (optional), and the code generator. C source file is an input to the parser which checks for syntax and semantic errors, and produces an internal representation of the program called an intermediate file. The optimizer is an optional pass that is executed before code generation.

The intermediate file provides input to the optimizer which produces a highly efficient version of the code in the same format as the intermediate file. The intermediate file from parser or optimizer (if used) provides input to the code generator. The code generator produces an assembly language source file. This provides input to an assembler which generates a Common Object File Format (COFF) file. The output file from assembler provides an input to the linker which produces an executable COFF object file <program_name.out>.

DSP Code Generation Process

1. Develop the real-time application software in ANSI C programming language.
2. Include a data file from PSCAD simulation into the real-time software.
3. Compile, assemble, and link the C source file using the single command:
`cl30 <program_name.c> -z <program_name.cmd>`

Three files are generated: <program_name.obj>, <program_name.map>, and <program_name.out>. The map file, <program_name.map>, shows the memory configuration, section composition and allocation, and various symbols used in the program with their storage addresses in the memory. The file with extension ‘obj’ is an executable object file. The output file, <program_name.out> is loaded into the memory of the TMS320C30 DSP for execution.

Execution of the DSP Code

1. The output file, <program_name.out>, from the linker is loaded into the evaluation module (EVM) in TMS320C30-based DSP board using the commands given below:

```
evm30
reset
load <program_name.out>
```

2. The loaded file is executed by using the 'run' command and the execution can be stopped by pressing the <escape> key.
3. The variables of interest can be displayed using following commands:

`disp *(int *) 0x000XXX`, for integer variables or
`disp *(float *) 0x000XXX`, for floating-point variables.

0x000XXX is the memory address at which the selected variable resides and is known from the map file. Variable name can be used instead of memory address.

4. Time taken to run the program on DSP can be obtained by using the process of benchmarking. Benchmarking involves creating breakpoints at the start and the end of the program and is carried out using the following command steps:

```
evm30
reset
load <program_name.out>
ba 0x000XXX (0x000XXX is the program start memory location)
ba 0x000YYY (0x000YYY is the program end memory location)
run
runb
? CLK
```

Complete program execution time including all passes through the program, in number of clock cycles of the DSP, is displayed on the screen. Program execution time in millisecond is calculated from the single-cycle instruction execution time which is 60 nanosecond for the TMS320C30. Time taken to execute a section of the program can also be calculated by using a similar procedure.

Appendix L. Real Time Playback (RTP) Simulator

This section gives a brief overview of the Real Time Playback (RTP) Simulator from the Manitoba HVDC Research Center. This simulator plays back, in real time, test signals generated from PSCAD/EMTDC power systems simulation software (Appendix E) or on-line recordings in COMTRADE format. These digital signals are converted into analog signals which are used for testing real-time systems including protective relays, fault location and other monitoring systems. The RTP Simulator was used for testing the implemented fault location system. Hardware and software aspects of the system are described below.

L.1 Hardware

The hardware is composed of a standard personal computer (PC) package fitted with the necessary additional hardware cards and output/input ports. The system is composed of four separate components: a tower case, display monitor, keyboard and mouse pointing device. The tower case encloses, among others, the following main items:

- 150 MHz Intel Pentium processor,
- 2.1 GB Hard Drive,
- 8x CD-ROM,
- 32 MB RAM
- 1.4 MB Floppy Drive,
- National Instruments 10-channel, 12-bit D/A (Digital to Analog) card and Front panel with 10 BNC connectors for access to the D/A card outputs.

L.2. Software

The operating system of the PC that is used as RTP Simulator is Microsoft Windows for Workgroups Version 3.11. In addition to a number of other programs, the main RTP software package (version 1.2) is also installed in a separate directory. This software enables interfacing with PSCAD/EMTDC (version 2.0) power systems simulation software. The waveforms of the signals that are loaded from PSCAD for

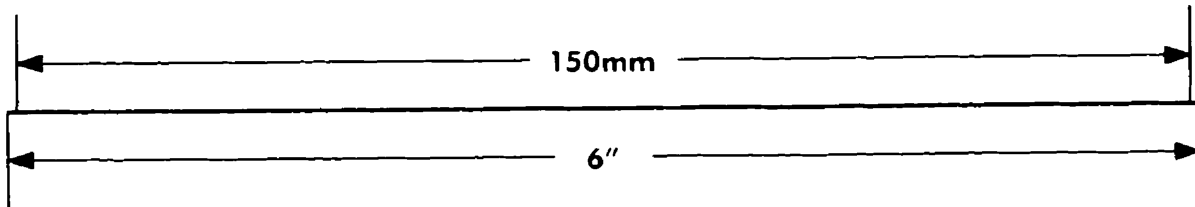
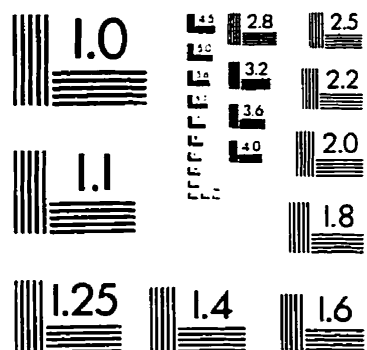
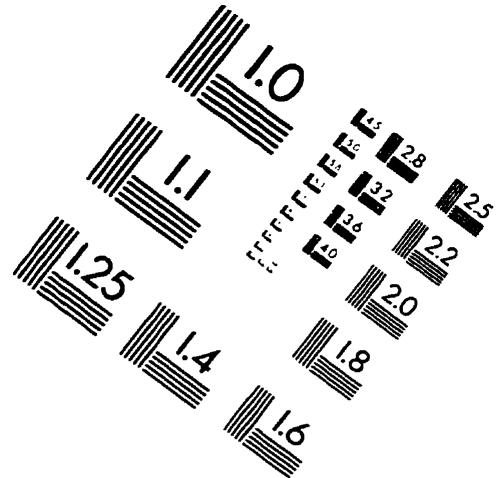
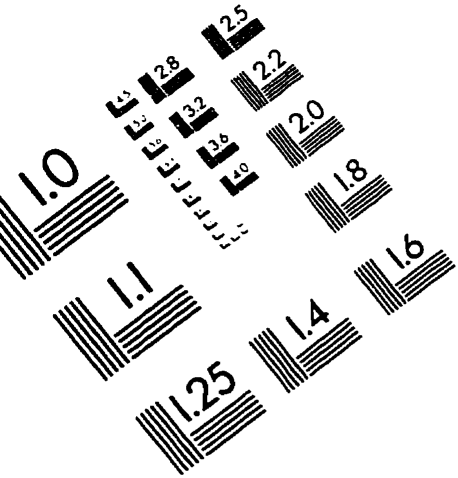
playback can be previewed using this software. On user command, the software plays these signals back through the output connectors.

The RTP Simulator software package includes an installation routine that introduces a recorder icon into the component pallet in DRAFT module of the PSCAD. There can be up to 9 recorders in a given power system simulation each having a maximum of 10 analog channels. System parameters to be recorded are selected by the user along with start and end times. The recordings can be user selected for COMTRADE or RTP format. The recordings are stored in a separate file, during Runtime. The name of the file is selected by the user in DRAFT module. The standard PSCAD output ASCII file is not affected by this process.

The generated recording file (with extension PBK) is then ported to the RTP Simulator for playback. Porting of these files can be done through the network connections or by the use of floppy disks. The former is preferable for speed of transfer and to avoid the size limitation of floppy disks.

When RTP playback software is started, any previously recorded files can be loaded for viewing on the screen and can be played back. When playback is initiated, RTP Simulator plays the first cycle in each channel repeatedly to create a pre-transient steady state waveform. Once the playback command is given, the RTP Simulator plays the transient data and then plays the last cycle repeatedly to create post-transient waveform. The last cycle is repeated 500 times by default, which can be reduced or increased by users.

IMAGE EVALUATION TEST TARGET (QA-3)



APPLIED IMAGE, Inc.
 1653 East Main Street
Rochester, NY 14609 USA
Phone: 716/482-0300
Fax: 716/288-5989

© 1993, Applied Image, Inc., All Rights Reserved

